

# Spectroscopic Atlas for Amateur Astronomers

A Guide to the Stellar  
Spectral Classes

Richard Walker

Version 4.0

04/2013

## Table of Content

<b>1</b>	<b>Introduction .....</b>	<b>11</b>
<b>2</b>	<b>Selection, Preparation and Presentation of the Spectra .....</b>	<b>13</b>
2.1	Selection of Spectra .....	13
2.2	Recording and Resolution of the Spectra .....	13
2.3	The Processing of the Spectra .....	14
2.4	Calibration of the Wavelength .....	14
2.5	Normalisation of the Intensity .....	15
2.6	Line Identification .....	15
2.7	Presentation .....	15
<b>3</b>	<b>Terms, Definitions and Abbreviations.....</b>	<b>16</b>
3.1	Parameters and Identification of the Stars .....	16
3.2	Galactic Nebulae and Star Clusters .....	16
3.3	Extragalactic Objects .....	16
3.4	"Early" and "Late" Spectral Types .....	16
3.5	Abbreviations and Units .....	16
3.6	Identifying of the Elements and Ions .....	17
3.7	The Metal Abundance Z (Metallicity) .....	17
<b>4</b>	<b>The Fraunhofer Lines.....</b>	<b>18</b>
<b>5</b>	<b>Overview and Characteristics of Stellar Spectral Classes .....</b>	<b>19</b>
5.1	The Temperature Sequence .....	19
5.2	The Luminosity Classes .....	22
5.3	Suffixes, Prefixes, and Special Classes .....	22
<b>6</b>	<b>Appearance of Elements and Molecules in the Spectra.....</b>	<b>24</b>
<b>7</b>	<b>Spectral Class O .....</b>	<b>25</b>
7.1	Overview .....	25
7.2	Parameters of the Early to Late O-Class Stars .....	26
7.3	Spectral Characteristics of the O-Class.....	26
7.4	General Remarks to the Classification of O-Stars .....	26
7.5	Commented Spectra .....	27
<b>8</b>	<b>Wolf Rayet Stars.....</b>	<b>32</b>
<b>9</b>	<b>Spectral Class B.....</b>	<b>38</b>
9.1	Overview .....	38
9.2	Parameters of the Early to Late B-Class Stars.....	38
9.3	Spectral Characteristics of the B-Class .....	38
9.4	Commented Spectra .....	39
<b>10</b>	<b>LBV Stars.....</b>	<b>45</b>
<b>11</b>	<b>Be Stars.....</b>	<b>49</b>
<b>12</b>	<b>Be Shell Stars.....</b>	<b>52</b>

<b>13 PMS Protostars .....</b>	<b>54</b>
13.1 Overview .....	54
13.2 Herbig Ae/Be and T Tauri Stars .....	54
13.3 Spectral Characteristics of PMS Stars.....	54
13.4 The FU Orionis Phenomenon.....	55
13.5 Commented Spectra .....	55
<b>14 Spectral Class A.....</b>	<b>60</b>
14.1 Overview .....	60
14.2 Parameters of the Early to Late A-Class Stars.....	60
14.3 Spectral Characteristics of the A-Class .....	60
14.4 Commented Spectra .....	61
<b>15 Spectral Class F .....</b>	<b>67</b>
15.1 Overview .....	67
15.2 Parameters of the Early to Late F-Class Stars.....	67
15.3 Spectral Characteristics of the F-Class .....	67
15.4 Commented Spectra .....	68
<b>16 Spectral Class G .....</b>	<b>72</b>
16.1 Overview .....	72
16.2 Parameters of the Early to Late G-Class Stars .....	72
16.3 Spectral Characteristics of the G-Class.....	72
16.4 Commented Spectra .....	73
<b>17 Spectral Class K.....</b>	<b>77</b>
17.1 Overview .....	77
17.2 Parameters of the Early to Late K-Class Stars.....	77
17.3 Spectral Characteristics of the K-Class .....	77
17.4 Commented Spectra .....	78
<b>18 Spectral Class M.....</b>	<b>85</b>
18.1 Overview .....	85
18.2 Parameters of the Early to Late M-Class Stars.....	85
18.3 Spectral Characteristics of the M-Class .....	85
18.4 Commented Spectra .....	86
<b>19 Spectral Sequence on the AGB.....</b>	<b>88</b>
19.1 Evolution of the Stars on the Asymptotic Giant Branch (AGB) .....	88
19.2 The Spectral Sequence of the Mira Variables on the AGB .....	89
<b>20 M(e) Stars on the AGB.....</b>	<b>90</b>
20.1 Overview .....	90
20.2 Spectral Characteristics of the M(e) Stars on the AGB.....	90
20.3 Commented Spectra .....	90
<b>21 Spectral Class S on the AGB .....</b>	<b>92</b>
21.1 Overview and Spectral Characteristics .....	92
21.2 The Boeshaar – Keenan S–Classification System.....	92
21.3 „Intrinsic“ and „Extrinsic“ („Symbiotic“) S-Stars .....	92

21.4	Hints for the Observation of <i>S</i> -Class Stars .....	93
21.5	Commented Spectra .....	93
<b>22</b>	<b>Carbon Stars on the AGB .....</b>	<b>98</b>
22.1	Overview and Spectral Characteristics .....	98
22.2	Competing Classification Systems.....	98
22.3	The Morgan Keenan (MK) – C System.....	98
22.4	The „Revised MK System 1993“ .....	99
22.5	Function of the Subclasses in the Evolution of Carbon Stars.....	100
22.6	Merrill Sanford Bands (MS) .....	100
22.7	Commented Spectra .....	101
<b>23</b>	<b>Spectra of Extragalactic Objects .....</b>	<b>104</b>
23.1	Introduction .....	104
23.2	Morphological Classification.....	104
23.3	Spectroscopic Classification .....	105
23.4	The phenomenon of AGN (Active Galactic Nuclei) .....	106
23.5	Commented Spectra .....	106
<b>24</b>	<b>Spectra of Emission Nebulae .....</b>	<b>115</b>
24.1	Short Introduction and Overview .....	115
24.2	Common Spectral Characteristics of Emission Nebulae .....	116
24.3	Emission Line Diagnostics and Excitation Classes <i>E</i> .....	116
24.4	Remarks to the Determination of Excitation Classes and Recording of Spectra .....	117
24.5	The Excitation Class as an Indicator for Plasma Diagnostics .....	118
24.6	Emission Lines identified in the Spectra of Nebulae.....	118
24.7	Commented Spectra .....	118
24.8	Distinguishing Characteristics in the Spectra of Emission Nebulae .....	123
<b>25</b>	<b>Reflexion Spectra of Solar System Bodies.....</b>	<b>133</b>
25.1	Overview .....	133
25.2	Commented Spectra .....	133
<b>26</b>	<b>Telluric Molecular Absorption .....</b>	<b>138</b>
<b>27</b>	<b>The Night Sky Spectrum.....</b>	<b>142</b>
27.1	Introduction .....	142
27.2	Effects on the Spectrum .....	142
27.3	Countermeasures .....	142
27.4	Comments to Table 96 .....	142
<b>28</b>	<b>Terrestrial Lightsources .....</b>	<b>144</b>
28.1	Spectra of Gas Discharge Lamps.....	144
28.2	Spectra of Gasflames.....	152
28.3	Spectra of Terrestrial Lightning Discharges .....	154
<b>29</b>	<b>Spectral Classes and <i>vsini</i> – Values of Important Stars.....</b>	<b>156</b>
<b>30</b>	<b>Required Ionisation Energies for the Individual Elements .....</b>	<b>159</b>
<b>31</b>	<b>Bright Planetary Nebulae sorted by Excitation Classes.....</b>	<b>160</b>



<b>32 Terminology of the Spectroscopic Wavelength Domains .....</b>	<b>161</b>
<b>33 Positions of the Atlas-Stars in the HRD .....</b>	<b>162</b>
<b>34 Appendix.....</b>	<b>163</b>
34.1 Constellations .....	163
34.2 Periodic Table of Elements .....	164
34.3 Some Excerpts of Historical and up to date Spectral Atlases .....	165
34.4 Instruments .....	168
<b>35 Bibliography and Internet .....</b>	<b>169</b>

## Change log of the atlas versions

Version 1.3: Corrections of some labeling-/typing errors and temperature of the O-class stars, some English language corrections.

Version 1.4: Corrections of some labeling and typing errors. *sect. 1:* correction of citation error regarding *Spectroweb*.

Version 1.5: *Sect. 7.4, (8) WR133*, expansion velocity of the stellar wind, *EW* value replaced by *FWHM* value.

*sect. 8.3 (9.3):* chart of the theoretical B-class continuum, correction of the wrongly labeled Ca II line (thanks to Robin Leadbeater!).

Version 2.0: New: *Sect. 12:* Be Shell stars and some adjustments to *sect. 11*.

New: *Sect. 18 – 21:* Spectral sequence of the *Mira Variables* on the *AGB* with the classes *M(e)*, *S-* and carbon stars *C*.

General revision of the title structure, the table of contents and the *sect. 31* "Bibliography and Internet".

Version 3.0:

*Sect. 3.5:* Additional Abbreviations,

*Sect. 3.7:* New: Formula for metallicity.

*Sect. 7:* General revision and expansion to the early O Class.

*Sec. 10:* P Cygni, higher resolved profile sections (900L grating) in the green and blue range of the spectrum.

*Sect. 13:* New: *Herbig Ae/Be* and *T Tauri Protostars*

*Sect. 21:* Correction of the wrongly labelled *BD Camelopardalis*: new HD 22649

*Sect. 24:* General revision of the section, new: determination of the excitation classes of emission nebulae and table 85: SNR M1/ NGC 1952.

*Sect. 25:* Reflexion spectra: former Tables 85 and 86 ==> new Tables 90 and 91

New: Comet C/2009 P1 Garradd, Table 94

*Sect. 27:* New: Nigth Sky Spectrum Table 96

*Sect. 28:* Table 106, Calibration spectrum of the glow starter OSRAM ST 111

*Sect. 31:* List of bright Planetary Nebulae sorted by excitation classes.

*All Parameter tables* of the individual spectral classes: Correction of the wrong (german) abbreviation "*Mrd*" by *bn* (thanks to Dave Dowhos!).

Version 4.0:

*Table of content:* Inserting of an additional subtitle level

*Sect. 2.2:* Supplement with the data of the SQUES Echelle spectrograph

*Sect. 3.7:* Correction of the formula

*Sect. 6:* Revised graphic

*Sect. 8:* New: Table 6, WR 136 and WR 142, supplements in the text

*Sect. 13:* New: FU Orionis Phenomenon with Table 19

*Sect. 15.3:* Revised graphic

*Sect. 23:* General revision of the section with spektroskopische classification of the Galaxies. New Tables 73 (M77) and 77, 78 (3C273)

*Sect. 24:* New: Table 86, Wolf Rayet Nebula NGC 6888, supplements in the text

*Sect. 26:* New: Table 95A, , Highly resolved spectra of telluric H<sub>2</sub>O and O<sub>2</sub> absorptions

*Sect. 28:* Table 106, Correction of the wrongly labelled H $\gamma$  line

*Sect. 28.3:* Table 111, Spectra of terrestrial lightning discharges

*Sect. 34:* New: Positions of the Atlas-Stars in the HRD

## Directory of Tables

Table	Page	Topic	Objects	Wavelength domain	Gra-ting
01	20	Overview on the spectral classes	Spectral strips of various stars	3950 – 6690	200L
02	21	Overview on the spectral classes	Intensity profiles of various stars	3950 – 6690	200L
1	29	Spectral features of the late O-class	Alnitak $\zeta$ Ori Mintaka $\delta$ Ori	3920 – 6710	200L
2	30	Detailed spectrum of a late O-class star	Alnitak $\zeta$ Ori	3950 – 4750 5740 – 6700	900L
3	31	Spectral features of the early to middle O-class	$\theta^1$ Ori C 68 Cygni	3800 – 6700	200L
5	36	Wolf-Rayet stars, type WN and WC final stage of the O-Class	WR 133 WR 140	3850 – 7250	200L
6	37	Wolf-Rayet stars, type WN and WO final stage of the O-Class	WR 136 WR 142	3860 – 7200 3750 – 7200	200L
10	40	Development of spectral features within the B-class	Alnilam $\epsilon$ Ori Gienah Corvi $\gamma$ CrV	3900 – 6700	200L
11	42	Effect of the luminosity on spectra of the late B-class	Regulus $\alpha$ Leo Rigel $\beta$ Ori $\phi$ Sagittarii	3920 – 4750	900L
12	44	Detailed spectrum of an early B-class star	Spica $\alpha$ Vir	3800 – 6750 3900 – 4750 4800 – 5100 5700 – 6050 6450 – 6600	200L 900L
13	47	LBV star, early B-class P Cygni profiles,	P Cygni, 34 Cyg	3900 – 6950 6000 – 6800	200L 900L
13A	48	Detailed spectrum LBV star, early B-class, P Cygni profiles	P Cygni 34 Cyg	3850 – 4650 4700 – 6050	900L
14	50	Be- star, early B-class	Dschubba $\delta$ Sco	3650 – 7000 4820 – 4940 6500 – 6700 6670 – 6690	200L 900L
14A	51	Be-star, early B-Class	Tsih $\gamma$ Cassiopeiae	3970 – 6750	200L
15	53	Be Shell Star, comparison to an “ordinary” Be Star	$\zeta$ Tauri Dschubba $\delta$ Sco	3800 – 6800	200L
17	57	Herbig Ae/Be Protostar	R Monocerotis NGC 2261	3900 – 7200	200L
18	58	T Tauri Protostar	T Tauri	3900 – 7000	200L
19	59	FU Orionis Protostar, comparison to the KO Giant Algieba, $\gamma$ Leonis	FU Orionis Algieba, $\gamma$ Leonis	3900 – 6800	200L
20	62	Development of spectral features within the A-class	Castor $\alpha$ Gem Altair $\alpha$ Aql	3900 – 6800	200L

Table	Page	Topic	Objects	Wavelength domain	Gra-ting
21	63	Detailed spectrum of an early A-class star	Sirius A $\alpha$ CMa	3900 – 6700 3900 – 4700 4780 – 5400	200L 900L
22	65	Effects of the luminosity on spectra of the early A-class	Vega $\alpha$ Lyr Ruchbah $\delta$ Cas Deneb $\alpha$ Cyg	3900 – 4700	900L
23	66	Metallicity: Vega vs. Sirius	Vega $\alpha$ Lyr Sirius A $\alpha$ CMa	3920 – 4700	900L
30	69	Development of spectral features within the F-class	Adhafera $\zeta$ Leo Procyon $\alpha$ CMi	3830 – 6700	200L
31	71	Effects of the luminosity on spectra of the early F-class	Porrima $\gamma$ Vir Caph $\beta$ Cas Mirfak $\alpha$ Per	3920 – 4750	900L
40	74	Development of spectral features within the G-class	Muphrid $\eta$ Boo Vindemiatrix $\epsilon$ Vir	3800 – 6600	200L
41	75	Detailed spectrum of an early G-class star	Sun	3800 – 7200 3900 – 4800	200L 900L
42	76	Detailed spectrum of an early G-class star	Sun	4700 – 5700 5650 – 6700	900L
50	80	Development of spectral features within the K-class	Arcturus $\alpha$ Boo Alterf $\lambda$ Leo	3900 – 6800	200L
51	81	Detailed spectrum of an early K-class star	Pollux $\alpha$ Gem	3900 – 6800 3800 – 4800	200L 900L
52	83	Effects of the luminosity on spectra of the late K-class	Alsciaukat $\alpha$ Lyncis 61 Cygni B	4000 – 4900	900L
53	84	Detailed spectrum of a later K-class star	Aldebaran $\alpha$ Tau	5150 – 5900 5850 – 6700	900L
60	87	Development of spectral features within the M-class	Antares $\alpha$ Sco Ras Algethi $\alpha$ Her	3900 – 7200	200L
63	91	Mira Variable M(e), comparison to a late classified M-Star	Mira $\circ$ Ceti Ras Algethi $\alpha$ Her	3900 – 7200	200L
65	94	Extreme S-Class star, comparison to a Mira Variable M(e)	R Cygni Mira $\circ$ Ceti	4100 – 7300	200L
66	96	Development of spectral features within the S-Class	Omikron1 Orionis Chi Cygni R Cygni	4100 – 7300	200L
66A	97	Comparison of an „intrinsic“ and „extrinsic“ S-Class star	BD Camelopardalis HR Pegasi	4300 – 7200	200L
67	102	Comparison of differently classified carbon stars	WZ Cassiopeiae Z Piscium W Orionis	4600 – 7300	200L
67A	103	<i>Merril Sanford Bands</i> , details at a higher resolved spectrum	W Orionis	4730 – 5400	900L
70	111	Comparison of Spectra: Spiral galaxy vs. star of the late G-class	Andromeda M31 Vindemiatrix $\epsilon$ Vir	3900 – 6700	200L

Table	Page	Topic	Objects	Wavelength domain	Gra-ting
73	112	Seyfert Galaxy, AGN	M77	3800 – 6800	200L
77	113	Quasar: Emission lines	3C273	3800 – 6600	200L
78	114	Quasar: Redshift	3C273	4400 – 7600	200L
80	124	Emission Nebula: <i>HII Region</i>	M42	3800 – 7300	200L
80A	125	Intensity profiles of H $\beta$ and [OIII] ( $\lambda$ 5007) in the central area of M42	M42	n.a.	200L
81	126	Emission Nebula: <i>Planetary Nebula</i>	IC418 Spirograph Neb	4100 – 7100	200L
82	127	Emission Nebula: <i>Planetary Nebula</i>	NGC6210 Turtle Neb.	3850 – 6600	200L
83	128	Emission Nebula: <i>Planetary Nebula</i>	NGC7009 Saturn Neb	3800 – 6700	200L
84	129	Emission Nebula: <i>Planetary Nebula</i>	M57 Ring Nebula	4600 – 6800	200L
84A	130	Intensity profiles of [O III] and [N II] in the longitudinal axis of M57	M57 Ring Nebula	n.a.	200L
85	131	Emission Nebula: <i>SNR</i>	M1 / NGC 1952	4600 – 6800	200L
86	132	Emission Nebula: Wolf Rayet <i>WR</i>	Crescent Nebula NGC 6888	4700 – 6800	200L
90	135	Reflexion spectra of solar system bodies	Mars, Venus	4300 – 7800	200L
91	136	Reflexion spectra of solar system bodies	Jupiter, Saturn	4400 – 7800	200L
94	137	Comet spectrum	C/2009 P1 Garradd	3800 – 6400	200L
95	139	Spectral absorptions due to the earth's atmosphere	Earth's atmosphere	6800 – 7800	900L
95A	140	Absorptions due to earth's atmosphere. High resolution spectrum: H <sub>2</sub> O lines around H $\alpha$	Sun $\delta$ Scorpii	6490 – 6610	SQUES Echelle
95B	141	Absorptions due to earth's atmosphere. High resolution spectrum: Fraunhofer A- und B-Band	Sun	6865 – 6940 7950 – 7700	SQUES Echelle
96	143	Night sky spectrum	Light Pollution Airglow	4000 – 7400	200L
101	146	Gas discharge lamp	Neon glow lamp	5800 – 8100	900L
102	147	Gas discharge lamp	ESL Osram Sunlux	3900 – 6400	200L
103	148	Gas discharge lamp	Xenon strobe tube	3900 – 8100	200L 900L
104	149	Gas discharge lamp	High pressure sodium vapor lamp	4700 – 7250	200L
105	150	Gas discharge lamp	High power xenon lamp	4900 – 6900	200L
106	151	Gas discharge lamp	Glow Starter OSRAM ST 111	4000 – 7700 3900 – 4800	200L 900L

Table	Page	Topic	Objects	Wavelength domain	Gra-ting
110	153	Swan Bands / Hydrocarbon gas flames: Comparison of superposed spectra	Butane-gas-torch Comet Hyakutake WZ Cassiopeiae	3800 – 6400	200L
111	155	Spectra of terrestrial lightning discharges	Lightning	3750 – 7200	200L

# 1 Introduction

Probably most amateur astronomers have a common experience at the beginning of their spectrographic "career". Full of expectations they test the new device for the first time and look with great pride at the first self recorded spectrum. This first enthusiasm then quickly gives way to the perplexity, how these numerous lines shall now be identified and even analyzed. Fortunately, some recommendable introductory literature, e.g. [1], to the interpretation of stellar spectra is available for amateurs. However, a real "*Spectral Atlas*", which systematically covers the classes *O, B, A, F, G, K, M*, by commenting most of the lines, visible in a medium resolved spectral profile, was still missing. In 2009 the extensive work "Stellar Spectral Classification" was published by R. Gray and C. Corbally [2]. It is aimed primarily at students and professional astronomers, but offers the significantly advanced amateur valuable information, eg for determining the decimal subclasses or the spectral characteristics of rare types of stars. In the Internet we find many professional papers, mostly focused on small sections of a spectral profile. Nevertheless, they often contribute valuable puzzle pieces to the exciting "detective work" of line identification.

Very well documented is the spectrum of the Sun (G2 V), where almost all of the lines are identified and commented. Here, at least two easily readable and freely downloadable atlases are available on the net [80], [81]. These sources can even help, with the necessary precautions, to identify spectral lines of adjacent spectral classes.

Spectral atlases from professional sources, published on the internet, and covering all important spectral classes can rarely be found. Amazingly, even in such professional papers, usually only a few intense lines, mostly in very lowly resolved spectra, are commented. However, the focus of many practical applications, even in professional works, is mostly reduced to relatively few, highly intense and isolated lines, e.g. for determination of the rotation speed or the metal abundance. In such publications the ultraviolet, the blue- and red-to far infrared part of the spectra are preferably treated - the sections "green" and "yellow" however only rarely.

In Appendix 34.3 some excerpts from several historical as well as state of the art spectral atlases are shown. Probably the best known, and highly important one, even for the history of science, is the out of print standard work "*An atlas of stellar spectra, with an outline of spectral classification*" by Morgan, Keenan and Kellman [50]. This seminal work from 1943 can now be downloaded from the Internet but is limited to the short-wavelength part of the visible spectrum, reflecting the state of technology in the 1940's. It presents photographic spectral strips, commented with handwritten notes! Made in a similar style is the "*Revised MK Spectral Atlas for Stars Earlier Than the Sun*" from 1978 by Morgan, Abt, and Tapscott [51].

Some spectral atlases were available in the past but are out of print today. The most comprehensive "reference work" is surely "*Bonner Spektralatlas*", the title of the English edition: "*Atlas for Objective Prism Spectra*" by Waltraut C. Seitter, 1975 [5]). This atlas, covering the spectral types from *O5* to *M2*, is out of print today, but recently available as download [5]! Still based on photographic spectral strips it's the only reviewed work, documenting most of the lines between about  $\lambda$  3400 – 5000, which are visible with low to medium resolving spectrographs. In the *green-red* range this atlas partly shows quite large gaps. It's striking, that despite this work undoubtedly being outdated, it has never been adapted to today's requirements, but is still referenced in various current papers. Written in a similar style, but much less detailed, are also the atlases [6], [7] and [8]. A stroke of luck that Martin Brunold [705] collected all these books and has kindly provided me with a review (see Appendix 34.3).

Nowadays calibrated and intensity-normalized profiles, plotted against the wavelength are required to meet the current standards. Fairly recent (2000) is "*A Digital Spectral Classifi-*

*cation Atlas*" by R.O. Gray [52]. However it's limited to a lowly resolved, short-wave part of the visible spectrum. Furthermore several atlases exist, focusing on specific wavelength ranges. Some of them are listed in the bibliography. For some of the brighter stars monographs are available, with fully commented spectra of e.g. Sirius, Procyon and Aldebaran. Unfortunately, such papers are mostly available as "abstracts" only. The download prices for the full versions are usually pretty high.

Very useful is *Spectroweb* [59], to find on the home page of *Dr. Alex Lobel*, Royal Observatory of Belgium. It's an interactive internet platform providing highly resolved and almost completely commented profiles of some bright stars, belonging to the middle and late spectral classes *F*, *G*, *K*, *M*. It is very useful for the interpretation eg of highly resolved Echelle spectra. Due to the enormous line density it's, particularly for beginners, very difficult to make the link to the highly blended lines of their own, in most cases lowly resolved profiles. Here at last it becomes clear, why spectral atlases need to be created for specific degrees of resolution.

Recently the pocket guide "*A Spectroscopic Atlas of Bright Stars*" [9] was published. It's essentially a collection of non-normalized pseudo-continua of bright stars, showing a few, intense spectral lines. These have been recorded by Jack Martin under the London night sky on conventional (chemical) film with a slitless transmission grating spectrograph. This huge diversity of information explains why different sources have been used for the line identification. References for each and every line would not be feasible. However, for each spectral class, the mainly used sources are referenced. An alternative option would be to compare the spectra with synthetically generated profiles, based on models of stellar atmospheres. This allows for example the software "*Spectrum*" from *R.O. Gray*, which runs on Linux with a command-oriented interface. The installation for non Linux users, and also the operation are demanding. So this is probably a realistic option for very few amateurs only.

This atlas is primarily intended to be used as a tool for the line identification – as a supplement to "*Analysis and Interpretation of Astronomical Spectra*" [30]. In this document also detailed information on the classification system of the spectra and the Hertzsprung-Russell diagram (*HRD*) is included. Knowledge of these topics are presupposed here and therefore treated briefly only. From the beginning it was clear, that this atlas would not be reduced to an isolated collection of some labeled spectral tables. Therefore, each spectral class is presented with their main characteristics and typical features. The atlas will be continuously updated if new information or characteristic spectra are available. This intended future expansion was considered in the numbering system of the tables. After such updates, direct or "hot links" on the file will necessarily lead to the void. Therefore, I strongly recommend linking to the atlas only to: <http://www.ursusmajor.ch/astrospektroskopie/richard-walkers-page/index.html>

Many thanks to *Martin Huwiler*, *Urs Flükiger* and *Dr. Helen Wider* for proofing the German edition, and Urs again for kindly providing his homepage for downloading!

Richard Walker, CH 8911 Rifferswil

© [richiwalker@bluewin.ch](mailto:richiwalker@bluewin.ch)

About the author: Born in 1951, I began to show interest in astronomy when I was about 12 years old – after my grandparents took me to a public astronomical observatory in Zurich one fine night, which led to my first glance at Saturn. Later I started my own observations with one of the typical department store telescopes, followed by a self constructed 6 inch Newton reflector. For the last 10 years, my interest has increasingly focused on theories about astrophysics and stellar astronomy, somewhat later also on the indispensable key to these topics – the spectroscopy. My professional background is civil engineering. For a long time I worked for a Swiss engineering company, specialized in planning powerplants, dams and tunnels. For the last 12 years of my professional career I was involved in risk assessments and worldwide inspections for a Swiss Reinsurance Company – for so-called "large risks" like dams, powerplants, large construction sites, highrise buildings etc. For a short time now I have been enjoying my early retirement. My further interests are archaeoastronomy, windsurfing, paragliding, diving and mountain climbing – and sometimes I am also busy with my granddaughters.



## 2 Selection, Preparation and Presentation of the Spectra

### 2.1 Selection of Spectra

Main criteria for the selection of the spectra have been the documentation of the spectral characteristics and further the demonstration of certain effects e.g. due to the different luminosity classes. The consideration of bright "common knowledge stars" was of secondary importance. In principle, every spectral class, including some extraordinary star types, is presented at least with an "early" and a "late" representative spectrum to show the development of characteristic features in the profile. Commented in separate chapters are spectra of emission nebulae, composite spectra of extragalactic objects, reflection spectra of solar system bodies, absorption bands generated by the earth's atmosphere and some profiles of terrestrial light sources.

### 2.2 Recording and Resolution of the Spectra

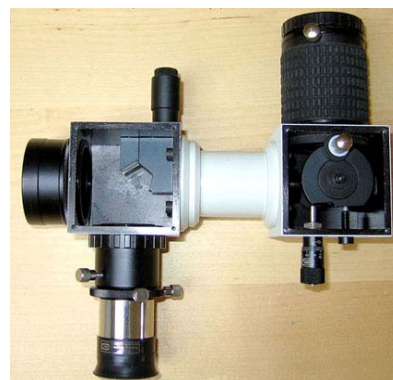
Most of the spectra have been recorded with the DADOS spectrograph [603], equipped with reflection gratings of 200- or 900 Lines/mm. Unless otherwise noted, the recording was made through the 8 inch Schmidt-Cassegrain *Celestron C8*, the  $25\mu\text{m}$  slit of the DADOS spectrograph. To display some highly resolved spectral details, the SQUES Echelle spectrograph was used [600], applying slit widths of about  $15\text{--}25\mu\text{m}$ . The recording was finally made with the monochrome camera Meade DSI III Pro or the cooled ATIK 314L+, both equipped with the same Sony chip ICX285AL. The spectra on the tables 5 (*WR133*), 70 and 84 have been recorded with Martin Huwiler through the CEDES 36 inch telescope of the *Mirasteilas Observatory* in Falera (see Appendix 34.4). Anyway applying longer exposure times, these objects are also within the reach of average amateur equipment!

The processing of the profiles with Vspec yields about following dispersion values [ $\text{\AA}/\text{pixel}$ ]: DADOS 200L  $\text{mm}^{-1}$ : 2.55, DADOS 900L  $\text{mm}^{-1}$ : 0.65, SQUES Echelle: 0.18.

Data of the Sony Chip ICX285AL: 1.4 Mega-pixel, 2/3" Monochrome CCD, Pixelsize  $6.45\mu\text{m} \times 6.45\mu\text{m}$  [606]. For longer exposure times a dark frame was subtracted, if necessary also the separately recorded light pollution (with Fitswork). The processing of a "flat-field" was omitted.

According to the Manual of the *DADOS Spectrograph* [603] the *R-value* (resolution), corresponds to  $R_{200L} = 647$  at  $6160 \text{ \AA}$  and  $R_{900L} = 3,000$  at  $5610 \text{ \AA}$  (slit width  $25 \mu\text{m}$ ). My own measurements in this wavelength domain, using several averaged *FWHM* values of Neon emissionlines, yielded *R-values* in the order of  $R_{200L} = 900$ , respectively  $R_{900L} = 4,000$ . Generally these resolutions have proven to be ideal for the presentation of the stellar spectral sequence. Therefore it's not surprising that Gray/Corbally [2] denote profiles with a resolution of  $\sim 3 \text{ \AA}$  as "*classification resolution spectra*". Even the professional astronomy uses spectrographs with lower resolutions for certain tasks. Substantially higher *R-values* would be soon comparable to reading a newspaper with the microscope.

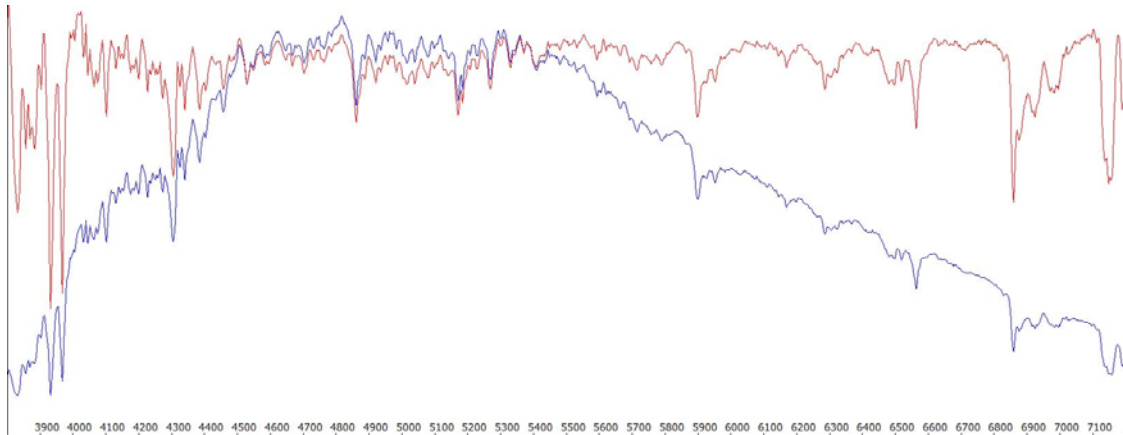
The *SQUES Echelle Spectrograph* [600], applied to present some higher resolved line details, reaches approximately  $R \approx 20,000$  at a slit width of  $\sim 15\mu\text{m}$ . The device can either be connected directly to the telescope or coupled via a fiber optics.



## 2.3 The Processing of the Spectra

The monochrome *fits* images have been processed with the standard procedure of *IRIS* [550]. In most cases, about 5–7 spectral profiles have been stacked, to achieve noise reduction. The generating and analyzing of the final profile was performed with *Vspec* [551]. The procedure is described in detail in the *IRIS* and *Vspec* manuals. For the software functions, applied to process the spectra in this atlas, a step by step description is available in [31] (German only).

With one exception (M31) in all broadband spectra (200L) the pseudo-continuum was removed. The profiles have been rectified – divided by the course of their own continuum. Thus, the intensity of the spectral lines becomes visually comparable over the entire range and further it results a flat (rectified), space-saving and easily readable profile [30]. The *relative depth or height* of a line *in relation* to the height of the according continuum level is crucial for the intensity comparison. The profile of a *pseudo-continuum* presents strong lines at the *blue or red end* of the spectrum optically as relatively *too weak* and vice versa, weak lines in the *middle part*, *-as too high*. But just this reasonable correction may confuse the beginners, if they try to find lines of their uncorrected pseudo-continuum in the flat, rectified atlas profile. The following graphic illustrates this effect with the superposition of the uncorrected pseudo-continuum (blue) and the atlas profile of the solar spectrum (red).



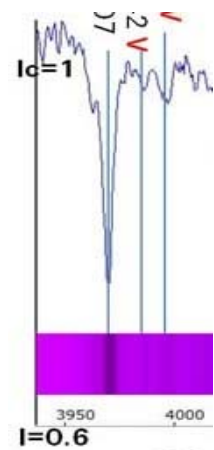
In rare cases with an increased noise level (by faint objects), the profile was sometimes smoothed, using filters such as the *Vspec* MMSE filter (minimum mean squared error). The goal of this process was here exclusively to improve the *readability* of the documented lines. A reduction of the telluric  $H_2O/O_2$  absorption in the yellow/red range of the spectral profile was omitted. Therefore the line documentation in this domain was restrained accordingly.

## 2.4 Calibration of the Wavelength

Most of the spectra have been calibrated *relatively*, based on *known lines* and *not absolutely* with the calibration lamp. This prevents that the profile, as a result of possible high radial velocities (Doppler Effect), is shifted on the wavelength axis. The focus here is the presentation of the spectral class and not the documentation of the individual star. Only for spectra of late spectral classes and extraordinary stars the calibration was carried out with the lamp. The *unit for the wavelength* is here generally *Angstrom* [Å]. These values are shown according to convention [2] with the prefix [ $\lambda$ ]. E.g.  $5000 \text{ Å}$  correspond to  $\lambda 5000$ .

## 2.5 Normalisation of the Intensity

An *absolute* flux calibration of the intensity profile would be very time consuming and is *not* necessary for the purpose of this atlas. But the continuum intensity of the rectified profiles was always normalised to unity, so that the medium continuum level yields about  $I_c = 1$ . An absorption line is usually saturated to the maximum if it reaches from the continuum level down to the wavelength axis  $I_c = 0$ . At the applied low to medium resolutions, in stellar spectra this can rarely, if at all, be seen. Hence, for space saving reasons, in most of the cases, not the entire range of saturation is presented. Instead the corresponding level on the wavelength axis is indicated with amounts mainly in a range of 0.3–0.6. In case of montages showing several spectra in one chart, the single profiles have been normalised to unity, based on the same continuum section, to enable a rough comparison of the line intensities.




## 2.6 Line Identification

For the sometimes complex identification process of spectral lines nearly all referenced information sources have been used. Some intensive, but in all the listed sources *not* documented lines, have been determined with *Vspec* (*Tools/Elements/line ident*). The values, implemented in this tool, are based on the *ILLSS Catalogue, Coluzzi 1993*. This procedure was applied very restrictively, i.e. in few cases with a clear profile, high line intensity and missing, plausible alternative elements in the immediate neighborhood. The labeling of such items is declared with a red "V".

The wavelengths of spectral lines are here usually labeled with an accuracy of two decimal places. These values were complemented from the *Vspec* tool, because in ancient sources (e.g. *BSA*), the indicated accuracy is only rounded to 1 Å. Labelings, lacking decimal places, here mostly indicate, that the line is a "blend", formed by several elements/ions with comparable intensity. Typically affected are metal absorption lines in spectra of the middle to late spectral classes. However, if in such cases the intensity of a blended line is clearly dominated by a certain element or ion it's also used to label the whole blend.

## 2.7 Presentation

All spectra are at least documented by a broadband profile (200L grating). In the presence of interesting lines or according information, higher resolved spectra are attached, recorded with the 900L grating or in some special cases even with the SQUES Echelle spectrograph [600]. The line profiles are supplemented on the wavelength axis by synthetically produced spectral strips (*Vspec*). Their color gradient shall chiefly serve as a rough visual reference for the wavelength domain.

Generally, only such details are commented, which are really recognizable in the profiles. Molecular absorption bands are marked with this icon: .

For densely labeled tables, I recommend to zoom it on the screen – even if inaccuracies of my drawings become relentlessly obvious this way. Due to this "online aspect", I avoided to separate the tables and the explanatory text in to different parts of the atlas. Due to numerous slim lines, hardcopies of this document require a *high printer resolution*.

### 3 Terms, Definitions and Abbreviations

#### 3.1 Parameters and Identification of the Stars

The information to the spectral and brightness classes comes largely from the *Bright Stars Catalogue* [505] or *James Kaler* [506], the distance information, if there available, from the *Karkoschka Atlas* [10]. The information to the "surface temperature" of the stars stems from a variety of sources, e.g. [506]. It is also referred to herein as *effective temperature*  $T_{eff}$ . It usually relates to the layer of the stellar *photosphere*, which is mainly responsible for the formation of the spectral lines as well as for the spectral distribution of the stellar radiation intensity (course of the continuum).

The *rotation velocity* of a star refers here to the part of the surface velocity  $v$ , which is projected to the direction of the earth –  $v \sin i$  – and can spectrographically be determined by using the Doppler principle (details and procedures see [30], [31]). These values are mainly derived from the *Bright Stars Catalogue* [505] or by *James Kaler* [506].

Brighter stars are referred in the atlas with the *proper name* and in the *Bayer system* with small Greek letters, combined with the abbreviated latin constellation name, e.g. *Sirius*  $\alpha$  *CMa* (see the corresponding lists in appendix 34.1). Fainter stars, lacking proper names, are identified with the *Bayer system*, or if necessary, with the *Flamsteed- or HD number* (Henry Draper Catalogue), e.g.  $\phi$  *Sagittarii*, 61 *Cygni*, HD 22649.

#### 3.2 Galactic Nebulae and Star Clusters

Such parameters are from NED [501], the *NASA/IPAC Extragalactic Database* or *Karkoschka* [10].

#### 3.3 Extragalactic Objects

Parameters of galaxies and Quasars, e.g. the  $Z$ -values of the redshift are from NED [501], the *NASA/IPAC Extragalactic Database*. From understandable reasons, information about the masses of such objects is missing there. Current estimates are still very uncertain, and accordingly the subject of debate – not least about the existence of dark matter. Therefore these values come from recent publications.

#### 3.4 "Early" and "Late" Spectral Types

At the beginning of the 20th Century, a hypothesis *wrongly* postulated that the spectral sequence from *O* to *M* represents the chronological development stages in the life of a star from very hot to cold. This misleading thesis has subsequently influenced the terminology, which is still in use today. Therefore the classes *O*, *B*, *A* are still called "early-", and *K*, *M* as "late" types. In this Atlas the classes *F* and *G* are referred as "middle".

This terminology is logically also applied *within* a class. So e.g. *M0* is called an "early" and *M8* a "late" M-type. In consequence e.g. *A2* is "earlier" than *A7*.

#### 3.5 Abbreviations and Units

*AU*: Astronomical unit, 149.6M km

*AGB*: Asymptotic Giant Branch (HRD)

*BSA*: Bonner Spektralatlas

*ESO*: European Southern Observatory

*ESL*: Energy saving lamp

*EW*: Equivalent width of a spectral line [ $\text{\AA}$ ] [30]

*FWHM*: Full width at half maximum height [ $\text{\AA}$ ] [30]

*HB*: Horizontal Branch (HRD)

*HD*: Henry Draper Catalogue

*HRD*: Hertzsprung-Russel Diagram

*HST*: Hubble Space Telescope      *LBV*: Luminous Blue Variable (sect. 10)

*MK*: Morgan, Keenan, Kellman: spectral classification system and spectral atlas

*PN*: Planetary Nebula

*PMS*: Pre-Main sequence Star. Young Protostar, not yet established on main sequence

*RGB*: Red Giant Branch (HRD)      *RSG*: Red Super Giant

*SB1*: SB 1 system. Spectroscopic binary stars with strongly different bright components.  
Only the spectrum of the brighter component can therefore be observed.

*SB2*: SB 2 system. Spectroscopic binary stars with two similar bright components.  
A *composite spectrum* of both components is therefore observed.

*SN*: Supernova

*VLT*: Very Large Telescope, ESO telescope group at Cerro Paranal, Chile

*WR*: Wolf-Rayet stars

*SuW*: German astronomical journal: *Sterne und Weltraum*

*K*: Kelvin temperature unit  $K \approx ^\circ\text{Celsius} + 273^\circ$

$\text{\AA}$ : unit of wavelength Angstrom.  $1 \text{\AA} = 10^{-10}\text{m}$


*ly*: light year  $1 \text{ ly} = 9,46 \times 10^{12} \text{ km}$       *parsec*:  $1 \text{ parsec} = 3.26 \text{ ly}$

Labeling of the Balmer Series:  $H\alpha$ ,  $H\beta$ ,  $H\gamma$ ,  $H\delta$ ,  $H\epsilon$ ,  $H8$ ,  $H9$ ,  $H10$  etc: Further lines after  $H\epsilon$  are labeled with the affected shell number, involved in the according electron transition.

*200L / 900L*: reflection grating of the DADOS spectrograph with 200 or 900 lines/mm.

*V*: Apparent magnitude of a celestial body

**V**: Spectral line identified with help of the *Vspec* Tool

: Molecular absorption band

$\odot$ : Comparison to the sun:  $M_\odot$ : solar mass,  $L_\odot$ : Luminosity of the sun

### 3.6 Identifying of the Elements and Ions

As usual in astrophysics, all the elements, except of *hydrogen* and *helium*, are called "*metals*" and identified in the astrophysical form - for details see [30].

The term "*ionisation stage*" refers here to the number of electrons, which an ionized atom has lost to the space (Si IV, Fe II, H II, etc.). The Roman numeral **I** is used for spectral lines associated with the *neutral* element, numeral **II** for those from the *first* ionization stage, – **III** for those from the *second*-, and so on. This must not be confused with the term "*Degree of ionisation*" in plasma physics. It defines for a gas mixture the *ratio* of atoms (of a certain element) that are ionised into charged particles, regarding the temperature, density and the required ionisation energy of the according element. This "*Degree*" is determined in astrophysics with the famous *Saha equation*.

So-called "Forbidden lines" are written within brackets, eg [O III].

### 3.7 The Metal Abundance Z (Metallicity)

Of great importance is the *iron to hydrogen ratio*  $N_{\text{Fe}}/N_{\text{H}}$ , considering the relative number of atoms  $N$  and not the mass! The metallicity  $Z$  in a stellar atmosphere, also called " $[Fe/H]$ ", is expressed as the decadic logarithm in relation to the sun:

$$Z = [Fe/H] = \log_{10} \frac{(N_{\text{Fe}}/N_{\text{H}})_{\text{star}}}{(N_{\text{Fe}}/N_{\text{H}})_{\text{Sun}}}$$

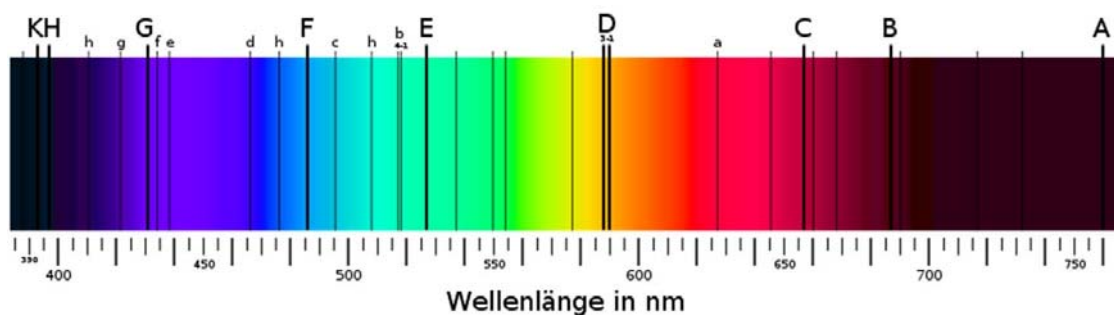
$Z$  values, smaller than found in the atmosphere of the Sun, are considered to be *metal poor* and carry a *negative sign* (–). The existing range reaches from approximately +0.5 to –5.4 (SuW 7/2010).

## 4 The Fraunhofer Lines

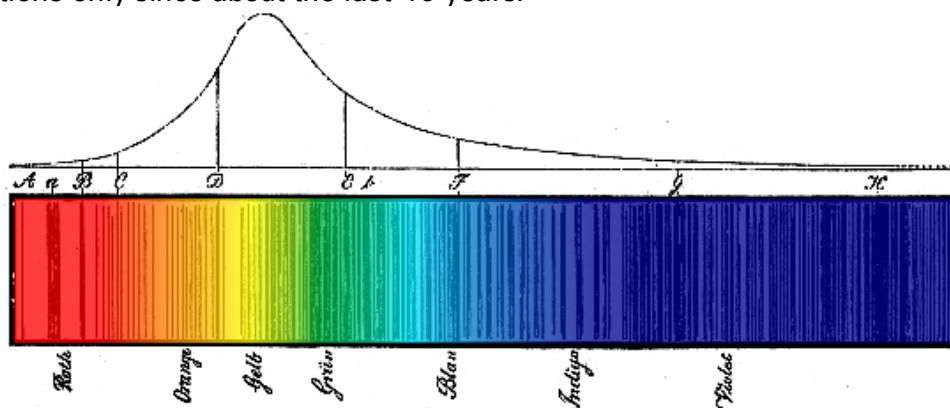
Fraunhofer has characterised the more prominent of the solar absorption lines with the letters *A* to *K* – this at a time when the physical relationships were still unknown. Later, additional lines were supplemented with small letters. These line designations are still in use even in current professional papers.

In this atlas some of the Fraunhofer lines are labeled in the solar spectrum and neighboring spectral classes. The table shows the listed Fraunhofer lines, rounded to 1 Å (Sources: Table: NASA, Graphic: Wikipedia).

Line ident.	Element	Wavelength [Å]
A – Band	O <sub>2</sub>	7594 - 7621
B – Band	O <sub>2</sub>	6867 - 6884
C	H (α)	6563
a – Band	O <sub>2</sub>	6276 - 6287
D 1, 2	Na	5896 & 5890
E	Fe	5270
b 1, 2, 3	Mg	5184/73/69
F	H (β)	4861
d	Fe	4668
e	Fe	4384
f	H (γ)	4340
G – Band	CH	4300 - 4310
g	Ca	4227
h	H (δ)	4102
H	Ca II	3968
K	Ca II	3934



Below: Original drawing of the solar spectrum by *Joseph Fraunhofer*. In contrast, the convention today requires the blue region of the spectrum to be left and vice versa the red to be right. Stunningly *visionary* appears to me the sketched, estimated intensity profile of the pseudo-continuum above the spectral strip! This type of plotted profiles, today of course normalised/calibrated and overprinted with the spectral lines, we can find again in publications only since about the last 40 years!





## 5 Overview and Characteristics of Stellar Spectral Classes

### 5.1 The Temperature Sequence

The rough, one-dimensional determination of the spectral classes *O*, *B*, *A*, *F*, *G*, *K*, *M*, is easy and even feasible for slightly advanced amateurs. This sequence of letters is further subdivided into decimal subclasses which follows directly the decreasing photospheric temperature, starting with the extremely hot O-type of several 10,000's K, and proceeding down to the cold *M*-class with about 2,400 – 3,500 K. The Sun is classified as *G2* with 5,800 K. Not treated here are the spectral types L and T which were first introduced in the 1990s as a low temperature extension of the M-Class, and include, among others, the so-called *Brown Dwarfs*. These cool objects are extremely faint and radiating primarily in the infrared range. Therefore, these classes remain unreachable by amateur means.

Spectral distinction criteria are prominent features such as lines in absorption or emission, which appear prominently in certain classes, and are entirely absent in others. The following charts show a montage with sample spectra of the entire class sequence of *O* – *M*. Here the original profiles of the stars are shown (200L grating), which are also used to present the individual spectral classes. This way, this resolution already enables the identification of the intense and therefore most documented spectral lines. Further also the influence of some elements, ions or molecules to the different spectral types becomes roughly visible.

Table 01 shows superposed the synthetically produced spectral strips – Table 02 shows the same but with the according intensity profiles.

What is already clearly noticeable here?

- In the upper third of the table (*B2*–*A5*), the strong lines of the H-Balmer series, i.e. *H $\alpha$* , *H $\beta$* , *H $\gamma$* , etc. They appear most pronounced in the class *A2* and are weakening from here towards earlier and later spectral classes.
- In the *lower quarter* of the table (*K5*–*M5*) the eye-catching shaded bands of molecular absorption spectra, mainly due to titanium oxide (*TiO*).
- Just underneath the half of the table some spectra (*F5*–*K0*), showing only few prominent features, but charged with a large number of fine metal lines. Striking features here are only the *Na I* double line (Fraunhofer D<sub>1,2</sub>) and in the “blue” part the impressive Fraunhofer lines of *Ca II* (K + H), gaining strength towards later spectral classes. *Fraunhofer H* at  $\lambda$  3968 starts around the *early F-class* to *overprint* the weakening *H $\epsilon$*  hydrogen line at  $\lambda$  3970. In addition, the H-Balmer series is further weakening towards later classes.
- Finally on the top of the table the extremely hot O-class with very few fine lines, mostly ionised helium (He II) and multiply ionized metals. The H-Balmer series appears here quite weak, as a result of the extremely high temperatures. The telluric *H<sub>2</sub>O* and *O<sub>2</sub>* absorption bands are reaching high intensities here, because the strongest radiation of the star takes place in the ultraviolet whereas the telluric absorption bands are located in the undisturbed domain near the infrared part of the spectrum. By contrast the maximum radiation of the *late* spectral classes takes place in the infrared part, enabling the stellar *TiO* absorption bands to overprint here the telluric lines.
- In the spectra of hot stars (~ classes from early A – O) the double line of *neutral* sodium *Na I* (Fraunhofer D<sub>1,2</sub>) must imperatively be of *interstellar* origin. Neutral sodium *Na I* has a very low ionisation energy of just 5.1 eV (see table in sect. 30) and can therefore exist only in the atmospheres of relatively cool stars. The wavelengths of the ionised *Na II* lie already in the ultraviolet range and are therefore not detectable by amateur equipment.

TABLE 01

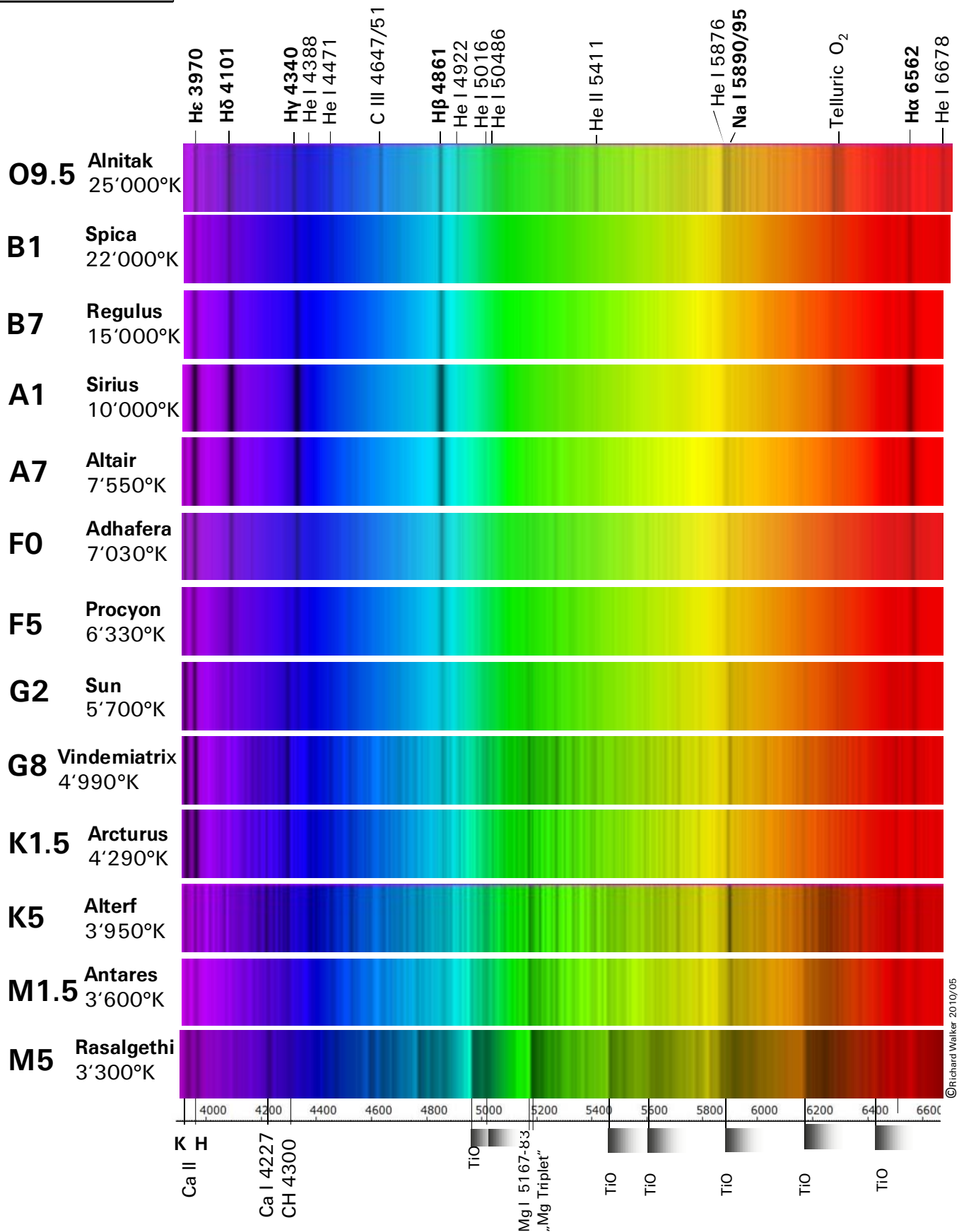
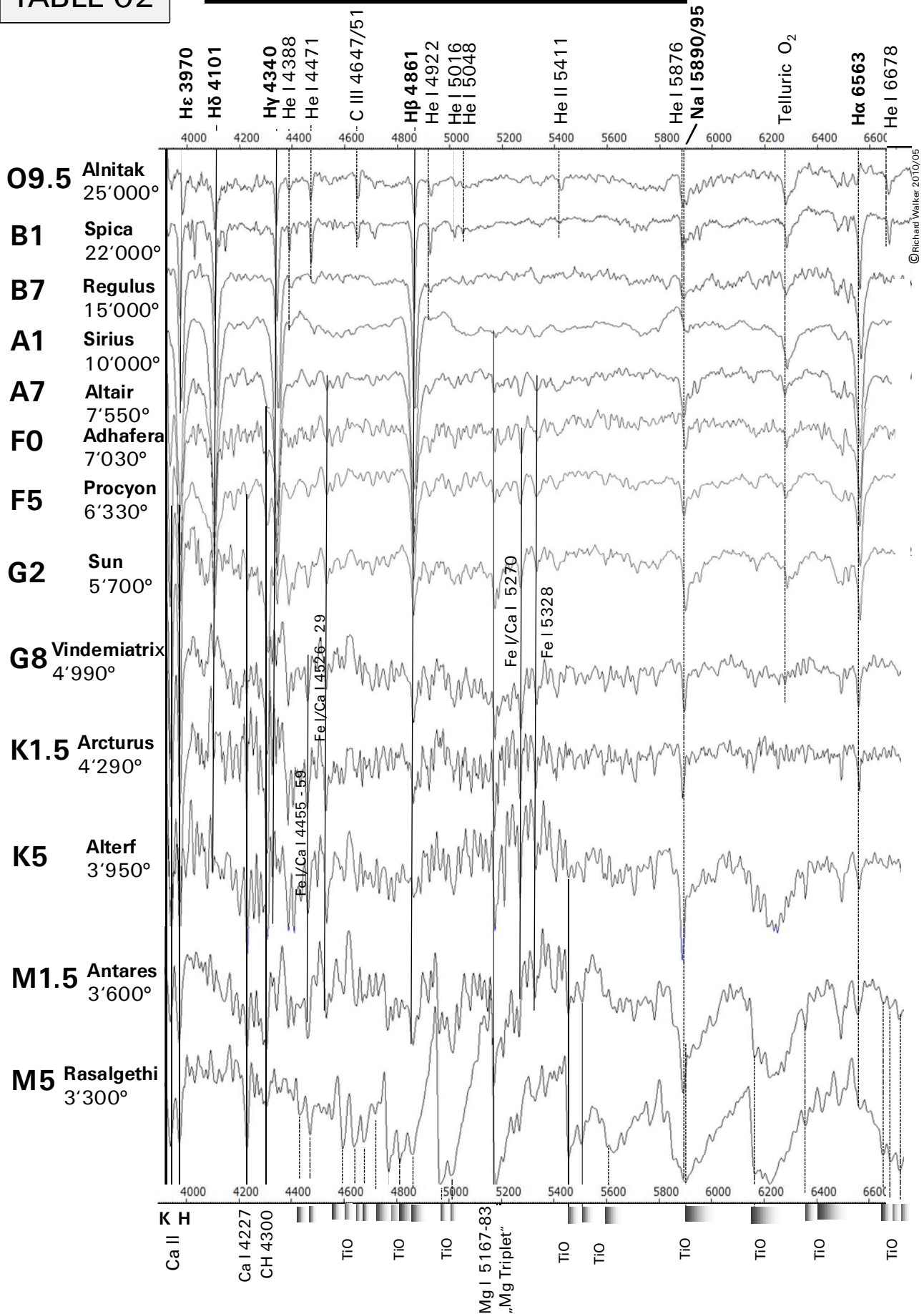
**Overview on the spectral classes**



TABLE 02

**Overview on the spectral classes**

## 5.2 The Luminosity Classes

Within the same spectral class, stars can show huge different absolute luminosities, due to different stages of their development. Since 1943, the spectral classes have therefore been expanded by an additional dimension in Roman numerals – the so called six *luminosity classes*. The Sun is classified with *G2V* since it's (fortunately) still located on the *Main Sequence* of the *HRD* with the luminosity class *V*.

Luminosity class	Star type
I	Luminous Super Giants
Ia-0, Ia, Iab, Ib	Subdivision of the Super Giants according to decreasing luminosity
II	Bright Giants
III	Normal Giants
IV	Sub Giants
V	Dwarfs or Main Sequence Stars
VI	Subdwarfs (rarely used, as specified by prefix)
VII	White Dwarfs (rarely used, as specified by prefix)

## 5.3 Suffixes, Prefixes, and Special Classes

With additional small letters, placed as prefix or suffix, extraordinary phenomena, such as a relative overabundance of a metal or the appearance of emission lines in the spectrum are specified. Some additives however are overdetermining, as e.g. *Giants*, unlike the *Subdwarfs* and *White Dwarfs*, are already specified by the luminosity class. Such labels are therefore hardly ever in use. Further with additional capital letters some special classes are specified.

Examples: Sirius A: *A1 Vm*, metal-rich *Main Sequence Star* (Dwarf) spectral class *A1*

Sirius B: *DA2*, White Dwarf or „Degenerate“ of spectral class *A2*

Omikron Andromedae: *B6 IIIep*,

Omikron Ceti (Mira): *M7 IIIe*

Kapteyn's star: *sd M1 V*, Subdwarf of spectral class *M1 V*

P Cygni: *B2 Ia pe*

Suffixes	
s	Sharp lines
b	Broad lines
c	Extraordinary sharp lines
comp	Composite spectrum
e	H- emission lines in B- and O- stars
f	He- and N- emission lines in O- Stars
em	Metallic emission lines
k	Interstellar absorptionlines
m	Strong metal lines
n / nn	Diffuse lines/ strongly diffuse lines eg due to high rotation speed
wk	Weak lines
p, pec	Peculiar spectrum
sh	Shell
v	Variation in spectrum
Fe, Mg...	Relatively high or low (–) abundance of the specified element

Prefixes	
d	Dwarf
sd	Subdwarf
g	Giant

Special Classes	
Q	Novae
P	Planetary Nebulae
D	Dwarf, +additional letter for <i>O</i> , <i>B</i> , <i>A</i> spectral class
W	Wolf-Rayet Star + additional letter for <i>C</i> -, <i>N</i> - or <i>O</i> - lines (see sect. 8)
S	Stars with zirconium oxide ab- sorption bands (see sect. 21)
C	Carbon stars (see sect. 22)
L, T,	Brown dwarfs
Y	Theoretical class for brown dwarfs < 600 K

Nowadays the special classes *P* (*Planetary Nebulae*) and *Q* (*Novae*) are barely in use!

The suffixes are not always applied consistently. We often see other versions. In the case of shell stars e.g. *pe*, or *shell* is in use.

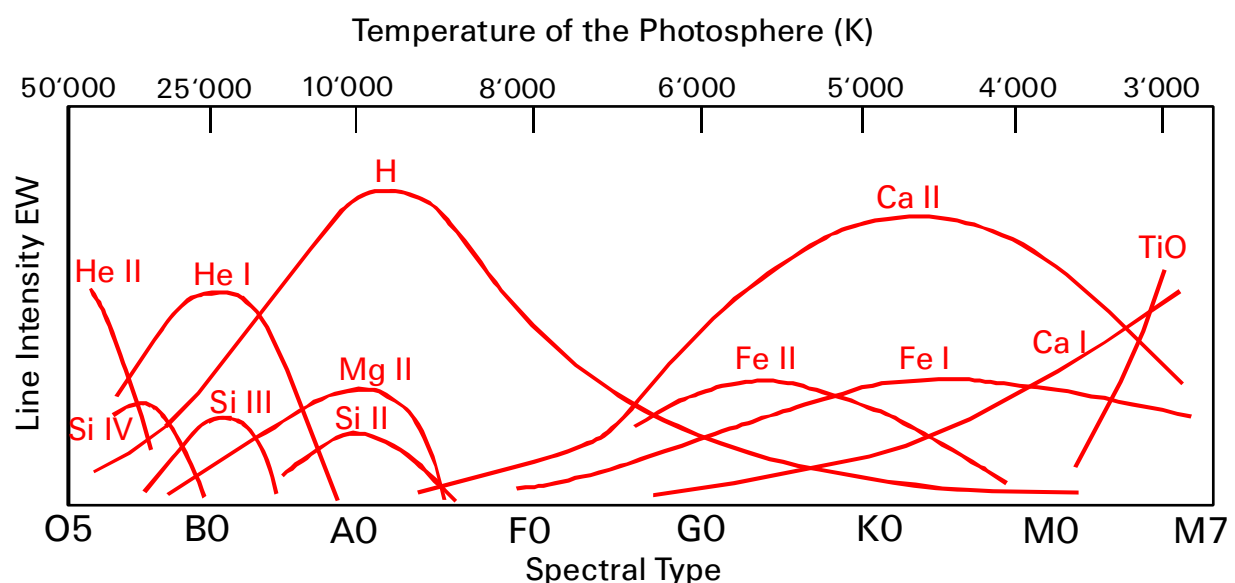
## 6 Appearance of Elements and Molecules in the Spectra

The spectrum of a star is primarily determined by the *temperature* of the photosphere. This temperature defines directly the spectral class in the *HRD*. From secondary importance is the density of the stellar atmosphere, primarily depending on the *luminosity class*, and further the specific *abundance* of certain metals. Another influential parameter is the *rotation speed* of the star, which, as a result of the Doppler Effect, broadens the spectral lines and reduces their intensity.

For the spectroscopy the following chart is from similar importance as the HRD. It shows roughly the appearance and the intensity (EW) of characteristic spectral lines, depending on the spectral class, respectively the "surface temperature" of a star. The latter determines for a certain element the *stage* and *degree* of ionisation. The theoretical foundations have been developed in 1925 by *Cecilia Payne-Gaposchkin* (1900-1979), according to *Otto Struve* "undoubtedly the most brilliant Ph.D. thesis ever written in astronomy". She was the first to apply the laws of atomic physics to the study of the temperature and density of stellar bodies and to conclude that hydrogen and helium, the two lightest elements, are also the two most common in the universe. She also disproved the old hypothesis that the chemical composition of the Sun is the same as of the earth. In addition to this scientific career, she was a mother of three children.



This chart is not only of great value for determining the spectral class, but also prevents by the line identification from large interpretation errors. Thus it becomes immediately clear that the *photosphere* of the Sun (spectral type G2V) is a few thousand degrees too cold to show helium *He I* in a normal (photospheric) solar spectrum. It also shows that the hydrogen lines of the Balmer series remain visible in varying degrees of intensity in nearly all spectral classes. Only in the late M-classes, they are increasingly overprinted by strong absorption bands of mainly *TiO*. The examples Sirius (A1V) and Regulus (B7V) show however that the influence of the *Fe* lines goes much further to the left, as indicated in this diagram.



## 7 Spectral Class O

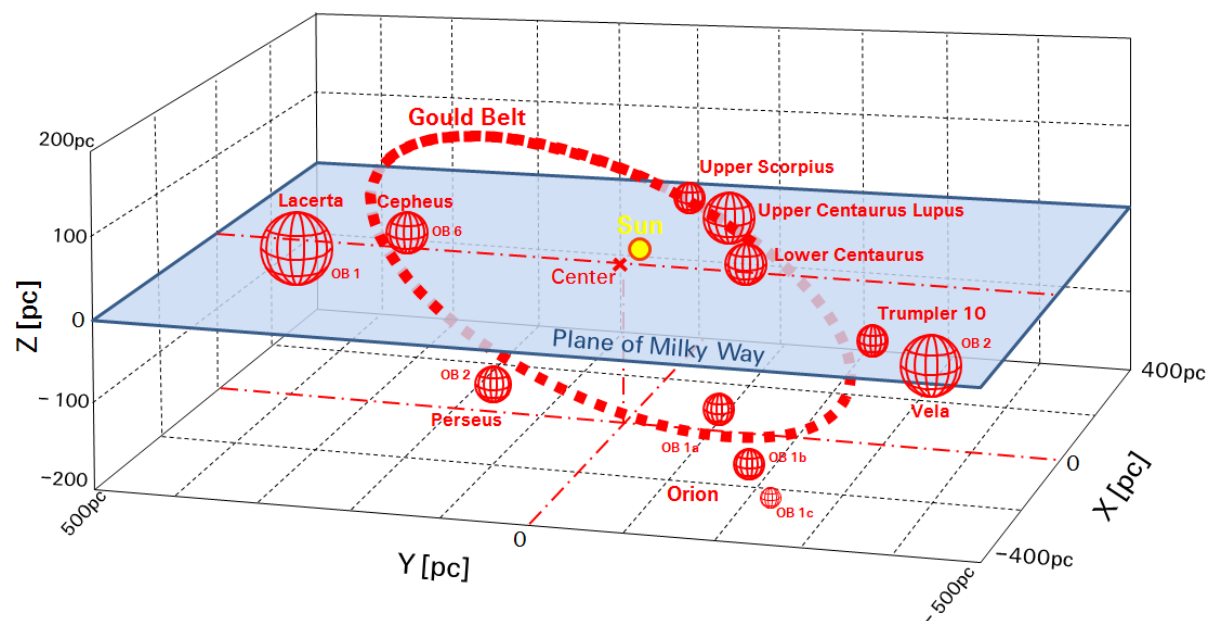
### 7.1 Overview

The O-Class comprises the hottest, most massive and shortest-living stars of the universe. At the end of their short lives, they will all end, due to their huge masses, in a *SN* explosion. Subsequently the only remains will consist of a very small, extremely compact *Neutron Star* or even a *Black Hole*. These blue shining, extreme types of stars are very rare. For the Milky Way only about 20,000 representatives of the O-type are estimated. As a result of their tremendous luminosity two bright representatives of this class are visible in a distance of some 1,000 ly in the constellation Orion: *Alnitak* ( $\zeta$  Ori) 1.8<sup>m</sup> and *Mintaka* 2.2<sup>m</sup> ( $\delta$  Ori). All these stars are *late O*-Types. Bright representatives of earlier *O*-types are only found in the southern sky, such as *Naos*, 2.3<sup>m</sup> ( $\zeta$  Puppis). The list on the right shows O- stars with an apparent magnitude V from about 5<sup>m</sup> upwards, which are spectroscopically accessible even for averagely equipped amateurs.

HD	Name	Spec. Class	V <sup>m</sup>
24912	Menkhib, $\xi$ Per	O7.5 III e	4.1
30614	$\alpha$ Cam	O9.5 Ia e	4.3
36486	Mintaka, $\delta$ Ori	O9.5 II+B0III	2.4
36861	Meissa, $\lambda$ Ori	O8 III	3.4
37022	$\theta^1$ Ori C	O6 pe v	5.1
37043	Nair al Saif, $\iota$ Ori	O9 III	2.8
37468	$\sigma$ Ori,	O9.5 V	3.8
37742	Alnitak, $\zeta$ Ori	O9.5 Ib	1.8
47839	15 Mon	O7 Ve	4.6
57060	29 CMa	O7	5.0
57061	30 CMa	O9 Ib	4.4
66811	Naos, $\zeta$ Pup	O4 I f(n) p	2.3
149757	$\zeta$ Oph	O9.5 V n	2.6
203064	68 Cyg	O7 III n(f)	5.0

Two other Orion stars  $\varepsilon$ - (*Alnilam*), and  $\kappa$ - (*Saiph*), are classified as *B0*, just scarcely missing the O-Class. Significantly fainter, but also much further distant, is the multiple *Trapezium star*  $\theta^1$  Ori. Its C-component  $\theta^1$  Ori C is a spectral type *O6pe V* and plays a key role for the ionisation of central parts in the Orion nebula M42.

This striking accumulation of extremely massive stars – known as so-called *OB Associations* – is not yet fully understood. Other slightly smaller clusters are located in the constellation *Scorpion*, *Perseus* and *Swan*. Together with other groups, they form the so-called "*Gould Belt*", (discovered by Benjamin Gould 1879) which is inclined some 20° to the galactic plane and has a diameter of about 2,000 ly. Our Sun is located somewhat off-center but still roughly within the ring plane [700] [700a].



## 7.2 Parameters of the Early to Late O-Class Stars

The following table shows the data *exclusively for the Main Sequence Stars* of the O-class compared to the Sun ( $\odot$ ) and according to [701] and other sources. Especially for the lower temperature limit, and even between reputable sources, are to find here clear differences in the published values (see also [30]).

Mass M/M $\odot$	Stay on <i>Main Sequence</i> [y]	Temperature photo- sphere [K]	Radius R/R $\odot$	Luminosity L/L $\odot$
60 – 20	1M – 10M	50,000 – 25,000	15 – 9	800,000 – 90,000

The O-class is open-ended. Currently, the top ranking is *O3* with a surface temperature of about 50,000 K [1]. The late *O9* class has been subdivided into decimal subclasses.

## 7.3 Spectral Characteristics of the O-Class

Spectra of the O-class are dominated by relatively low intense absorptions of singly or multiply ionised elements. The extremely high temperatures cause in addition to neutral helium He I, also lines of ionised helium (*He II*). In the early O-classes *He II* may also appear as *emission line*. In earlier times the appearance of He II in the spectrum was used as the main criterion for the definition of the O-class [2]. Today, in higher-resolved spectra, it can be detected already in the B0 class. Further appear also multiply ionised metals, as *C III*, *N III*, [*O III*] and *Si IV*. Due to the extreme temperatures, the *degree of ionisation* is here too high for the *H*-Balmer Series and their line intensity therefore only weak [30]. If *H*-lines appear in emission, the suffix "e" is added to the class letter (*Oe*). If *He* and/or *N* are seen in emission, the suffix "f" is added. "*Of*" stars seem to form the link between the O-Class and the Wolf-Rayet Stars, probably also to the LBV stars (see *sect. 8/10*).

The maximum intensity of the real continuum is in the UV range. The graph shows the theoretical continuum for a synthetic O9V standard star (Vspec *Tools/Library*).



## 7.4 General Remarks to the Classification of O-Stars

In no other spectral class, even among reputable databases, such different classifications can be found as in the O-class. Perhaps this can also be justified by the typically highly variable spectral features. This particularly affects the suffixes. But even by the decimal subclasses we see significant differences. Further in the early O-classes indications for the luminosity class are often missing.



## 7.5 Commented Spectra

**Table 1:** *Alnitak* (ζ Ori) and *Mintaka* (δ Ori)

This table shows two broadband spectra (200L grating) providing an overview on the spectral features of the late O-class.

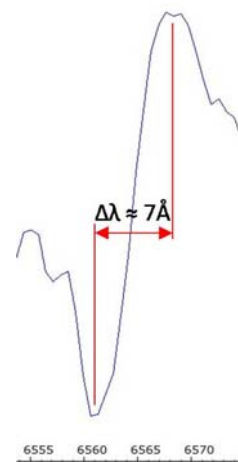
*Alnitak* (1200 ly) belongs to the spectral class *O9.5 Ib*, representing the lower level of the so-called *Super Giants*. The Wikipedia picture shows the size of the star compared to the Sun.



*Mintaka* (1200 ly) is classified slightly below with *O9.5 II (Bright Giant)*. Both stars are dominant components in multiple star systems and their surface temperature is about 25,000 K. In spite of the minimal class difference even in these low-resolution spectra, some differences can be observed (see comment below).

**Table 2:** Detailed spectrum of *Alnitak* (ζ Ori)

This table shows for *Alnitak* (1200 ly), a late O-Type star, two higher resolved spectra in the blue- and red wavelength domains (900L grating). Here, the main distinguishing feature between the two spectra of *Table 1* is clearly visible. The *Hα* line at λ 6562 forms here a textbook example of a *P-Cygni profile* with a red shifted emission- and a blue-shifted absorption line. This is always an indication for radially ejected matter by the star, a common process for some members of this extreme stellar class. The wavelength shift results here to about 7 Å. According to the Doppler law this yields a gas-expansion velocity  $v_r \approx 320 \text{ km/s}$ .



$$v_r = \frac{\Delta\lambda}{\lambda_0} \cdot c$$

$\lambda_0$  = Wavelength of the line,  $c = 300'000 \text{ km/s}$  (speed of light)

For further information, refer to *Table 13* for *P Cygni* or [30].

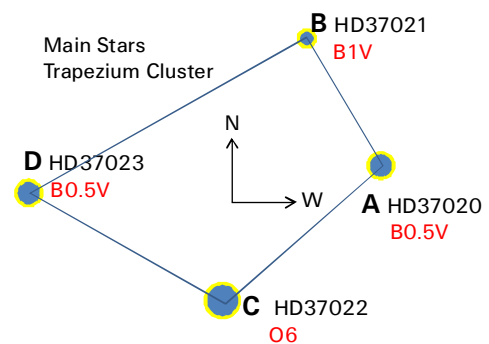
### Line identification:

The line identification is based amongst others on [1], [5], [51], [56], [57]

**Table 3:** *θ¹ Ori C*, HD37022 V=+5.13<sup>m</sup> and *68 Cygni* HD203064 V=+5.04<sup>m</sup>

This table shows two apparently faint representatives of the early to mid-O-class, which are easily accessible for the averagely equipped amateur (200L grating).

*θ¹ Ori C* (~1400 ly) is the brightest component of the famous Trapezium in M42. This stellar giant with its ever-changing spectral characteristics is being investigated intensively. The interferometric study [351] provides a good overview on these efforts. The data concerning the spectral type show a wide variation range eg *O4–O6 pV* [500], *O5–O7* [351] or *O6* [506]. Depending on the source the stellar mass is estimated to about 31-34 solar masses. Like nearly all other stars of the Trapezium, also *θ¹ Ori C* has at least one companion of spectral type *O9.5*, maybe also *B0*, with an orbital period of about 11 years. Recently, still another, very closely orbiting companion, with about one solar mass and a period of ~ 50 days is presumed. The data for the surface temperature vary approximately in the range of the proposed spectral types between 39'000K and 45'000K. The C- component generates some 80% of the total amount of photons [223], exciting the H II region of the Orion Nebula (see tables 80/80A)!



Most of the absorption lines appear here similar to those of Alnitak and Mintaka. H $\beta$  is striking, because the emission line, generated in the surrounding nebula, grows out of a broad, photospheric absorption dip of the star. The two [O III] emissions must be generated by the surrounding nebula, because the hot and dense stellar atmospheres can impossibly generate "forbidden" lines. The H $\alpha$  emission is produced by the recombination of the encircling H II region, totally veiling here the stellar line (sect. 24).

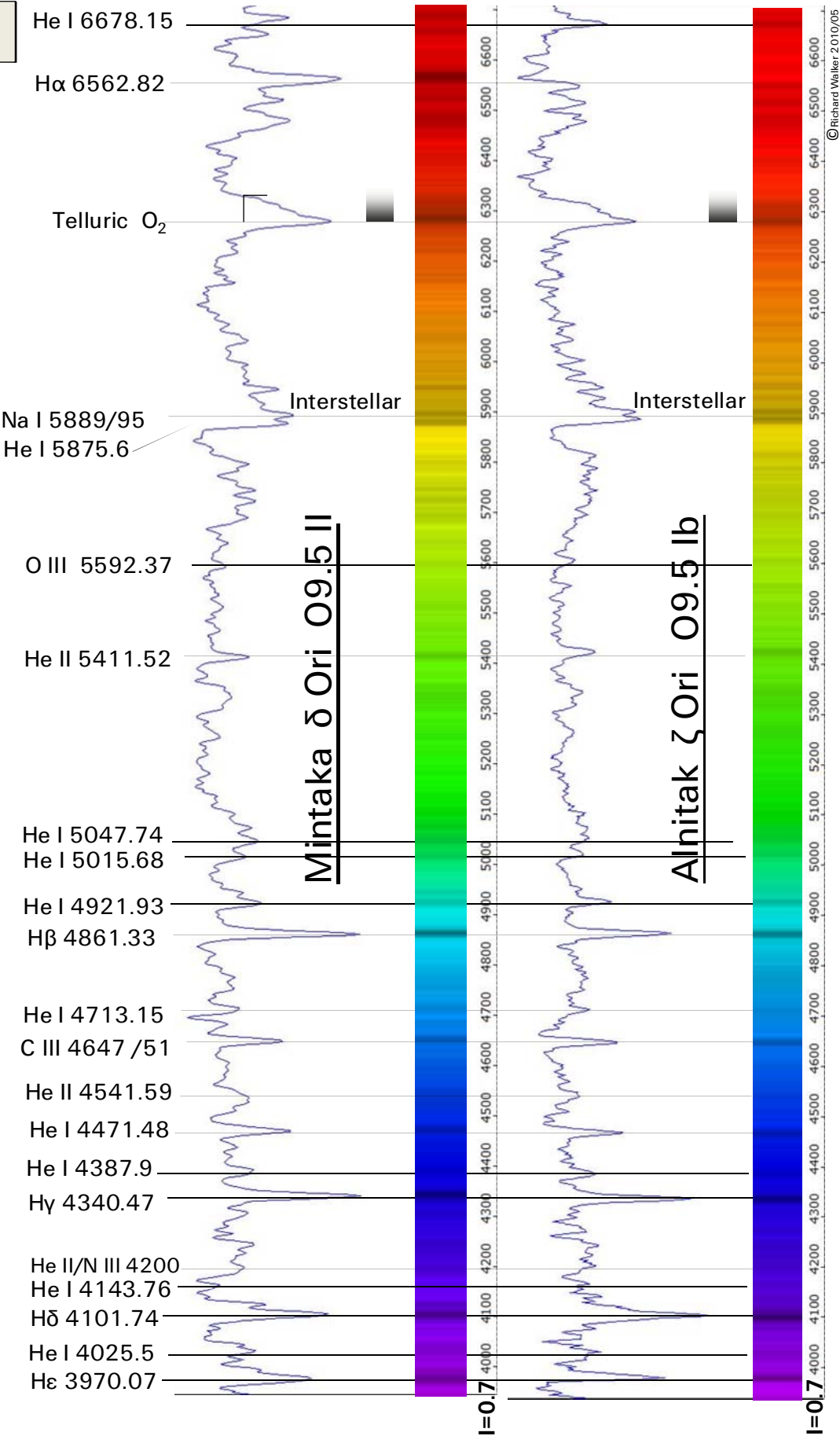
It is strongly recommended to record  $\theta^1 Ori C$  with autoguiding to ensure the tracking on the correct trapezium star. The orientation of the slit axis should be optimised accordingly. The sketch above should facilitate the orientation. The exposure time for the profile in Table 3 is 340 seconds.

68 Cygni (~2300 ly) is surrounded by the weakly developed H II region *Sharpless 119*. It is the brightest of total 6 ionising stars. Most of the sources classify this star with 30 solar masses and a surface temperature of about 35'000K as *O7 III n (f)* [505]. "Of" stars are considered as a transitional phase on the way to Wolf Rayet stars and show eg He and N lines in emission - a clear indication that material is repelled. As classification lines for the Of-type the blends N III  $\lambda\lambda$  4634–40–42 and He II  $\lambda$  4686 are used [2]. Since only N III appears here in emission, *68 Cygni* is considered as a "mild" Of star, and the suffix "f" is therefore set in parentheses (f) [2]. In the intensive Of -phase both features, N III and He II, show up in emission. Compared to the O9-types the C IV lines ( $\lambda\lambda$  5801/5812) are quite intensive here. This indicates that *68 Cygni*, as well as  $\theta^1 Ori C$ , are stars of the rather *early* O-class. C IV requires with 47.9 eV almost twice the ionisation energy as He II.

According to [505] 68 Cygni passed about 1959-70 a phase with H $\alpha$  in emission. Because of the high proper motion, it is regarded as so called "runaway star" and originates probably from the OB2 region of Cepheus. As a possible scenario, the acceleration by the supernova explosion of a companion star is discussed. Perhaps the remaining black hole with ~3  $M_{\odot}$  still orbits around the star very closely. Observed fluctuations of equivalent widths at certain spectral lines indicate a possible orbital period of about 5 days. The prior information is mainly based on [352].



TABLE 1



© Richard Walter 2010/05

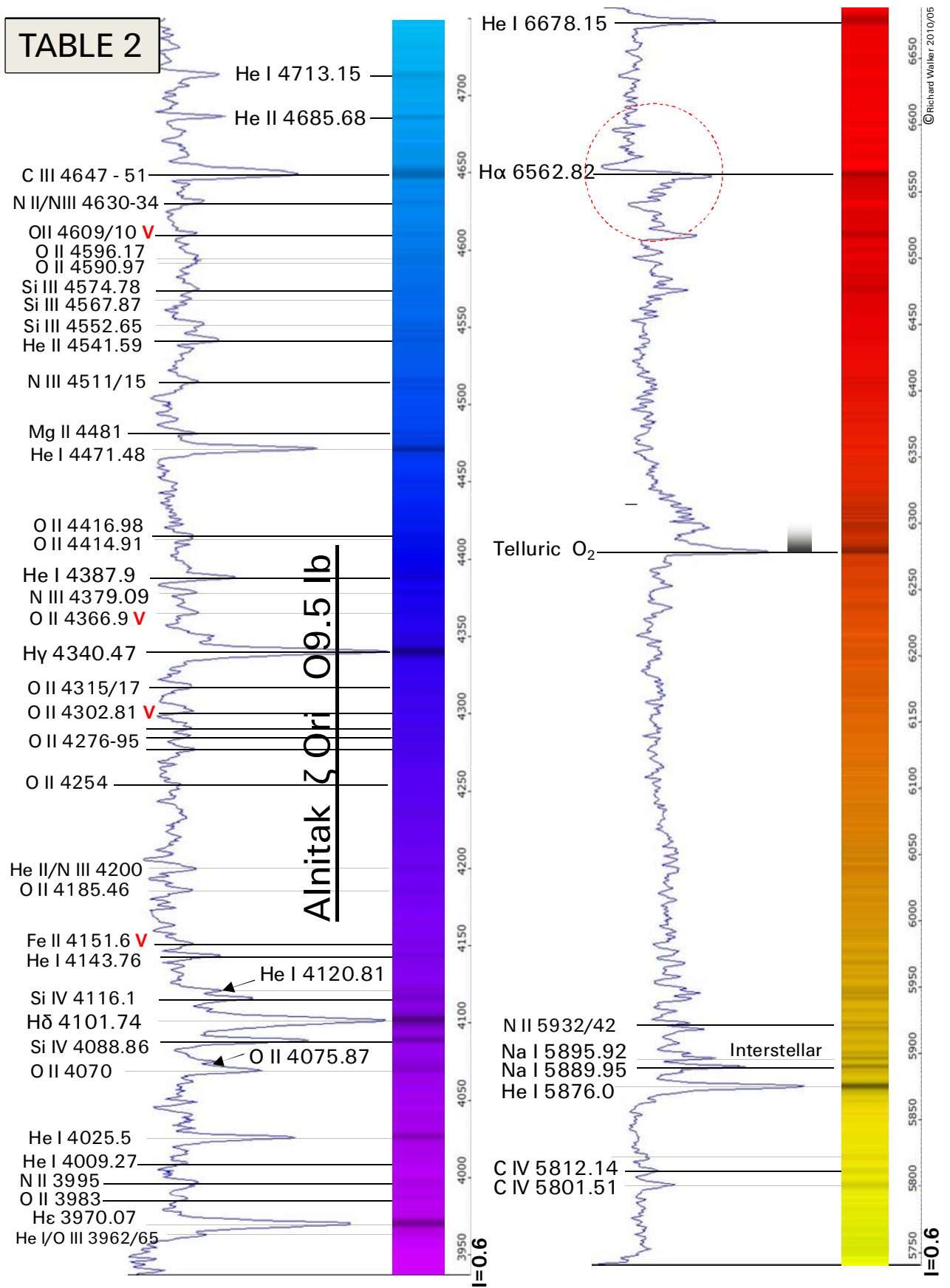
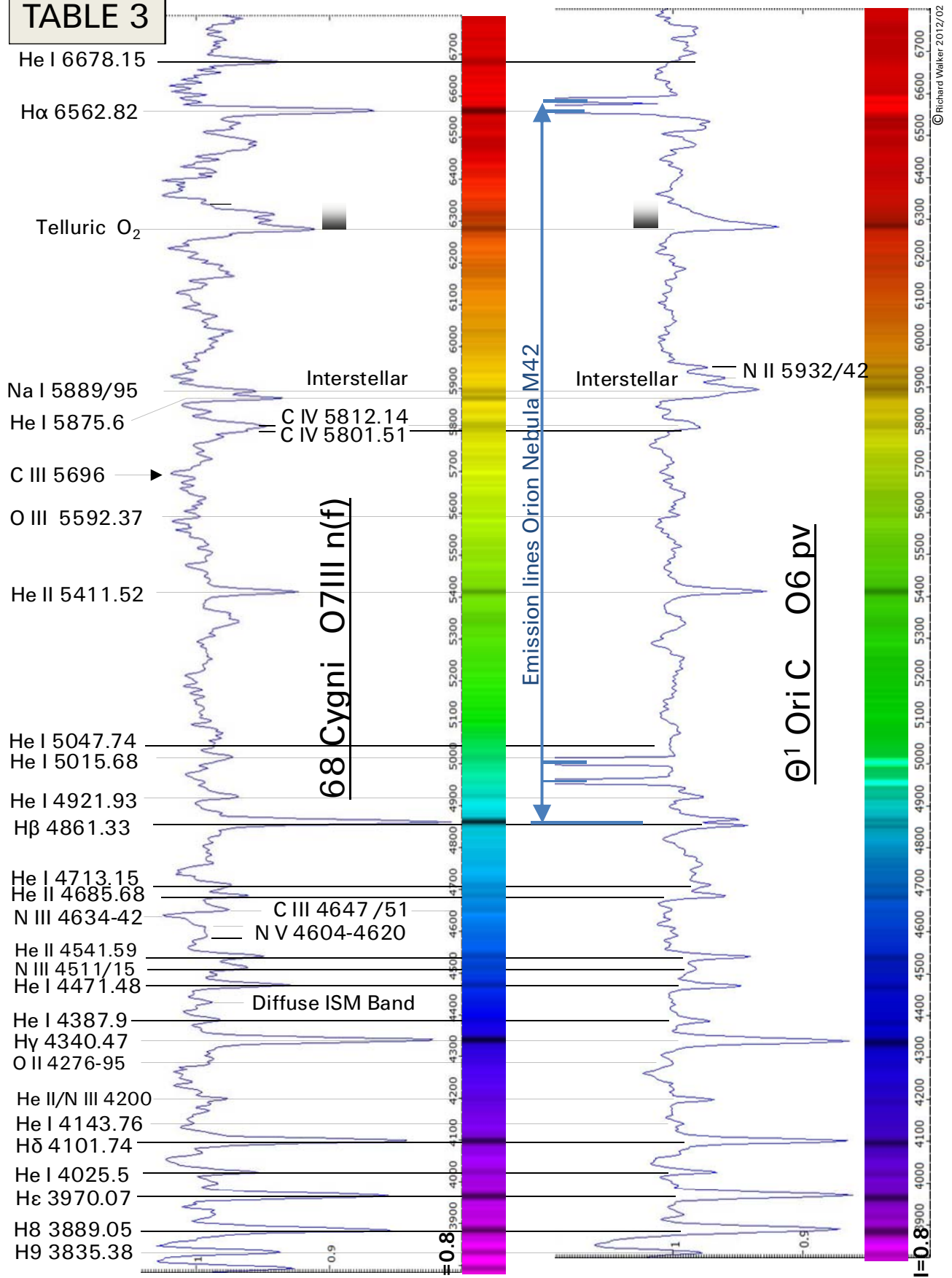


TABLE 3



## 8 Wolf Rayet Stars

The French astronomers *Charles Wolf* and *Georges Rayet* discovered in 1867 very rare stars, whose spectra are standing out by massively broadened, intense *helium emission lines* and the *almost complete absence of hydrogen*. These objects are grouped in an *extra class*, marking the *final stage* of massive O-type stars approx.  $\geq 20 M_{\odot}$ . Below this mass limit of  $< 20 M_{\odot}$ , the SN explosion takes place directly at the end of the Red Giant stage, without to pass a subsequent WR phase.

At the begin of the WR phase, the star blasts away its entire outer hydrogen shell by a huge stellar wind with velocities of up to 2000 km/s (see Table 86). On the further path to the SN of the category 1b or 1c, similar to the peeling of an onion, also the layers of the stellar core are removed from the top down. This causes an annual mass loss rate of about  $10^{-5}$  to  $10^{-4} M_{\odot}$  [236]. On the surface of the star the extremely hot, former nuclear H and He fusion zones become exposed where, in addition to helium, the metals C, N, and O have been formed. The total duration of the entire WR stage is estimated to be about 200,000 years [238].

Therefore, the spectrum differs now completely from the previous O-class stage. The broad lines of ionised helium *He II* appear now together with the emissions of *highly ionised* C, N, or O – depending on the “currently” exposed surface layer of the former H and He fusion zones [236]. These metals determine the classification of the *WR* stars and their high stage of ionisation is an indicator of the involved, extremely high temperatures and the corresponding excitation energies (*see table sect. 30*).

WN: WR stars with nitrogene emissions (WNL with H-lines, WNE without H-lines [236])

WC: WR with carbon emissions (by partial helium fusion [236])

WO: WR with oxygene emissions (by complete helium fusion, very rare[236]).

Similar to the other spectral types also the WR stars are subdivided into decimal subclasses. The classification system according to Smith (1968) was later improved by van der Hucht, Crowther et al. It is based on comparison of individual line intensities, following the principle “The earlier the subclass, the higher the stage of ionisation”. A current version of this system can be found in [2].

One of the possible, mass-dependent, evolutionary sequence on the way to a supernova is: O  $\rightarrow$  Of  $\rightarrow$  LBV/RSG  $\rightarrow$  WN  $\rightarrow$  WC  $\rightarrow$  WO  $\rightarrow$  SN [241]. In contrast to the “semantic logic” of the subclass system the evolution of the individual WR subclasses runs here from “late” to “early”. Thereby the temperature, as well as the associated ionisation stage of the metals, is rising.

In the early stages of the WR evolution, the H-Balmer series of the not yet completely repelled hydrogen shell, can still be detected within blends at the “late” WN (WNL) types [2] [236].

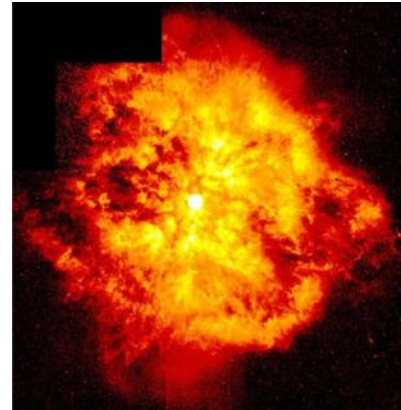
In the later stages of WR-development, the “early” WC subclasses show, though still weakly, the highly ionised oxygen O VI doublet at  $\lambda\lambda$  3811/3834.

In the final WO phase, this O VI doublet appears strongly developed, together with other, highly ionised oxygen emissions (Table 6). Pure WO stars are extremely rare and the corresponding final phase probably very short – in addition associated with a significant X-ray radiation.

Also the central stars of Planetary Nebulae PN repel their shells (sect. 24.7). In their final stage, they show similar spectra, which are also classified as *WR* types (*WRPN*). However, their absolute magnitude and mass is significantly lower and they finally end up, much less spectacular, as *White Dwarfs* (see sect. 24.7).

The HST image (NASA) shows the star WR 124 located in the constellation *Arrow*. With the spectral class WN8 it is still at the very beginning of the WR stage. Just about 10,000 years ago, he started to repel his hydrogen envelope with a stellar wind of about 2000 km/s.

In the southern sky, some 1100 ly distant,  $\gamma$  *Velorum*, alias WR 11, with the spectral class WC8, is much more advanced than WR 124 and with an apparent brightness of 1.74<sup>m</sup> the by far brightest representative of all WR stars. On the northern hemisphere mainly in the constellation *Cygnus*, a concentration of such extreme stars can be found, which are members of the *Cygnus OB associations*. Here 23 WR stars are located – 14 are classified as WN-type, 8 as WC-, and just one as WO- type (WR 142). The two brightest ones reach an apparent magnitude in the range of 6–7<sup>m</sup> and are therefore well accessible with a slit spectrograph, even for moderately sized amateur telescopes. By chance they just represent the two main types WN and WC.



During the final *SN* explosion the remains of such bizarre “stellar monsters” with originally about 20–80 solar masses and surface temperatures of 30,000–100,000 K, will most probably implode in to a *Black Hole*. This event will be accompanied by a high-energy gamma-ray burst, emitted in both directions of the stellar rotation axis.

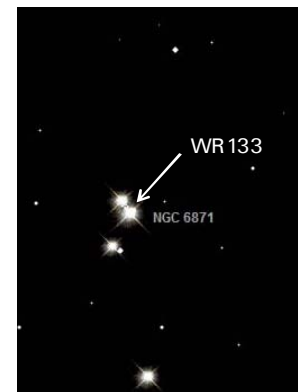
Table 5: *Wolf-Rayet Stars WR 133 and WR 140*

The montage of two overview spectra (200L grating) presents the subtypes WN and WC of *Wolf-Rayet Stars*.

WR 133 spectral class WN4: HD 190918

J2000 RA: 20h 05' 57.3" Dec: +35° 47' 18.2" V=+6.78<sup>m</sup>

Some 6,500 ly distant, the very well explored *WR 133* in the constellation *Cygnus* hides itself inconspicuously within the central members of the open cluster NGC 6871. Despite to the use of “Goto Telescopes” here is a certain risk to record the wrong star – what is instantly recognisable in the spectrum. In particular, the bright *He II* “emission knots” can hardly be overlooked.



*WR 133* forms a spectroscopic binary (SB2) with an *O9 I Supergiant* in an orbital period of about 112 days. Therefore, we see a composite spectrum, which is however clearly dominated by the emission lines of the *WR star* (labeled *red* in *Table 5*). Striking here are the numerous lines of differently high ionised *nitrogen*, responsible for the classification WN. However one faint carbon emission shows up here, *C IV* at  $\lambda$  5801-12 [230]. This spectral feature is significantly weaker, compared to the WC type *WR 140* (see below).

The very close-by *O9* companion star generates here some absorptions of helium- and some *H*-Balmer lines (labeled *black* in *Table 5*), as well as the sodium double line, which is of interstellar origin [344]. The continuum is here, in comparison to *WR 140* presented below, relatively intense. The strong *He II* emission at  $\lambda$  6560 poses a *considerable risk* to be misinterpreted as *H $\alpha$*  line at  $\lambda$  6562! The most intense line here is clearly the *He II* at  $\lambda$  4686. The expansion velocity of the stellar wind can be estimated from the *FWHM* values

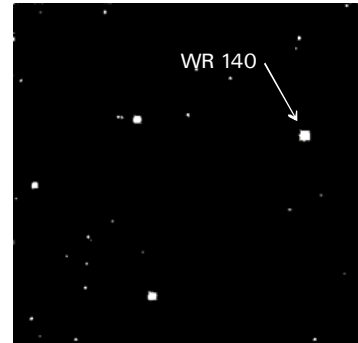


of the two intense *He II* emissions. If these figures are put in to the Doppler formula and the results are finally corrected by the *instrumental broadening* [30], velocities of  $v_r \approx 1800 \text{ km/s}$  at  $\lambda 4686$  and  $v_r \approx 1500 \text{ km/s}$  at  $\lambda 6560$  are resulting. In the order of magnitude, these figures agree quite well with literature values ( $v_r < 2000 \text{ km/s}$ ). The spectrum was recorded with the 90 cm (36 inch) CEDES Cassegrain Telescope in Falera – exposure: 4x30 sec. The line identification is based amongst others on [230] [231] [232] [233] [344].

WR 140 spectral class WC7: HD 193793

J2000 RA: 20h 20' 28" Dec: +43° 51' 16.3" V=+6.93<sup>m</sup>

Also located in the constellation Cygnus and some 4,700 ly distant, *WR140* is a member of a spectroscopic binary (SB2) with an *O4 V Main Sequence Star* in a *highly excentric orbit* with a period of some 2,900 days. During the periastron passages this binary system usually attracts the worldwide attention of professional- and amateur astronomers, mainly observing effects, caused by the colliding stellar winds (*colliding wind binary*) [346] [347]. The map shows the star pattern in the immediate vicinity of the WR star. It's relatively isolated and therefore much easier to find than WR 133.



This composite spectrum is clearly dominated by the *WR star*. One of the reasons is presumably the time of the last periastron passage of January 2009. At the time of recording it dated already back more than 1½ years. In contrast to the very close binary system *WR 133*, absorption lines are barely visible here, besides the well known telluric lines and the double line of sodium, which could also be of interstellar origin. The numerous different lines of highly ionised carbon show clearly, that *WR 140*, with the classification *WC7*, is a representative of the *carbon type* among the *WR stars*. Nitrogen is not detectable. The intense *C III/C IV* emission at  $\lambda 4650$  is blended with the *He II* line at  $\lambda 4686$ . This feature is even the most striking of the spectrum, followed by the *C IV* emission line at  $\lambda 5801-12$  and the *C III* "hump" at  $\lambda 5696$ . The *He II* emission at  $\lambda 6560$  is relatively weak. The spectrum was recorded with the *Celestron C8* – exposure: 10x90 sec. The line identification is based amongst others on [230] [231] [232] [233] [344].

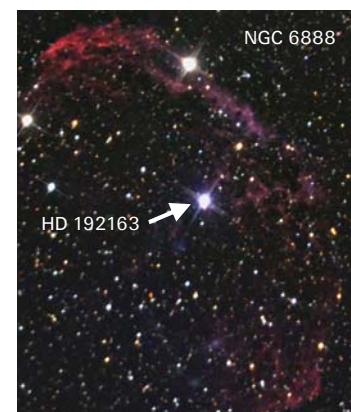
Table 6: *Wolf-Rayet Stars WR 136 and WR 142*

The montage of the two overview spectra (200L grating) allows for the WR sequence the direct comparison of the early stage *WN* with the final stage *WO*, shortly before the SN explosion.

WR 136 spectral class WN6: HD192163

J2000 RA: 20h 12' 07" Dec: +38° 21' 18" V=+7.65<sup>m</sup>

In a distance of about 4,700 light years, located in the constellation Cygnus, WR 136 belongs to the Cygnus OB1 association. With  $T_{eff} \approx 55'000 \text{ K}$  [239], it forms the origin and ionising source of the elliptical shaped *Crescent emission nebula NGC 6888* (see Table 86). Within about 30,000 years this repelled hydrogen shell has expanded to  $\sim 16 \times 25 \text{ ly}$  [237] and is still visible. Therefore WR 136 is at the beginning of the WR sequence, whose duration is estimated to be about 500,000 years [237]. The velocity of the stellar wind is  $v_r \approx 1700 \text{ km/s}$  [232]. It generates the visible shock wave (NGC 6888) by collision with



interstellar matter, which still propagates with about 75 km/s [240]. WR 136 has no proven companion star (image: Wikipedia, M. Schopfer).

The spectrum is dominated by numerous striking He II emissions. The more intense of them belong to the so-called *Pickering Series*, which was discovered in 1896 by E. Pickering (see table). To shorter wavelengths it shows a similar decrement, ie intensity loss, like the Balmer Series of hydrogen (sect. 24.2). Further some of these He II emissions are located very close to the H-Balmer lines. If hydrogen is present in the spectrum, this becomes evident in the blends with the He II lines, whose peaks then clearly exceed the decrement line of the Pickering Series [2]. At WR 136, hydrogen is theoretically detectable at  $\lambda \leq H\beta$  [239]. The spectrum was recorded with Celestron C8/Atik 314L+/6x120 seconds.

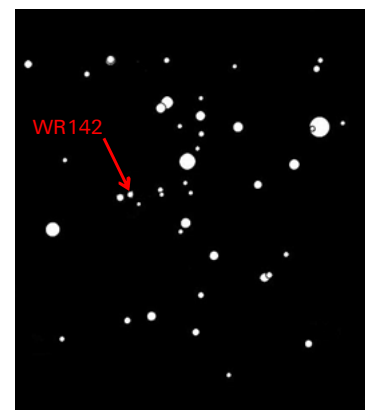
Balmer H I	Pickering He II
6563	6560
–	5412
4861	4859
–	4542
4340	4339
–	4200
4102	4100

The line identification is here based on [230] [231] [232] [233] [237] [238] [239].

WR 142 spectral class WO2: Sand 5 (Sanduleak 1971) ST3 (Stephenson 1966)

J2000 RA: 20h 21' 44.35" Dec: +37° 22' 31" V=+13.82<sup>m</sup> [232] +13.4<sup>m</sup> [241]

A complete contrast to WR 136 forms the some 4,000 ly distant WR 142 in the constellation Cygnus, inconspicuously embedded in the open star cluster Berkeley 87. It is currently one of four in the Milky Way detected, oxygen types of the WR stage – in addition to WR 142 and a recently discovered specimen in the Scutum arm of the Milky Way [243], also WR 102 (V = 15.8<sup>m</sup>). All are close to the end as a *SN*. In the Magellanic Clouds three other WO stars have been detected. Like most of the WO class stars also WR 142 is an active X-ray source [241].



With V= +13.82<sup>m</sup> WR 142 is by far the brightest WO- representative and for sure the only one, which can be recorded with a DADOS/C8 setup.

Five of these WO stars are numbered with *Sand 1... 5*, named after Nicholas Sanduleak, who was looking with objective prism for these “exotic stars” in the 70s of the 20th century. These extremely rare and interesting objects are well researched and documented.

Compared to WR 136, WR 142 shows mainly extremely broad and highly ionised emissions of oxygen. These obviously exorbitant amounts of energy, generated in the final stage of a WO star, can be estimated with help of the detected ionisation stages. The required energy to ionise oxygen to the stage O VI is 113.9 eV (table sect. 30). This is as much as 4.6-fold to generate He II and 8.3-fold to ionise hydrogen H II. In addition to the extremely high temperatures, this is also caused due to the photoionisation by X-ray sources [235].

The Doppler analysis of the line widths obtained here stellar wind speeds of about 3,600 up to >5000 km/s, after all ~1.6% of the speed of light! Suitable for own measurements is the relatively isolated, unblended O VI line at  $\lambda 5290$ .

The spectrum was recorded with Celestron C8/Atik 314L+/4x1300 seconds, 2x2 binned, chiptemperature–10°C. The line identification is here based on [242] [243] [2]. Further the light pollution had to be subtracted.

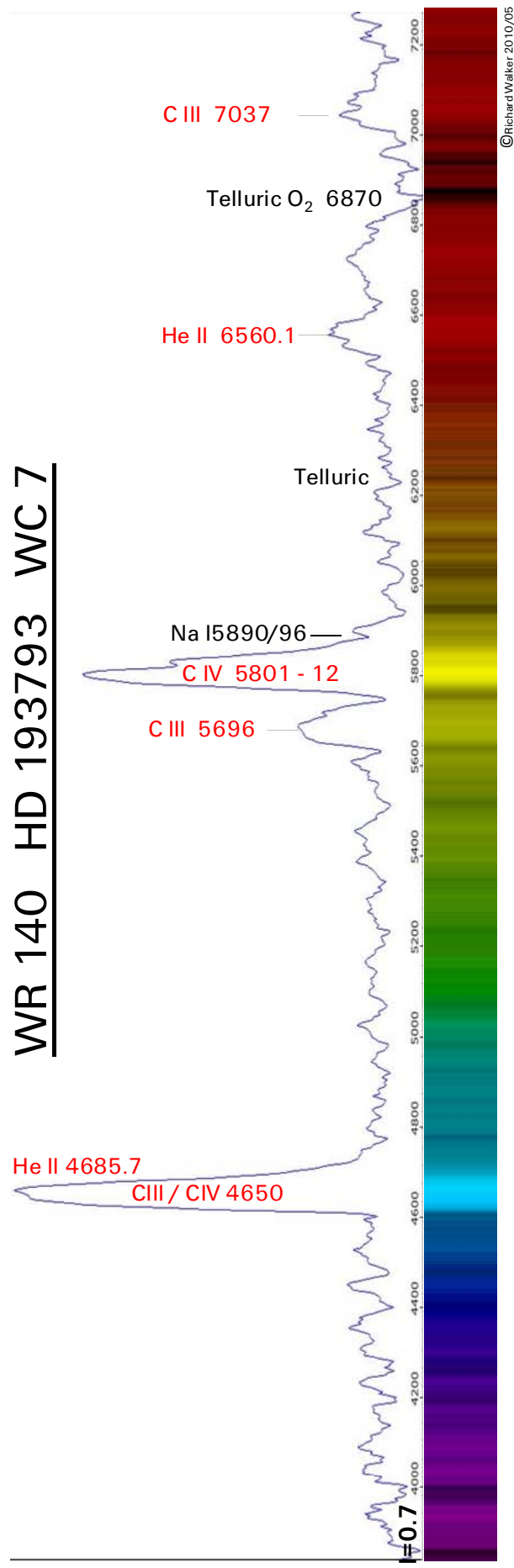
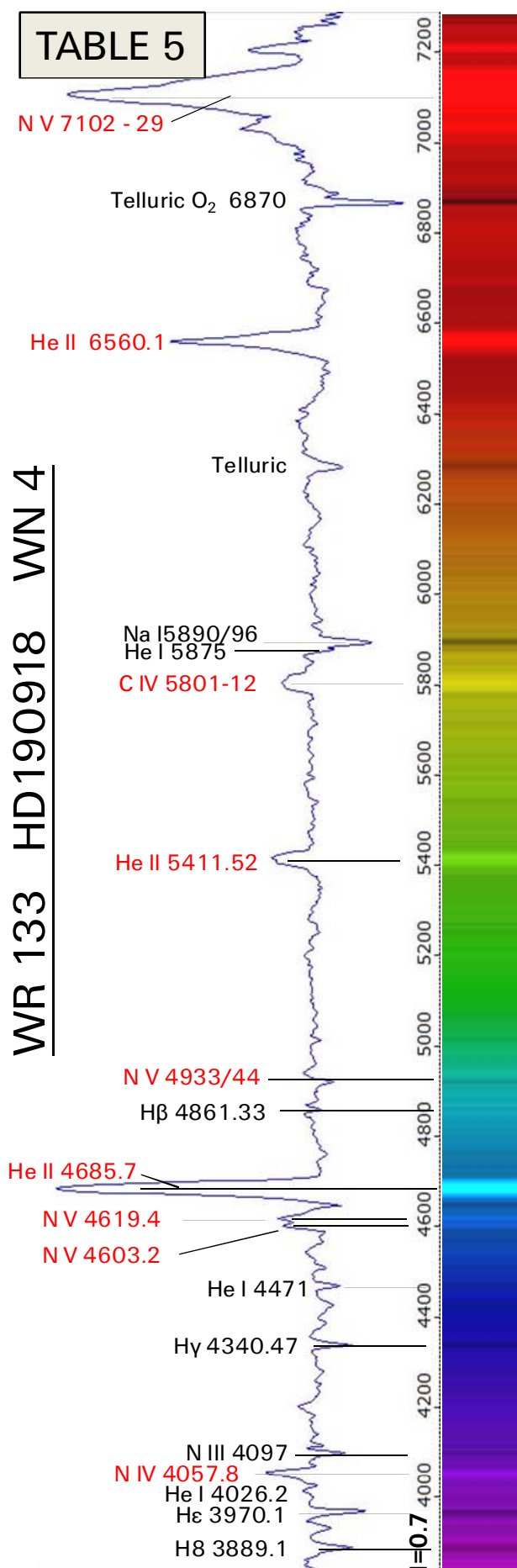
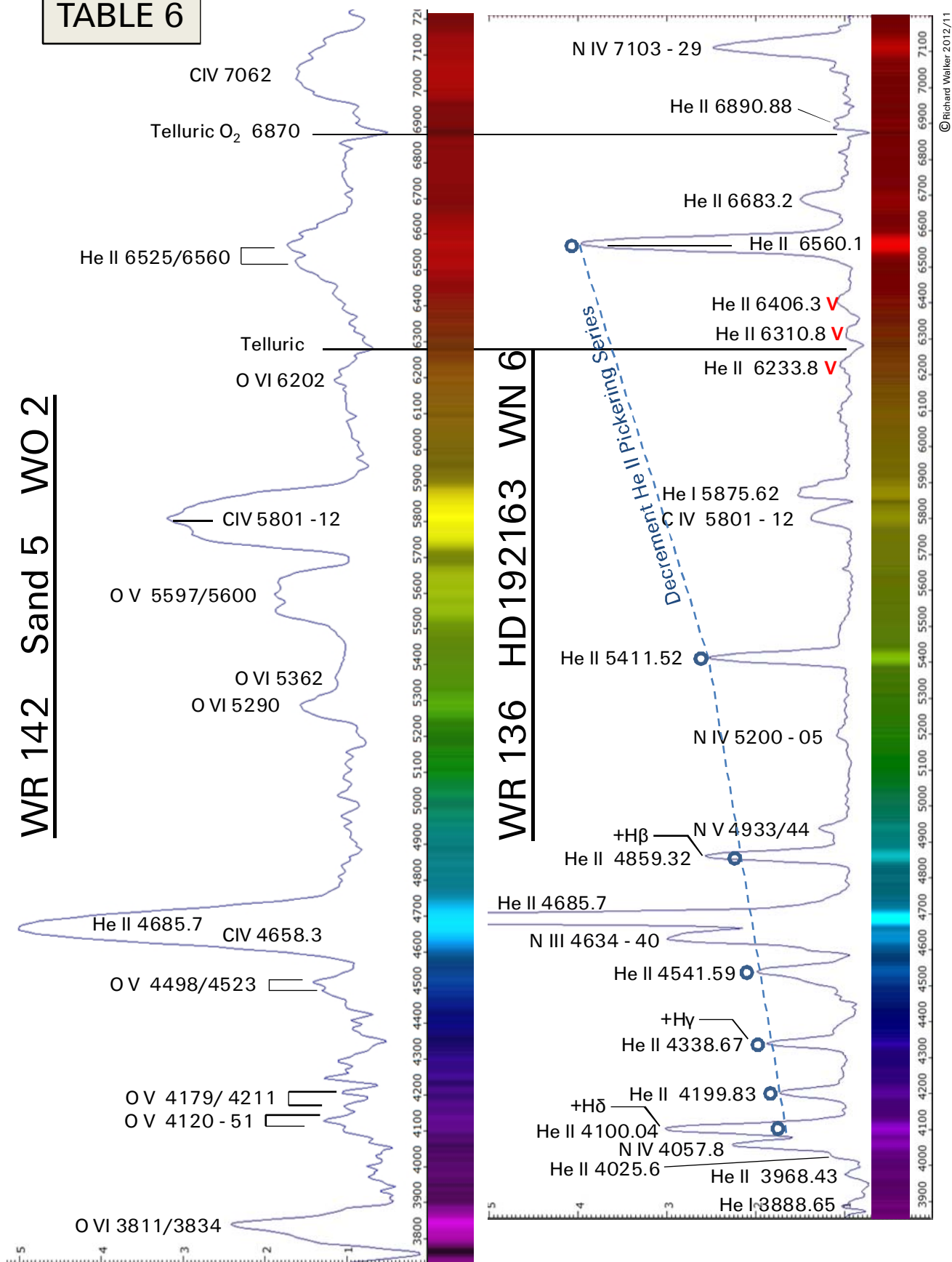




TABLE 6



## 9 Spectral Class B

### 9.1 Overview

Below the extreme O-category seamlessly follows the B-class. Several of the bright Orion stars are early *BO*-types and differ therefore from the above presented late *O9.5* stars, only by small nuances within the spectral profiles. These blue-white luminous B-stars are less massive and hot and therefore living much longer. Further they are much more numerous, dominating a considerable part of the brighter constellations. Here some examples: all bright members of the *Pleiades*, all the bright *Orion stars* except Alnitak, Mintaka and Betelgeuse, all bright stars in the head of the *Scorpion*, except the reddish Antares. Further mentionable are *Regulus*, *Spica*, *Alpheratz*, and the weaker blue component of the well known double star *Albireo B* (B8V). Even the famous, unstable giant *P Cygni*, as well as most of the *Be*- and *Be-Shell stars* (Tables 14 – 15) are members of the B-class.

### 9.2 Parameters of the Early to Late B-Class Stars

The following table shows the data, exclusively valid for the *Main Sequence Stars* of the B-class, compared to the Sun ( $\odot$ ) and according to [701] and other sources (\*). Here, the *enormous spread* becomes evident, covered by this class from the *BO–B9* types. Particularly impressive is the difference in the luminosity – that is about a factor of 550! The huge luminosity is one of the reasons, why the some 1000 ly distant, mostly *early B-class stars* in the Orion constellation, are able to show such a great brightness. Within this class, in the range of about 8–10 solar masses, it's decided whether single stars explode as a *SN* or end up as *White Dwarfs*.

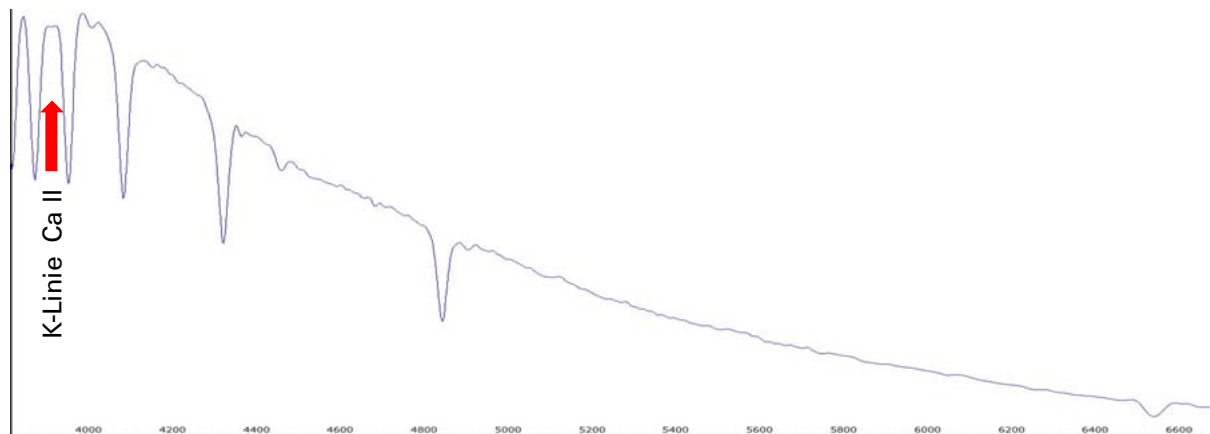
Mass M/M $\odot$	Stay on <i>Main Sequence</i> [y]	Temperature photosphere [K]	Radius R/R $\odot$	Luminosity L/L $\odot$
18 – 3	10M – 400M	25,000 (*) – 10,500	8.4 – 3.0	52,000 – 95

### 9.3 Spectral Characteristics of the B-Class

This class is characterised by the absorption lines of neutral helium, *He I*, reaching their maximum intensity at about class *B2* and weakening downwards the subclasses to *B9*. Further dominating are spectral lines of singly ionised metals *O II*, *Si II*, *Mg II*. Towards later subclasses, the Fraunhofer K line of *Ca II* becomes faintly visible and the H-Balmer series gets significantly stronger. Due to lower temperatures and thereby decreasing *degree of ionisation* the simply ionised *He II* is only visible in the top *BO* subclass, but limited here to the *Main Sequence Stars* of the luminosity class *V*. Absorption lines of higher ionised silicon *Si III* and *Si IV* appear until down to type *B2*.

Highly abundant in the B-class are so called "*Fast Rotators*". Such stars with high rotation speed (about 150–400 km/s) influence the appearance of the spectrum significantly. For details, see the comments to the tables below.

The maximum intensity of the real continuum is still in the UV range, but with a significantly higher share in the visible spectrum. The following graph shows the theoretical continuum for a *B6 IV* standard star (*Vspec Tools/Library*). Marked with a read arrow is here the small kink of the emerging but still very weak Fraunhofer K-line of singly ionised calcium *Ca II*.



## 9.4 Commented Spectra

Table 10: Anilam ( $\epsilon$  Ori) and Gienah Corvi ( $\gamma$  Crv)

The development of the B-subclasses is demonstrated here by a montage of two overview spectra (200L grating) representing an early and late subtype.

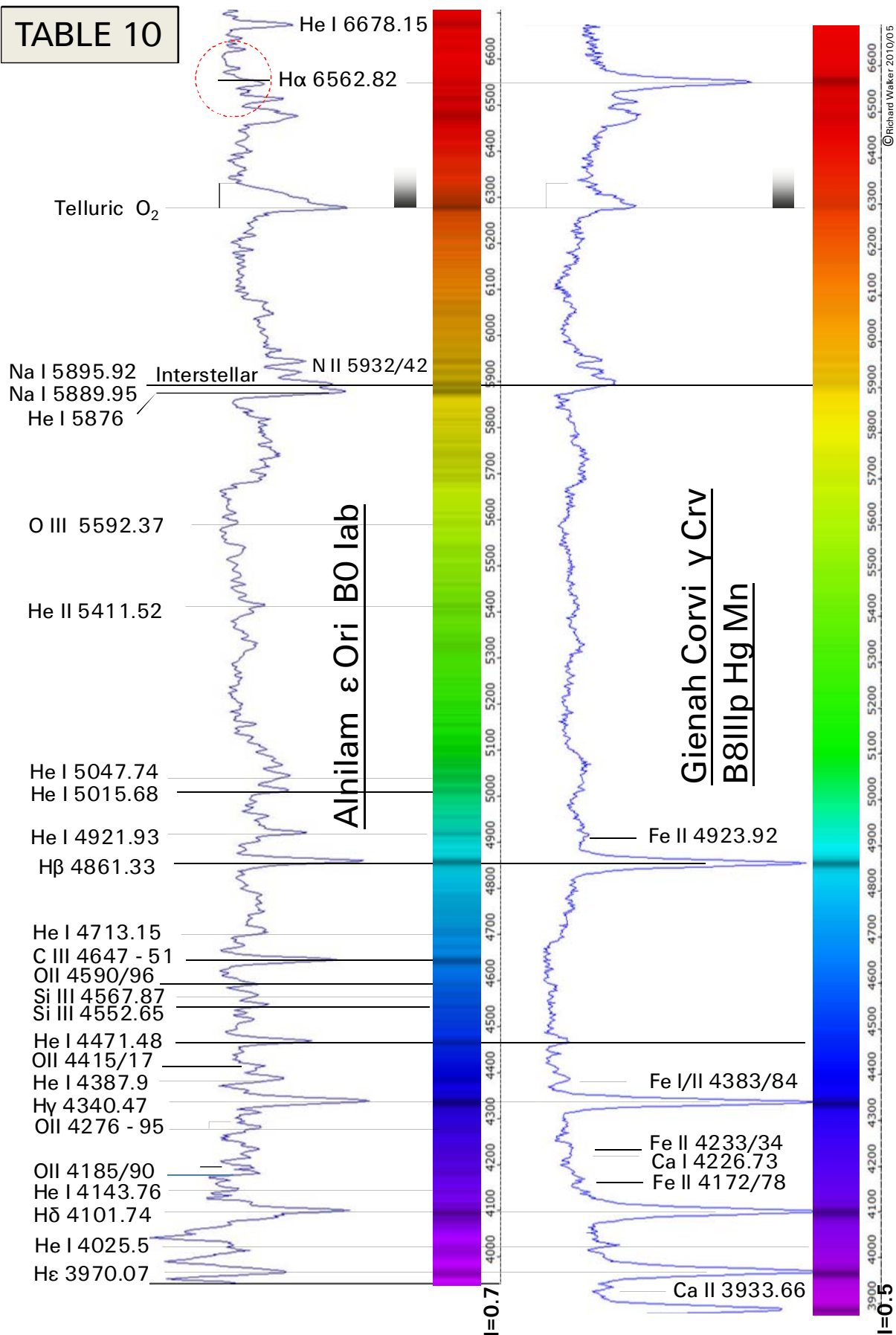
Anilam (1200 ly) belongs to the spectral class *B0 Iab*, and is a so-called *Supergiant*. The surface temperature is about 25,000 K. The star ejects permanently matter, visible here by the somewhat stunted *P Cygni profile* of the *H $\alpha$*  line. About this detail, a PhD thesis exists [340], which analyses a time series of the line-profile change. For more information, refer to Table 13, *P Cygni*.

Gienah Corvi (165 ly) is classified with *B8 IIIp Hg Mn*. It's in the Giant stage and shows overabundances of mercury *Hg* and manganese *Mn* (at this resolution not visible in the profile). For a giant, it has a remarkably high apparent rotation speed of some 150 km/s [506]. This flattens the spectral lines, as the following example of Regulus will show more detailed. According to [506] this effect explains, why the overabundances of some metals have been discovered here so late.

The comparison of these spectra clearly demonstrates the remarkable change in the spectra within the enormous span from the early to the late *B*-Class. The *He I* lines of *Gienah Corvi* are only very faint. Moreover, they are now blended by numerous, still weak, singly ionised or even neutral metal absorptions, such as *Fe I/II*, *Mg II*, *Ca I/II*. These lines appear very diffuse, additionally flattened by the enormous rotation speed. Clearly visible however is the striking increase in the intensity of the *H*-Balmer series towards the late subclasses.

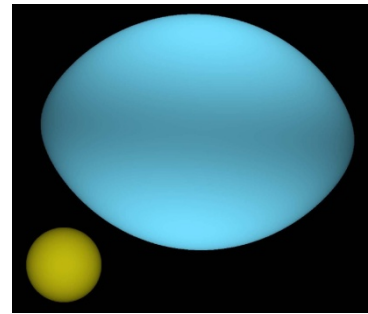
Here appears, for the first time and tentatively only, the Fraunhofer *K-line*, *Ca II* at  $\lambda$  3933. The remarkable small kink in the continuum peak between *H $\epsilon$*  and *H $\delta$* , will grow dramatically within the following *A*-class and becomes the most dominant spectral feature for the middle- to late spectral types! Their "twin-sister", the Fraunhofer *H-line* at  $\lambda$  3968, has still no chance to compete against the strong Balmer absorption line *H $\epsilon$*  at  $\lambda$  3970.

TABLE 10



**Table 11:** Effect of the luminosity on spectra of the B-class: *Regulus* ( $\alpha$  Leo),  $\phi$  *Sagittarii* and *Rigel* ( $\beta$  Ori).

*Regulus* (77 ly) is classified as *B7V* and is, like our Sun, as so-called *Dwarf* still remaining on the *Main Sequence* of the HRD. It's the dominant component of a quadruple star system with a surface temperature at the poles of about 15,000 K. Its very high apparent rotation speed at the equator is about 315 km/s, which is not exceptional for stars of the late B-class. *Albireo B* (B8Ve) for example has an apparent rotational speed of some 250 km/s [506]. Thereby the spectral lines of *Regulus* are strongly widened and the star itself gets impressively flattened. (Computer drawing by W. Huang: *Regulus* in size compared to the Sun). The *H $\alpha$*  line is already well developed in this late B-class.



$\phi$  *Sagittarii* (230 ly) is classified with *B8III* and therefore a so-called *Normal Giant*. Its surface temperature is about 12,300 K and the apparent rotation speed is indicated by Kaler [506] with relatively low 52 km/s. This has hardly a noticeable influence on the *line width* in this spectrum.

*Rigel* (800 ly) is classified as *B8Iab*, belonging to the *Super Giants*. It has a small companion, which is even visible in amateur telescopes, but hardly affects this spectrum of medium resolution (Photo NASA). The surface temperature is about 11,500 K. The apparent rotation speed is indicated in the range of about 40–60 km/s, depending on the info source.



The comparison of these three spectra, equally normalised, shows a clear decrease of the width and intensity of the *H-Balmerlines* with increasing luminosity. Conversely to this, the metal lines in the giants become more intense and narrower at the same time, caused by the less dense stellar atmosphere and thus a lower *pressure- and collision broadening*. For the *Regulus* spectrum, an additional role plays the so-called *rotational broadening*. With its apparent rotation speed of 315 km/s it's a real "*Fast rotator*". This value is about 5 – 6 times higher than by *Rigel* and  $\phi$  *Sagittarii*. Due to this effect particularly the fine metal lines of the *Regulus* spectrum become additionally broadened and their intensity considerably reduced.

F. Royer [401] has shown this effect in a chart for the A-class stars and the *Mg II* line at  $\lambda$  4481 (marked in Table 11 with a red ellipse). Due to this effect, the absorption lines of *Regulus* become additionally "ironed out". Remarkable that the *Mg II* line in Table 11 shows a slightly different behavior than the directly adjacent *He I* absorption at  $\lambda$  4471.

*Caveat:* This synthetic spectrum is calculated for a much higher resolution than shown in Table 11. Therefore the lines appear in the DADOS spectrum considerably wider, as a result of the greater *instrumental broadening*!

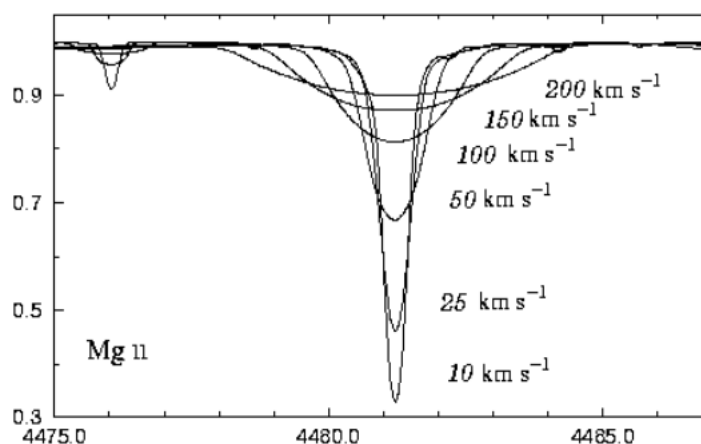
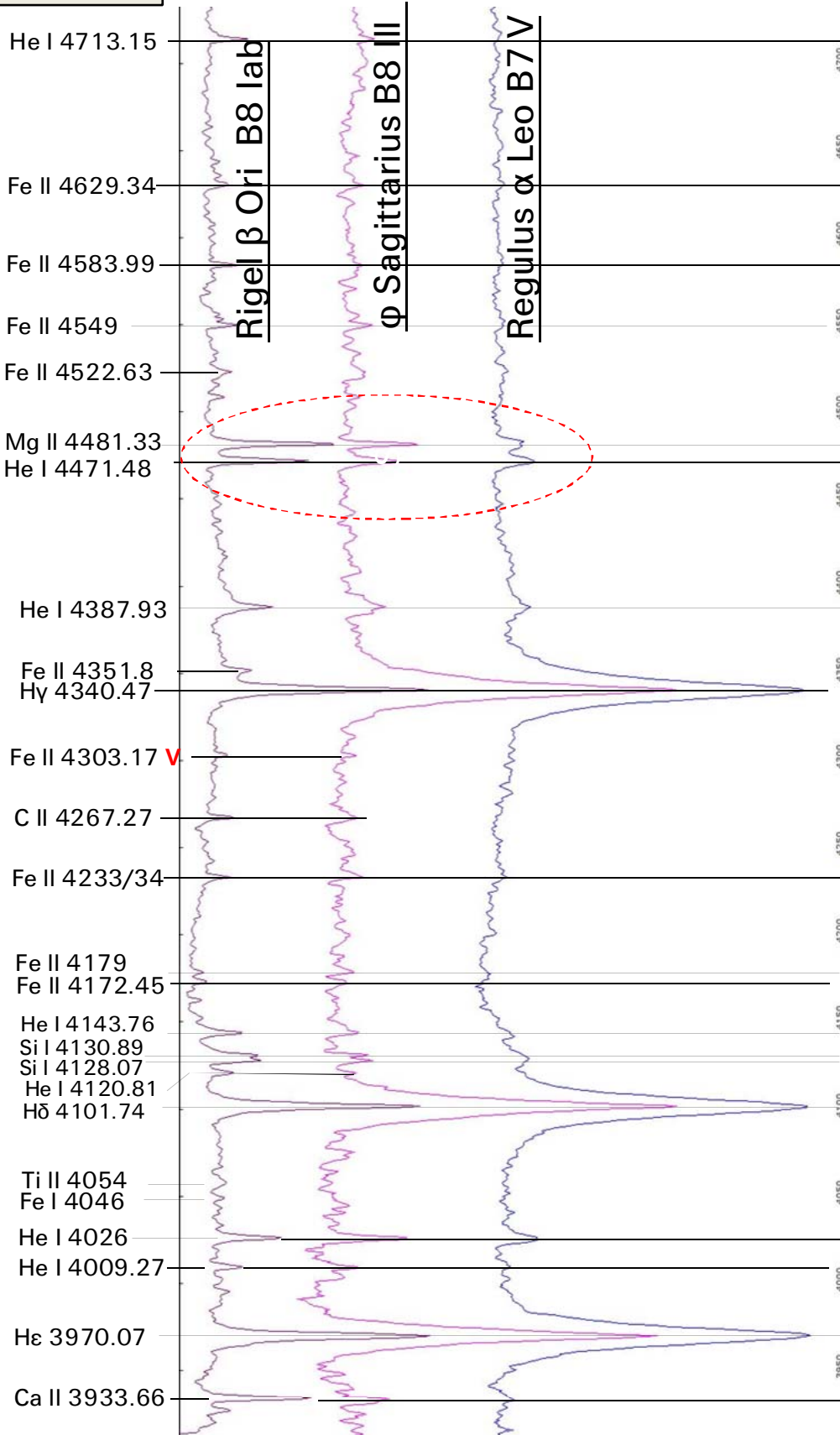


TABLE 11

Effect of the luminosity on spectra of the B-class



Rigel

$\phi$  Sgr

Regulus



Table 12: Detailed spectrum of *Spica* ( $\alpha$  Vir)

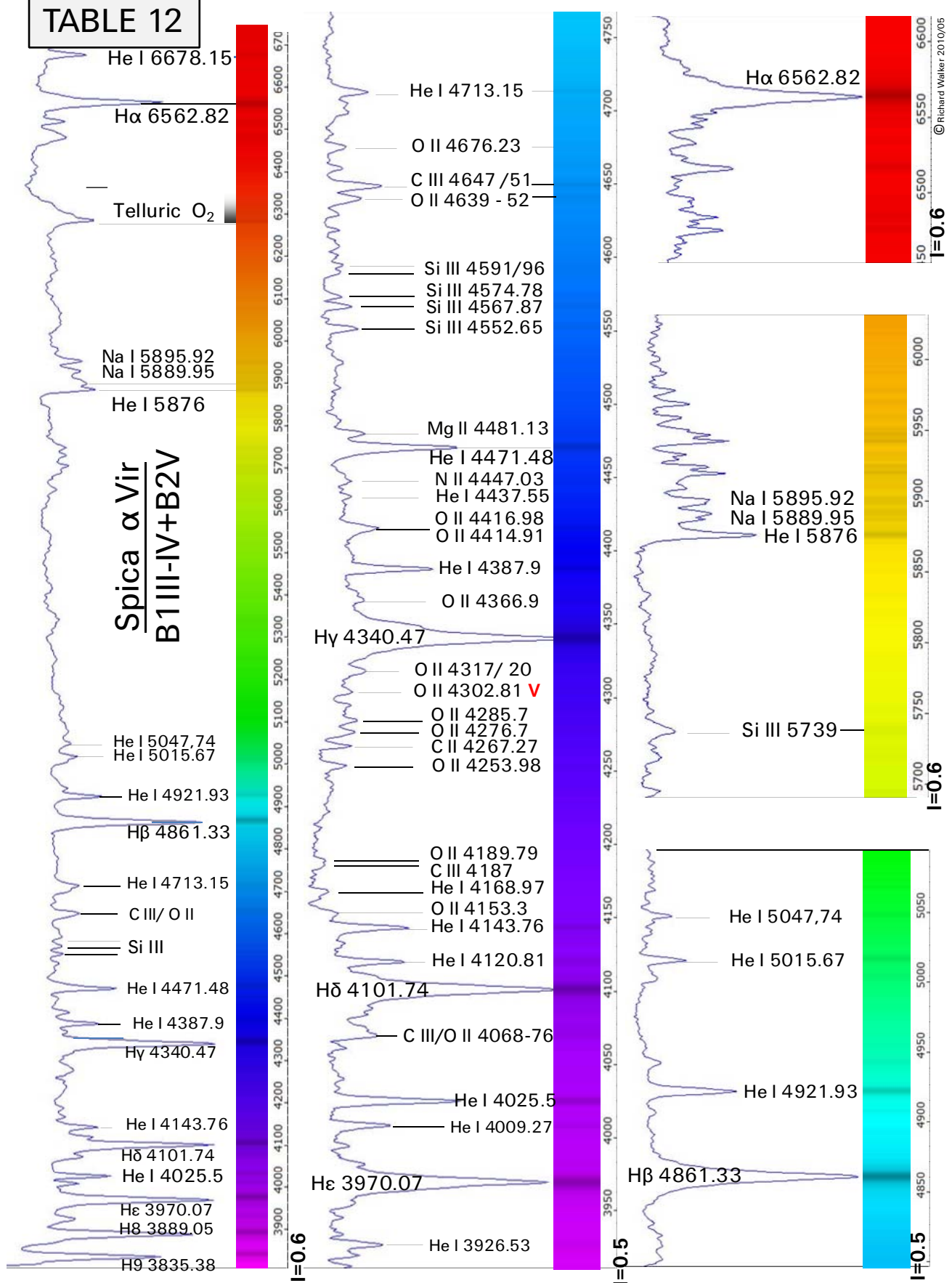
Overview spectrum (200L grating) and higher resolved profiles (900L grating)

*Spica* (260 ly) is a spectroscopic binary with an orbital period of about four days. The dominant *A*-component is in the Giant stage and has a surface temperature of about 22,000 K, corresponding to the spectral type *B1 III-IV*. The smaller *B*-component with the spectral type *B2V* is still on the *Main Sequence* and with a temperature of about 18,500 K significantly less hot and luminous. This very close orbit of the two stars causes, due to the Doppler effect, a periodic splitting of spectral lines (SB2 system), which is not recognisable in these profiles here. Ionised helium *He II* is here no more recognisable however still several absorption lines of multiply ionised metals.

Line identification:

The line identification is based amongst others on [1], [51], [56], [57]

TABLE 12

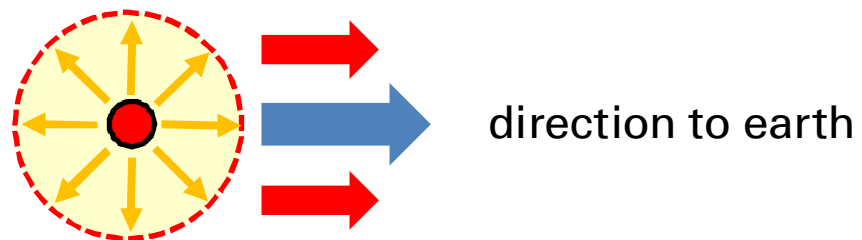
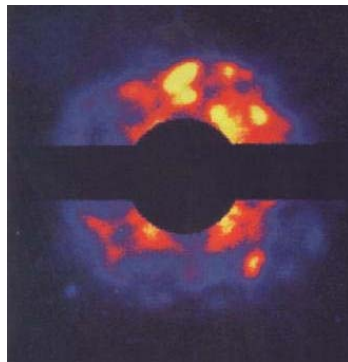




## 10 LBV Stars

*P Cygni* is one of the so-called *Luminous Blue Variables* (LBV), most probably progenitors of *WR stars*! It's an unstable and variable *Supergiant* of spectral class *B2 Ia pe*, with a surface temperature of about 19,000 K. Its distance is according Karkoschka some 5000 ly. What we analyse here with our spectrographs, apparently "realtime", tooked therefore really place at the end of the Neolithic period – a genuine "time machine" at its best! At the beginning of the 17th century, he showed a tremendous outburst, which is known as *Nova Cygni 1600*. After about six years as a star of the third magnitude, the brightness decreased to  $<5^m$ . Apart from a few minor episodic outbursts, the luminosity increased again in the 18th century, until it reached the current, slightly variable value of about  $+4.7^m$  to  $+4.9^m$ .

*P Cygni* is the *prototype* for the already presented *P Cygni profiles* in *Table 2* (Alnitak) and *Table 10* (Alnilam). Such spectral features are found in nearly all spectral classes and are a reliable sign for a huge amount of radially ejected matter by the star. Not surprisingly this effect is sometimes also visible in the spectra of Novae and Supernovae.



The left image shows parts of the expanding star shell, taken with the *HST*. The star in the center is covered here. The chart above right shows how the resulting *P Cygni profiles* are generated. In the direction of the *blue arrow* a small part of the expanding shell of gas moves right in our direction, so the resulting *absorption lines* appear blueshifted by the Doppler Effect. The *red arrows* symbolise the light, generated by the ionised shell areas, ejected sideways, and therefore are visible as emission lines. Both phenomena cause now the overall layout of the spectral line with a blue-shifted absorption part, which transits continuously into the mostly more intensive, red shifted emission peak. As already demonstrated in *Table 2* and in [30], the difference  $\Delta\lambda$  between the two peaks enables the estimation of the expansion velocity of the shell (here some 200 km/s).

Profile to the right (900L): The "original" *P Cygni* star shows a highly impressive *H $\alpha$*  emission line. Therefore the other spectral features appear strongly compressed, so they are barely recognisable. The blue absorption part of this line is strongly stunted. In contrast to this, the helium emission at  $\lambda$  6678 shows here and in the lower profile of *Table 13* (900L) a textbook-like *P Cygni profile* – the same does *H $\delta$*  in the upper profile of *Table 13* (200L). To show the other lines, overprinting here the telluric absorptions, the profiles in *Table 13* are strongly zoomed in the vertical intensity axis. The top of the *H $\alpha$*  emission is therefore cutted. Noteworthy, that the continuum appears significantly elevated in an area of some 100 Å around *H $\alpha$* .

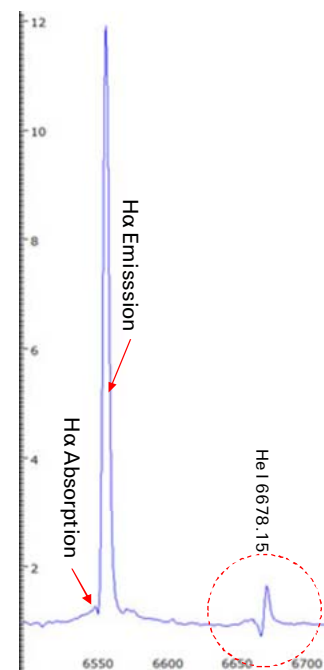


Table 13: Overview and detailed spectrum of *P Cygni* (34 Cyg)

Overview spectrum (200L grating, recorded September 16, 2009) and a higher resolved profile around the H $\alpha$  line (900L grating, recorded June 22, 2010). The line identification is based on [341].

Table 13 A: Detailed spectrum of *P Cygni* (34 Cyg)

Higher resolved profile sections (900L grating), recorded May 07, 2011) in the green and blue area of the spectrum. The line identification in the range  $>\lambda$  4100 is based on [341], in the range of  $<\lambda$  4100 according to [341a], [341b].

Remarks:

What appears in these profiles as absorptions turns out at a higher resolution in most cases as emission lines or P Cygni profiles!

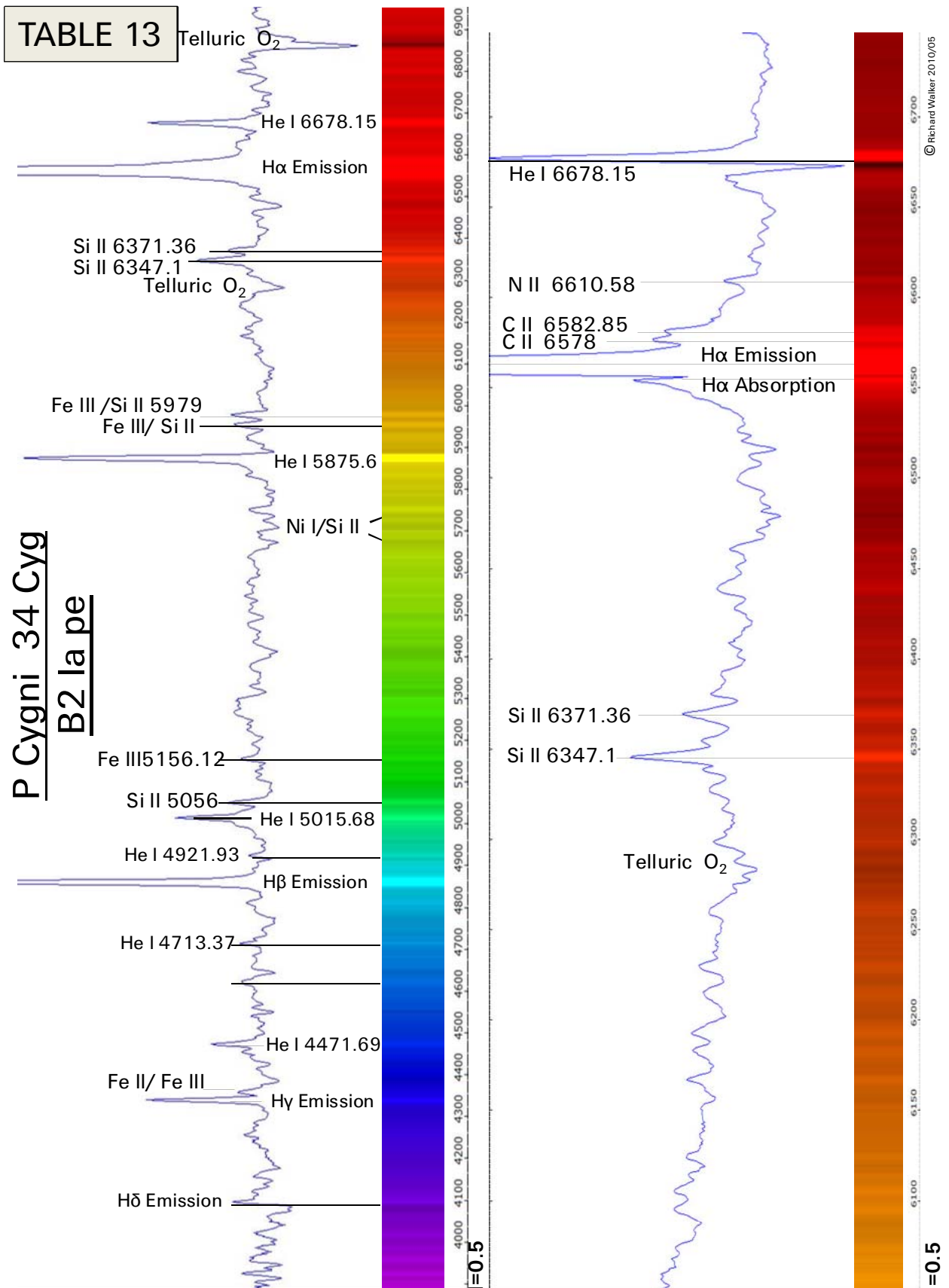
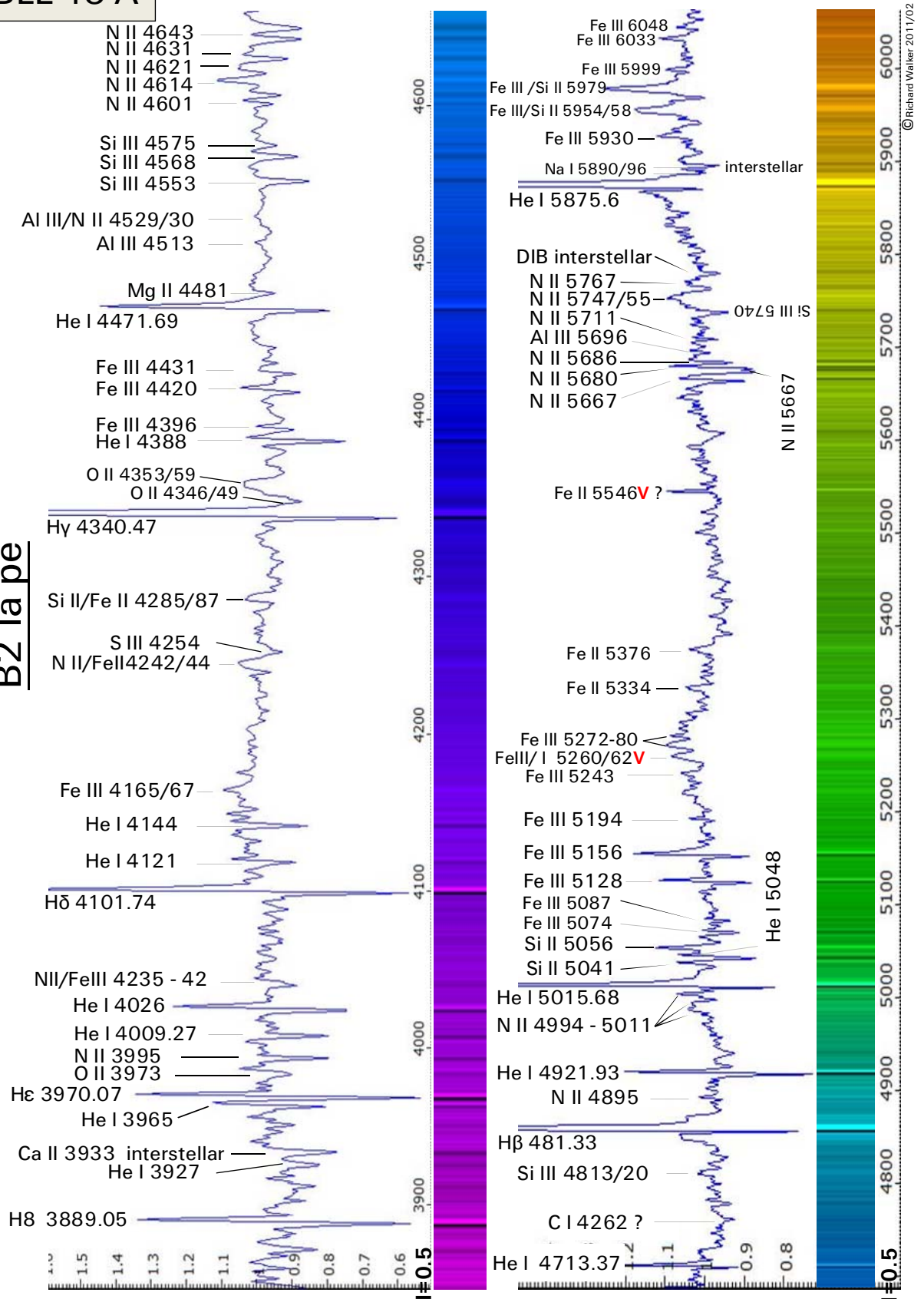


TABLE 13 A

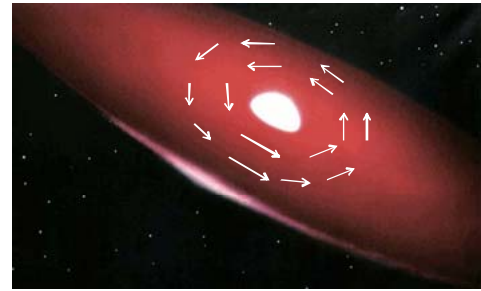
P Cygni 34 Cyg

B2 Ia pe



## 11 Be Stars

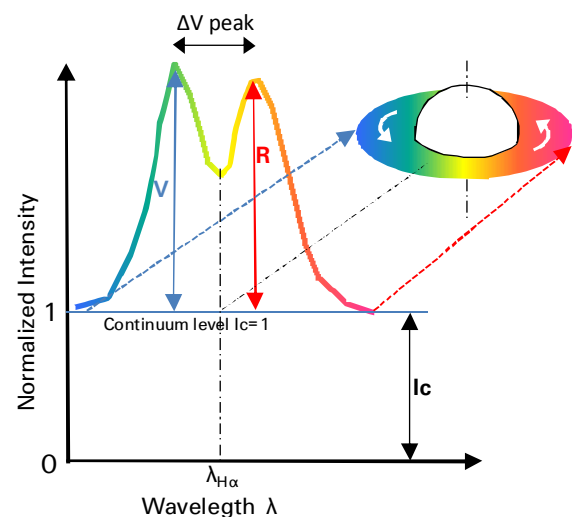
*Be stars* form a large subgroup of the spectral class *B*, and all of them show a *high rotation speed*. A small number is still to find in the early *A*-class. These stars are mostly located on or near the *Main Sequence* of the *HRD*. A few *Be*-stars only have reached the giant stage with an upper limit of *luminosity class III*. The first *Be*-star,  $\gamma$  *Cassiopeiae*, was discovered in 1868 by Father *Angelo Secchi*, who wondered about the "bright lines" in this spectrum. The suffix *e* (*Be*) suggests that emission lines occur here. Due to the sometimes temporary only occurrence of the *Be* stage, the suffix *e* for emission lines is missing in some stellar classification databases.



University Western Ontario

In contrast to the stars, showing *P Cygni profiles* due to expanding matter (*Table 13*), the *Be stars* develop, often just episodically, a *rotating circumstellar disk* of gas in the equatorial plane. The mechanism is not yet fully understood. This phenomenon is accompanied by *H I* and *He I* emissions in the spectrum, as well as strong infrared and *X-ray* radiation. Outside such episodes, the star can seemingly spend a normal "life" in the *B* class.

The approximately 450 ly distant *Dschubba*, dominant member in a quadruple star system, has mutated since about 2000 from the *B0.3 IV* spectral type in to a *Be*-star and developed a typical circumstellar disk of gas. The apparent rotation speed of the central star is approximately 180 km/s [505]. The spectra in *Table 14* show the state of the gas disk at different dates. The  $H\alpha$  emission line was taken on August 18, 2009. Its intensity is significantly lower than by *P Cygni*, but although still so high, that the interesting, much weaker double peak profile of the helium line at  $\lambda$  6678, could be overlooked. To make such details visible, the profiles in *Table 14* are strongly zoomed in the intensity axis. The chart shows, how this double peak arises due to a combination of Doppler- and perspective effects. The intensities of *V* and *R*, as well as the distance between the two peaks, inform about the apparent "current" state of the disk. For detailed information with examples and formulas refer to [30] and [31].



The main interest of the research seems to be focused on these spectral features. Anyway here are even more remarkable effects to see. Also  $H\beta$  shows an emission line, which grows up here in the middle of a broad *photospheric absorption* line of the central star [250]. Such spectral features are therefore called *emission-* or *shell cores* [2]. However  $H\gamma$ ,  $H\delta$  and  $H\epsilon$  appear at this resolution as "normal" absorption lines, a suggestion for amateurs, to observe these lines with higher resolutions. Further at about  $\lambda$  3700 the profile shows a kind of double peak emission. A similar structure within this wavelength domain was commented in [702] by *H.A. Abt* as a "Disk Line". In [2] a six-stage classification system is presented according to *Lesh*. The more lines of the *H* Balmer series show up as emission lines, the more intense the *Be* phenomenon is classified. Following the required excitation energies [eV], for some of the *H* Balmerlines, starting from the ground state  $n = 1$ :  $H\alpha$ : 10.2,  $H\beta$ : 12.1,  $H\gamma$ : 12.7,  $H\delta$ : 13.0

Overview spectrum (200L grating) and higher resolved profiles (900L grating) around the  $H\alpha$  and  $H\beta$  lines, further a zoomed detail of the Helium doublepeak at  $\lambda$  6678.

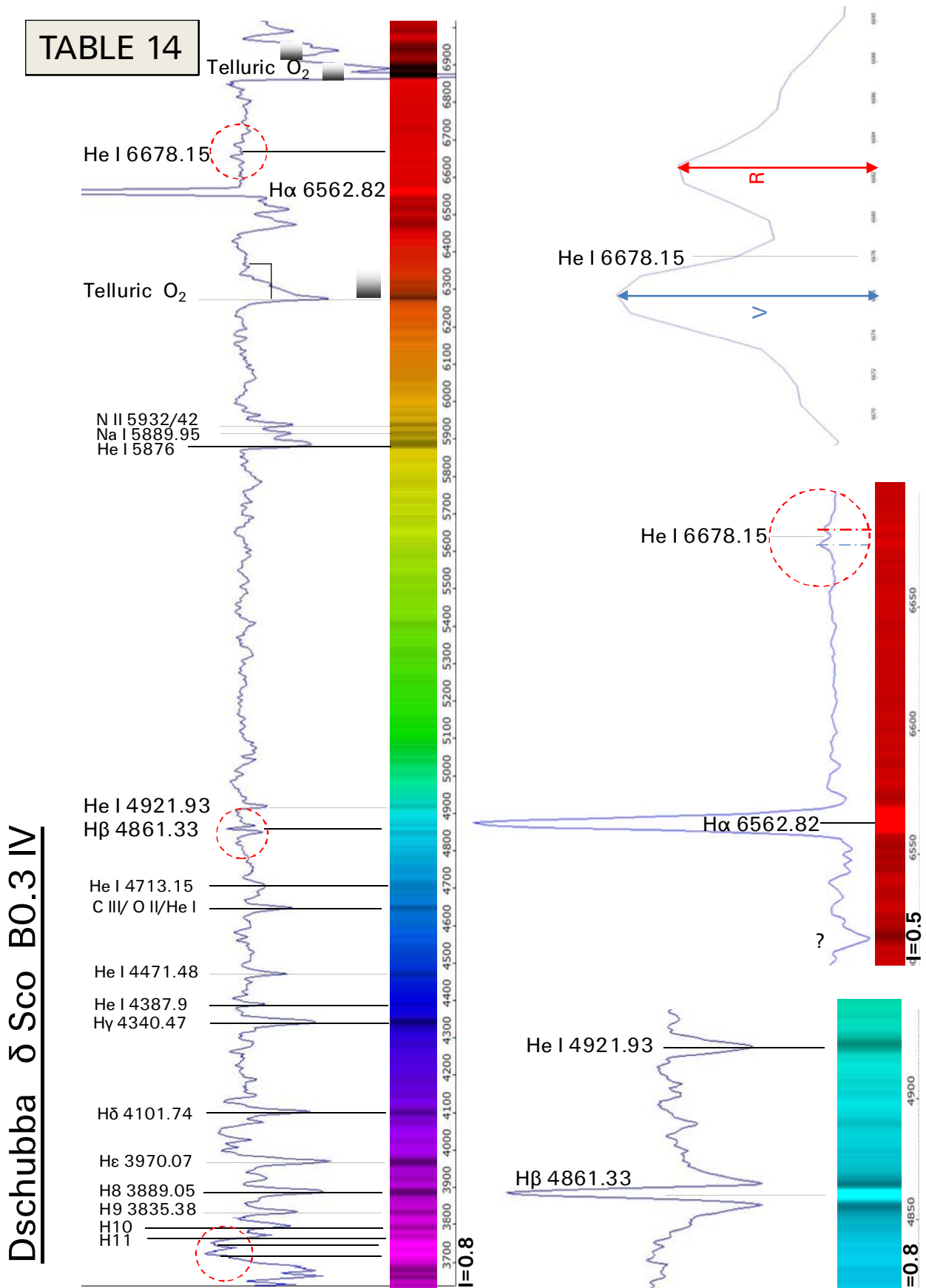
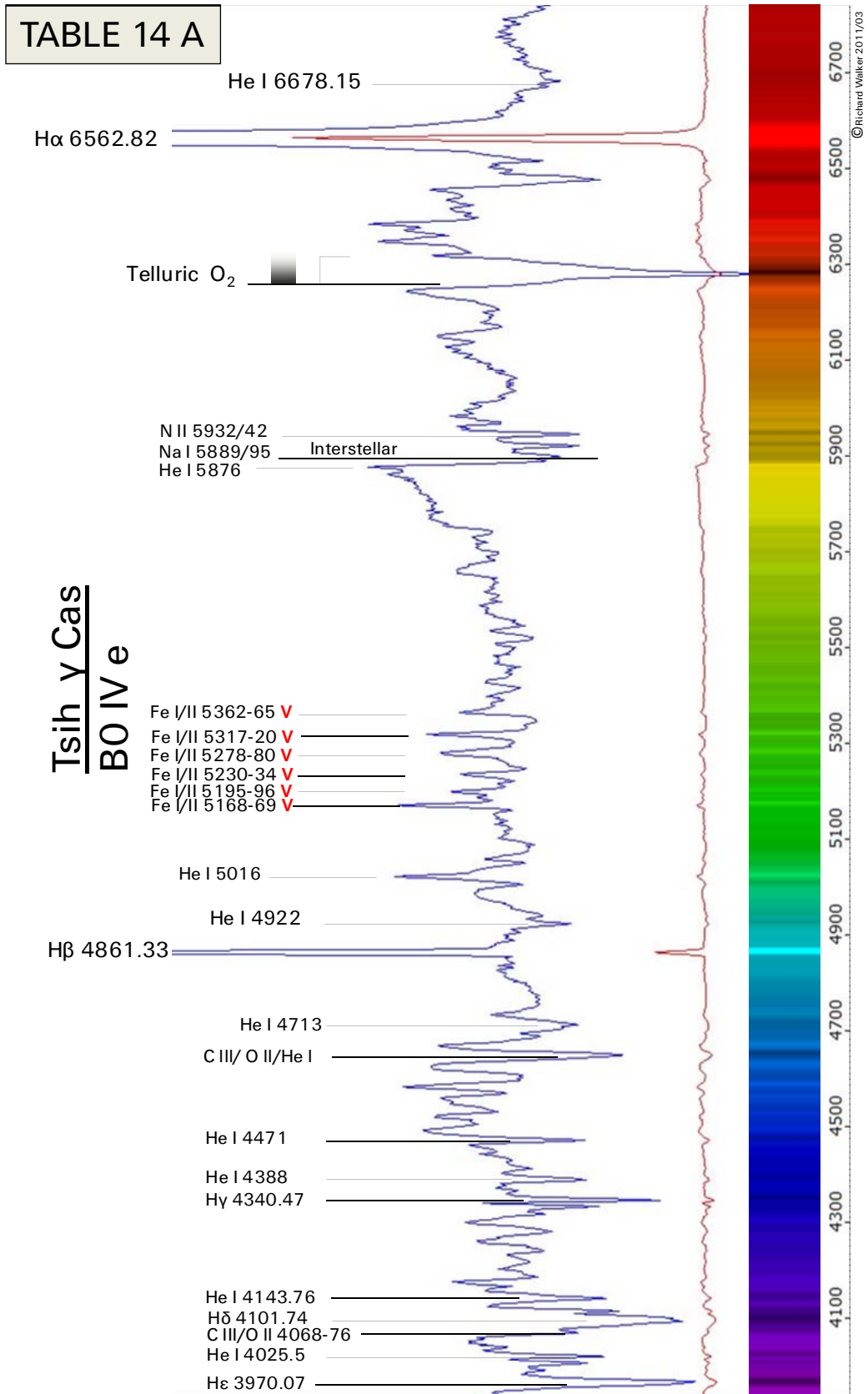




**Table 14 A:** Be- Star *Tsih γ Cassiopeiae* B0 IVe (610 Lj)  $V = 2.47^m$ 

Overview spectrum (200L grating). The apparent rotation speed of the central star is typically very high,  $\sim 300$  km/s. The spectrum was taken on April 9, 2011. In contrast to  $\delta$  *sco* much more lines are here in emission. Some of them are caused by *Fe I/Fe II*. The *He I* line at  $\lambda$  6678 is hidden within a broad absorption and barely visible in this lowly resolved profile. The red profile represents the actual intensity ratios with the dominant *H $\alpha$*  and *H $\beta$*  emission. The blue one is strongly zoomed to make the fine lines better visible.





## 12 Be Shell Stars

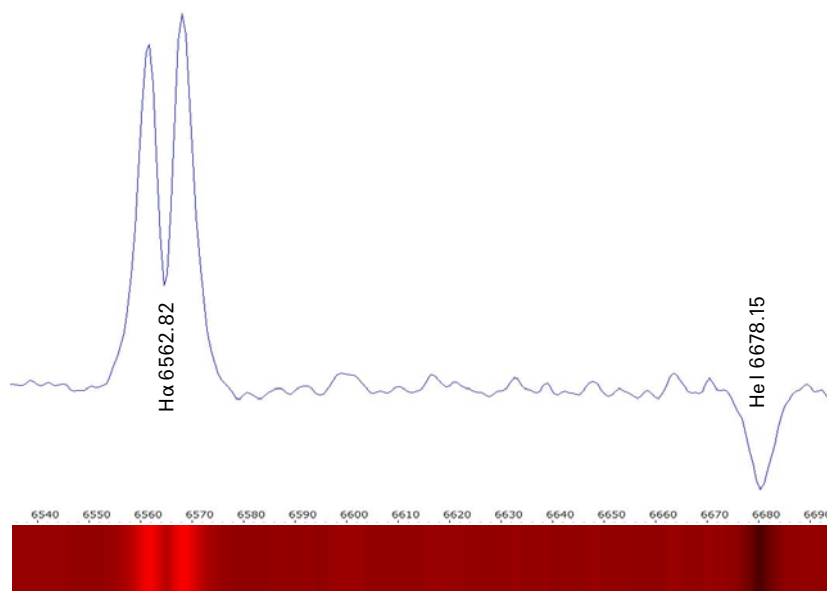
During the *Be* phase a star can pass in some cases also the extreme *shell stage*. In this case it forms not only a disk, but rather a large scale, low density shell (“pseudo photosphere” [2]), which has similar characteristics like the photosphere of the supergiants with a luminosity class of approximately I-II. Accordingly, only few emission lines are showing up here, however much more very narrow but strikingly intense absorption lines with low FWHM values. Prototype for this star category is  $\zeta$  *Tauri*. Also *28 Tauri* (Pleione) is undergoing this extreme shell stage from time to time. Sometimes the suffix *pe* is added to the spectral classification of such stars.

**Table 15:** Comparison Be Shell star  $\zeta$  *Tauri*, and Be star  $\delta$  *scorpii*.

$\zeta$  *Tauri* (HD 37202), *B4 IIIpe* [505],  $V_{\text{var}} = 2.88^{\text{m}} - 3.17^{\text{m}}$

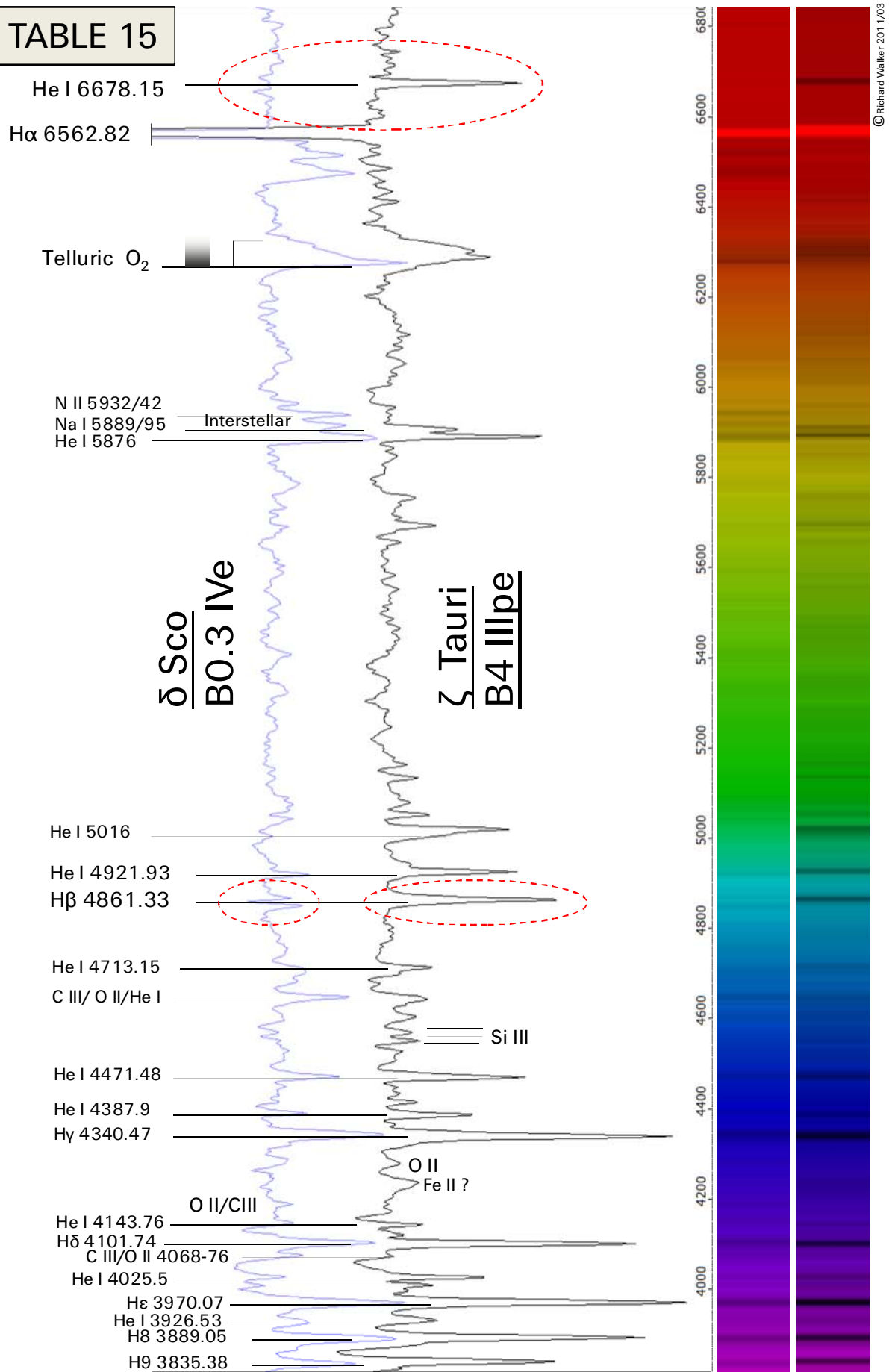
The approximately 417 ly distant  $\zeta$  *Tauri* has a surface temperature of some 22,000 K. The apparent rotation speed of the central star is some 330 km/s, which is not unusual high for this type of star. It forms the main component of a binary system with a much smaller *B*-component of spectral class G8III. The orbital period is some 0.36 years, the distance between the components some 1 AU. The behavior of the spectral lines is sometimes very volatile. According to [505] the width of the H-lines may change within some 10 minutes – not unusual for *Be* shell stars! The spectral class of  $\zeta$  *Tauri* is specified inconsistently by different datasources. So it’s classified by [2] with *B2 IIIIn shell*, instead of *B4 IIIpe* according to [505].

The Montage of the two spectra in *Table 15* shows the difference between the two stars. In contrast to  $\delta$  *scorpii*, *H $\alpha$*  is the only recognisable *emission line* in the spectrum of  $\zeta$  *Tauri* (200L grating). The following profile (900L grating) shows *H $\alpha$*  as an asymmetrical double peak emission line. Their shape can change within a very short time – a highly rewarding monitoring project for amateur astronomers!



Unlike to  $\delta$  *scorpii* the spectrum of  $\zeta$  *Tauri* shows the *He I* line at  $\lambda$  6678 and the *H $\beta$*  line at  $\lambda$  4861 *not* as emission- but relatively intensive absorption lines. (marked in *Table 15* with red ellipses). Furthermore all absorptionlines appear much more intensive compared to  $\delta$  *scorpii*, corresponding approximately to those of early B Giants. Striking however is the strong absorption around the *He I* line at  $\lambda$  5016. Due to the strong zoom in the vertical intensity axis, the peaks of the *H $\alpha$*  emissions appear here “cutted”. Their real intensity is similar in both spectral profiles.

TABLE 15

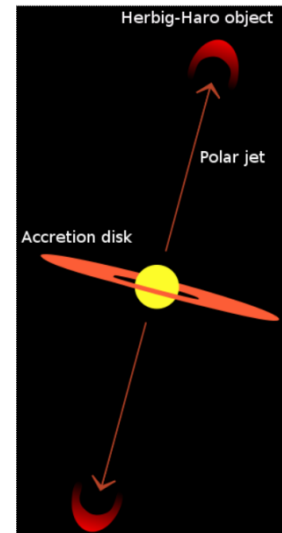


## 13 PMS Protostars

### 13.1 Overview

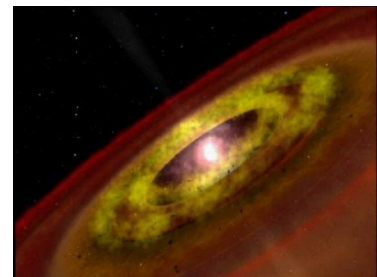
These objects represent the stellar birth phase. These so-called *YSO* (Young Stellar Objects) are formed from contracting gas and dust clouds. Due to this gravitational process the temperature in the center rises until the onset of the hydrogen fusion. Finally the star begins to shine. From now on, within the rough time frame of several hundred thousand to millions of years, it approaches from top, downward to the main sequence of the HRD. Therefore, these objects are also called *PMS stars* (Pre-Main Sequence) [2]. The highly irregular optical brightness variations proof, that the PMS stars are still very unstable. In a later phase planets are formed from the residual, protoplanetary disk material.

In this phase, the material forms a rotating accretion disk, which at least temporarily veils the central star. A part of the so-called *accretion flow* doesn't hit the emerging protostar [275]. It is deflected and ejected on both side of the disk, forming a cone-shaped, bipolar nebula (graphics Wikipedia). At some distance from the protostar, this jet may collide with interstellar matter, forming rather short living, nebulous structures, so-called *Herbig Haro* objects. These are named after *George Herbig* and *Guillermo Haro*. A detailed and illustrated presentation of these effects can be found in [275].



### 13.2 Herbig Ae/Be and T Tauri Stars

The *Herbig Ae/Be objects* represent the birth stage of the stellar spectral classes A – O. For the later F – M types these are the *T Tauri stars*, which are still subdivided into *Classical T Tauri Stars (CTTS)* with intense emission lines and *Weak T Tauri stars (WTTS)* with predominantly absorption lines. The limit is determined here by the equivalent width *EW* of the H $\alpha$  emission line. According to [2] the object is a *CTTS* if  $EW > |10\text{\AA}|$  and according to other sources  $EW > |5\text{\AA}|$ .



### 13.3 Spectral Characteristics of PMS Stars

This striking instability becomes also evident in the spectrum. Typically, it shows emission lines of the H-Balmer series, as well as of the H- and K (Ca II) Fraunhofer lines. Depending on the state of the accretion disk, and our perspective on the object, in addition numerous Fe I and Fe II lines, as well as Ti II may show up [270]. Mainly late *WTTS* T Tauri stars sometimes generate more or less pure absorption spectra, which enable a fairly accurate classification of the star.

*Gray Corbally* [2] presents a classification system for Herbig Ae/Be stars with the following main criteria:

- The presence and intensity of emission lines of the H-Balmer series
- The presence and a possible  $\lambda$  shift of so-called *Shell Cores*, mainly observed by the Balmer series. These are emission lines, raising up from rotationally broadened, photospheric absorption sinks.
- The presence of emission lines of ionised metals, particularly the *Fe II (42) Multiplet*
- The appearance of the Fe II (42) multiplet as *emission lines, absorption lines, or P Cygni profiles* (see below)
- Strength of the Balmer Decrement

### 13.4 The FU Orionis Phenomenon

FU Orionis is the eponymous star of this phenomenon, which occupies a special position in the birth phase of stellar evolution. In astronomical jargon such objects are also called "FUors". 1936–37 FU Ori increased its apparent brightness within 120 days by about 6 classes from  $\sim 16^m$  to  $\sim 9^m$  [289]. At first an ordinary nova eruption was suspected. Anyway, the subsequently expected decrease in brightness did not take place, but remained, with slight fluctuations, more or less on this level until today. In the 1970s, V1057 Cygni showed a similar behavior. Today it is believed, that the long-lasting increase in brightness at T Tauri stars is caused in their late phase by a dramatic increase of matter, falling from the accretion disk down to the protostar [286] – [290]. Thereby the spectrum is changing dramatically and it resembles to that of a supergiant of the spectral classes F – K (details see the following comment on table 19). In my personal opinion, this effect could possibly be caused by a temporarily formed pseudo photosphere, similar to the Be shell stars (sect. 12). Further it is believed, that this stage is passed through several times and further limited to stellar masses  $\leq 1 M_{\odot}$ , what consequently means, restricted to the T Tauri class [289].

### 13.5 Commented Spectra

Table 17: NGC 2261 („Hubble's Variable Nebula“) with *R Monocerotis*

*R Monocerotis* (approx. 2500 ly) is a *Herbig Ae/Be* star. Of its bipolar nebula from our perspective only one of the two conical halves is visible as NGC 2261 (image: HST). The star itself and the second symmetrical half of the nebula remain hidden behind the accretion disk. The brightness of *R Monocerotis* varies between approx.  $10-12^m$ . Quite recently it became clear, that this well-hidden object is a *Herbig Ae/Be* star of spectral type B0. Like most of the representatives of early spectral classes, *R Monocerotis* is also orbited by a smaller companion.



In the 1970's it was still considered by many authors as a T Tauri object of middle spectral class. In such cases, the spectral type can, with reasonable accuracy, be determined only with today's methods and means.

The spectrum in table 17 was taken on March 12, 2012 in the brightest tip of the nebula, near the not directly visible *R Mon*. With the 50  $\mu\text{m}$  slit of DADOS at the C8, an exposure time was applied of 4x780 seconds: Atik 314L,  $-10^{\circ}\text{C}$ , 2x2 binning mode. As for table 85 (M1), it was here also necessary, to record separately the disturbing light pollution spectrum just outside the nebula and to subtract it afterwards from the NGC 2261 signal (with Fitswork).

The most striking features are the strong H Balmer lines, which are seen here in emission. The Balmer Decrement in this profile yields  $I_{H\alpha}/I_{H\beta} \approx 5$ . For such objects, this selective reddening of the profile is significantly influenced by the density of the circumstellar dust cloud and poses even an important classification criterion (see above). The high degree of dust occultation is probably one reason why here almost exclusively emission lines can be seen. C.A. Grady et al [273] noted the correlation between the intensity of the Fe I and Fe II emissions, and the degree of dust occultation, combined with the associated infrared excess. Striking in this profile appears further the so called *Fe II (42) Multiplet* at  $\lambda\lambda$  4923, 5018 und 5169 [2]. This feature can also be found in the spectra of Novae and Supernovae as well as in Active Galactic Nuclei (AGN). Herbig already noted in the 1960's that the short-wave K-line of the two Ca II emissions mostly appears more intense.

Here it was also confirmed, that the spectrum, taken in a wider area of the NGC 2261 nebula, looks similar to a profile, recorded very close to R Monocerotis. Thus NGC 2261 is apparently rather a reflection than an emission nebula. The quality of the obtained noisy profiles however is insufficient for this publication. The line identification is inter alia based on [2] and [270].

This highly interesting object is also very popular amongst astrophotographers who record the short-term brightness variations in spectacular series of images. On January 26, 1949 NGC 2261 became famous, because Edwin Hubble himself photographed this nebula as the official First Light Object of the new 5m telescope at Mount Palomar Observatory!

Table 18: T Tauri HD 284419, Prototype of the T Tauri Stars

T Tauri (approx. 462 ly, [Loinard et al.]) is a *Classical T Tauri Star CTTS* with highly intense emission lines. This clearly demonstrates here the EW value of H $\alpha$ :  $EW_{H\alpha} \approx -87\text{\AA}$ . At first glance, the two profiles of Table 17 and 18 look very similar. The Fe II (42) multiplet however is here much weaker, but the Ca II emission significantly stronger. T Tauri is classified as *G5 Ve*, much later than Type A. This can only be recognized here at the CH absorption band ( $\lambda \sim 4300$ ).

A highly interesting detail are the forbidden [O I] line, the strikingly intense sulfur lines [S II] and the H $\gamma$  emission, which at the time of recording on March 27, 2012 appeared as *inverse P Cygni profiles!* These indicate large-scale *contraction* movements within the accretion disk, headed towards the star – this in contrast to the normal P Cygni profiles, which are always a reliable sign for an *expansion*. The Doppler analysis showed here contraction velocities of some 600 km/s (formula and example see Table 2).

According to AAVSO the apparent brightness of the object at the time of recording was  $\sim 10^m$ . The spectrum in Table 18 was taken with DADOS and the 25 $\mu\text{m}$  slit; exposure time 3x724 seconds: Atik 314L,  $-10^\circ\text{C}$ , 2x2 binning mode. As for table 17, it was here also necessary, to subtract the disturbing light pollution spectrum from the T Tauri signal. At T Tauri, as a by-product of this star birth, a closely neighboring *Herbig Haro object* is to observe. Here it is the variable nebula NGC1555, named after *John Russell Hind* (1823-95) visible in large telescopes next to T Tauri (image: CDS).



Table 19: FU Orionis, *G3 lav + K*, [500],  $V_{\text{var}} = \sim +9.6^m$  and  $\gamma$  Leonis, Algieba, *KO IIIb+G7III*

Spectral comparison of the protostar FU Orionis (approx. 1300 ly, [289]), with the KO IIIb giant  $\gamma$  Leonis (approx. 126 ly). Recording data with C8/DADOS/Atik 314L+: 25 $\mu\text{m}$  slit, 8x600 seconds, 2x2 binning mode,  $-20^\circ\text{C}$ , including subtraction of the light pollution. In the short-wave range the "Fuor" spectra look generally like those of F–G supergiants, but in the near-infrared rather like those of K-giants. In comparison to  $\gamma$  Leonis (KO IIIb), this is easily recognisable here and is also expressed by the spectral class of G3 lav + K. In comparison with the  $\gamma$  Leonis profile we see the following striking differences:

- At FU Orionis the H $\alpha$  line forms a distorted P-Cygni profile. Typically, the red shifted emission part appears here strongly stunted [286], [290].
- The strong, broad absorption of lithium Li I at  $\lambda$  6708 shows, that FU Orionis must necessarily be a very young object, because at high temperatures (due to convection) this element is reduced to helium [11].
- Very slim but intense appears here the H-Balmer series, with the exception of H $\alpha$ , as well as the D<sub>1,2</sub> sodium absorptions at about  $\lambda$  5900.





TABLE 17

NGC 2261 / R Monocerotis (Recorded March 12. 2012)

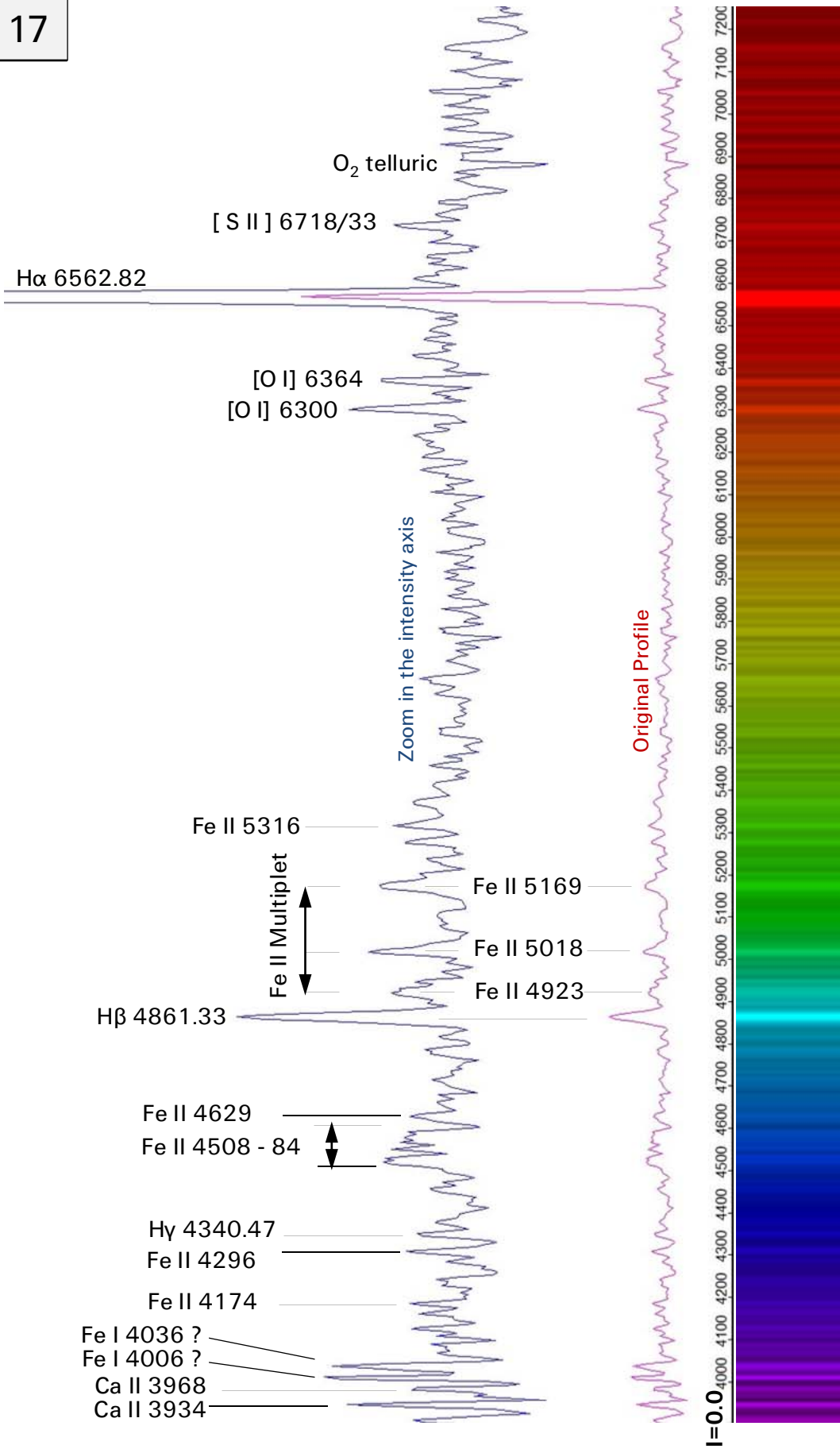
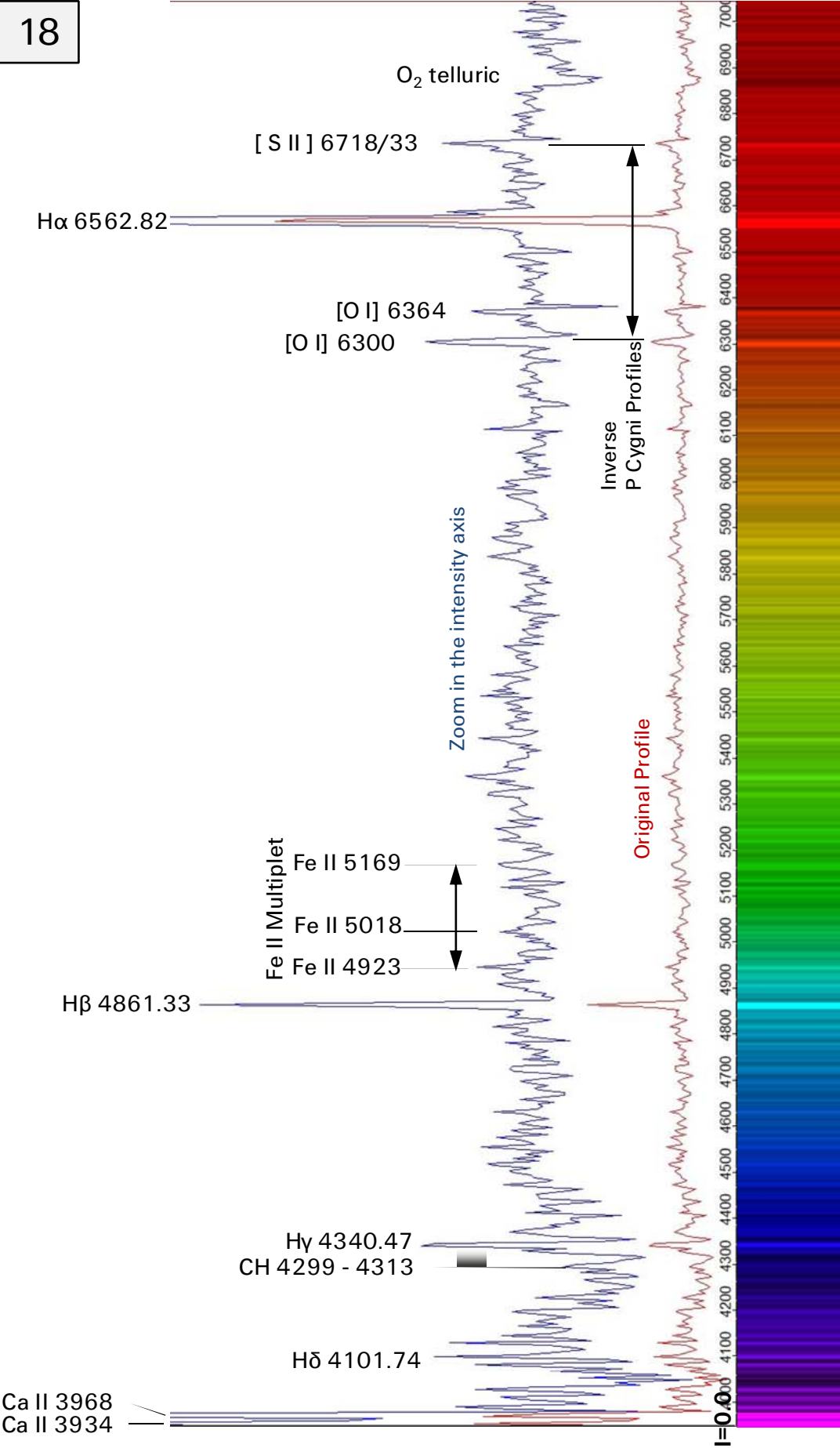
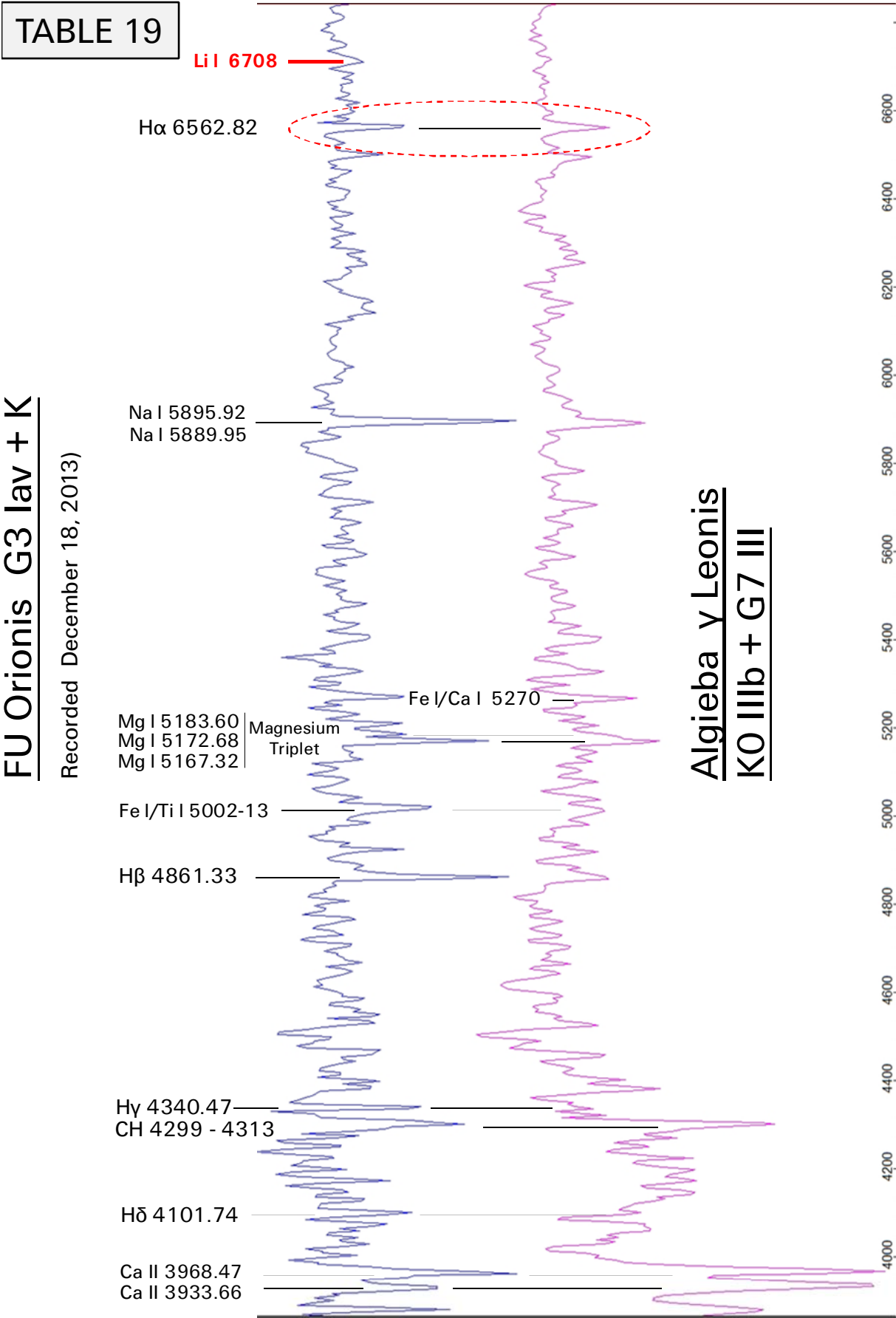


TABLE 18

T Tauri HD 284419 (Recorded March 27, 2012)







## 14 Spectral Class A

### 14.1 Overview

Several of the best known and most striking, bright white stars, like *Sirius*, *Vega*, *Castor*, *Deneb*, *Denebola*, *Altair*, and most of the stars in the *Great Bear* are classified as *A-types*. In this and all the following later classes, the single stars on the *Main Sequence* will pass at the end of their life a *Giant phase*, combined with an impressive "farewell tour" through almost the entire HRD. They will end their lives as extremely dense *White Dwarfs*. During this final process at least some of them will eject a photogenic *Planetary Nebula*.

### 14.2 Parameters of the Early to Late A-Class Stars

The following table shows the data exclusively for the *Main Sequence Stars* of the *A-class*, compared to the Sun ( $\odot$ ) and according to [701]. Compared with the enormously broad *B-Class*, the low mass range (factor 1.5) is striking here. Nevertheless impressive is the huge influence of this relatively small mass difference on the luminosity and life expectancy.

Mass M/M $\odot$	Stay on main sequence [y]	Temperature photosphere [K]	Radius R/R $\odot$	Luminosity L/L $\odot$
3 – 2	440M – 3bn	10,000 – 7,500	2.7 – 1.7	55 – 8

### 14.3 Spectral Characteristics of the A-Class

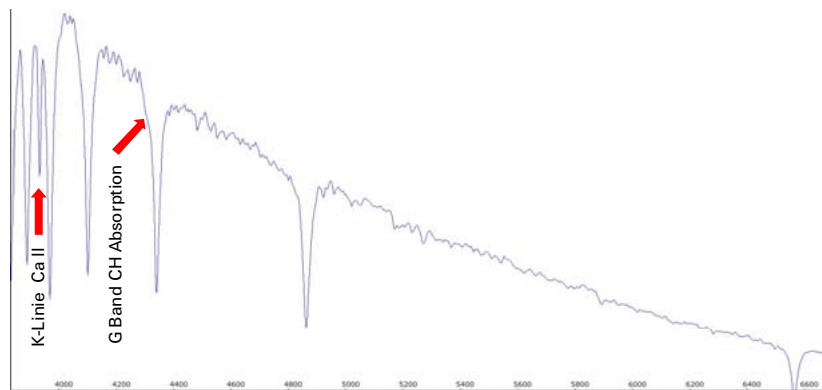
Since the beginning of spectroscopy in the 19th century this class has fascinated by their impressive hydrogen lines, but otherwise very "tidy" and esthetically looking spectra. This was at least one reason for numerous false hypotheses. Father *Angelo Secchi* already classified these spectra in the mid-19th Century as "*Type I*" (see appendix 34.3). Edward Pickering labeled these in his later refined system as "*A-Type*". Today, this class has still Pickering's "*A-label*", but unobtrusively in the upper middle of the MK-stellar classes.

These distinctive and clear spectra are very well suited as a didactic introduction to the practical spectroscopy. Moreover, the pattern of the strong *H-Balmer* lines is an excellent aid for first calibration attempts. This feature gains intensity since the late *B-class* and reaches its maximum in type A2 [1]. Quantum mechanically, this can be explained with the surface temperature of about 9,800 K. This way the hydrogen atoms are thermally excited so that a maximum number of electrons stay already on the level  $n_2$ , the "takeoff level" for the electron transitions in the shell system  $n_2 - n_\infty$  of the *H-Balmer* series [30].

From here on, the later *A-classes* are characterised by a gradual, but still moderate intensity loss of the *H-Balmer* series. Conversely, the two Fraunhofer *H + K* lines of *Ca II* become significantly stronger. The Fraunhofer *K*-line penetrates now deeper into the continuum peak between *H $\epsilon$*  and *H $\delta$*  and exceeds between *A7* and *F0* the intensity of the hydrogen absorption. Within the same range also the growing Fraunhofer *H*-line ( $\lambda$  3968) overprints now the weakening *H $\epsilon$*  absorption. In the late *A-classes* the "Blue Wing" of the *H $\gamma$*  line shows a small kink. At the latest in the *F0* class, it's revealed as the fast growing molecular *CH-absorption* of the Fraunhofer *G-band* (in the following graph marked with red arrow).

Higher resolved spectra show immediately that the first impression of the "simple spectrum" is deceptive. The continuum between the hydrogen lines is interrupted by numerous metal absorptions. The absorptions of neutral atoms become now more intensive at the expense of the singly ionised ones. In the early subclasses, a few *He I* lines still appear but very faintly. The intensity maximum of the real continuum moves here already to the "blue" short wave edge of the visible spectrum. The graph shows the theoretical continuum for a

synthetic *A5V* standard star (*Vspec Tools/Library*). Marked with red arrows are the two above-mentioned details.

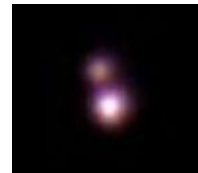


## 14.4 Commented Spectra

Table 20: Castor ( $\alpha$  Gem) and Altair ( $\alpha$  Aql)

The development within the A-subclasses is demonstrated here by a montage of two overview spectra (200L grating), representing an early and late subtype.

Castor (52 ly) is a very rare 6-fold star system. The two brightest components can be resolved even in smaller amateur telescopes (own picture by C8, and Meade DSI II). They dominate the spectrum and their early A-classifications, *A1Vm* and *A2Vm*, are very similar. The surface temperature – some 9,800 K – is therefore similar as for *Sirius* (*A1Vm*).



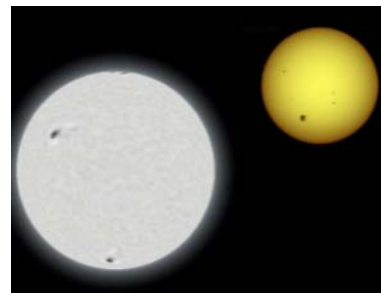
Altair (17 ly) is an *A7V Main Sequence Star* of the late A-Class. Correspondingly lower is therefore the surface temperature of some 7,550 K. For this late A-class it shows an extremely high apparent rotation speed of 210 km/s [506]. The equatorial diameter is therefore enhanced by about 22% (interferometric survey in 2007 by J. Monnier et al.).

Table 21: Detailed spectrum of Sirius A ( $\alpha$  CMa)

Sirius A (8.6 ly), spectral type *A1 Vm* with a surface temperature of about 9,880 K, is similar to Vega and Regulus, a Dwarf star on the *Main Sequence* of the *HRD*. It forms the main component of a binary system with *Sirius B* (White Dwarf).

The table shows an overview spectrum (200L grating) and two higher-resolved profiles in the blue/green and red wavelength domain (900L grating). Within the blue/green part most of the interesting metal absorptions are concentrated.

They look very slim, compared to the huge *H*-Balmer lines. Here, as well as in the spectrum of castor, the so-called *magnesium triplet* appears, still faintly, for the first time at  $\lambda$  5168 – 83 (Fraunhofer **b**).



*Sirius* is one of the metal-rich stars, which are labeled with the suffix [m] (see *Table 23*). Computer graphic Wikipedia: *Sirius* compared in size to the *Sun*.

Its apparent rotation speed of about only 13 km/s is unusual low for the early A-Class. According to [1] however, such statistical outliers correlate significantly with an overabundance of metals.

The line identification is based amongst others on [1], [5], [50], [51], [52],

TABLE 20

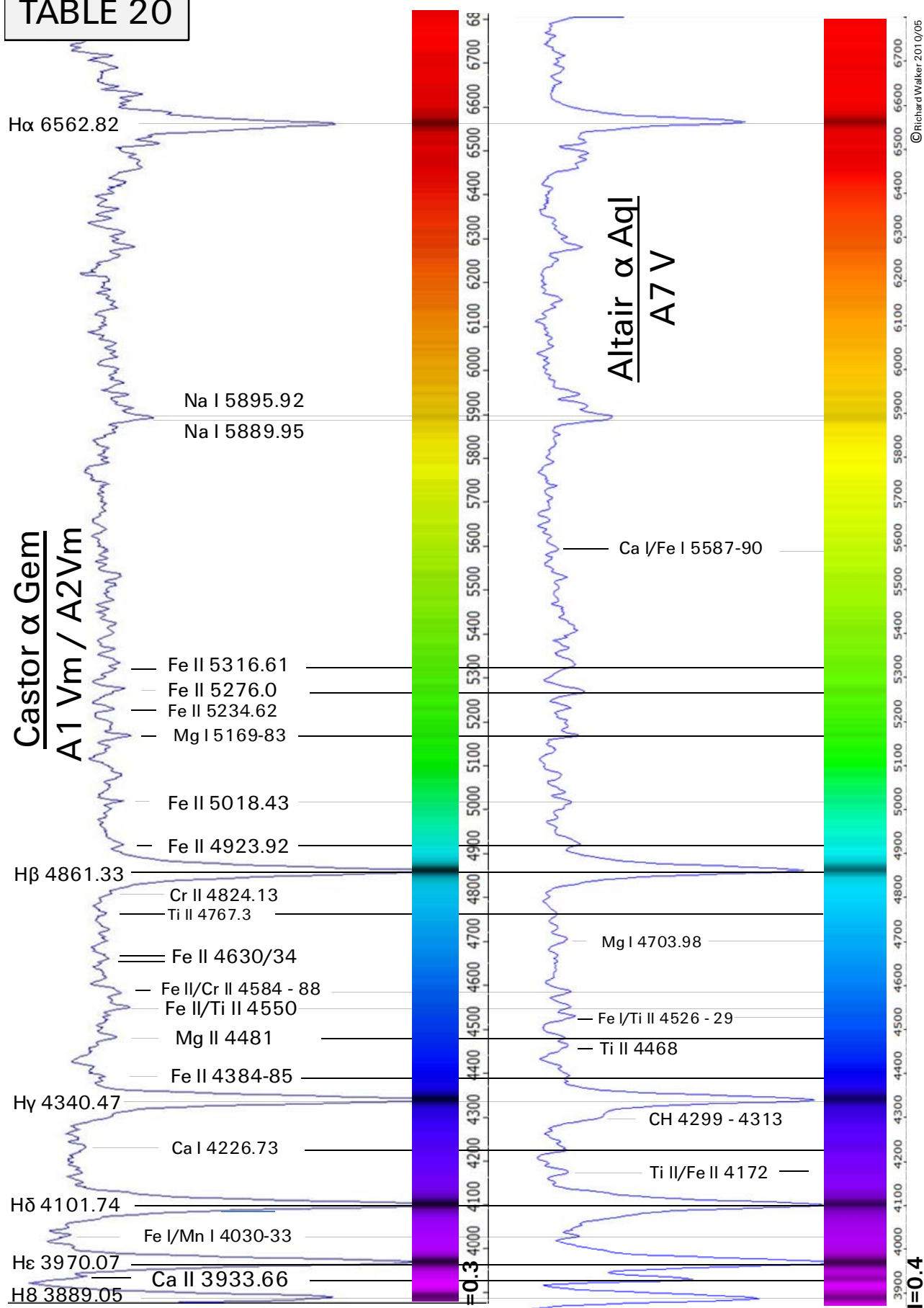


TABLE 21

H $\alpha$  6562.82Telluric O<sub>2</sub>

Na I 5895.92

Na I 5889.95

He I 5876

Sirius  $\alpha$  CMa  
A1 Vm

H $\beta$  4861.33

Fe II 4630/35

Mg II 4481

Fe II 4384-85

H $\gamma$  4340.47H $\delta$  4101.74

He 3970.07

Fe II/Cr I 4666

Fe II 4634.6

Fe II 4629.9

Cr II 4617/19

Cr II 4588

Fe II 4583.8

Ti II 4571.97

Fe II 4556

Fe II 4550

Fe II 4541

Fe II 4534

Fe II 4520/23

Fe II 4515

Fe II 4508

Ti II 4501.27

Fe II 4489/91

Mg II 4481

Ti II 4470

Fe II 4451

Ti II 4444

Fe II 4416.8

Ti II 4400.63

Ti II 4395.04

Fe II 4384-85

Ti II 4375.35

Fe II 4366.17

H $\gamma$  4340.47

Sc II/Ti II 4314

Ti II 4307.9

Fe II 4303.2

Ti I 4289

Fe I 4271-72

Fe II/Cr II 4258/62

Fe I 4250 - 51

Cr II 4242.38

Fe II 4233.17

Ca I 4226.73

Sr II 4215.77

Fe I 4198.31

Fe I 4187.04

Fe II/Cr II 4178-79

Fe II 4173.1

Fe I 4152 - 61

Fe I 4143-44

Si II 4128/31

H $\delta$  4101.74

Sr II 4077.71

Fe I 4071.74

Fe I 4067.6

Fe I 4062.4

Mn I 4055.54

Fe I 4045.82

Mn I 4031 - 36

Ti II/V II 4023/24

Cr II/Ti II 4012

Fe I 4002/05

He 3970.07

Cr II 3945

Ca II 3933.66

Fe II 5316.61

Fe II 5276.0

Fe II 5234.62

Fe I 5227.19 V

Fe II 5197.6

Mg I 5183.60

Mg I 5172.68

Mg I 5167.32

Fe II 5100.66 V

Si II 5056.02

Si II 5041.06

Fe II 5018.43

Fe II 5002/4

Fe I 4957 V

Fe I 4933 V

Fe II 4923.92

Fe II 4890 V

H $\beta$  4861.33

Cr II 4824.13

Ti II 4807

Ti II 4793



**Table 22:** Luminosity effect on spectra of the early A-class: *Vega* ( $\alpha$  Lyr), *Ruchbah* ( $\delta$  Cas) and *Deneb* ( $\alpha$  Cyg).

*Vega* (25 ly) is classified with *A0V* and is, like our Sun, a so-called *Dwarf* on the *Main Sequence* of the *HRD*. Its surface temperature is about 9,500 K its apparent rotational speed at the equator with some 15 km/s is very low. However, recent interferometrical studies show that's why we see *Vega* almost "Pole on" and the *effective* rotational speed is >200 km/s.

*Ruchbah* (100 ly) is classified with *A5 III-IV*. Thus it's moving in the *HRD* on the way from the *Main Sequence* to the *Giant Branch*. Its surface temperature is about 8,400 K. Its rotation speed is indicated by *Kaler* [506] with 113 km/s, an inconspicuous value for this class.

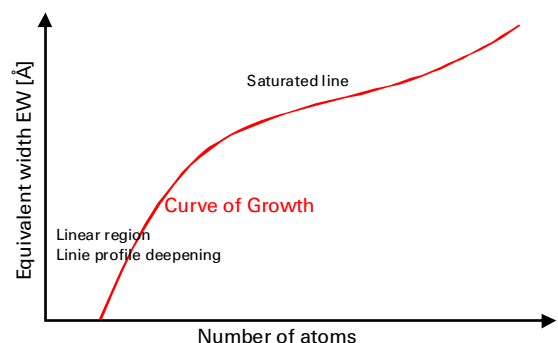
*Deneb* (2,000 ly) is classified with *A2 Ia* and thus belongs to the *Supergiants*. The surface temperature is about 8,500 K. The apparent rotation speed is indicated with about 21 km/s. This *Supergiant* was during its former stay on the *Main Sequence*, an early *B*- or even a late *O*-star [506].

The comparison of these three equally normalised spectra shows clearly a *decrease* of the *intensity* and *width* of the *H*-lines by *increasing* luminosity. Conversely the metal lines in the *Giant* become more intense, what is expected due to the less dense stellar atmosphere and thus a lower *pressure* and *collision broadening*. Due to the relatively moderate  $v \sin i$  values the *rotational broadening* has here not a dominant influence on the appearance of the profiles.

**Table 23:** Different metal abundance of *Vega* and *Sirius*

The comparison of the "metallicity" between *Vega* and *Sirius* has been the subject of numerous professional studies in the past, such as [703], [704]. Besides the different metal abundance these two stars are almost equally classified and have also a similarly low, apparent rotation speed. Differences in the spectrum must therefore primarily be caused by the different metal abundance, which predestines the two bright stars for such investigations.

At this resolution (900L grating) it can immediately be noticed, that the *Ca II* line (Fraunhofer *K* at  $\lambda$  3933) in the *Vega* spectrum is *much intenser*, even though the star is classified slightly earlier than *Sirius*. This is already visible, even without measuring of the *EW* values. But most, *if not all* other metal absorptions, are significantly stronger in the profile of *Sirius*. The graph shows the shape of the so-called "*Curve of Growth*" according to *Keith Robinson* [3]. We are interested here only in the approximately linear range, covering the area of the *unsaturated* spectral line in the left part of the graph. Here the *EW* of a particular spectral line is nearly proportional to the number of atoms of the corresponding element within a certain gas mixture.



A Chinese study by *H. M. Qiu* et al. [703] summarises that *Sirius*, with a *Fe/H* ratio of +0.5 is relatively metal rich, *Vega* with a ratio of -0.57, however, is relatively metal poor. Here is also confirmed that for *Sirius* *Ca* and *Sc* are *underabundant* and vice versa *Fe overabundant*. According to this study this *deficit* of *Ca* and *Sc* and the *overabundance* of *Fe* are generally used as defining markers for metal rich *Am stars*. The Fraunhofer *Ca II* line ( $\lambda$  3934) also serves in various other studies as an important indicator of metal abundance.

TABLE 22

Effect of the luminosity on spectra of the A-class

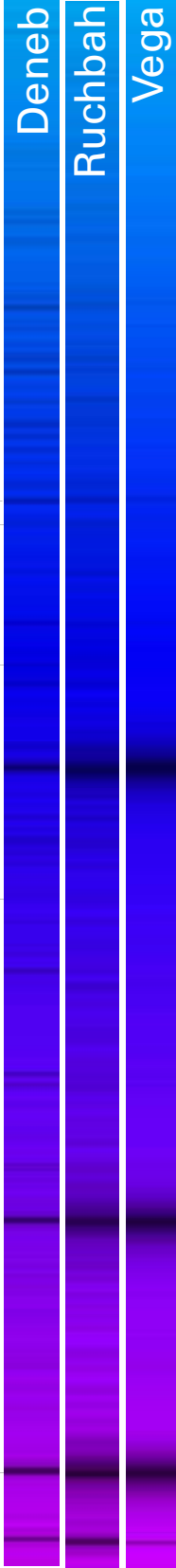
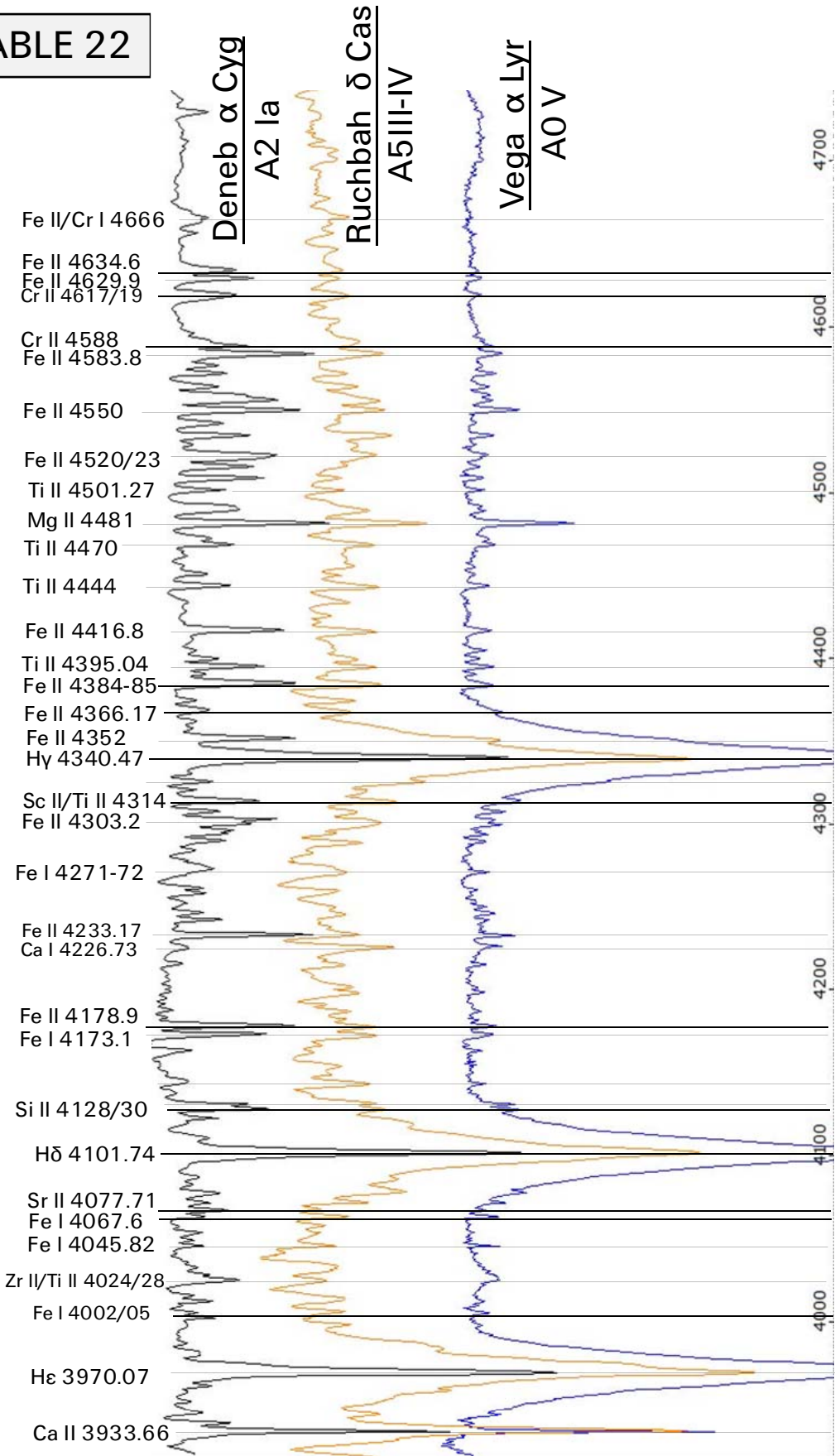
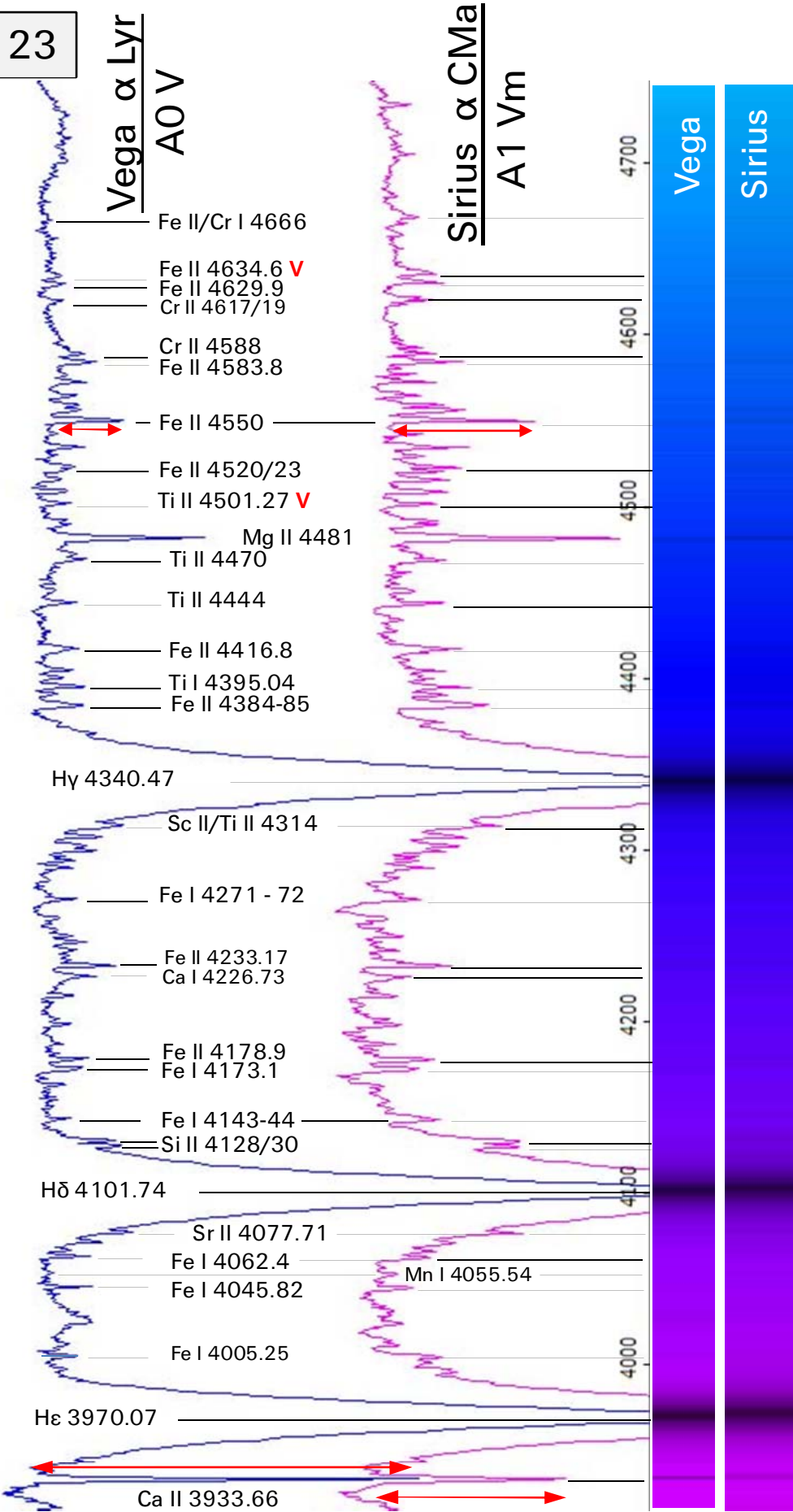




TABLE 23

Comparison of metallicity Vega vs. Sirius



## 15 Spectral Class F

### 15.1 Overview

The *F*-class is located directly above the *G*-category, where our Sun is classified. It includes several well-known, bright yellow shining stars like *Procyon*, *Caph* ( $\beta$  Cas), *Porrina* ( $\gamma$  Vir), *Mirfak* ( $\alpha$  Per), *Canopus* in the southern sky and even the *Pole Star*. On the *Giant Branch* of the *HRD* we find here several pulsation variables, belonging to the categories of  $\delta$  Cephei and RR Lyrae.

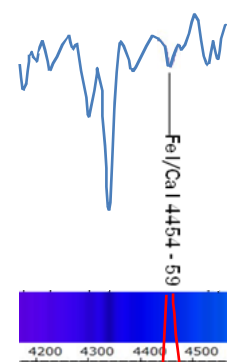
### 15.2 Parameters of the Early to Late F-Class Stars

The following table shows the data exclusively for the *Main Sequence Stars* of the *F*-class, compared to the Sun ( $\odot$ ) and according to [701].

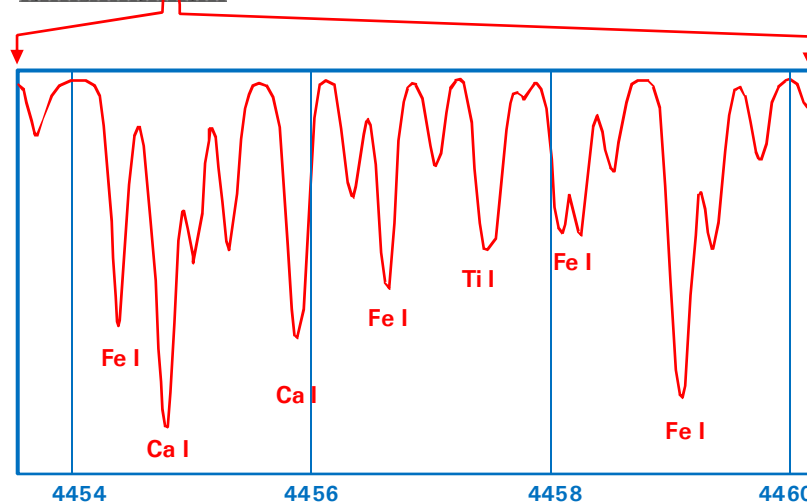
Mass M/M $\odot$	Stay on main sequence [y]	Temperature photosphere [K]	Radius R/R $\odot$	Luminosity L/L $\odot$
1.6 – 1.1	3bn – 7bn	7,200 – 6,000	1.6 – 1.2	6.5 – 2.0

### 15.3 Spectral Characteristics of the F-Class

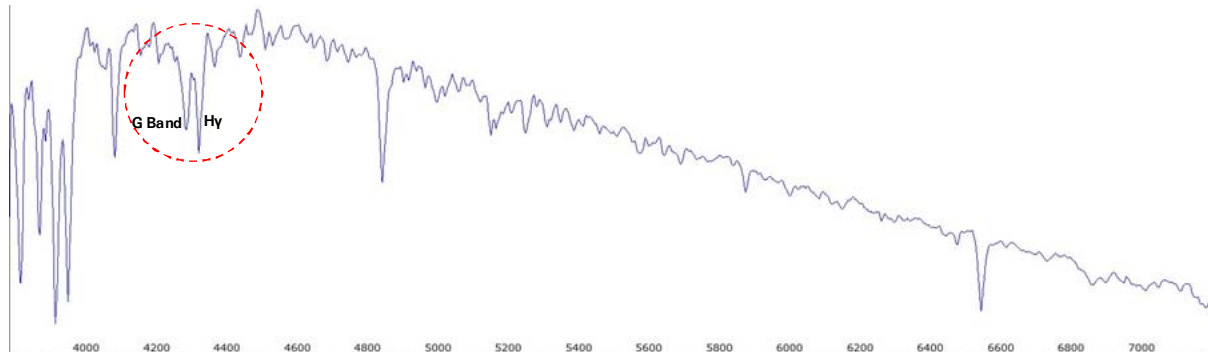
The H-Balmer lines are now much weaker and the Fraunhofer *H + K* lines (*Ca II*) become the dominant features, so that the Fraunhofer *H* absorption now clearly displaces the *H $\epsilon$*  line. Towards the late subclasses the *neutral* elements, e.g. *Fe I*, *Cr I*, replace now increasingly the absorption of the *ionised* ones. The *Ca I* line at  $\lambda$  4227 clearly intensifies, as well as the *G-band* (*CH* molecular) which surpasses within the *F*-Class the intensity of the neighboring *H $\gamma$*  line. This striking "line double" can therefore only be seen here so it forms essentially the unmistakable "Brand" of the *F*-class! The *Magnesium Triplet* ( $\lambda$  5168–83) becomes here stronger, compared to the *A*-Class.



At this resolution, at the latest since the early *A*-class, most of the absorptions are formed by *several* metal lines of slightly different wavelengths, so called "blends". These can only be resolved with high-resolution spectrographs. Labeled here are therefore only the chiefly involved elements, causing these blends. In *Table 30*, one of the absorption lines within the *Procyon* profile is summarily labeled with *Fe I/Ca I* 4454 – 59 (small graph left). The large graph below shows a highly resolved profile (*Spectroweb* [59]) in the corresponding wavelength domain. The imagination of isolated single lines must be abandoned here!



The intensity maximum of the real continuum is now clearly located within the visible range of the spectrum. The graph shows the theoretical continuum for a synthetic *F5 V* standard star (*Vspec/Tools/Library*). Highlighted with a red circle is here the "Line-double" of the *G-band* and *H $\gamma$* , the striking "Brand" of the *F*-class.



## 15.4 Commented Spectra

Tafel 30: *Adhafera* ( $\zeta$  Leo) und *Procyon* ( $\alpha$  CMi)

The development of the *F*-subclasses is demonstrated here by two superposed overview spectra (200L grating) representing an early and middle subtype.

*Adhafera* (260 ly), classified as *F0 III*, is located at the top of the *F*-class and has already reached the Giant stage (III). The surface temperature is about 7,030 K and its apparent rotation speed some 84 km/s [506]. Even within this early *F*-class, the Fraunhofer-*H* and *K* lines have already *surpassed* the intensity of the *H*-Balmer series, where the *K*-line at  $\lambda$  3968 has overprinted the *H $\epsilon$*  absorption.

*Procyon* (11 ly) is classified as *F5 IV-V* and thus representing approximately the "center" of the *F*-class. Like *Sirius*, it has a white dwarf companion. The luminosity class IV-V reveals that it has begun to leave the *Main Sequence* in the *HRD* towards the *Giant Branch*. The apparent rotation speed is only some 6 km/s. The surface temperature with about 6,630 K is expectedly lower than for the earlier classified *Adhafera*. At the first glance this has little effect on the spectral profile.

The most noticeable and important difference relates to the "Brand" of the *F*-class - the increasing intensity of the *CH* molecular absorption band (at  $\lambda$  4300) and conversely the shrinking of the neighboring *H $\gamma$*  line. Further the growing intensity of the *Ca I* line ( $\lambda$  4227), at this resolution clearly visible only by the somewhat colder *Procyon*. Some further differences may be caused by the difference in luminosity class.

Line identification:

The line identification is based amongst others on [1], [5], [51], [52], [59]

TABLE 30

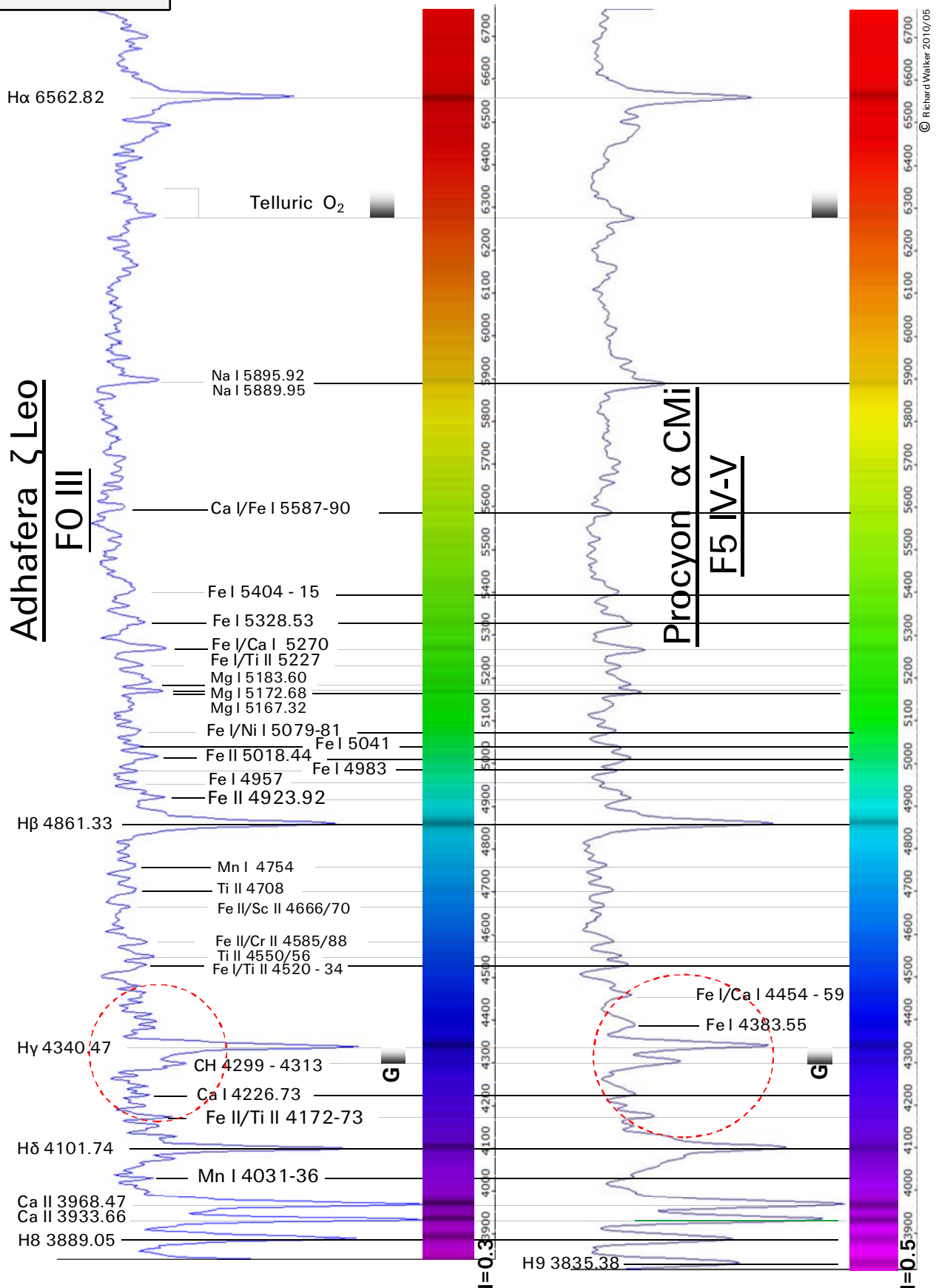


Table 31: Effect of the luminosity on spectra of the *F*-class: *Porrima* ( $\gamma$  Vir), *Caph* ( $\beta$  Cas) and *Mirfak* ( $\alpha$  Per).

*Porrima* (39 ly) is classified with *F0V* and is, like our Sun, a *Dwarf* on the *Main Sequence* of the HRD. Its surface temperature is about 7,100 K and its apparent rotation speed remains here unknown.

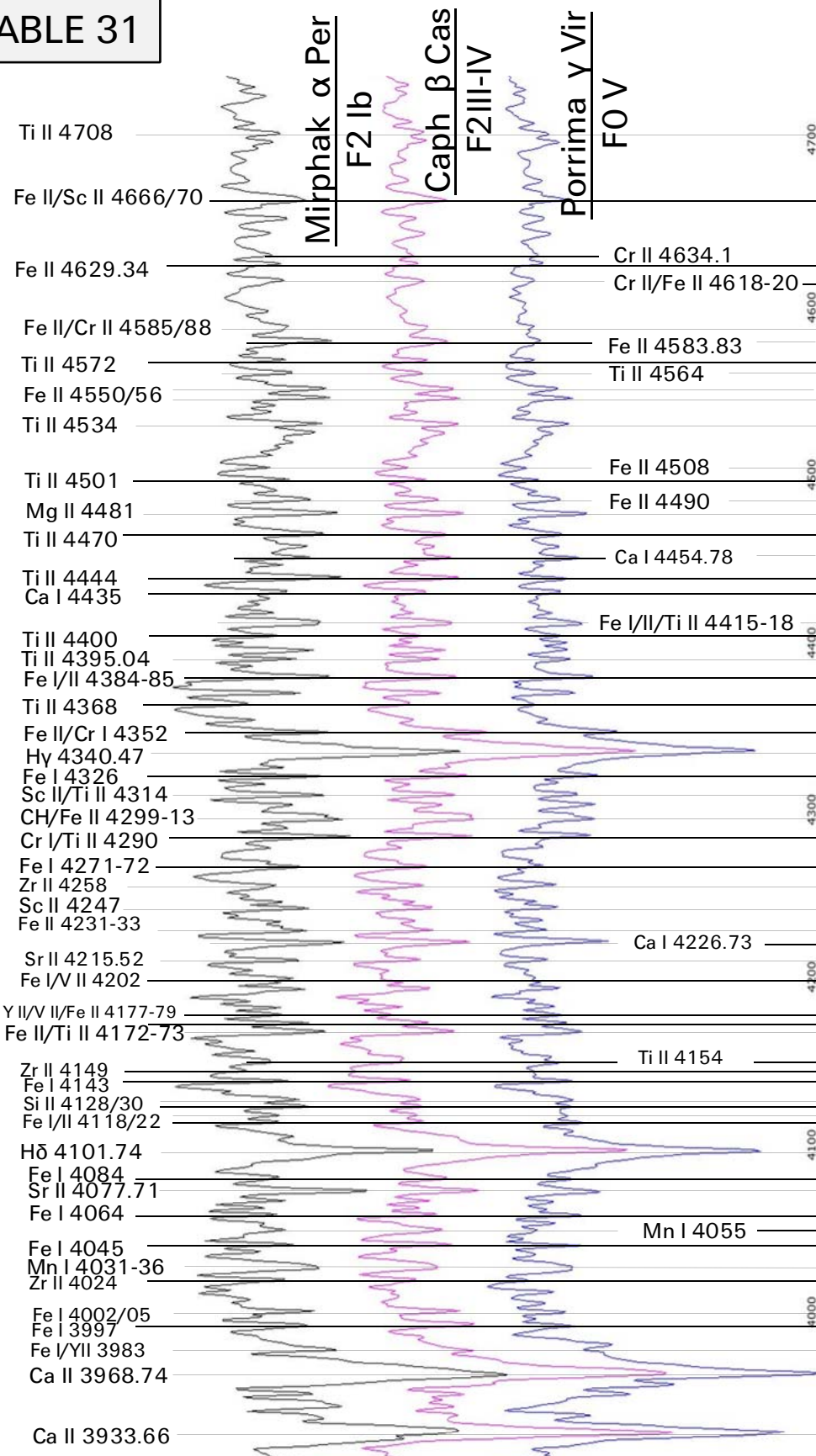
*Caph* (55 ly) is classified with *F2 III-IV*, thus moving from the *Main Sequence* to the *Giant Branch* in the HRD. Its surface temperature is about 6,700 K. His apparent rotation speed is reported by *Kaler* [506] with 70 km/s.

*Mirfak* (600 ly) is classified with *F2 Ib* and therefore one of the *Supergiants*. The surface temperature is about 6,180 K. The apparent rotation speed is reported with 18 km/s. *Mirfak* is a former *Main Sequence Star* of the *B*-Class [506].

The comparison of these three equally normalised spectra shows no striking differences between the luminosity classes. A difference regarding the intensity and width of the H-lines is here *visually* not recognisable. The metal lines of the *Supergiant Mirfak* are somewhat more intensive than in the profile of the *Giant Caph*. Between *Caph* and the *Main Sequence Star Porrima* differences are hardly discernible.

TABLE 31

Effect of the luminosity on spectra of the F-class





## 16 Spectral Class G

### 16.1 Overview

The yellow shining stars of the *G*-class have, from a spectroscopic view, a special status, because their spectra are more or less similar to that of our Sun, which is probably one of the best explored and documented.  $\alpha$  *Centauri* in the southern sky is with *G2V* equally classified as the Sun. It shows therefore nearly the same surface temperature like our central star. In the northern sky *Muphrid* ( $\eta$  *Boo*) with *G0 IV* is classified relatively close to the Sun. Otherwise among the bright stars no further similar classified can be found. *Capella* with its two binary components of *G5IIIe* and *G0III* is already settled on the *Giant Branch* of the *HRD*. The same applies for *Sadalsuud* ( $\beta$  *Aqr*) with *G0Ib*.

Other well-known *G*-stars can only be found in the classes *G7* and later, such as *Kornephoros* ( $\beta$  *Her*),  $\gamma$  *Leo*,  $\gamma$  *Per*,  $\delta$  *Boo*, *Vindemiatrix* ( $\epsilon$  *Vir*).

### 16.2 Parameters of the Early to Late G-Class Stars

The following table shows the data exclusively for the *Main Sequence Stars* of the *G*-class, compared to the Sun ( $\odot$ ) and according to [701].

Mass M/M $\odot$	Stay on main sequence [y]	Temperature photosphere [K]	Radius R/R $\odot$	Luminosity L/L $\odot$
1.05 – 0.9	7 bn – 15 bn	6,000 – 5,500	1.1 – 0.85	1.5 – 0.66

Striking is the percental *very low mass range*, which is covered by the *G*-class. Nevertheless, the life expectancy and luminosity of the star respond almost grotesquely sensitive to this difference. Our Sun with a surface temperature of about 5,800 K (*G2V*) belongs to the early *G*-class, spending some 7 billion years on the *Main Sequence*.

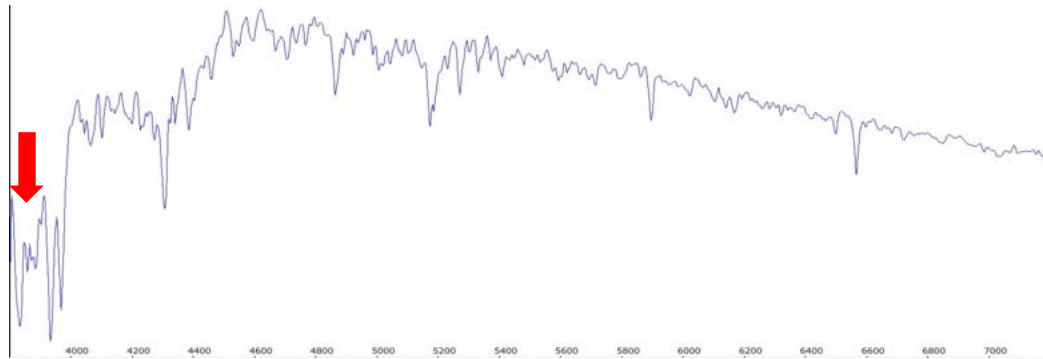
### 16.3 Spectral Characteristics of the G-Class

The Fraunhofer *H* + *K* lines of ionised *Ca II* become here impressively strong achieving theoretically the maximum intensity in the *late G classes*. This becomes also evident in the chart in sect. 6. In the solar spectrum (*G2V*) they are by far the strongest lines generated by the star itself. For *Main Sequence Stars* of the *G*-Class, the *K*-line is always slightly more intense than the *H*-line.

The *H*-Balmer series becomes significantly weaker, so these lines are now surpassed even by various metal absorptions. Therefore they lose from here on their function as welcome orientation marks, e.g. for the calibration and line identification. The intensity of the so-called *Magnesium Triplet* ( $\lambda\lambda$  5169-83) has increased during the *F*-Class and achieves a considerable strength here, so with "*b*" it's even labeled with its own Fraunhofer letter. The *Ca I* line by  $\lambda$  4227 also impressively gained intensity since the early *F* classes and becomes here a striking spectral feature also with an own Fraunhofer letter "*g*".

In general, the trend here continues by growing intensity of *neutral metals* e.g. *Fe I* and the Fraunhofer-*D* lines (*Na I*). Towards the later subclasses they increasingly replace the absorption of the ionised elements. Due to the dominance of fine metal lines, the spectra become now more and more complex. Therefore, our Sun is not really a suitable object for beginners. The temperature here is sunken to such a low level that simple and robust *diatomic* molecules can survive in these stellar atmospheres. Most prominent of such features is the Fraunhofer *G*-band of the *CH molecule*, which already surpassed in the late *F*-class the intensity of the *H $\gamma$*  line. Further mentionable are also the strong *CN* and *CH* absorption bands

in the violet area, overprinting here the  $H8$  and  $H9$  Balmer lines beyond recognition. In highly resolved spectra now finer absorption bands of carbon monoxide  $CO$  appear. The intensity maximum of the real continuum shifts now to the green part of the visible spectrum, hence the evolution has optimised our eyes to this wavelength domain (Sun  $G2V$ ). The graph shows the theoretical continuum for a synthetic  $G5 V$  standard star (*Vspec/Tools/Library*). Highlighted with a red arrow is here the area on the violet side of the H+K Fraunhofer lines, where strong molecular  $CN$  and  $CH$  absorption bands overprint the former  $H8$ - and  $H9$ -Balmer lines.



## 16.4 Commented Spectra

Table 40: *Muphrid* ( $\eta$  Boo) und *Vindemiatrix* ( $\epsilon$  Vir)

The development of the  $G$ -subclasses is demonstrated here by two superposed overview spectra (200L grating) representing an early and late subtype.

*Muphrid* (37 ly) with  $G0 IV$  has already moved away from the *Main Sequence* towards the *Giant Branch* in the *HRD*. Of all naked eye visible stars in the northern sky, it's the closest "class neighbor" to the Sun ( $G2V$ ). Its surface temperature is about 6,100 K, i.e. slightly hotter than our central star – hence the earlier classification. It's a part of a spectroscopic binary. The  $B$ -component however, is so small that, in contrast to *Spica*, no splitting of the spectral lines can be observed (SB1 system). *Muphrid* is classified by several sources as above average metal rich. Nevertheless, the suffix  $m$  is missing here in the classification.

*Vindemiatrix* (103 ly) with  $G8 IIIab$  is a late representative of the  $G$ -class and has already developed to the Giant stage. Its apparent rotation speed is  $<17\text{ km/s}$  [505] what is usual for this class. According to [506] *Vindemiatrix* was formerly a  $B$ -class *Main Sequence Star*.

The comparison of these spectra demonstrates mainly the intensity loss of the  $H$ -Balmer lines, well visible by the  $H\beta$  line. The profile of *Vindemiatrix* shows also a massively shrunken  $H\gamma$  line which is now difficult to identify, particularly besides the now dominant  $G$ -band (CH). Otherwise, no spectacular changes can be seen. However in highly resolved spectra, significant intensity differences of individual lines would be detectable, particularly within the blends.

Table 41 and 42: The Sun, spectra recorded from reflected daylight.

Our central star ( $G2V$ ), with a surface temperature of approx. 5,800 K, is a normal *Dwarf* on the *Main Sequence*. On these tables the Sun is documented with an overview spectrum (200L grating) and three higher-resolved profiles in the blue, green and red domain (900L grating). The Sun has a very low rotation speed of just below 2 km/s, which is usual for middle and late spectral types. The increased thickness of the convective shell generates strong magnetic fields with a considerable breaking effect on the stellar rotation. The image shows a picture in the  $H\alpha$  light by the SOHO satellite. Line identification: is based mainly on [80], [81], [59].

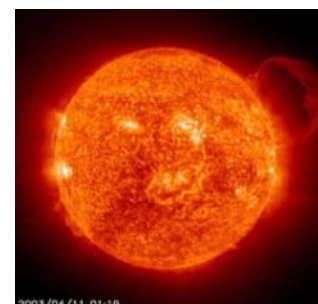


TABLE 40

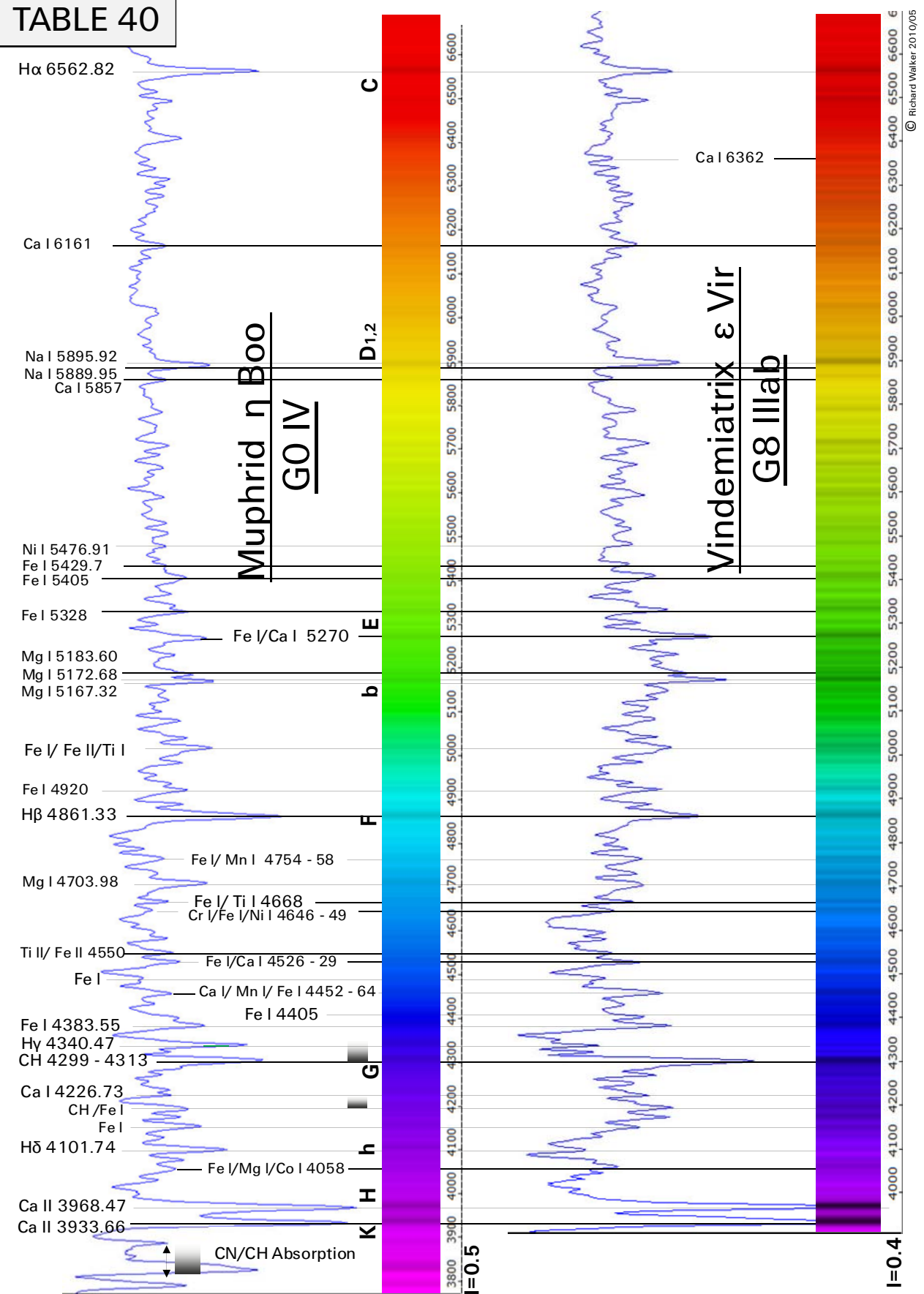


TABLE 41

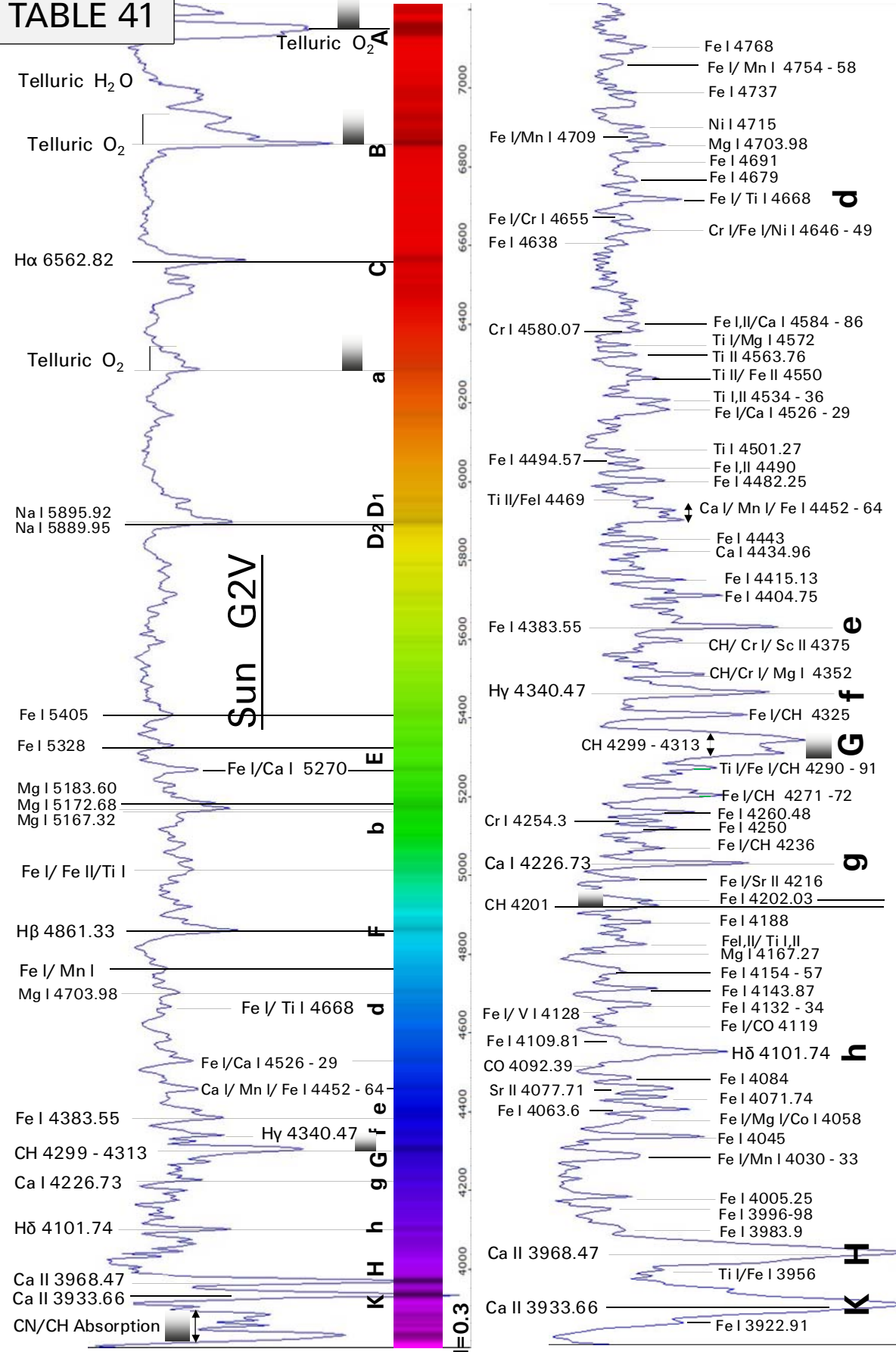
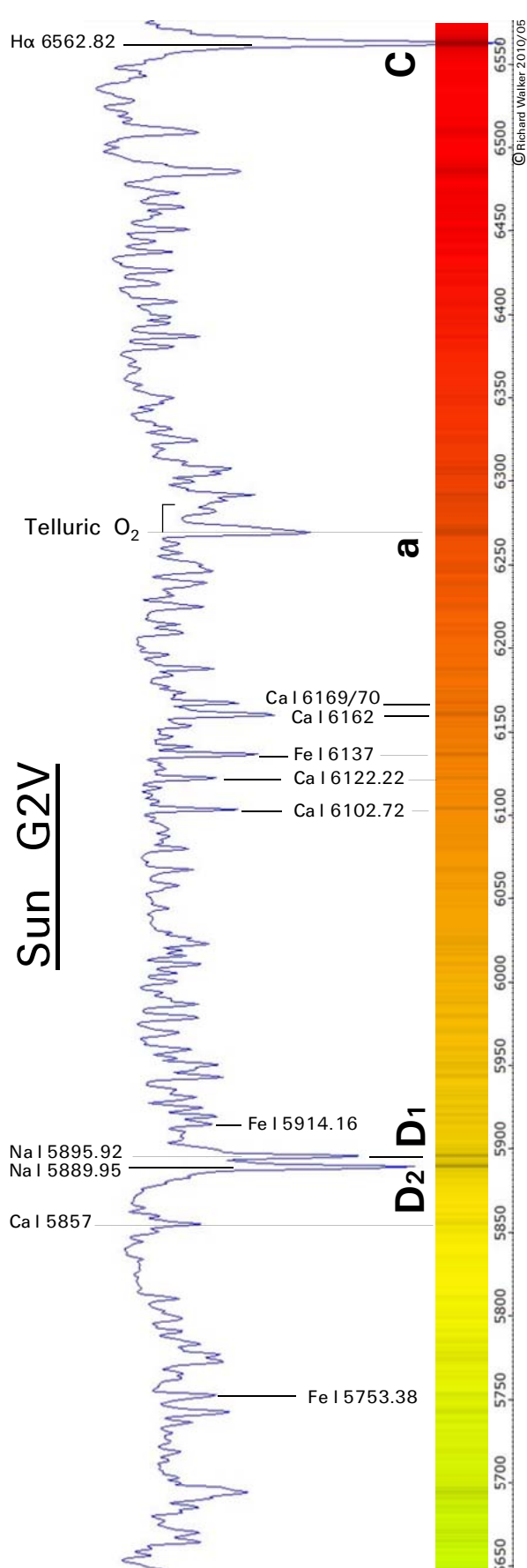
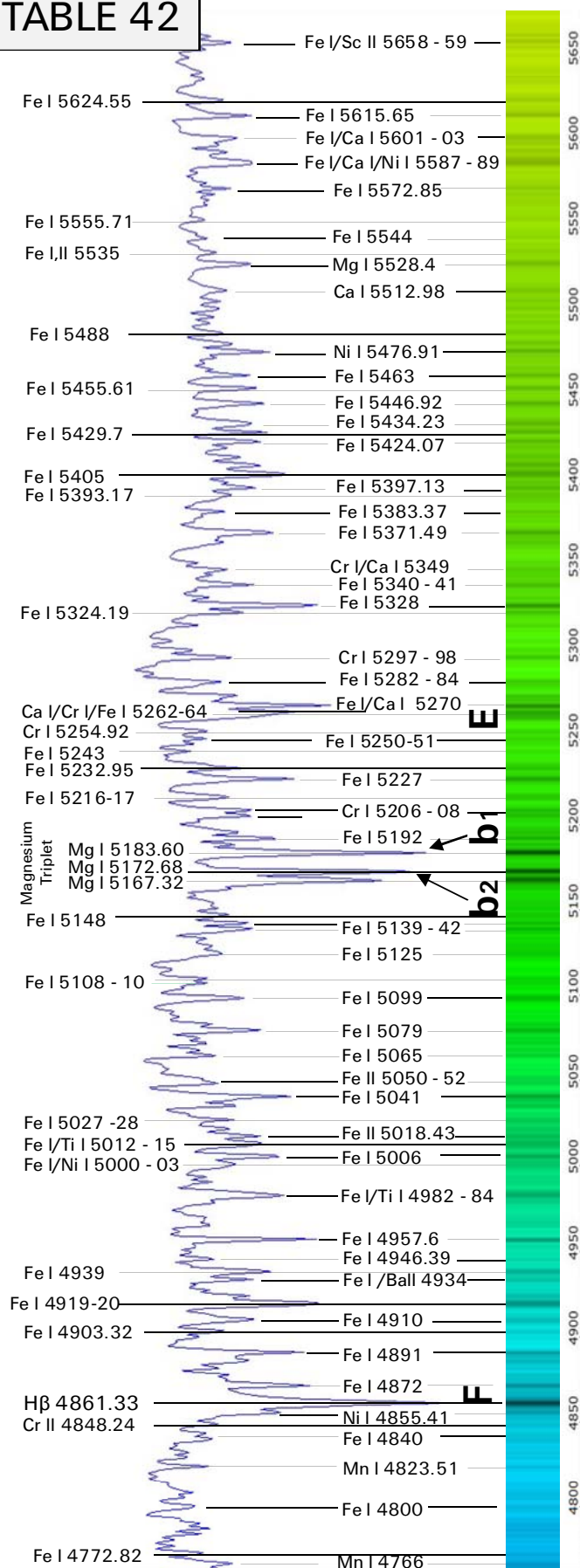




TABLE 42



## 17 Spectral Class K

### 17.1 Overview

The stars of the orange yellow shining *K*-class includes familiar names such as *Pollux*, *Aldebaran*, *Arcturus*, *Hamal*, *Alphard*, as well as the lighter, yellow bright orange component of the famous double star *Albireo A* (K3 II).

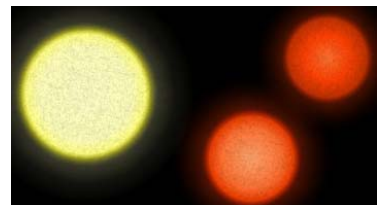
### 17.2 Parameters of the Early to Late K-Class Stars

The following table shows the data exclusively for the *Main Sequence Stars* of the *K*-class, compared to the Sun ( $\odot$ ) and according to [701].

Mass M/M $\odot$	Stay on main sequence [y]	Temperature photosphere [K]	Radius R/R $\odot$	Luminosity L/L $\odot$
0.8 – 0.6	>20bn	5,250 – 4,000	0.8 – 0.65	0.42 – 0.10

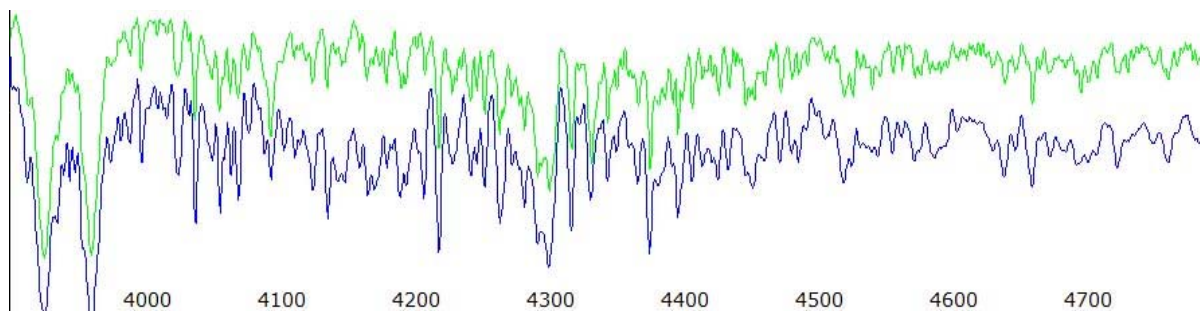
Striking is also here the percental low mass range, which is covered by this class. All *K*-class dwarfs stay longer on the *Main Sequence* than the estimated age of the universe of some 13.7 billion years. This means that in the entire universe, not a single star of this class is migrated to the *Giant Branch*! The luminosity of the *K-Main Sequence Stars* is so low that they are only visible at relatively short distances. Therefore, all above listed "highlights" of this class are located on the *Giant Branch*. These massive stars were classified much earlier during their former stay on the *Main Sequence*. Their parameters are therefore far outside of the table values above. Here they spend only a relatively short time before they explode as a *SN* or end up as *White Dwarfs*.

Only a *few real K-Main Sequence Stars* are visible with the naked eye. In the northern sky the best-known is probably the only 11 ly distant binary *61 Cygni*, with a total apparent brightness of just 4.8<sup>m</sup> and the spectral classes *K5V* and *K7V* (see *Table 52*). The Wikipedia graphic shows the size of the two *K*-class components compared to the Sun.



### 17.3 Spectral Characteristics of the K-Class

The temperature of this class is considerably lower than in the G-category, but still as high as within the solar sunspots. Correspondingly, the spectra of the early K-class look still very similar as in the whole G-category. The following chart shows in the blue short-wave domain the superimposed profiles of Pollux (blue) and Sun (green). Already Fraunhofer has noticed the striking similarity of the two spectra.



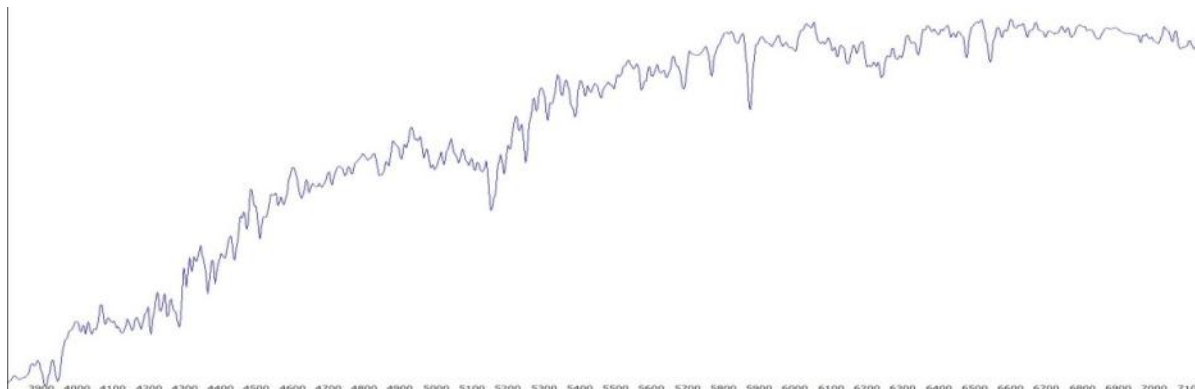


On a glance, the two profiles look indeed very similar, although *Pollux* (K0 IIIb) is a *Giant* and the *Sun* (G2V) is still a *Main Sequence Star*. Apparently the trend continues that the luminosity-related differences in the profiles become increasingly smaller towards later spectral classes.

Within the G- and early K-subclasses apparently no spectacular changes of spectral characteristics take place. Considered more in detail, several differences in the line intensity and in the shape of the continuum become visible. Now the spectral lines are mainly caused due to neutral atoms or by simple *diatomic* molecules. The intensity of the neutral metals continues to increase. The neutral calcium *Ca I* at  $\lambda$  4227 has excelled the G-Band in the class *K5* (detail in Table 50 marked in red). The G-Band becomes now very faint and about at *K5* it's even splitted into several discrete lines. The H-Balmer series is now very weak and difficult to identify, except of the *H $\alpha$* - and the considerably shrunken *H $\beta$*  line. The *Magnesium Triplet* still appears quite prominently.

In the spectra of the later K-subclasses a remarkable break occurs and the similarity to the solar spectrum gets increasingly lost. Since the class *K5* and later, particularly in the long wave-(red) part of the spectrum, titanium oxide (TiO) bands appear and start to overprint the telluric *H<sub>2</sub>O* and *O<sub>2</sub>* absorptions. Therefore already Father *Angelo Secchi* noticed *Aldebaran* (K5III) as a transition star for the appearance of the impressive *TiO* band spectra.

In use are only the classes *K1* - *K5* and *K7*. *K6*, *K8* and *K9* have not yet been allocated. The intensity maximum of the real continuum is shifted here into the red region of the visible spectral range. The graph shows the theoretical continuum for a synthetic *K4 III* standard star (*Vspec/Tools/Library*).



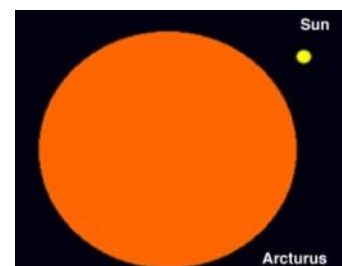
## 17.4 Commented Spectra

Table 50: *Arcturus* ( $\alpha$  Boo) and *Alterf* ( $\lambda$  Leo)

The development of the *K*-subclasses is demonstrated here by two superposed overview spectra (200L grating) representing an early and late subtype.

*Arcturus* (37 ly), classified with *K1.5 III Fe-0.5*, is an early *K*-star and stays on the *Giant Branch* of the *HRD*. Its surface temperature is about 4,290 K. The suffix indicates a relative *underabundance* of *iron*.

Compared to the Sun the *Fe/H* ratio of *Arcturus* is only about 20% [506]. The graph shows the proportions of *Arcturus* compared to the Sun. The apparent rotation speed is given in [505] with <17km/s. Like *Pollux* also the spectrum of *Arcturus* is very similar to that of the Sun. The main differences are in the intensity of individual lines, as already pointed out above.



*Alterf* (320 ly) is a *K5 III* giant of the later *K*-class. Its surface temperature is 3,950 K, almost 340 K lower than that of *Arcturus*. The apparent rotation speed is indicated in [505] with <17 km/s. Such low values are normal for late spectral types and have no detectable effect on the spectra of this resolution.

Particularly the short-wave side of the *Alterf* profile is still dominated by discrete absorption lines, which are mostly the same, as seen in the spectra of *Pollux* and *Arcturus*. However the shape of the continuum in the yellow-red range is already similar to that of *Betelgeuse* and *Antares*, albeit much less intense. This shows the beginning influence of the molecular *TiO* absorption. At this spectral resolution, these absorption bands can be reliably identified only in the near infrared part, close to the telluric A-line which is *outside* of the chart in *Table 50*. The following detailed spectrum of *Aldebaran*, however, shows complementarily this section. With *K5 III* this star has the same spectral class like *Alterf*. The spectrum shows here clearly the absorption bands of titanium oxide *TiO* and calcium hydride *CaH*.

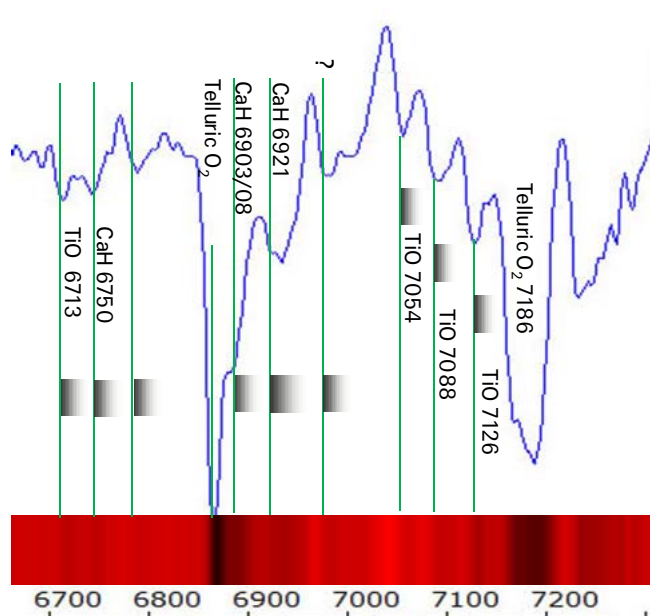


**Table 51:** *Pollux* ( $\alpha$  Gem)

*Pollux* (34 ly) is classified as *K0 IIIb*, an early *K*-star already established on the *Giant Branch* of the *HRD*. Its surface temperature is about 4,770 K. The apparent rotation speed is given in [505] with <17km/s. On this table *Pollux* is documented with an overview spectrum (200L grating) and a higher resolved profile in the blue area (900L grating).

The line identification is based amongst others on [1], [5], [50], [52], [53], [55], [58], [59]

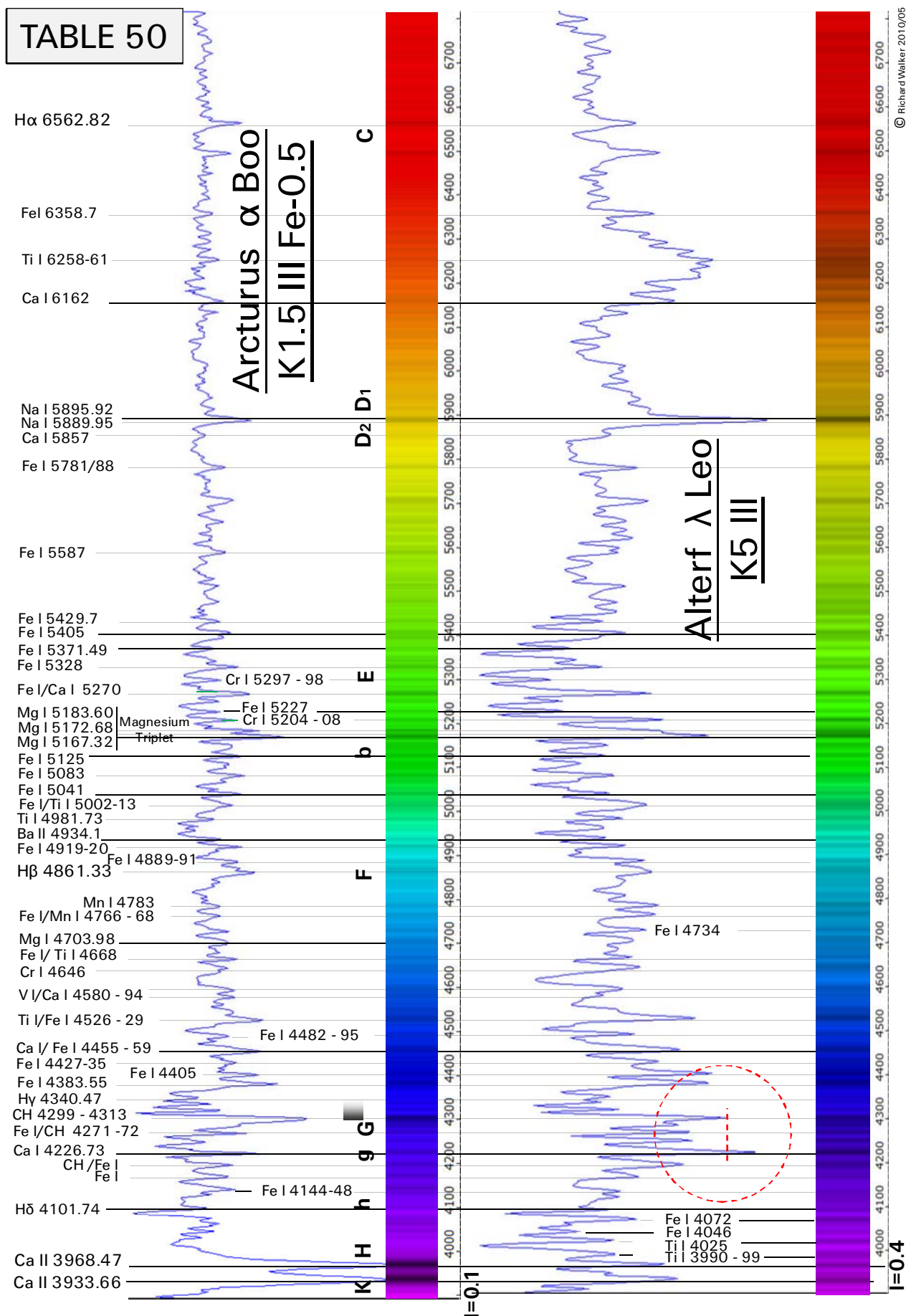


TABLE 51

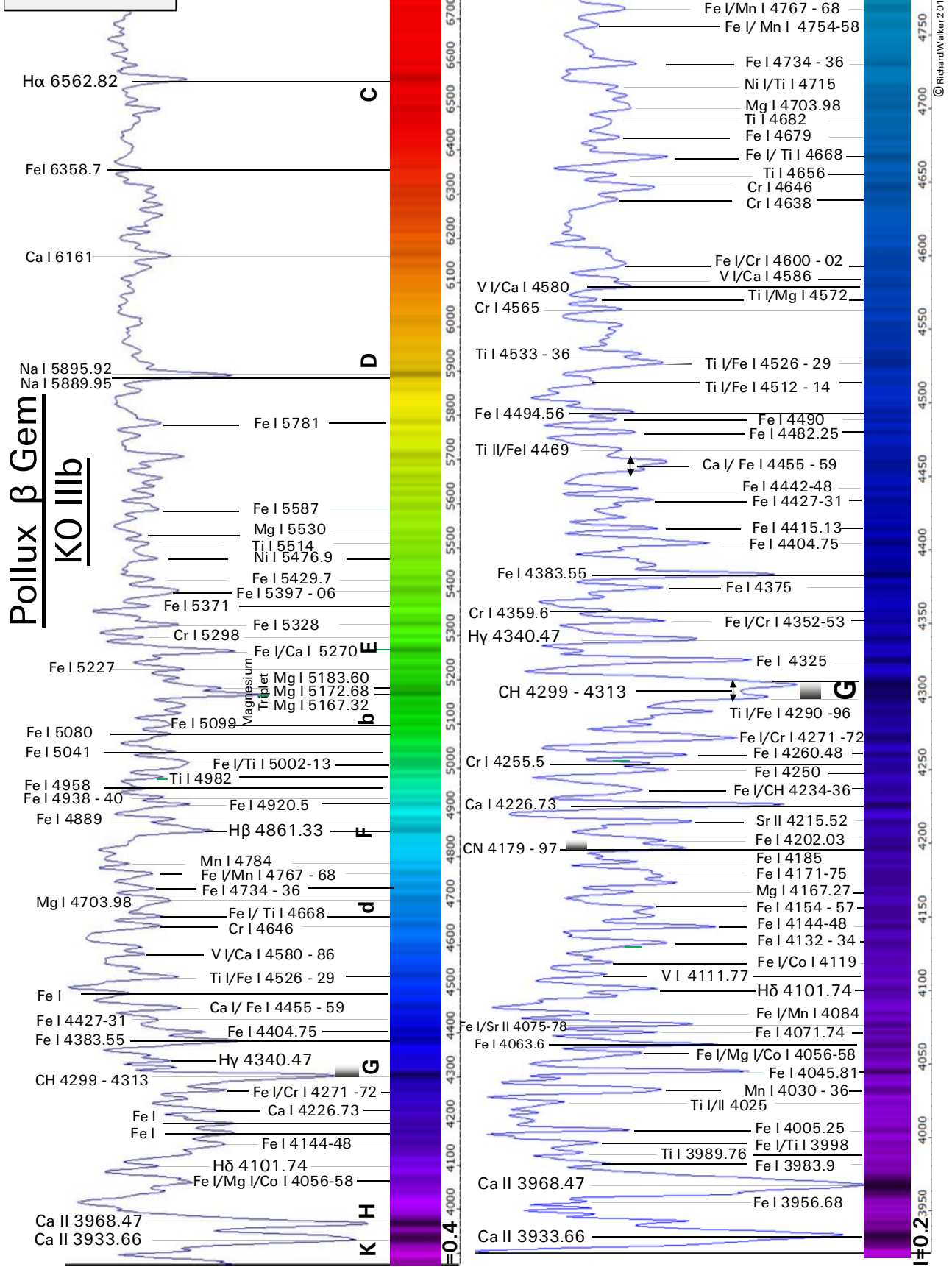


Table 52: Luminosity effects on spectra of the late *K*-class: *Alsciaukat* ( $\alpha$  *Lyncis*) and *61 Cygni B*.

*61 Cygni B* (11 ly) is the weaker of two binary components. With *K7 V* it's classified as an ordinary *Dwarf* on the *Main Sequence*. The surface temperature is some 4,120 K, its apparent rotation speed is <2km/sec. The two components belong to the few true *Main Sequence Stars* of the *K*-class which are spectroscopically accessible to moderate sized telescopes.

*Alsciaukat* (220 ly): This star with the jaw-breaking, Arabic name is classified with *K7 III*, and thus a *Normal Giant*. Its surface temperature is about 3,860 K. Its apparent rotation speed could not be found. Its slight variability suggests that it stands just before a long-period, Mira-type variable stage [506].

The comparison of the two equally normalised spectra shows in this section a similar profile shape for the different luminosity classes. In each section, however, clear differences and even different lines are visible. The spectrum of *Alsciaukat* shows at this resolution (according to BSA) clearly the splitting of the former Fraunhofer *G* -band into *three* discrete absorption lines: *Ti I* ( $\lambda\lambda$  4301 and 4314) and *Fe I* ( $\lambda$  4308).

Table 53: *Aldebaran* ( $\alpha$  *Tau*)

Complementary to *Table 52* some higher-resolved detail spectra of the *K*-star *Aldebaran* (66 Lj) in the green and red region are added here (900L grating). *Aldebaran* with *K5 III* represents the later *K*-class and is established on the *Giant Branch* of the *HRD*. Its surface temperature is about 4,010 K. The apparent rotation speed is given in [505] with <17km/s. The graphic shows the proportions of *Aldebaran* compared to the Sun.

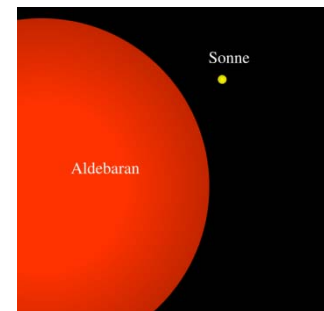




TABLE 52

Effect of the luminosity on spectra of the K-class

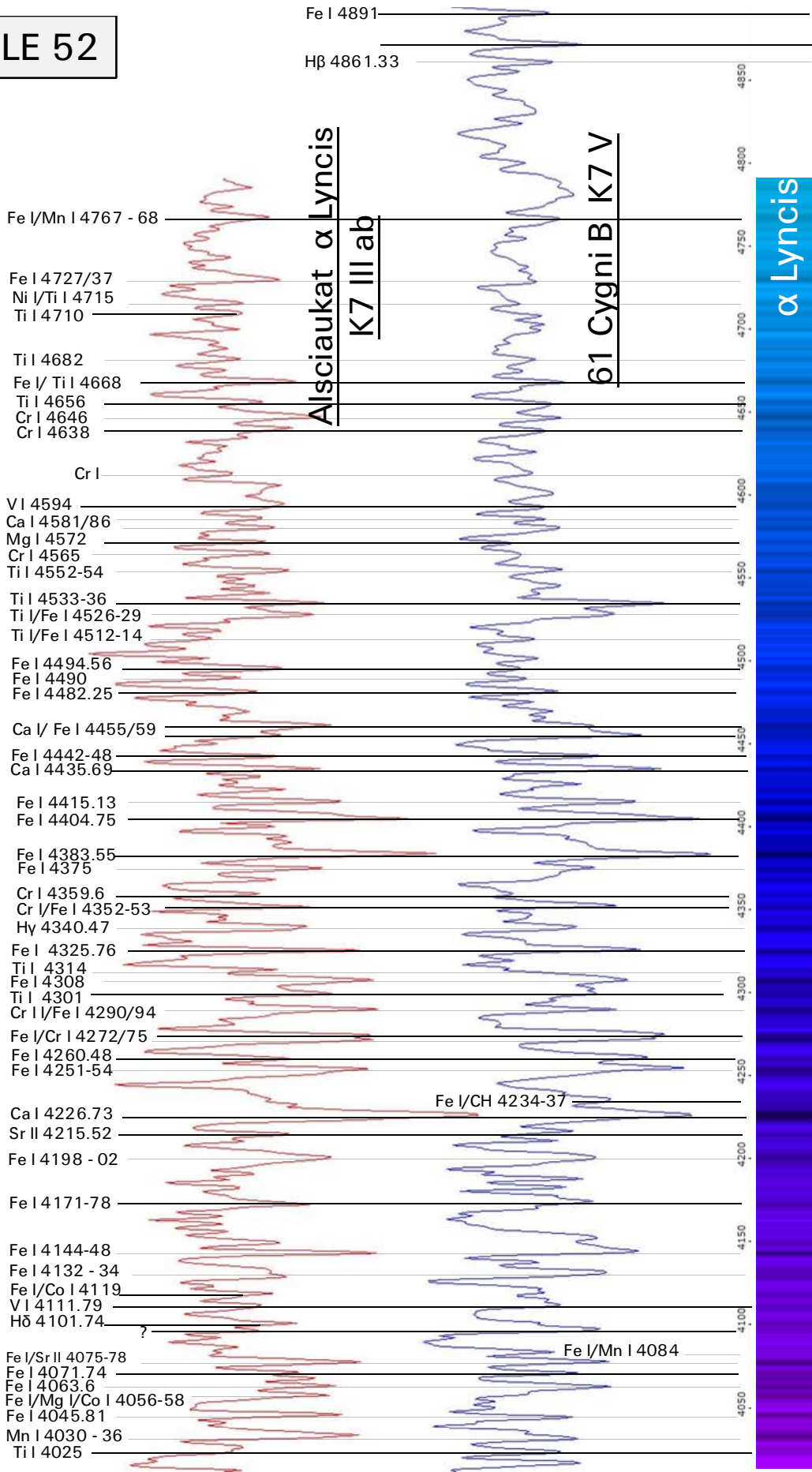
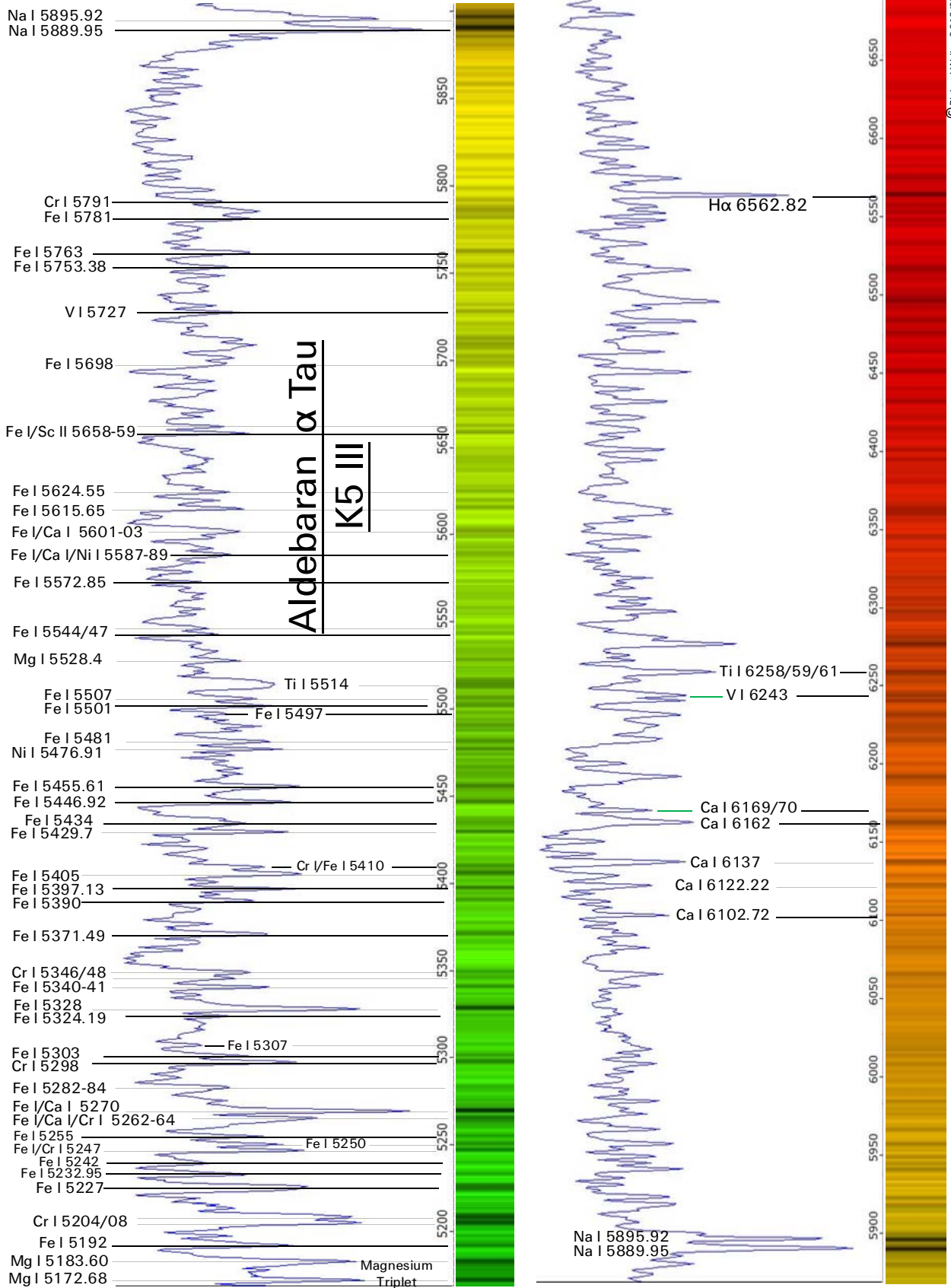




TABLE 53



## 18 Spectral Class M

### 18.1 Overview

Some of the orange-red shining stars of the *M*-class are well-known names such as *Betelgeuse*, *Antares*, *Mirach* ( $\beta$  And), *Scheat* ( $\beta$  Peg), *Ras Algheti* ( $\alpha$  Her), *Menkar* ( $\alpha$  Cet), *Tejat Posterior* ( $\mu$  Gem). Some late types of this class are long period variables such as *Mira* (M7IIIe).

### 18.2 Parameters of the Early to Late M-Class Stars

The following table shows the data exclusively for the *Main Sequence Stars* of the *M*-class, compared to the Sun ( $\odot$ ) and according to [701].

Mass M/M $\odot$	Stay on main sequence [y]	Temperature photosphere [K]	Radius R/R $\odot$	Luminosity L/L $\odot$
0.5 – 0.08	>100bn	3,850 – 2,600	0.63 – 0.17	0.08 – 0.001

Striking is here the huge percental increase of the covered mass range compared to the earlier classes *A*, *F*, *G*, *K*. The "late half" of this class already touches the range limit of the *Brown Dwarfs*, which are separately classified with *L*, *T* and *Y* (not yet be treated here). As the *K*- also the *M*-Dwarfs stay longer on the *Main Sequence* than the estimated age of the universe of some 13.7 billion years. This means that in the entire universe, not a single star of the *M*-class is migrated to the *Giant Branch* in the *HRD*! All with the naked eye visible *M*-type stars are former class *B* to *G* *Main Sequence Stars* which spend here only a relatively short time until the end of their *Giant Stage*. Their parameters are therefore far outside of the table values above.

With the naked eye, no real *M*-type *Main Sequence Stars* are visible, although they provide 76% of the Sun's near neighbors! The most famous and apparently "brightest" representative is in the southern sky *Proxima Centauri* with the spectral class *M5 Ve*. With a distance of 4.22 ly it's the very nearest neighbor to the Sun, but reaching an apparent magnitude of only 11<sup>m</sup>! Therefore, it was discovered very late in 1915.

The graphic (Wikipedia) shows the proportion of *Proxima Centauri* compared to the *Sun*. Its diameter was determined with the *HST* to about 200,000 km. His life expectancy on the *Main Sequence* is estimated to some 4 trillion years! Whether our universe then still exists – in whatever form – must be answered by cosmological models.



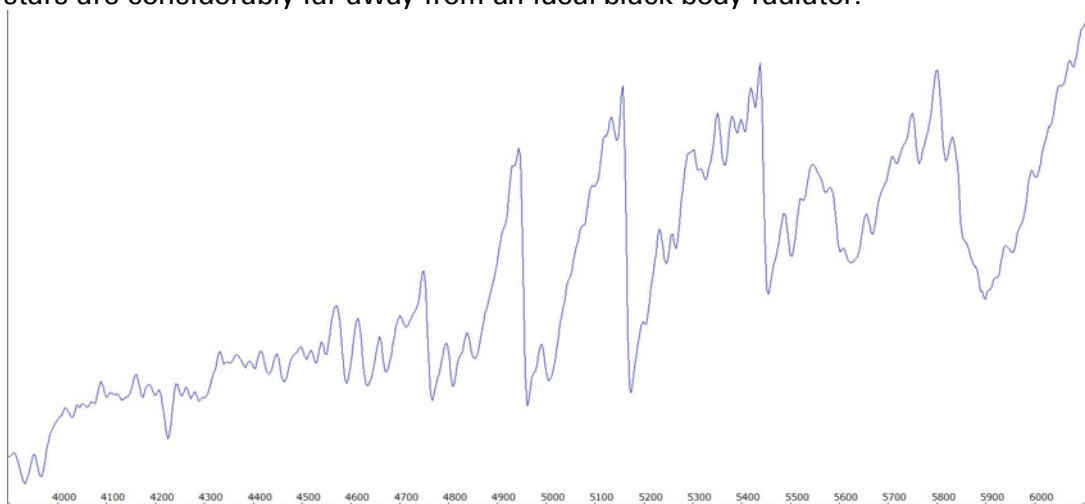
### 18.3 Spectral Characteristics of the M-Class

The Fraunhofer *H* + *K* lines remain striking in the entire *M*-class. In addition to the *H $\alpha$*  line neutral calcium *Ca I* at  $\lambda$  4227 and the sodium double line at about  $\lambda\lambda$  5890/95, are the dominant *discrete* absorptions, which are still visible at this resolution. The once prominent *G*-band breaks now up in at least three discrete lines (BSA). The main features here are undoubtedly the huge absorption bands of *titanium oxide TiO*. Their intensity rises significantly towards the late subclasses, overprinting now thousands of neutral, atomic absorption lines which would otherwise visible here [1]. Although they show up already in the late *K*-classes, they form here the unmistakable "Brand" of the *M*-category. Much less frequent and with smaller intensity we find here a few absorption bands of *CaH* (calcium hydride) and *MgH* molecules (magnesium hydride). In the late *M*-subclasses the lower temperature

allows even the formation of further *diatomic* molecules like *vanadium oxide* (VO) and *molecular hydrogen*  $H_2$ .

The wavelengths of the *absorption bands* are defined by the "*most distinct edges*" the so called *band heads* of the profile. As a result of this characteristic, sawtooth-shaped curve, these *edges* are much more diffuse than discrete absorption lines, which show in theory approximately a Gaussian bell shape. The wavelength values for the individual bands can sometimes vary, depending on the source, up to 2 Å! These absorption bands are therefore totally inappropriate for a precise calibration of the spectrum, based on known lines. Only the calibration with the lamp can meet here reasonable standards.

The intensity maximum of the real continuum is shifted here into the infrared range of the spectrum. Therefore the telluric  $H_2O$  and  $O_2$  absorptions in the red range of the spectrum are almost completely overprinted by the stellar molecular bands. The graph shows the theoretical continuum for a synthetic *M5 III* star (*Vspec/Tools/Library*). Due to the specific radiation characteristics, influenced by the massive gaps in the continuum, the M class stars are considerably far away from an ideal black body radiator.



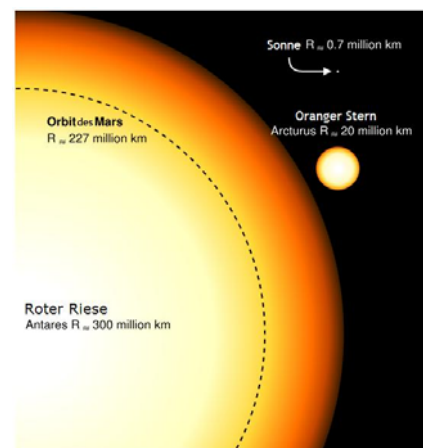
## 18.4 Commented Spectra

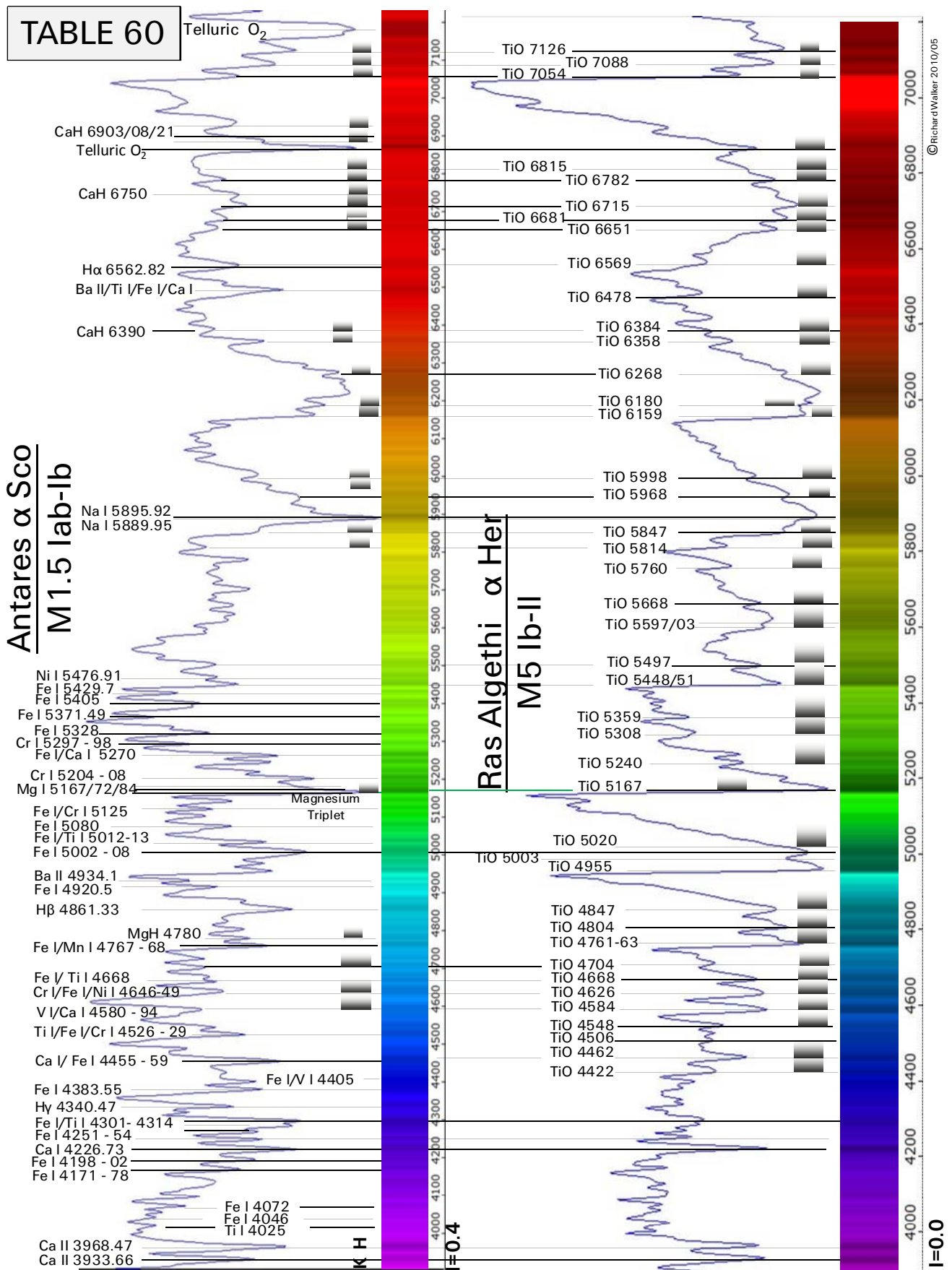
**Table 60:** *Antares* ( $\alpha$  Sco) and *Ras Algethi* ( $\alpha$  Her)

The development of the *M*-subclasses is demonstrated here by two superposed overview spectra (200L grating) representing an early and late subtype.

*Antares* (450 ly) is a *Supergiant* of the early *M*-Class with *M1.5 lab* and the dominant component of a binary star system. Its surface temperature is about 3,600 K. The apparent rotation speed is given in [505] with <20 km/s. The graphic shows the proportions of *Antares*, compared to *Arcturus* and the Sun.

*Ras Algethi* (400 ly) is a multiple star system. The spectrum is dominated by the *Supergiant* classified as *M5 II* and represents a later *M*-Type. As expected its surface temperature of 3,300 K is lower than by the earlier classified *Antares*. *Ras Algethi* is smaller than *Antares*, but also surrounded by a cloud of gas and dust. The line identification is based amongst others on [1], [5], [50], [52], [53], [55], [58], [59], [61]





## 19 Spectral Sequence on the AGB

### 19.1 Evolution of the Stars on the Asymptotic Giant Branch (AGB)

The following simplified presented sequence is applicable for stars with 1 to 8, depending on the source, even up to about 10 solar masses.

#### Red Giant Branch RGB

After leaving the *Main Sequence* the star moves in the *HRD* first up to the right on the *Red Giant Branch* (RGB). In this phase, the hydrogen fusion zone grows outwards on a shell around the increasing helium core. Thus the radius and the luminosity of the star dramatically increase, while the density and temperature of the atmosphere substantially decrease.

#### Horizontal Branch HB

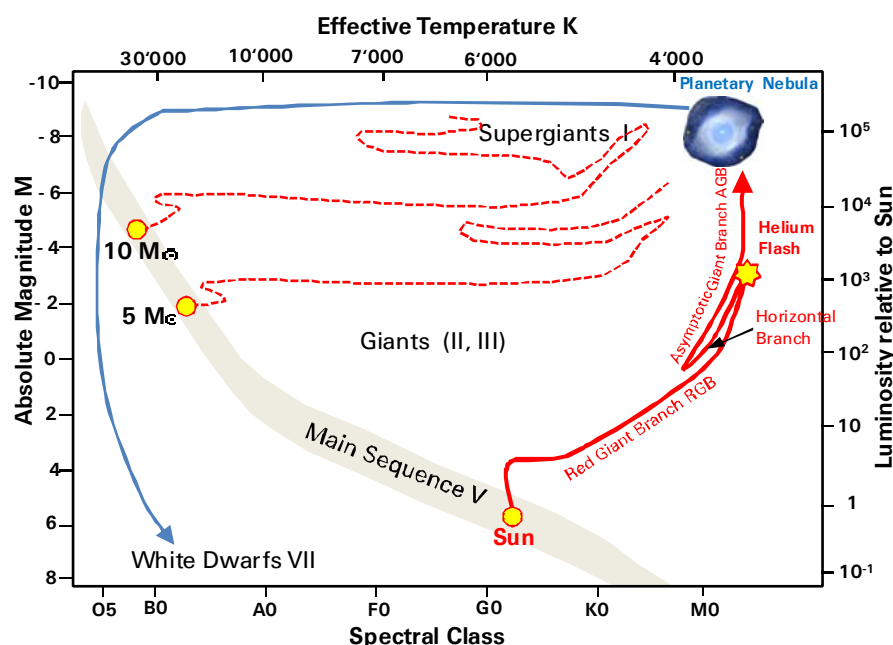
The so-called *helium flash* stops abruptly this ascent on the *RGB*. This event is triggered by the nuclear ignition of the helium core, which was formed during the *RGB* phase. From now on by helium fusion and other highly complex nuclear processes, carbon and oxygen is formed in the core of the star. As a result, the star first moves somewhat to the left and down on the *Horizontal Branch* (HB).

#### Asymptotic Giant Branch AGB

In a later phase, the helium begins to "burn" within a shell around the core of carbon and oxygen and in addition triggers now the hydrogen fusion in a further outer shell of the star. This multiple or alternating "shell burning process" causes now the rise of the expanding and unstable star along the *AGB*. At one solar mass the stellar radius reaches now some 1.5 AU and the luminosity is about 10,000 times that of the former *Main Sequence Star*.

#### Post AGB Phase

In the final stage these stars eject their outer shells as a *Planetary Nebula* (see sect. 24), which is excited to the emission of light by the remaining, extremely hot core. These objects initially show similar spectra like *Wolf Rayet Stars* (sect. 8). Later on, they cool down and end as *White Dwarfs* on the stellar "cemetery" in the lower part of the *HRD*. The following chart (excerpt from the *HRD*) shows schematically the *Post-Main Sequence Evolution* for stars of about 1, 5 and 10 solar masses.

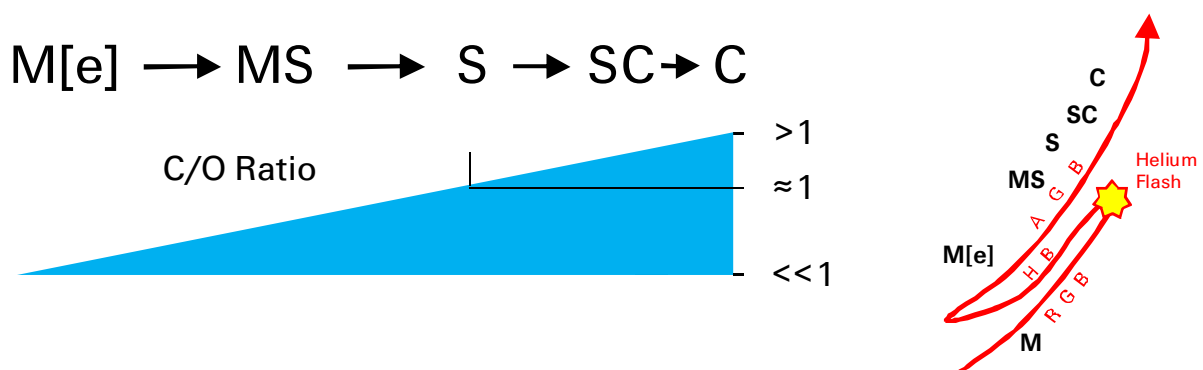




## 19.2 The Spectral Sequence of the Mira Variables on the AGB

This sequence consists of stars in their unstable *AGB* phase, limited to the range of about 1 – 2 solar masses and the spectral class *M* as well as to some late *K*-types. This category is for amateur astronomers not only interesting for photometric monitoring, but also in terms of spectral analysis. The astrophysical context is still not fully understood and shown here strongly simplified, mainly based on [2].

Once arrived on the *AGB* the star becomes unstable, as a result of the above mentioned complex fusion processes. It starts now pulsating and pushing off a lot of material. Therefore most but not all of these stars, show now the behavior of long-period *Mira Variables*. Current theories postulate at this stage strong, so-called *Thermal Pulses*, which trigger deep convective "dredge up" processes inside the star. As a result, carbon, and products of the nuclear *S*-process, is conveyed to the stellar surface (e.g. barium, lithium, zirconium, technetium, etc.). During its ascent on the *AGB* the star passes the following sequence of spectral classes (schematic diagram):



On this course the oxygen in the stellar atmosphere is not only bound by the formation of metal oxides (eg *TiO*, *ZrO*, *YO*). The rest of it combines now with the rapidly increasing carbon mainly to *CO* molecules [1]. Thus the *content of free oxygen* gets now continuously reduced. It's expressed in this context as *ratio of carbon to oxygen C/O*.

In the M(e) phase, at the "bottom" of the *AGB*, the stellar atmosphere is still *oxygen-rich*  $C/O \approx 0.5$ . Here *TiO* absorptions still dominate the profile, usually associated with individual atomic emission lines. Therefore I added the "index" (e) to this class to distinguish it clearly from the relatively stable, only hydrogen "burning" giants of spectral types *K* to *M* on the *RGB*.

Within the MS to S class the stellar atmosphere increasingly shows an oxygen deficiency. Therefore absorption of diatomic zirconiumoxide (*ZrO*) displaces now more and more the former dominating titanoxide bands (*TiO*). Within the spectral class S, the ratio becomes  $C/O \approx 1$  and therefore no more unbound oxygen exists in the stellar atmosphere.

Above the spectral class S the  $C/O$  ratio becomes  $C/O > 1$ . This creates a *carbon excess*, which accumulates in a circumstellar cloud and dominates now impressively the star's spectrum. Thus, in the intermediate SC-class, and increasingly in the following C-Class moderately high resolved spectra only show absorptions of diatomic carbon molecules (*CH*, *CN*, and *C<sub>2</sub>*). Increasingly here also show up atomic lines of *S*-process products, but also impressive absorptions of *Na I*.

Once arrived at the top of the AGB the star ejects due to intense thermal pulses its outer shell as a photogenic *Planetary Nebula*.

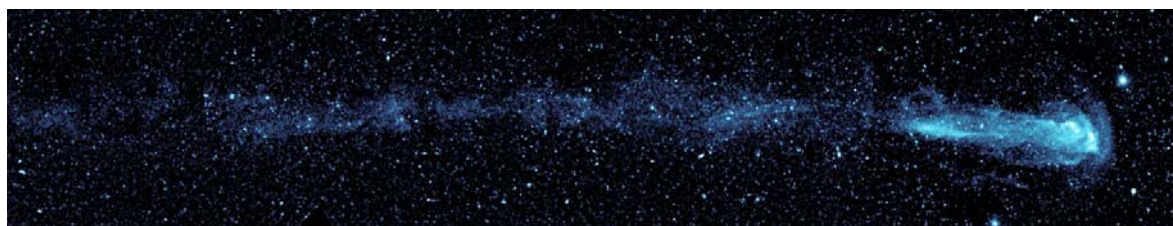


## 20 M(e) Stars on the AGB

### 20.1 Overview

The unstable M(e) stars on the AGB still have an oxygen-rich atmosphere ( $C/O < 1$ ) and are usually long-period variable of type *LPV* (*Long Period Variable*) or *Mira Variable*. The period of the brightness variation is in the order of about 100 to 1000 days. Prototype of this class is *Mira (o Ceti)*. This instability leads to shock waves in the stellar atmosphere, which expands and contracts by the rhythm of the brightness variations (radius up to a factor 2!).

As a result of this spectacular process the star loses continuously matter, as documented by recent photographs of *Mira*. The star produces on its way through the galaxy an impressive trace of stellar material, which can be seen in the ultraviolet region on a length of about 13 ly. This spectacular image was taken with GALEX (Galaxy Evolution Explorer, NASA), recorded in August 2008: [http://www.nasa.gov/mission\\_pages/galex/](http://www.nasa.gov/mission_pages/galex/).



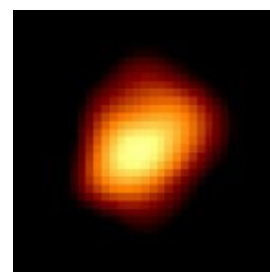
### 20.2 Spectral Characteristics of the M(e) Stars on the AGB

Parallel to the "pulsations" of the stellar atmosphere, emission lines of variable intensity appear in the spectrum, predominantly the short wave *H*-Balmerlines on the "blue side" of *H $\gamma$* . The maximum intensity mostly shows *H $\delta$*  (see Table 63). According to the *Balmer decrement* the *H $\alpha$* , *H $\beta$*  and *H $\gamma$*  emissions are in fact much more intensive. But highly intense *TiO* absorption bands overprint here completely *H $\alpha$*  and *H $\beta$*  and strongly diminish *H $\gamma$* . According to [1] this is evidence that the emission lines are formed in much deeper layers of the stellar atmosphere as the titanium oxide absorptions. The spectral type of the star itself is often variable within the range of decimal subclasses. Apart from the emission lines no further differences to a normal *M*-star can be detected in a moderately resolved spectrum.

### 20.3 Commented Spectra

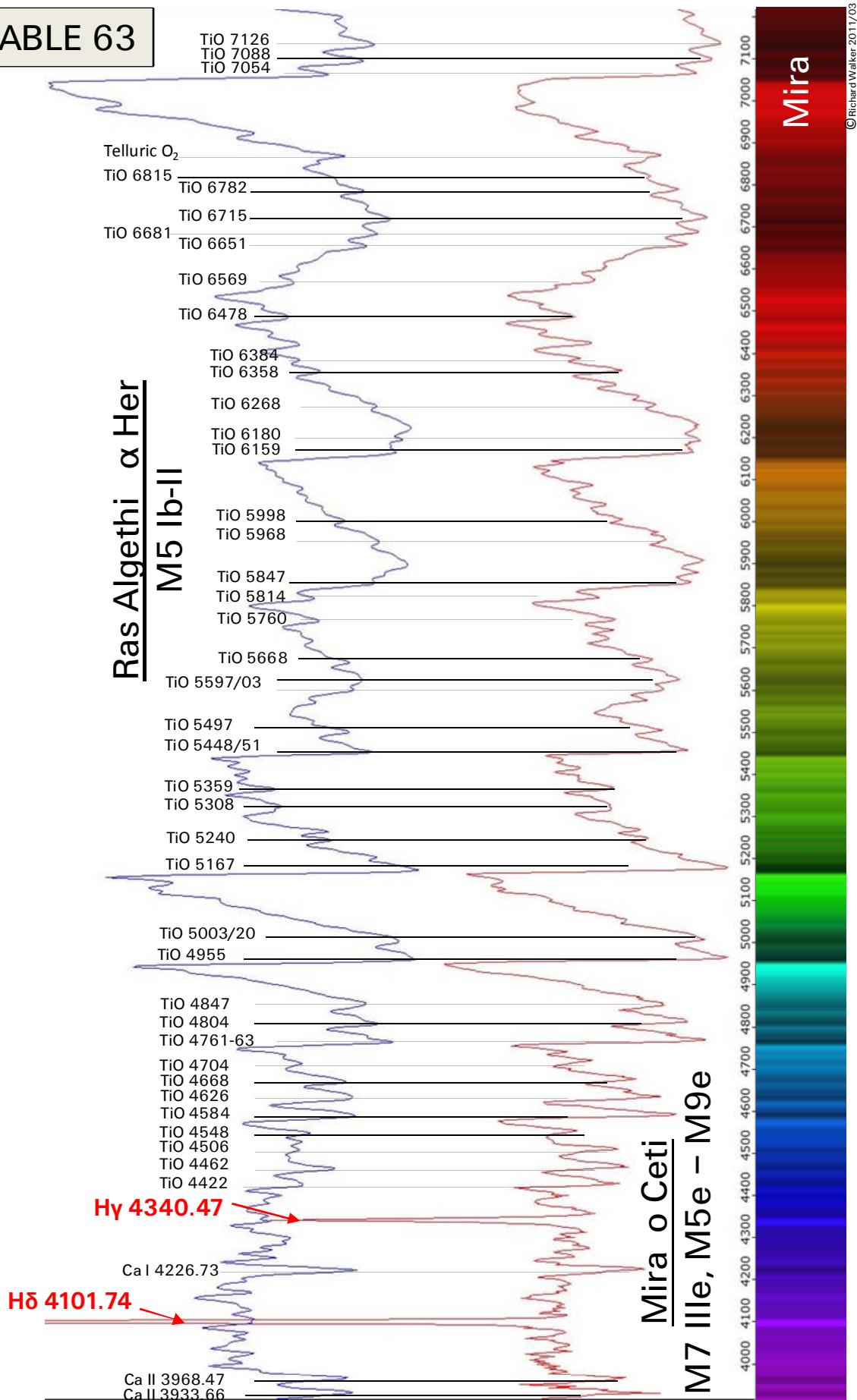
**Table 63:** A montage of two overview spectra (200L grating). Comparison of the *M(e)* star *Mira*, (*o Ceti*, *M7 IIIe*, alternatively *M5e–9e [505]*) and the ordinary *M-Type* star *Ras Algethi* ( $\alpha$  *Her*, *M5 II*), which is still located on the *RGB* (see Table 60).

*Mira A*, probably one of the most popular variables, steadily losing matter to its binary partner, the white dwarf *Mira B* (VZ Ceti). It shows an impressive brightness variation  $V_{\text{var}} \approx 3^{\text{m}} - 10^{\text{m}}$ , with a period of about 331 days (LPV). In some cases it becomes much brighter than  $2.0^{\text{m}}$ . Its spectacular variability was discovered in 1639 by *Holwarda*. The *HST* image (NASA) shows *Mira* in a phase with a slightly oval shape. Thanks to its diameter of  $> 500\text{M km}$ , the star (by interferometry) can still be recorded as a disc at a distance of about 300 ly!



Apart from some differences in the intensity of *TiO* bands, the emission lines *H $\delta$*  and *H $\gamma$*  are essentially the only spectral differences that distinguish the *AGB* star *Mira* from the *RGB* star *Ras Algethi*. *H $\delta$*  is here in fact significantly more intensive than *H $\gamma$*  what was already explained above. The profile was recorded December 13, 2010 (JD 2455544.46), some 60 days after the maximum brightness,  $V \approx 4.1\text{m}$  (AAVSO).

TABLE 63



## 21 Spectral Class S on the AGB

### 21.1 Overview and Spectral Characteristics

The spectrum of a star is influenced on the further ascent along the *AGB* by:

- the *increase of carbon* in the stellar atmosphere
- the consequential *decline of the oxygen content*
- “dredged up” *S-process products* (eg, zirconium, lithium, etc.)

This development changes at first the spectral type *M(e)* in to the intermediate class *MS*. If at all, then only small differences are detectable here with moderate resolution spectrographs. However at higher resolution appear first signs of zirconium oxide (*ZrO*). within the still dominant *titanium oxide* bands. The share of *ZrO* increases now continuously up to the extreme types of the spectral class *S*, where *ZrO* almost entirely replaces the *TiO* absorption. In [2] this effect is explained with the higher affinity of *ZrO* to oxygen, and the greater temperature resistance of this molecule. The dissociation energy of *ZrO*, (and also of *LaO* and *YO*), is  $>7\text{eV}$ , in contrast to *TiO*  $<7\text{eV}$ .

### 21.2 The Boeshaar – Keenan S-Classification System

The spectral class *S* is specified with the following format. It forms a temperature sequence, analog to the normal *M*-giants on the *RGB*. Since all *S*-stars are already giants, a luminosity class is usually not indicated.

**SX/n(e)**

**X:** stands for the temperature sequence of the *M*-class from 1 – 9 (some 3,800–2,500 K).

**n:** *C/O index* on a scale of 1 – 10, estimated from the relative intensities of *TiO* and *ZrO*.

The *C/O ratio* itself can not be obtained directly from the spectrum. It can only be estimated by means of the *C/O index* (table values according to *Scalo, Ross*)

(e) indicates that the spectrum sometimes shows emission lines.

This classification can be supplemented with characteristic elements/molecules showing up in the spectrum. The following table shows the spectral class *S* between the intermediate classes *MS* and *SC*, based on [140] and [2], where also detailed classification details can be found.

Spectraltype with <i>C/O Index</i>	Criteria for the <i>C/O Index</i>	~ <i>C/O Ratio</i>	Comment
MXS	<i>TiO</i> still dominates, some signs for <i>ZrO</i> bands are recognisable in highly resolved spectra		Transition class from <i>M(e)</i> to <i>S</i>
SX/1	<i>TiO</i> >> <i>ZrO</i> , <i>YO</i>	< 0.95	Spectralclass <i>S</i>
SX/2	<i>TiO</i> > <i>ZrO</i>	0.95	
SX/3	<i>TiO</i> ≈ <i>ZrO</i> , <i>YO</i> intensive	0.96	
SX/4	<i>ZrO</i> > <i>TiO</i>	0.97	
SX/5	<i>ZrO</i> >> <i>TiO</i>	0.97	
SX/6	<i>ZrO</i> very intensive, no <i>TiO</i> recognizable	0.98	
SX/7 = SC X/7	<i>ZrO</i> weaker, intensive <i>Na</i> lines	0.99	
SC X/8	No <i>ZrO</i> recognizable, intensive <i>Na</i> lines	1.00	Transition class from the <i>S</i> – to the carbon stars
SC X/9	Very intensive <i>Na</i> lines, <i>C<sub>2</sub></i> very weak	1.02	
SC X/10 = C-N	Intensive <i>Na</i> lines, <i>C<sub>2</sub></i> weak	1.1	

### 21.3 „Intrinsic“ and „Extrinsic“ („Symbiotic“) S-Stars

According to [2], this classification system does not explain the whole *S*-Class and carbon stars. Many *non*– or only *slightly variable* *S*–stars, which lie often outside the *AGB*, show *no*

short-living and unstable  $^{99}\text{Tc}$  (technetium) isotopes in the spectrum – hence called "*Tc - poor*". This affects at least 40% of all registered *MS* and *S* types [160]. A recent, still debated scenario postulates a mass transfer, which brings the *ZrO* from a nearby companion star in to the stellar atmosphere. Therefore these special types are also called "*extrinsic*" or "*symbiotic*". Textbook example is the relatively bright and only slightly variable ( $V \approx 5.2^m$ ) *BD Camelopardalis* (Table 66a). In fact, such objects are relatively hot and form components of close binary systems. These properties, as well as a low variability and the absence of  $^{99}\text{Tc}$  in the spectrum, are currently the main distinguishing characteristics of an "*extrinsic*" *S*-class star. In such cases the spectral classification is sometimes supplemented by "*symbiotic*" or "*extrinsic*".

In contrast, the *S*-Type stars on the *AGB* show *thermal pulses*, are usually *highly variable* and classified as "*Tc - rich*" or "*intrinsic*". Intrinsic means, that the elements and molecules, responsible for the *S*-classification, are produced by the star itself.

## 21.4 Hints for the Observation of S-Class Stars

On the *AGB* the stellar atmospheres meet the condition  $C/O \approx 1$  only during a very short period. Therefore *S*-classified stars are very rare. For our galaxy, only some 1300 are registered [160]. In the amateur literature unfortunately *Chi Cygni* is very often proposed as a "showcase object" of the *S*-Class stars, whose brightness can reach up to  $3.3^m$ . Regrettably it has a very low *C/O* index, like all other bright *S*-stars. The disappointment is respectively great for beginners, when in low-resolution spectra, if at all, only weak signs of zirconium can be seen. But there are some members with a high *C/O* index, reaching a maximum brightness up to some  $7^m$ . At this stage they become recordable with slit spectrographs at guided telescopes of medium aperture, including *R Cygni* HD185456 and *R Geminorum* HD 53791 – further also *R Lyncis* HD 51610, *U Cassiopeiae* HD 4350, *S Ursae Maioris* HD 110813 and *V Cancr* 70276. For the observation planning, the current brightness level for most of the variable *S* stars is displayed by AAVSO [507].

## 21.5 Commented Spectra

**Table 65:** For comparison, a montage of two broadband spectra (200L grating) is presented. *M(e)* star *Mira (o ceti)* (see Table 63) and the *S*-class star *R Cygni (S4/6e)* with a very high *C/O Index* = 6. The comparison of the two profiles shows impressively the transition from the spectral type *M(e)*, dominated by *TiO* bands to an extreme *S*-type star which shows *ZrO* absorptions only.

*R Cygni*, HD185456 (distance?), is strongly variable, according to AAVSO:  $V_{\text{var}} \approx 7.5^m - 13.9^m$ , and shows a period of about 429 days (*LPV*). The maximal and minimal brightness may differ considerably, compared between the individual periods. In the oxygen-rich *Mira* atmosphere the prominent *TiO bands* are still dominating. In the profile of *R Cygni*, due to the strong lack of oxygen, only impressive *ZrO* absorption bands, atomic lines of *S*-process elements, as well as a strong *Na I* absorption can be seen. Following a number of other physical effects (see [2]), the outer layers of the atmosphere become more "transparent" by the extreme *S*-Class. Therefore all emission lines of the *H-Balmer series* show up here – *H $\alpha$*  however, significantly dampend, compared to the law of the Balmer decrement. In the *Mira* profile only *H $\alpha$*  and *H $\beta$*  are in emission. The identification of the  $^{99}\text{Tc}$  *I* lines (marker for the "intrinsic" type) at  $\lambda\lambda$  4238, 4262 and 4297 is uncertain at this low resolution. The profile was taken on April 3, 2011 (JD 2455654.56) in the region of the maximum brightness  $V \approx 7.5^m$  (AAVSO) with the Celestron C8, 4x240 seconds. The detailed *ZrO* line identification was chiefly enabled by [141] - in second priority by [2].

TABLE 65

Mira o Ceti  
M5e – M9e

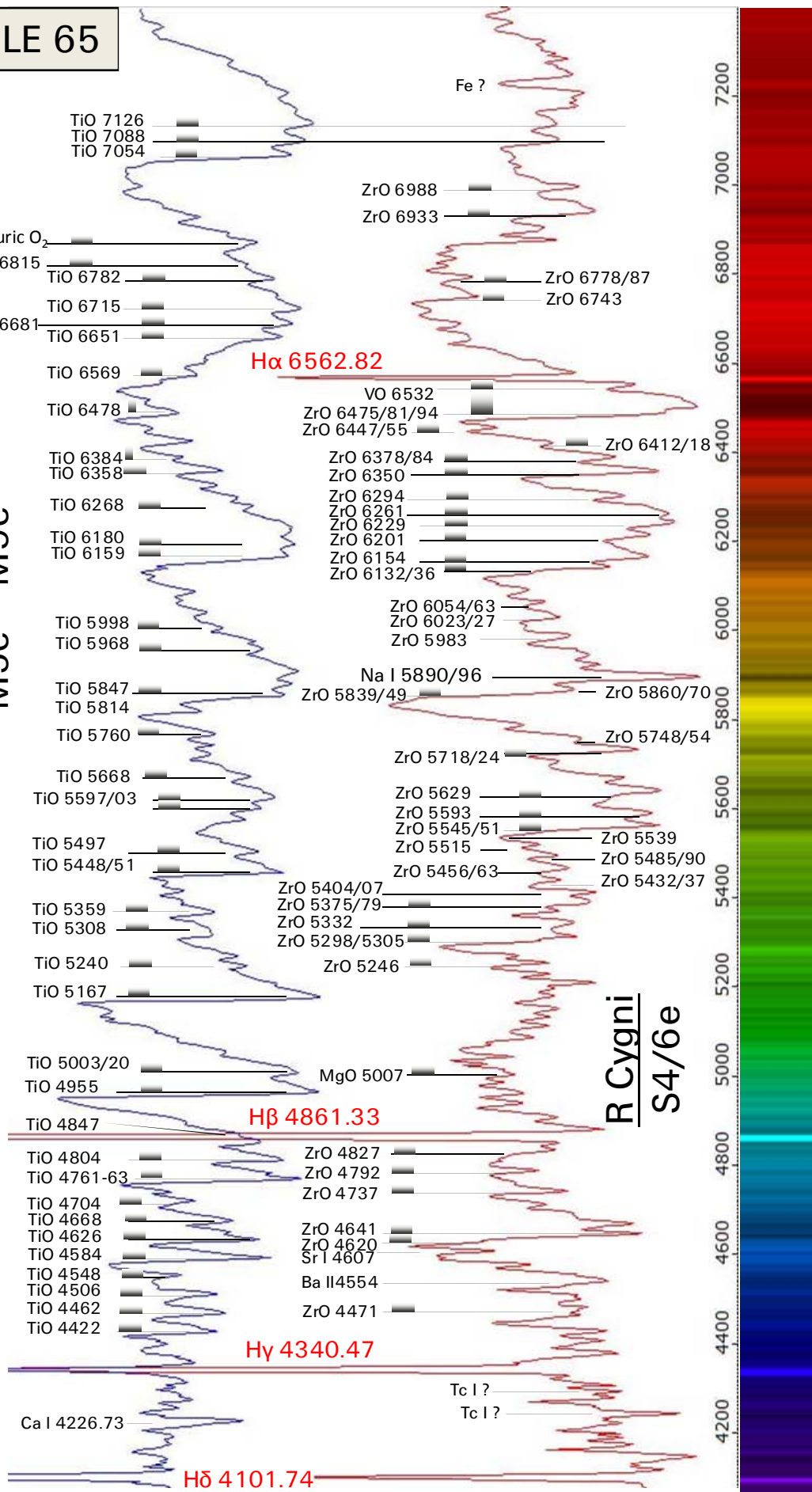




Table 66: A montage of three broadband spectra (200L grating) is presented to demonstrate the spectral development within the S-Class. To optimise the clarity, only the prominent lines are labeled here.

Omicron1 Orionis (4 Ori) HD 30959, (540 ly).

This star, with an apparent magnitude of about 4.74<sup>m</sup>, is only slightly variable. With *M3.2S* it forms the transition class between the *M(e)* and *S*-types. Alternatively, the star is also classified as *S3.5/1-*. According to the very low *C/O* index *ZrO* is barely visible in this low-resolution spectrum. *TiO* bands here still dominate the profile.

Chi Cygni HD 187796, (340 ly).

With a classification of *S6/1e* (alternatively *S7/1.5e*), the *C/O* index is here only slightly higher compared to *Omicron1 Orionis*. Thus the zirconiumoxide absorptions can overprint here the still dominant *TiO* bands only within a few small sections of the profile at  $\lambda\lambda$  5298/05, 5375/79, 5839/49 and 6475/81/94 (blend with *TiO*  $\lambda$  6478). This star shows with  $V_{\text{var}} \approx 3.3^{\text{m}} - 14.3^{\text{m}}$ , the highest brightness variation of all known variables – period length about 408 days (*LPV*).

R Cygni HD 185456.

As already shown in *Table 65*, the *ZrO* absorptions have fully overprinted here the *TiO* bands, due to the high *C/O* Index.

Observation hint: *R Cygni* is easy to find. It's located just nearby of *Theta Cygni*, HD 185395 ( $V \approx 4.5^{\text{m}}$ ).

Table 66 A: Shows a montage of two broadband spectra (200L grating) to compare an “*intrinsic*” and an “*extrinsic*” *S*-class star. Both stars have nearly the same spectral classification. Despite of some minor differences the two profiles run almost identically – regardless of the suspected different origin of the *ZrO* in the stellar atmospheres.

The *intrinsic* *HR Pegasi*, HD 216672, (970 ly), is only slightly variable  $V_{\text{var}} \approx 6.1^{\text{m}} - 6.5^{\text{m}}$  with a periode of some 50 days (Type *SR*, semi-regular). It is classified as *S4/1+* with a very low *C/O* Index.

The *extrinsic* *BD Camelopardalis*, HD 22649, (510 ly), is only slightly variable  $V \approx 5.1^{\text{m}}$ . It forms a component of a close binary system, is classified as *S3.5/2 symbiotic* and therefore relatively hot.



TABLE 66

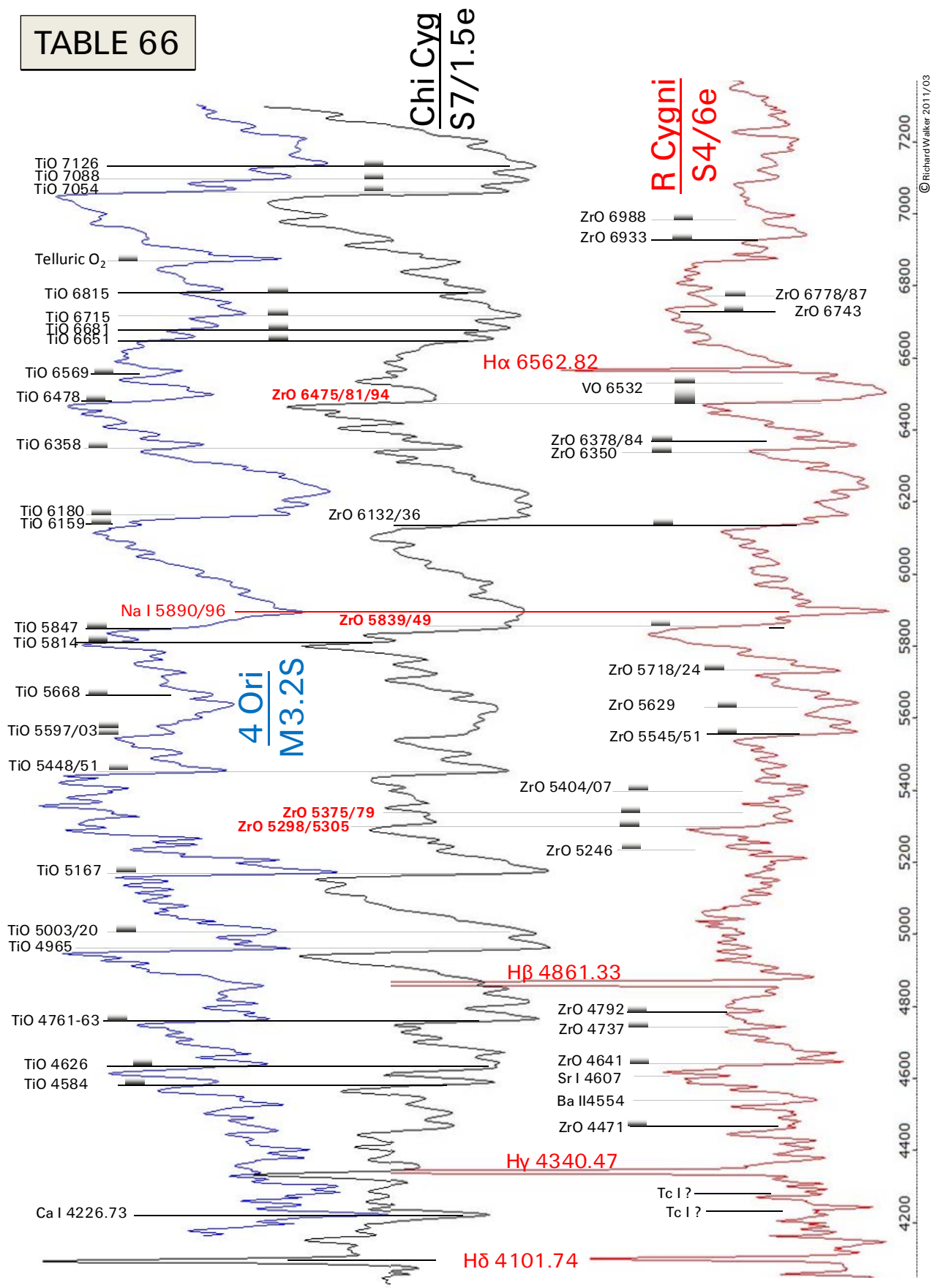
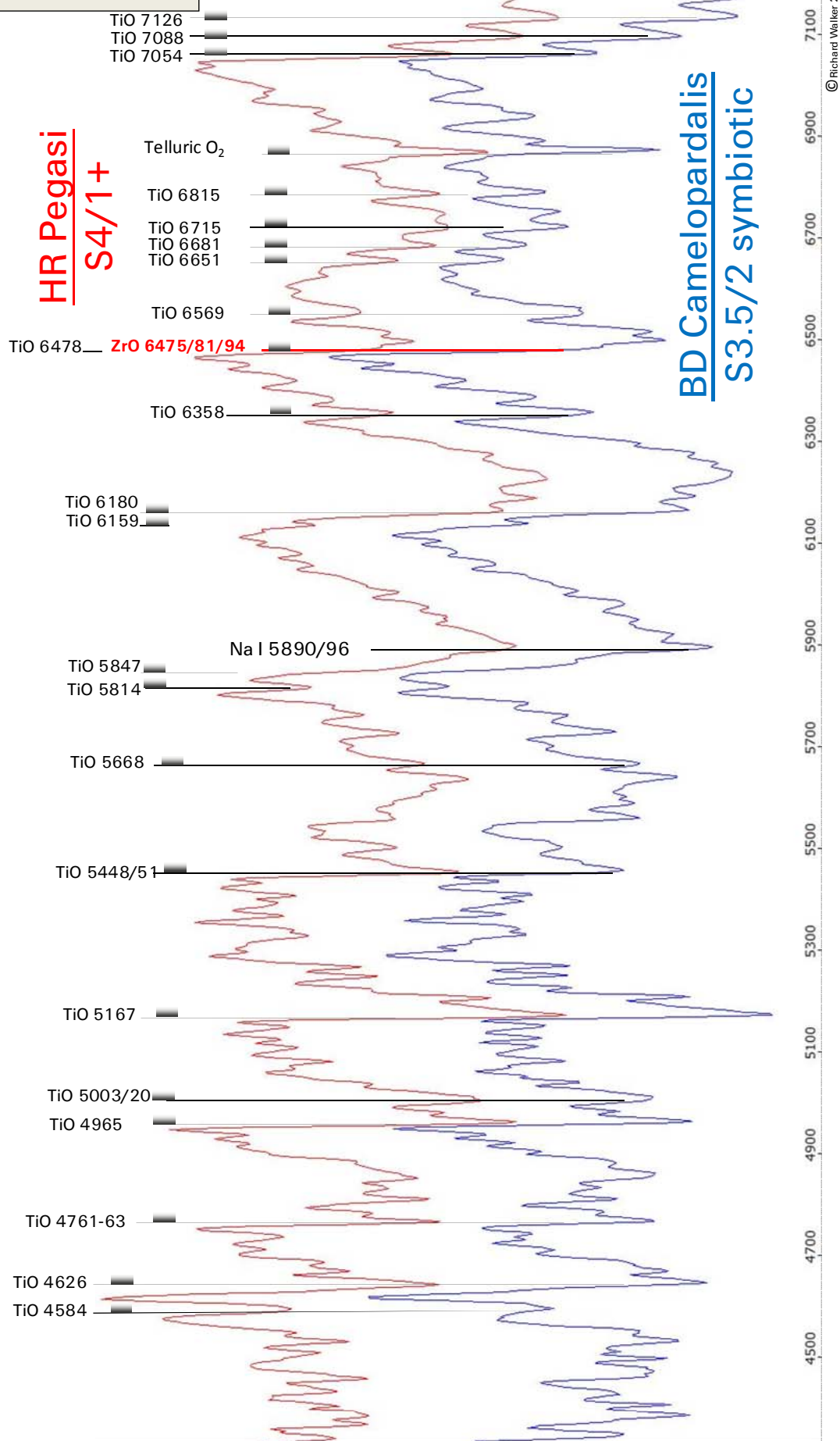


TABLE 66 A



## 22 Carbon Stars on the AGB

### 22.1 Overview and Spectral Characteristics

The final stage of the stellar evolution on the *AGB* is formed by the deeply red shining carbon stars, in most of the cases also *Mira Variables* or „*Carbon Miras*“. In the atmosphere of a star, finally moving to the upper part of the *AGB*, the *C/O* ratio becomes  $C/O > 1$ . This results in a *carbon excess* which accumulates in a circumstellar cloud, dominating now impressively the star's spectrum. Thus, in the intermediate class *SC*, and increasingly in the following *C*-Class, moderately high resolution spectra show now predominantly absorptions of diatomic carbon molecules. In addition to *CH* and *CN* the so-called *Swan bands* due to *C<sub>2</sub>* are particularly striking – discovered in 1856 by the Scot *William Swan*. (see also *Table 110*). Further visible are atomic lines of *S*-Process products and impressive absorptions of *Na I*. Angelo Secchi was the first to discover that the intensity gradient of the *C<sub>2</sub> Swan bands* is reversed [ ] in contrast to other molecular absorptions, such as *titanium-* and *zirconium oxide*. For this feature, he created the separate spectral class *IV*. (see appendix 34.3).

### 22.2 Competing Classification Systems

The phenomenon of carbon stars is still far from being fully understood (see e.g. [106]). For the *S*-class, in spite of ongoing disputes exists a generally accepted and consistently applied classification system. However for the carbon stars – the situation is still confusing and unsatisfactory. The „*Revised MK-System 1993*“, propagated in most of the textbooks, is applied obviously rarely. Its precursor from the 1960's, the so-called *MK-C system*, however, very often! Surprisingly frequent one can see even classifications according to the much older *Harvard system*, with the *R* and *N* classes.

### 22.3 The Morgan Keenan (MK) – C System

This simple, old classification system is still very popular, both in many professional publications, as well as in most of the stellar databases. It uses the following format:

**CX,n**

- X:** defines on a scale of 0 – 7, the position of the star in the temperature sequence. This scale is temperature equivalent to the spectral classes from *G4* to *M4* (see table below). The system appears to have been extended down to *C9* (e.g. *WZ Cas*).
- n:** This index rates on a scale from 1 – 5, the intensity of the *C<sub>2</sub> Swan bands*. In individual cases, appropriate supplements may be added, for example (e) for emissionlines, further also intensive lines of *S*-Process elements.

C0	C1	C2	C3	C4	C5	C6	C7
G4-G6	G7-G8	G9-K0	K1-K2	K3-K4	K5-M0	M1-M2	M3-M4
4500	4300	4100	3900	3650	3450		

This classification system squeezes the entire complex class of carbon stars in one seven-stage temperature sequence, supplemented just with one single intensity index!

Example: *C 2.5* indicates a stellar temperature, equivalent to the spectral *G9 – K0*, combined with very intense *C<sub>2</sub> Swan bands*.

## 22.4 The „Revised MK System 1993“

In 1993, the old "C system" was revised to the "Revised MK System 1993" and adapted to new findings [107]. It comprises five sub-classes (!), ordered by spectral symptoms – whose astrophysical background however remains widely unclear. Perhaps this could be one reason why the acceptance of this complex system, even some 20 years after its introduction, seems to be still limited. The "Keenan 1993 system" uses the following format:

### C-Sub X n

- Sub:** corresponds to the subclass of the carbon star according to the following table  
**X:** defines the position of the star in the temperature sequence of the C-Class. This forms a parallel sequence to the spectral classes from *G4* to *M4* (see table)  
**n:** Various indices as listed below.

Sub-class	Supposed status [106]	Criteria, spectral symptoms
C-R	Intrinsic	Intensive <i>Swan bands</i> ( $C_2$ ) in the blue part of the spectrum. Considerable flux in the blue/violet area – decreasing with lower temperatures. Later types show weaker <i>H</i> – Balmerlines, $H\beta$ line serves as a temperature indicator. <i>S</i> -process elements show average intensity. Intensity of $^{12}C^{13}C$ Band head at $\lambda$ 4737 is above average.
C-N	Intrinsic	<i>S</i> -Process elements are exceptionally intensive. Early <i>C-N</i> types show a tendency to <i>Merril Sanford Bands</i> ( $SiC_2$ silicon carbide). Strong, broad and diffuse absorption, or even a barely detectable flux in the blue range $\lambda < 4400$ . <i>Swan bands</i> $C_2$ weaker than with the <i>C-R</i> types
C-J	Intrinsic	Very intensive <i>Swan bands</i> ( $C_2$ ) and <i>CN</i> absorptions, further <i>Merril Sanford bands</i> ( $SiC_2$ ) and an <i>infrared excess</i> .
C-H	Extrinsic	Dominant <i>CH</i> absorptions in the blue/violet area. Fraunhofer <i>G</i> band at $\lambda$ 4300 exceptionally- and <i>S</i> -Process elements above average intensive.
C-Hd	?	<i>Hd</i> indicates <i>Hydrogene deficient</i> . Hydrogen lines or <i>CH</i> absorptions weak or even absent. <i>CN</i> and <i>Swan bands</i> ( $C_2$ ) above average intensive, very often irregular <i>R Crb Variables</i> , showing sudden dramatic brightness dips, due to veiling of the photosphere by circumstellar dust clouds.

Temperatur equivalent of the <i>Main Sequence</i>	~Temperatur range [K]	<i>C-R</i> -Sequence	<i>C-N</i> -Sequence	<i>C-H</i> -Sequence
G4 – G6	4500	C-R0		C-H0
G7 – G8	4300	C-R1	C-N1	C-H1
G9 – K0	4100	C-R2	C-N2	C-H2
K1 – K2	3900	C-R3	C-N3	C-H3
K3 – K4	3650	C-R4	C-N4	C-H4
K5 – M0	3450	C-R5	C-N5	C-H5
M1 – M2		C-R6	C-N6	C-H6
M3 – M4			C-N7	
M5 – M6			C-N8	
M7 – M8	~2500		C-N9	

This classification can be supplemented with the following indices [107], [2]:

Index	Specification
$C_2$ – Index	Intensity of the molecular $C_2$ <i>Swan bands</i> Scale 1 – 5
$CH$ – Index	Intensity of the molecular $CH$ absorption. Scale 1 – 6.
$MS$ – Index	Intensity of the <i>Merril Sanford Bands</i> ( $SiC_2$ ), Scale 1 – 5
$J$ – Index	Intensity ratio of the $C_2$ molecular absorption with the Isotopes $^{12}C^{13}C$ and $^{12}C^{12}C$ , Scale 1 – 5.
<i>Elements</i>	In some cases, for strong lithium and sodium lines index values are specified

Not included in this system is the still *not* understood class of the *dC* carbon dwarf stars located on the *Main Sequence*.

## 22.5 Function of the Subclasses in the Evolution of Carbon Stars

Current professional publications provide a rather diffuse picture about the functions of these subclasses within the evolution of carbon stars. Many details, so e.g. about the "*dredge up*" processes, are obviously far from being fully understood. Further the theoretical modeling of "*carbon atmospheres*"  $C/O > 1$  seems to be difficult.

Analog to the *S*-Class also carbon stars on the *AGB* are referred as "*intrinsic*". It's assumed, that the subclass *C-N*, as well as the late representatives of *C-R*, form the last development stage of the *AGB* sequence. These subgroups show a behavior like *M*-giants with very similar spectra. Furthermore they are also so-called "*Low Mass Objects*" with  $\leq 3$  solar masses, typically show a *mass loss* and all of them are *Variables*.

Early representatives of C-R Type shows in contrast, neither variability nor a significant mass loss. Further they seem *not* to be *AGB* stars and show a behavior like *K*-giants. One of the discussed scenarios postulates a star on the *Horizontal Branch* (*HB*) with a helium "burning" core. However it remains here a mystery how the formed carbon will be conveyed to the surface. A further hypothesis is a former binary system whose masses fused into one single star.

The position of the *C-J* class on the *AGB* is unclear. It's argued that these "*Low Mass Objects*" could be descendants of the *C-R* class on the *AGB*.

The *C-H* class seems to be "*extrinsic*". Most representatives are on the *Horizontal Branch* (*HB*) and components of close binary stars. This suggests a mass transfer scenario similar to the extrinsic *S*-Class.

## 22.6 Merrill Sanford Bands (MS)

Already at the beginning of the 20th Century in spectra of certain carbon stars, in the range of some  $\lambda\lambda$  4640 to 5200, intensive absorptions attracted attention, which for a long time could not be interpreted. The most intense bandheads are at  $\lambda\lambda$  4977, 4909, 4867, 4640 and  $\lambda$  4581. These absorption bands are named after the two explorers, who first described these in 1926. Not until 1956 *Kleman* could prove with laboratory spectra, that these bands are caused by  $SiC_2$  silicon carbide. For this purpose he heated silicon in a graphite tube up to 2500 K.

*P. J. Sarre* et al. have also shown [109] that the *Merril Sanford Bands* are generated in cooler layers of the stellar atmosphere, far beyond the photosphere. *Merril Sanford Bands* are most common in the entire *C-J* and the early *C-N* classes.



## 22.7 Commented Spectra

The majority of carbon stars is part of the sub-class *C–N*, documented here with some examples. The spectral classes are here indicated in the old *MK–C system*, according to Stephenson's 1989 catalog [500]. If available [107], also the classification, corresponding to the "*Revised MK System 1993*" is specified.

Table 67: A montage of three broadband spectra (200L grating) is presented to demonstrate the difference between the profiles of differently classified carbon stars.

*WZ Cassiopeiae*: HD 224855, spectralclass *C9,2 Li* or *C-N7 III: C<sub>2</sub> 2 Li 10*.

J2000 RA: 00h 01' 16" Dec: +60° 21' 19"  $V_{\text{var}} \approx +6.5 - 8.5^{\text{m}}$

*WZ Cas* (1,500 ly) is an extremely late classified, cool *Supergiant* (2,500 K). It's the dominant component of a binary star system, impressively contrasting with its white-blueish shining companion star ( $V \approx 8^{\text{m}}$ , *A0*). It's located in the constellation Cassiopeia (image: [www.astro.sci.muni.cz/](http://www.astro.sci.muni.cz/)).



Besides the rather weak *Swan bands* (here classified with index value 2), this spectrum is dominated by the striking, almost fully saturated (!) *Na I* line. Further by the impressive absorption of *lithium Li I* ( $\lambda$  6708), whose intensity is rated here with 10. Therefore *WZ Cassiopeiae* is often called "Lithium star" [348]. According to [349] this intense *Li I* absorption line was the first evidence of *Lithium* outside the solar system, found by *McKellar* 1941 – a small but anyway interesting detail in the history of science! Further the profile is dominated by *CN*- und *C<sub>2</sub>*-absorption bands and the *H*-Balmerlines are barely recognisable here. The spectrum was recorded with the Celestron C8 – exposure: 3x85 sec. The line identification is based amongst others on [100], [104], [110], [348], [349].

*Z Piscium*: HD 7561, spectral class *C7,3* or *C-N5 C<sub>2</sub> 4*

J2000 RA: 01h 16' 05" Dec: +25° 46' 10"  $V_{\text{var}} \approx \text{max.} +6.8^{\text{m}}$

This star is a *Supergiant* with a surface temperature of some 3,000 K and located some 1,500 ly distant in the constellation *Pisces* [105]. With *C7,3* it's classified earlier than *WZ Cas* (*C9.2*). The carbon absorptions are here much intenser and the *Na I* line somewhat weaker, but still very impressive! Instead of the exceptional *Lithium* line ( $\lambda$  6708) the undisturbed *CN* absorption at  $\lambda$  6656 is visible here.

The spectrum was recorded with DADOS 50 $\mu$ m slit and the Celestron C8/ 3x60sec. The line identification is based amongst others on [100], [104], [110], [348].

*W Orionis*: HD 32736, spectral class *C5,4*

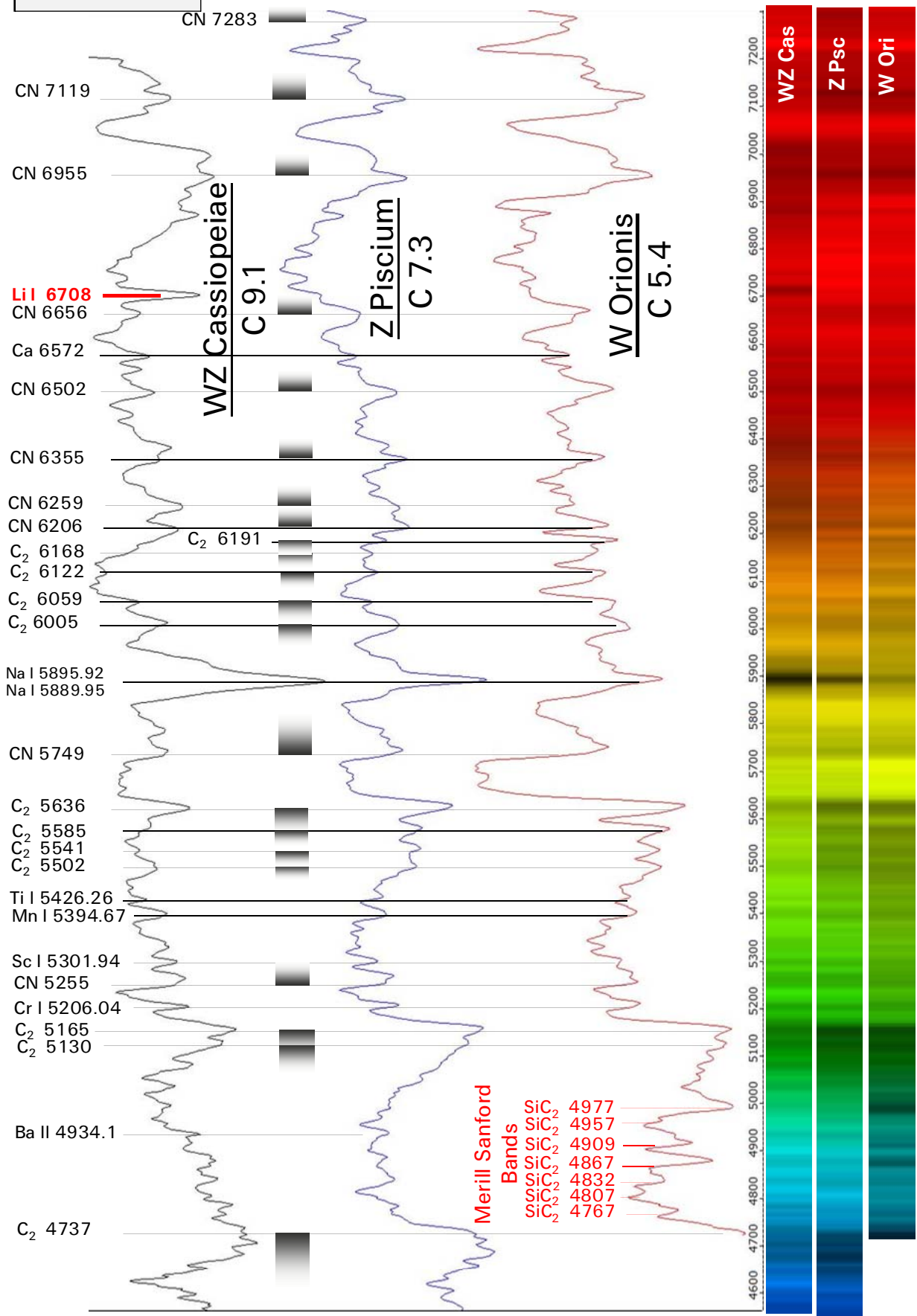
J2000 RA: 5h 05' 59" Dec: +1° 11' 27"  $V_{\text{var}} \approx \text{max.} +5.88^{\text{m}}$

The luminosity class of this carbon giant (some 700 ly distant), is difficult to determine [506]. *Merrill Sanford Bands* are striking here. In the profiles of the two other, much later classified carbon stars, these absorption bands of triatomic *SiC<sub>2</sub> silicon carbide* are hardly recognisable. The spectrum was recorded with DADOS 25 $\mu$ m slit and Celestron C8/ 5x42 sec. The line identification is based amongst others on [100], [104], [110], [107], [109] [348].

Table 67a: *W Orionis*. Higher resolved spectrum (900L grating) in the wavelength domain of the *Merrill Sanford Bands*. The line identification is based here additionally on [108].



TABLE 67



W Orionis C 5.4 Merrill Sanford Bands



## 23 Spectra of Extragalactic Objects

### 23.1 Introduction

It's impossible with amateur equipment, to record spectra of single stars within external galaxies. However it's possible to record *composite spectra* of galaxies and Quasars! In contrast to profiles of individual stars the composite (or integrated) spectra show the superposed characteristics of hundreds of billions individual star spectra. Using Doppler spectroscopy thus also the radial velocities, respectively the  $z$ -values of such objects can be measured. Further by "edge on" galaxies the rough distribution of the rotation speed within the galactic disk can be estimated [30].

On a professional level, this has been practiced successfully since the beginning of the 20th century and has contributed substantially to our present understanding of the universe. The first, who tried this with M31, was in 1912 *Vesto M. Slipher* at the Lowell Observatory in Flagstaff Arizona. He was able to measure the *blue shift* of the spectrum and derived a radial velocity of  $-300$  km/s. Further he detected the rotation of this "nebula". The fact that M31 is a galaxy outside the Milky Way was proved only later in the early twenties. Further, he also noted that most of the other galaxies appearing *red shifted* and thus are removing from us. Hubble used these shift measurements later for the correlation with the distance (Hubble constant).

### 23.2 Morphological Classification

The characteristics of the spectra are partly correlated with the morphological types of galaxies. The following graph shows the so-called Hubble Sandage tuning-fork diagram.

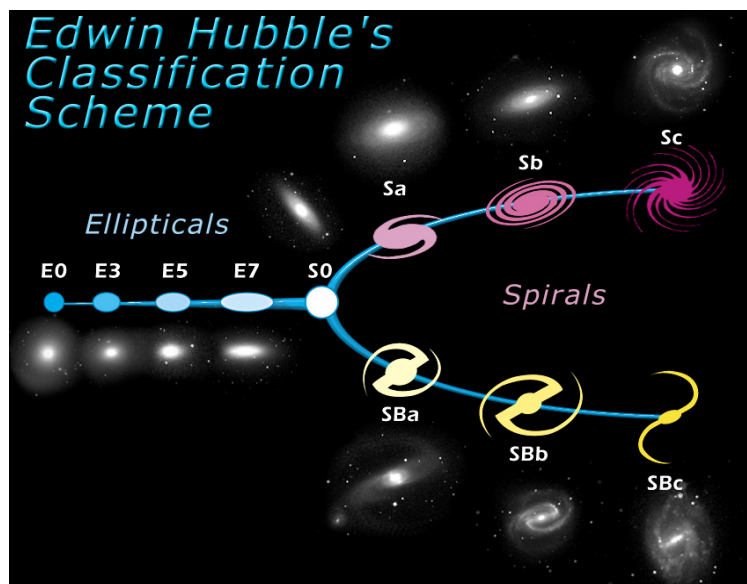


Image: NASA/ESA

It is based on the former faulty hypothesis that this sequence should represent the evolution of galaxies, starting from the elliptical shape of E0 and ending with the spiral types Sc, or SBc. Similar to the stellar spectral classes, we therefore call, even today, the ellipticals as "early" and the spirals as "late" types. However, according to current knowledge, the elliptical galaxies represent rather the final stage, merged by a number of smaller galaxies. During this process also the irregular stage *Ir* is passed through. Examples are M82 and the Antenna Galaxy NGC4038/4039.

### 23.3 Spectroscopic Classification

The spectroscopic classification distinguishes these objects according to spectral features. Already in the 1920ies it was recognised that such composite- or integrated spectra have a similar information content like those of individual single stars. They also show profiles e.g. with or without emission lines, chiefly depending on the kind and activity of the galactic nuclei. Such spectral profiles are powerful means to determine e.g. the content of stars, and the development state of the galaxy [301]. The relative similarity of the galactic composite spectra to those of single stars, was also a powerful argument in the historical dispute (mainly between *H. Shapley* and *H. Curtis*), that galaxies are not dust or gas nebulae like M42 (see *Tables 80/80A*), but extremely distant, huge clusters of individual stars!

In the second half of the 20th Century, classification systems have been developed, which were based on the similarity with stellar spectral types. The galaxies were classified this way by W. Morgan, beginning with A, AF, F- and ending by the late K-systems. The following correlations have been noticed [2]:

- The later the stellar spectral type, with which the profile shows similarities, the stronger the galaxy is centrally concentrated.
- The elliptical classes E1 – E4, remain still dominated by features of later spectral types. From here on however, the characteristic changes until the profiles of the types *Sc/SBc* and *Irr* look similar to those of early spectral classes. Furthermore emission lines show up here with increasing intensity.

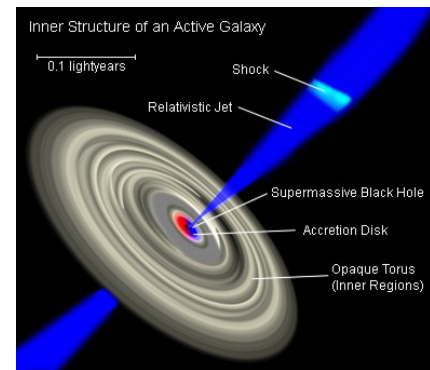
Another, also rather rough classification system, is based on the presence, intensity and shape of emission lines. It also includes peculiar shapes such as Seyfert galaxies and Quasars, which stand out by an extremely high core activity and therefore belong to the category of AGN (Active Galactic Nuclei).

	Absorption line Galaxy	Starburst Galaxy	Seyfert Galaxy	Quasar
Features within the optical spectral range	Almost exclusively absorption lines, sporadically weak emissions may show up	Intensive H-emission lines, just weakly may appear: [N II] ( $\lambda\lambda 6583$ ), [S II] ( $\lambda\lambda 6716/31$ ) and [O I] ( $\lambda 6300$ ), generally little or no absorptions	Intensive and Doppler-broadened H- and slim [O III] emission lines, [N II], [S II], and [O I] are intensive, generally little or no absorptions	Intensive and extremely Doppler-broadened H- emission lines
Affected objects and responsible effects	Mainly elliptical galaxies with old star inventory, low star formation rate and weakly active nuclei	Colliding, gravitationally interacting, or gas-rich young galaxies with giant H II regions and a correspondingly high rate of star birth	Central, supermassive black hole with high accretion rate	Central, supermassive black hole with extremely high accretion rate
Examples	M31, M33, M81,	M82, NGC 4038/4039	M77, M106, NGC 4151	3C273, Makarian 421

Somewhat outside of this system are the numerous, so-called LINER galaxies. LINER means "Low-Ionisation Nuclear Emission-Line Region". The spectral features are emission lines of weakly ionised or neutral atoms such as O I, N I and S I. Just weakly appear emissions of highly ionised atoms such as He I, Ne II and O II. Well-known examples are M104 (Sombrero) and M94. Morphologically mainly the types E0 – S0 are represented. This phenomenon, especially the origin of the involved ionisation processes is still subject of debate.

### 23.4 The phenomenon of AGN (Active Galactic Nuclei)

The AGN phenomenon in Seyfert galaxies and Quasars is caused by so-called supermassive black holes, collecting vast amounts of matter from their surroundings and generating thereby exorbitant amounts of energy and intense X-ray radiation. This process is accompanied by an accretion disk in the equatorial plane and jets of matter which are ejected parallel to the rotation axis of the object with almost the speed of light (image: Wikipedia). Seyfert galaxies are the largest group with AGN [307].



### 23.5 Commented Spectra

Table 70: Absorption line Galaxy Andromeda M31/NGC224

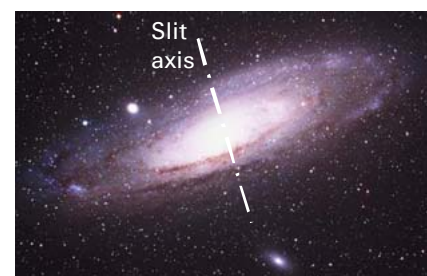
The table shows heliocentric parameters according to NED [501], and Evans, N.W. Wilkinson (2000) [1] (Value including suspected dark matter).

Radial Velocity	Redshift $z$	Distance	Morphology	Diameter	Mass <sup>1</sup>
-300km/s	-0.001	2.6 M ly	Sb	141,000 ly	$1.23 \cdot 10^{12} M_{\odot}$

Table 70 shows a composite spectrum of M31. The slit axis of the DADOS spectrograph was adjusted nearly parallel to the apparently smaller crossaxis of the galaxy, since no rotation effects are intended to show here [30].

According to [301] composite spectra of the galaxy types *Sa – Sb* are dominated mainly by *developed Giant stars*.

As a matter of fact the pseudo-continuum of the recorded *M31* spectrum fits here best to that of a single star of the late G-class! For a comparison, the *M31* profile is therefore shown here superposed with the pseudo-continuum of *Vindematrix* ( $\epsilon$  Vir). *M31* belongs obviously to the category of absorptionline galaxies. The most dominant common features are the *Fraunhofer G-band*, the *Calcium Triplet*, and the *Sodium Double Line* (Fraunhofer D line). The *H-Balmer* lines are just faintly visible in absorption. According to [301], this finding fits rather to *elliptical galaxies (type E)*. For the type *Sa–Sb* also few emission lines, caused by a younger stellar population, may sporadically be recognisable. However this is not detectable in this spectrum of *M31*.



The *H-Balmer* lines are just faintly visible in absorption. According to [301], this finding fits rather to *elliptical galaxies (type E)*. For the type *Sa–Sb* also few emission lines, caused by a younger stellar population, may sporadically be recognisable. However this is not detectable in this spectrum of *M31*.

The profile was recorded in the Nasmyth focus of the 90 cm CEDES Cassegrain Telescope in Falera – exposure: 3x340 sec. Clearly visible here is the expected blueshift of several Angstroms by the *absolutely* wavelength-calibrated *M31* profile, compared to the *relatively* calibrated spectrum of  $\epsilon$  Vir, based on known lines.



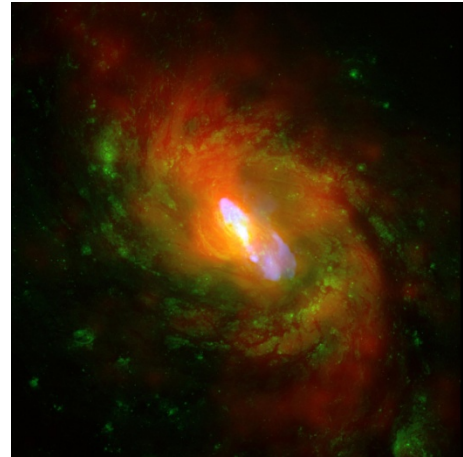
**Table 73:** Seyfert Galaxy M77/NGC1068

The table shows heliocentric parameters according to NED [501] and other sources [<sup>1</sup>].

Radial Velocity $v_r$	Redshift $z$	Distance	Morphology	Diameter	Mass [ <sup>1</sup> ]
+1137km/s	+0.0037	60 M ly	Sb / Sy2	115'000 ly	$\sim 1.0 \cdot 10^{12} M_\odot$

Table 73 shows a composit spectrum of the core of M77. The galaxy is classified as type Seyfert 2 (image: NASA/Wikipedia). In the 1940ies Carl Kennan Seyfert (1911 – 1960) discovered in the core of some galaxies intensive emission lines of the H-Balmer series with Doppler-broadenings of more than 1000 km/s.

In addition, emissions of forbidden transitions, such as [O III] and [N II] can be detected. However, they can't substantially be broadened, due to the shock sensitivity of the metastable initial states. In contrast to the emission of the H-Balmer series, they are probably generated far away from the turbulent core around the supermassive black hole, whose mass is estimated to be  $\sim 15$  Million  $M_\odot$  [Hubble ESA, Garching]. In contrast to the permitted lines they show therefore virtually no intensity fluctuations.



Also remarkable are the *double peaks* at the H $\gamma$  and the Ne III (3967) emission. B. Garcia-Lorenzo et al. [304] and other authors suggest here Doppler effects due to differently running streams of gas in the close vicinity around the black hole.

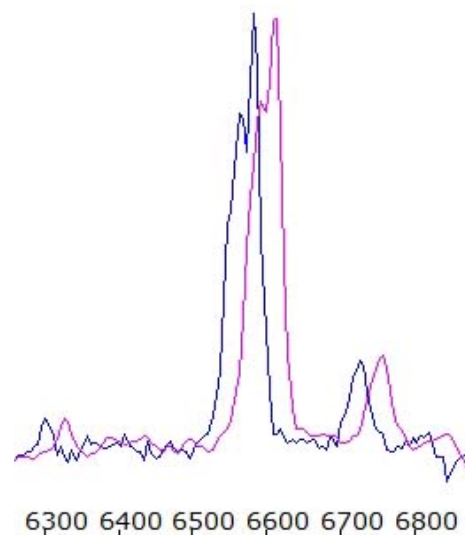
Seyfert galaxies are divided into:

- Subclass 1 with strongly broadened lines, limited to the *permitted transitions*
- Subclass 2 with only slightly broadened lines, limited to the *permitted transitions*

It is now generally assumed, that this class difference is rather caused by effects of different perspectives, see "Seyfert Unification Theory" [306]. Thus, at subclass 2, the forming regions of the broad, permitted lines are obscured by dust clouds and/or an unfavorable viewing angle.

M77 shows one of the strongest red shifts of the entire Messier catalog. In the area of the H $\alpha$  line it is about  $24 \text{ \AA}$  ( $z \cdot \lambda_0$ ). In the graph on the right the scale and the blue profile are based on the rest length  $\lambda_0$ , calibrated with known lines. The red profile is absolutely scaled with the calibration light; that on Table 73 refers to the rest wavelength  $\lambda_0$ .

For obvious reasons the spectrum shows strong similarity to profiles of galactic emission nebulae, which are presented in sect. 24. Accordingly, the excitation class  $E$  can also be determined here. Already the He II line at  $\lambda 4686$  shows, that it must be  $E > 4$ . The criterion  $\log(I_{N1+N2}/I_{He II (4686)})$  results here in  $\sim 1.5$ , corresponding to an excitation class  $E 10$  on the 12-step Gurzadyan scale (sect. 24). This high excitation





level is also documented by the considerable intensity of the forbidden [O III] and [N II] lines, compared to the rather weak H-Balmer series. So here even [N II] (6583) surpasses clearly the H $\alpha$  emission. Comparable to the supernova remnant M1 (sect. 24), the sulfur [S II] doublet ( $\lambda\lambda$  6718/6733) is here also strikingly intense – probably as well due to shock wave-induced excitation.

*Veilleux* and *Osterbrock* use in their classification scheme [307] inter alia the decadic logarithms of the intensity ratios  $[O\ III]_{(5007)}/H\beta$  and  $[N\ II]_{(6583)}/H\alpha$ . According to *Shuder* and *Osterbrock* (1981), the intensity ratio  $[O\ III]_{(5007)}/H\beta > 3$  applies as a rough criterion to distinguish Seyfert from H II- or starburst galaxies.

The supermassive black hole appears in the center of Seyfert galaxies, almost starlike, very bright, while the rest of the galaxy remains relatively dark. This considerably simplifies the recording of the spectrum of M77 with an apparent magnitude of V 8.9<sup>m</sup>.

The spectrum from the core was recorded with the 25 $\mu$ m slit and the 200L grating. Exposure time: C8/DADOS/Atik 314L+: 2x1200 seconds, 2x2 Binning Mode, –20°C. In addition the subtraction of light pollution was necessary.

**Table 77:** Quasar 3C273, details of the spectral profile

Preliminary remarks: Here follows a summary of my publication "*Quasar 3C273, Optical Spectrum and Determination of the Redshift*" [36]. There further information, as well as a finder chart and details, about the recording of this object, can be found.

The table shows heliocentric parameters according to NED [501] and other sources [1].

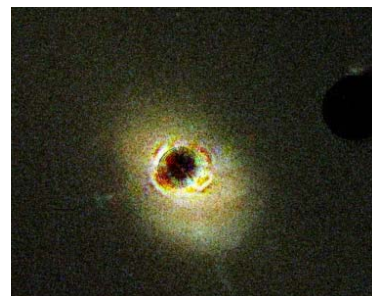
Redshift [501] $z = \Delta\lambda/\lambda_0$	Doppler Radial velocity [501] $v_r = c \cdot z$	Relativistic Radial velocity [500]* $v_{rel} = c \cdot \frac{(z+1)^2 - 1}{(z+1)^2 + 1}$	Distance [bn ly] <sup>[1]</sup>
+0.1583	+47'469 km s <sup>-1</sup>	+43'751 km s <sup>-1</sup>	2.4

\***Remark:** The value for the relativistic radial velocity is currently no longer included in [500]

The apparently brightest Quasar 3C273 in Virgo is often (wrongly) called the most distant object which can still be seen with average amateur means, purely visually and without the use of astro cameras. The designation means the object number 273 in Ryle's third Cambridge catalogue of radio sources from 1959.

### The Quasar Phenomenon

The term "Quasar" is derived from *Quasistellar Object (QSO)*, because these objects appear as point shaped light sources. Maarten Schmidt discovered the first in 1963 at the coordinates of a corresponding entry in the mentioned radio source catalogue (HST image: 3C273). It quickly became clear that this object showed the largest Redshift, known at that time, and therefore could impossibly be a star. In addition, the obtained spectra differed dramatically from stellar profiles and appeared more like those of Wolf Rayet stars, Nova outbursts, or even Supernova explosions. According to today's knowledge, Quasars are considered as the most energetic and luminous version of galaxies with active nuclei (AGN). The center of such an object always hosts a supermassive Black Hole which accumulates matter from the surrounding galaxy by an accretion disk and ejects a jet with relativistic speed. Therefore, Quasars are also strong sources of X-ray and radio emission. The mass estimation of the Black Hole is still difficult and uncertain. The literature shows



strongly scattering values for example [311], proposing a mass of some 1 bn  $M_{\odot}$ . Their point shaped appearance can be explained by the enormous brightness of the nuclei, which in most cases totally outshine the rest of their host galaxies. Apart from the episodically occurring Supernova explosions they are by far the most luminous objects in the universe.

### Spectral features

The spectrum is dominated by extremely broadened emissions of the H-Balmer series and by forbidden [OIII] lines at  $\lambda\lambda$  5007 and 4959, fusing here to a blend. Because of quantum mechanical reasons, the forbidden O III lines can not appear significantly broadened, it is discussed, whether the  $\lambda$  5018 emission of the Fe II (42) multiplet ( $\lambda\lambda$  4923, 5018 and 5169), supplies the major contribution to the intensity of this emission [309], [312]. This multiplet frequently appears in the spectra of Active Galactic Nuclei (AGN), as well as in the profiles of Protostars (see PMS sect. 13). Striking is the much lower intensity of the O III emission, relative to  $H\beta$ . This observation is in contrast to the spectral profiles of active Seyfert-type Galaxies (Table 73), planetary nebulae and H II regions (sect. 24). This phenomenon has already been noted by the discoverers of Quasars in the 1960ies. Even today just hypotheses exist about this issue.

Undisputed is the Ne III emission at  $\lambda$  3869. The other features are mostly broad-band blends of different emissions, generated by various ions. This significantly complicates the line identification [312]. Consequently, their exact composition is still unclear. Striking is a broad emission between  $\lambda\lambda$  4500 – 4700. *J. B. Oke* [313] suggested as the cause the He II line at  $\lambda$  4686 and numerous emissions of C III and N III - this in analogy with similar spectra of Supernovae and Wolf Rayet stars. In [312] it is assumed that the striking emission in the range of  $\lambda$  5870 is caused by He I at  $\lambda$  5876. Under discussion is also the Na I doublet, which in certain phases can be observed during Nova eruptions. Due to the extreme shock sensitivity of the metastable initial states of the forbidden O III lines, and the very low ionisation energy of Na I, these emissions must necessarily be generated at a considerable distance to the supermassive Black Hole. An indication for the contraction process within the accretion disk are the inverse P Cygni profiles in the area around  $\lambda\lambda$  6100 - 6400, also observable in the spectra of the much smaller disks around the T Tauri and Ae/Be- Protostars (see sect. 13).

The  $H\alpha$  emission is here redshifted so far (1017 Å !) that it coincides with the intense, telluric Fraunhofer A line. This is the cause why  $H\alpha$  appears split here [313]. This circumstance complicates the determination of the Redshift, using this line, and seems at least to be one of the reasons for the by far too low Balmer Decrement ( $I_{H\alpha}/I_{H\beta} < 2.85$ ) [313].

Because  $H\alpha$  appears split, the radial velocity in the vicinity of the Black Hole is estimated here, using the FWHM of the Doppler-broadened and Gauss fitted  $H\beta$  line. Infos to the formula see [30], sect. 17. At such extreme line widths the correction of the instrumental broadening can be neglected. It results in  $FWHM_{Emission\ H\beta} \approx 88\text{Å}$ . The radial velocity of the matter, calculated with the Doppler principle results in:

$$v_r \approx \frac{FWHM_{Emission\ H\beta}}{\lambda_{0\ H\beta}} \cdot c \approx 5400\text{ km/s}$$

This is roughly within the strongly scattering literature values. For the jet however, based on X-ray analyses, up to 70% of the light speed are postulated [308].

Not only the brightness of the object can vary considerably (see AAVSO), also the spectral characteristics can change dramatically within a short time, such as the half-width  $EW$  of the  $H\beta$  emission (for details see [36]). It also shows that this central region can't be indefinitely large, and according to [www.hubblesite.org](http://www.hubblesite.org) can therefore hardly exceed the diameter of our solar system. 3C273 would certainly be a highly interesting candidate for a monitoring project. In addition to such considerations we should always be aware that these

changes, observed within a very short time, took place about 2.4 billion years ago, when our earth was still in the Precambrian geological age!

Table 78: Quasar 3C273, Redshift

On this table, redshifted wavelengths are indicated, measured at Gaussian fitted lines and related to the original wavelength scale, calibrated with a calibration light source [35]. The amounts of redshift are not constant but, for a given radial velocity  $v_r$ , proportional to the rest wavelength  $\lambda_0$  of the corresponding spectral line.

$$\Delta\lambda = \frac{v_r \cdot \lambda_0}{c}$$

In the field of astrophysics for such highly red shifted objects, the distance is usually expressed directly as  $z$ -value. It can easily be determined by the measured Redshift in the spectrum and is independent of assumptions for cosmological model parameters (eg  $\Omega$ ). Due to the constant speed of light  $c = const$ ,  $z$  is also used as a measure of time for the past.

$$z = \frac{\Delta\lambda}{\lambda_0}$$

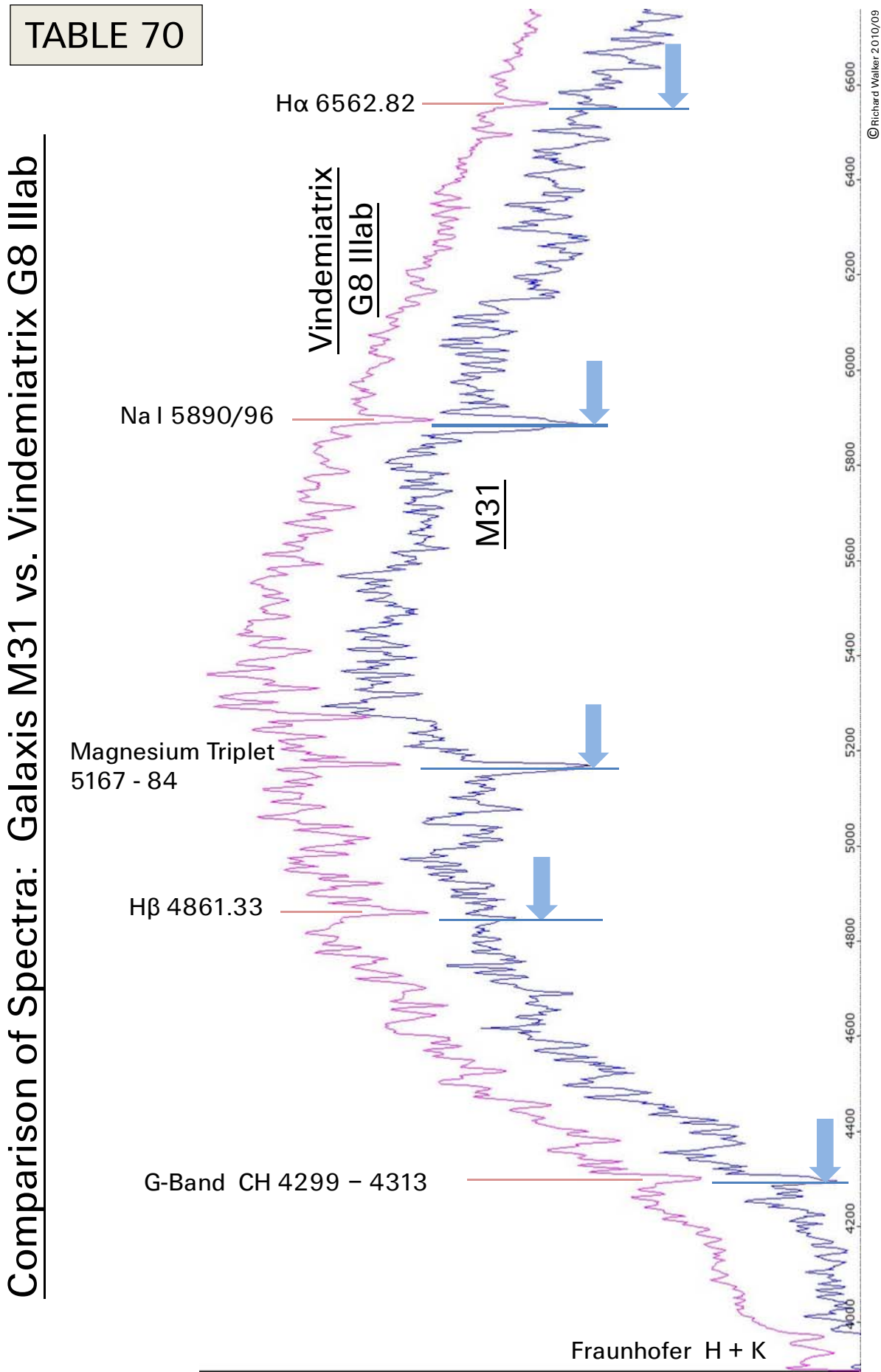
The  $\Delta\lambda$  values allow the calculation of the radial velocity  $v_r$  with the usual Doppler formula. With such high redshifts ( $z > 0.1$ ), however, the relativistic formula should be used for  $v_{rel}$  [16].

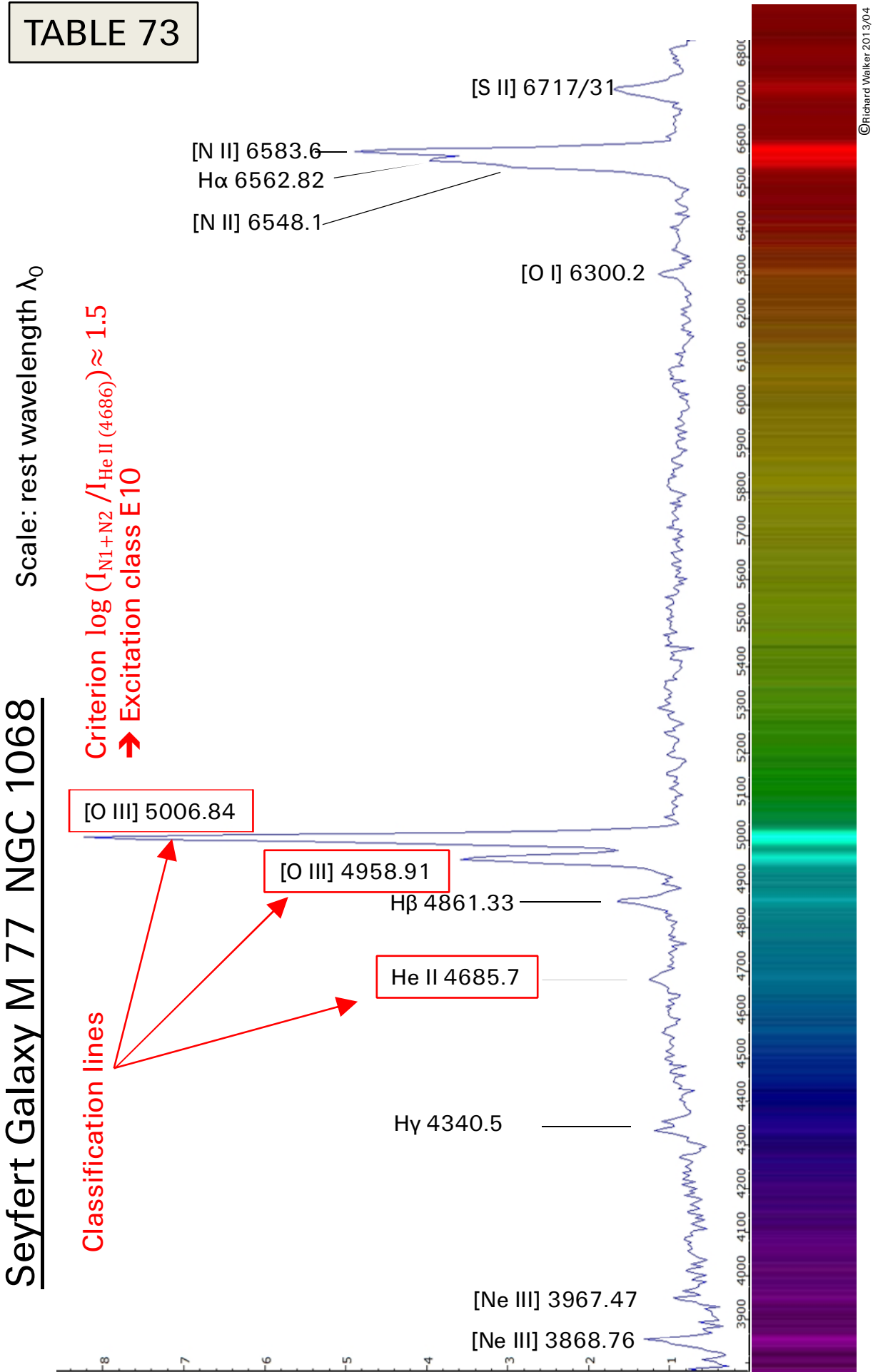
$$\text{Doppler formula: } v_r = \frac{\Delta\lambda}{\lambda_0} \cdot c \quad \text{relativistic: } v_{rel} = c \cdot \frac{(z + 1)^2 - 1}{(z + 1)^2 + 1}$$

Results of measurements and calculations:

$$z = 0.158 \quad v_r = 47'490\text{km/s} \quad v_{rel} = 43'808\text{km/s}$$

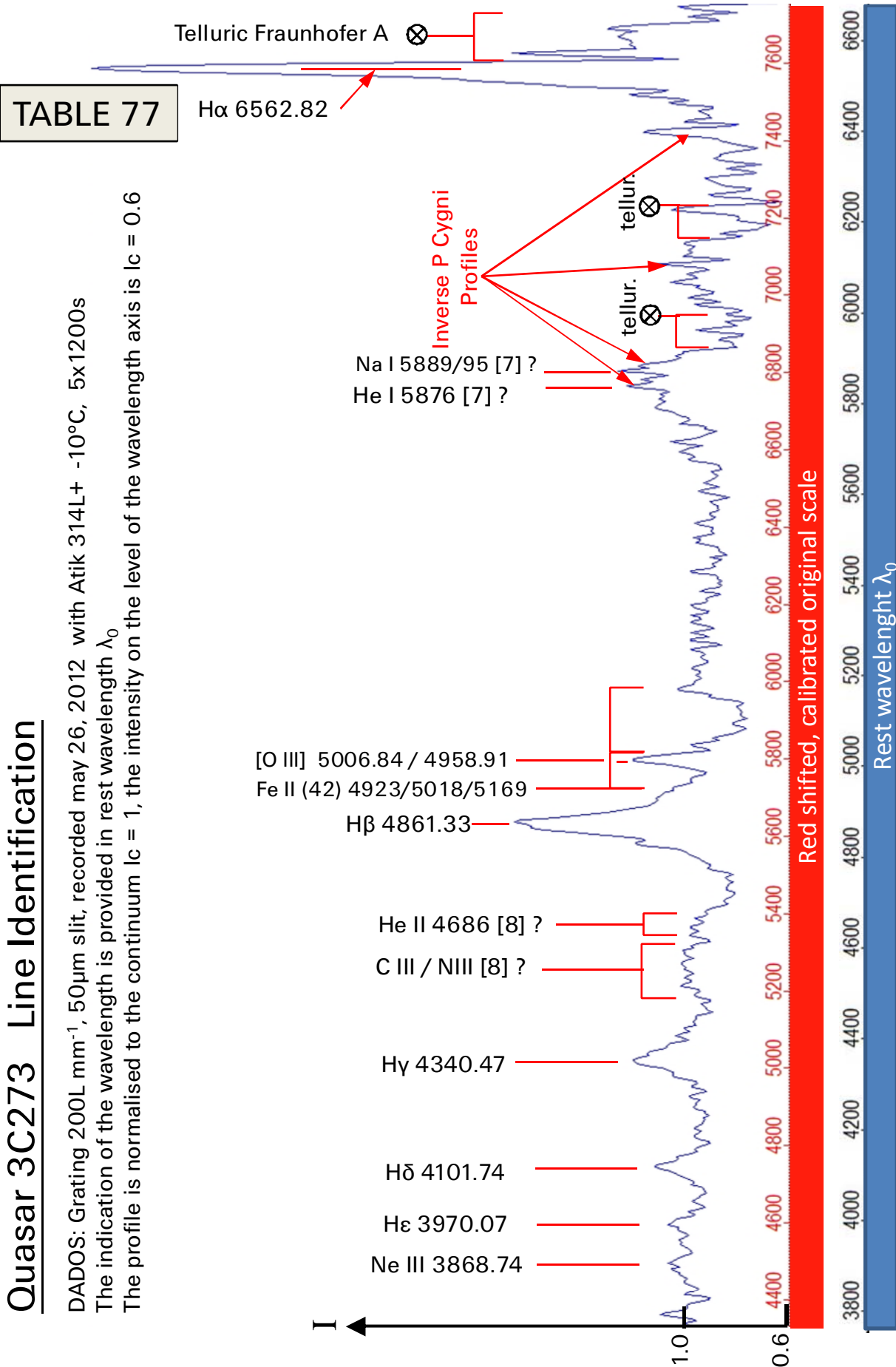
More information and distance determination, see [36].





# Quasar 3C273 Line Identification

DADOS: Grating 200L mm<sup>-1</sup>, 50μm slit, recorded may 26, 2012 with Atik 314L+ -10°C, 5x1200s  
The indication of the wavelength is provided in rest wavelength  $\lambda_0$   
The profile is normalised to the continuum  $I_c = 1$ , the intensity on the level of the wavelength axis is  $I_c = 0.6$

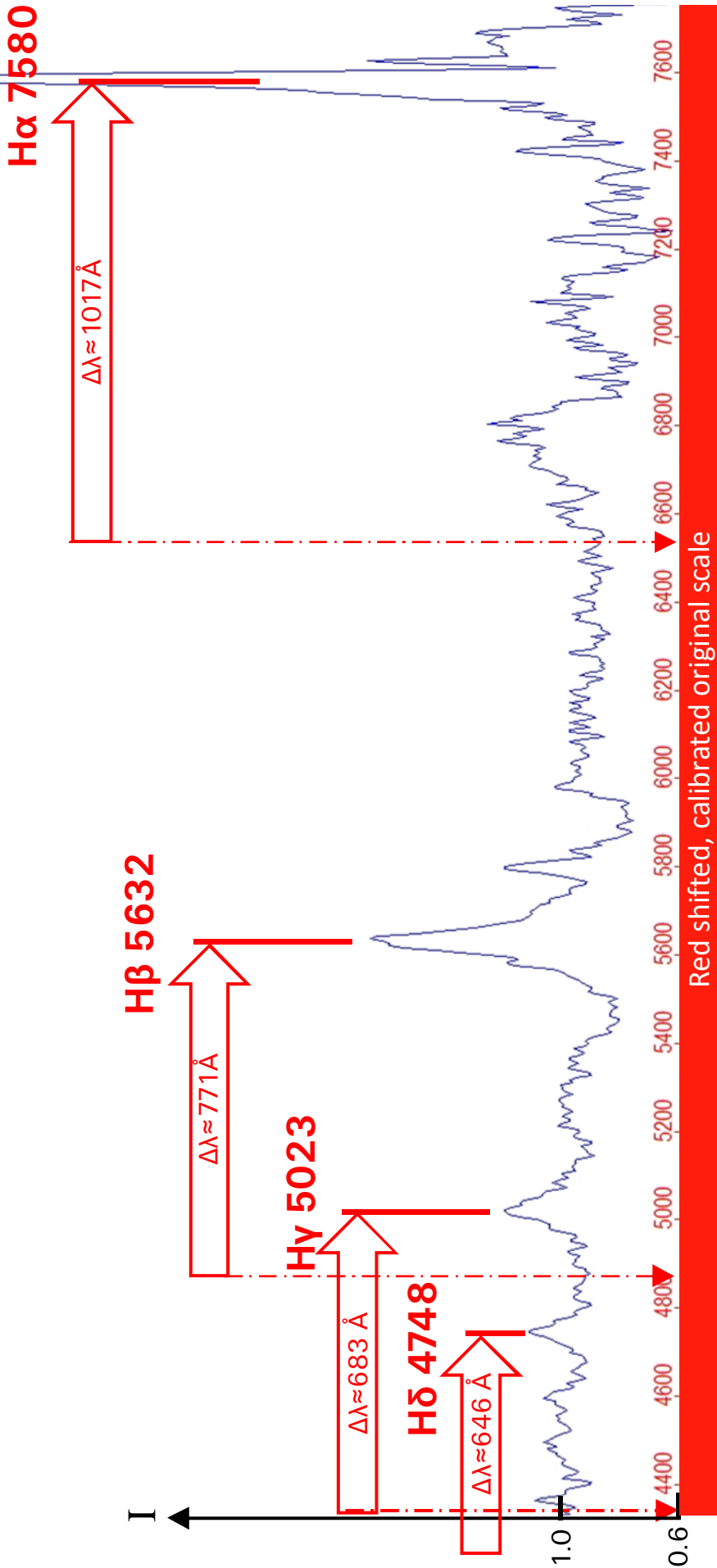




# Quasar 3C273, Redshift of the Hydrogen Balmer Lines

DADOS: Grating 200L mm<sup>-1</sup>, 50μm slit, recorded may 26, 2012 with Atik 314L+ -10°C, 5x1200s  
The indication of the wavelength, determined with Vspec at Gaussfits, is provided red shifted on the original scale. The profile is normalised to the continuum I<sub>c</sub> = 1, the intensity on the level of the wavelength axis is I<sub>c</sub> = 0.6.

TABLE 78



## 24 Spectra of Emission Nebulae

### 24.1 Short Introduction and Overview

*Reflection nebulae* are interstellar gas and dust clouds which passively reflect the light of the embedded stars. *Emission nebulae* however are shining actively. This process requires that the atoms are first ionised by hot radiation sources with at least 25,000K. The density of the nebulae is so extremely small that on earth it can be generated only as the best ultra-high vacuum. In [30], sect. 20, these processes are explained more in detail. The requirements for the development of *emission nebulae* are mainly met by the following astronomical “object classes”:

#### H II Regions:

Textbook example is the Orion Nebula *M42* (Photo: NASA). Here extremely hot stars of the O- and early B class ionise – in addition to helium, oxygen and nitrogen – primarily hydrogen atoms of the surrounding nebula. This requires UV photons, above the so-called Lyman limit of 912 Å and corresponding to an ionisation energy of >13.6 eV. This level is only achievable by very hot stars of the O- and early B-Class. Such H II regions tend to have a clumpy and chaotic structure and may extend over dozens of light years. They show a high star formation rate and can still be detected even in distant galaxies. The reddish hue is caused by the dominant H $\alpha$  emission.



#### Planetary Nebulae PN – The most significant sub-group of the emission nebulae

In the central part of these much higher energetic objects are mostly extremely hot white dwarfs with up to > 200,000K. This is the final stage of stars at the end of the AGB (sect. 19 – 22) with originally <8 solar masses. They ionise the atoms of their rather slowly expanding former stellar envelopes (some 20-40 km/s). Photo: NGC 6543 Cat’s eye nebula (NASA). About 10% of central stars show similar spectra in the final stage like Wolf Rayet stars, and thus have WR-classifications (WRPN). Their absolute magnitude however is considerably lower. PN often show an ellipsoidal shape, in some cases with a regular fine structure. The reasons for the numerous other existing forms are only partially understood.



#### Super Nova Remnants SNR and Wolf Rayet Nebulae WR

SNR show a striking filamentary structure. The main part of the ionisation energy is provided here by the collision of the rapidly expanding stellar envelope (a few 1000 km/s) with the interstellar matter. Photo: M1 Crab Nebula (NASA). The shells around the Wolf-Rayet Stars, such as the *Crescent Nebula NGC 6888* (table 86) are excited in a similar way, but anyway much less intensive.



In the center of SNR the remaining Neutron Star or Pulsar emits a wind of relativistic electrons with nearly light speed. It is deflected or slowed by magnetic fields within the plasma or electric fields around the ions. Such energy transformations are compensated by emitted photons, causing broadband *Synchrotron*- or *Bremsstrahlung*, predominantly in the X-ray domain.

## 24.2 Common Spectral Characteristics of Emission Nebulae

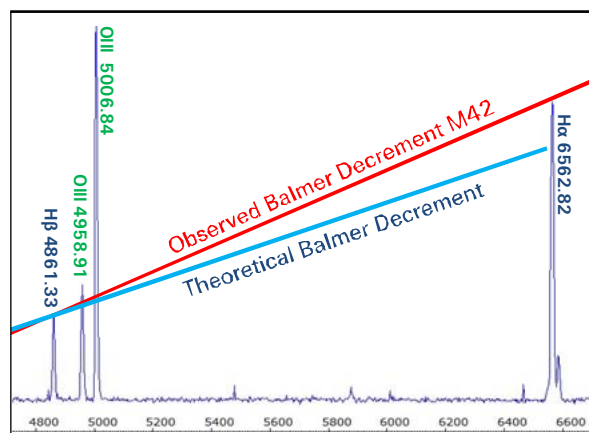
Besides of the chemical composition the local state of the plasma is determined by the power of the UV radiation as well as the temperature  $T_e$  and density  $N_e$  of the free electrons. By recombination the ions recapture free electrons which subsequently cascade down to lower levels, emitting photons of well defined discrete frequencies (fluorescence effect). According to the Plank formula:  $\Delta E = h \cdot \nu$ , the frequency of the emitted photon  $\nu$  [nu:] is exactly proportional to the energy difference  $\Delta E$  between the levels, of the downward electron transition. For these reasons, *emission nebulae* generate, similar to a gas discharge lamp, predominantly “quasi monochromatic” light, not as a continuum, but rather as several discrete emission lines. Accordingly effective are therefore specifically designed, narrow band nebula filters. With the exception of SNR, emission nebulae show only a very faint continuum radiation.

Since the main part of the light is concentrated on a few, more or less intense emission lines, these objects can be still detected even at extreme distances. The brightest [O III] lines become photographically visible just after very short exposure times. In all types of emission nebulae physically the same ionisation processes are responsible for the line formation, albeit with very different excitation energies. This explains the very similar appearance of the spectra. The graph below shows a section of the emission spectrum of M42 with two noticeable features:

1. The intensity ratio of the brightest [O III] lines is always:  $I(5007)/I(4959) \approx 3$ .
2. The intensity ratio between the hydrogen lines, called *Balmer Decrement D*, represents the quantum-mechanically induced intensity loss of these lines in the direction of decreasing wavelength. Detailed description see [30], sect. 18.

Important for astrophysics is the intensity ratio  $D = I(H\alpha)/I(H\beta)$ . The theoretically calculated value for thin gases is  $D_{Th} \approx 2.85$ .

The steeper the curve, the greater is the selective interstellar extinction (reddening) of light by dust particles, what in Photometry is called *red color excess*. As a result, the lines at shorter wavelengths are increasingly shown too short. Most of the galactic PN, reachable for amateurs, show values of  $D \approx 3.0 - 3.3$  [203]. Therefore, for a rough determination of the excitation class this effect can be neglected, especially as the diagnostic lines are relatively close together (see below). However, there are stark outliers like NGC 7027 with  $D \approx 7.4$  [14]. For extragalactic objects  $D$  becomes  $> 4$ , which in any case requires a correction of the intensities ("Dereddening") [204], (procedure see [30] sect. 19).



## 24.3 Emission Line Diagnostics and Excitation Classes E

Since the beginning of the 20th Century numerous methods have been proposed to determine the excitation classes of emission nebulae. The 12-level “revised” *Guradyan* system [14], which has been developed also by, *Aller, Webster, Acker* and others [204, 205, 206] is one of the currently best accepted and appropriate also for amateurs. It relies on the simple principle that with increasing excitation class, the intensity of the forbidden [O III] lines becomes stronger, *compared* with the H-Balmer series. Therefore as a classification criterion the intensity sum of the two brightest [O III] lines, relative to the H $\beta$  emission, is used. Within the range of the low excitation classes E: 1–4, this value increases strikingly. The [O III] lines at  $\lambda\lambda 4959$  and  $5007$  are denoted in the formulas as  $N_1$  and  $N_2$ .

$$\text{For low Excitation Classes } E1 - E4: \quad I_{N1+N2} / I_{H\beta}$$

Within the transition class E4 the He II line at  $\lambda 4686$  appears for the first time. It requires 24.6 eV for the ionisation, corresponding to about 50,000K [202]. That's almost twice the energy as needed for H II with 13.6 eV. From here on, the intensity of He II increases continuously and replaces the now stagnant  $H\beta$  emission as a comparison value in the formula. The ratio is expressed here logarithmically (base 10) in order to limit the range of values for the classification system:

$$\text{For middle and high Excitation Classes } E4 - E12: \quad \log(I_{N1+N2} / I_{He II (4686)})$$

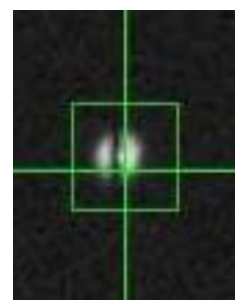
The 12 E-Classes are subdivided in to the groups Low ( $E = 1 - 4$ ), Middle ( $E = 4 - 8$ ) and High ( $E = 8 - 12$ ). In extreme cases  $12^+$  is assigned.

Low		Middle		High	
E-Class	$I_{N1+N2} / I_{H\beta}$	E-Class	$\log(I_{N1+N2} / I_{4686})$	E-Class	$\log(I_{N1+N2} / I_{4686})$
E1	0 - 5	E4	2.6	E9	1.7
E2	5 - 10	E5	2.5	E10	1.5
E3	10 - 15	E6	2.3	E11	1.2
E4	>15	E7	2.1	E12	0.9
		E8	1.9	E12 <sup>+</sup>	0.6

## 24.4 Remarks to the Determination of Excitation Classes and Recording of Spectra

The determination of the low E classes 1–4 is easy, since the  $H\beta$  line, compared to the [O III] emission, is relatively intense. At level E4 the He II line ( $\lambda 4686$ ) starts very weak, requiring very low-noise spectra, and a strong zoom into the intensity axis.

Quite easy to record are spectra from the very small, disc-shaped and blue-greenish shining PN. Thus they are very quickly to localize within a stellar group and the exposure time for the bright representatives takes only a few minutes (200L reflection grating). The brightest [O III] line appears often just after a few seconds on the screen (eg NGC 6210). The intensity of the lines is here integrated along the very short, exposed part of the slit. But along this very short appearing diameter the individual lines show considerably different intensities (see sect. 24.7). Furthermore, during long exposure times, small changes in the slit position with respect to the nebula are to observe as a result of inadequate seeing and/or guiding quality. Tests have shown that several spectra of the same object may show significantly different results including for the Balmer Decrement. Anyway the influence on the excitation class was observed as quite low! The picture shows the small sliver of the *Spirograph Nebula* (IC 418) on the 25  $\mu$ m slit (PHD Guiding). Between the green autoguiding cross and the slit the bright central star is visible.



By contrast the large appearing nebulae as M27 and M57 require, with the C8 and the Meade DSI III, at least 20–30 minutes of exposure time (without binning) and a totally cloud- and haze-free section of the sky. But they allow a selective recording of spectra within specific areas of the nebula, and to gain an intensity curve along the quite long exposed part of the slit (sect. 24.7). In this case, tests with several spectra of the same object showed consistent results. More detailed information on this topic, as well as remarks to the correction of the raw profiles, can be found in [30] sect. 20 and 21.

## 24.5 The Excitation Class as an Indicator for Plasma Diagnostics

Gurzadyan (among others) has shown that the excitation classes are more or less closely linked to the evolution of the PN [14], [206]. The study with a sample of 142 PN showed that the E-Class is a rough indicator for the following parameters; however in the reality the values may scatter considerably [13].

### 1. The age of the PN

Typically PN start on the lowest E- level and subsequently step up the entire scale with increasing age. The four lowest classes are usually passed very quickly. Later on this pace decreases dramatically. The entire process takes finally about 10,000 to > 20,000 years, an extremely short period, compared with the total lifetime of a star!

### 2. The Temperature $T_{eff}$ of the central star

The temperature of the central star also rises with the increasing E-Class. By repelling the shell, increasingly deeper and thus hotter layers of the star become "exposed". At about E7 in most cases an extremely hot White Dwarf remains, generating a WR-like spectrum. This demonstrates impressively the table of the PN in sect. 31. Hence, for  $T_{eff}$  [K] the following rough estimates can be derived:

E-Class	E1-2	E3	E4	E5	E7	E8-12
$T_{eff}$ [K]	35,000	50,000	70,000	80,000	90,000	100,000 – 200,000

### 3. The Expansion of the Nebula

The visibility limit of expanding PN lies at a maximum radius of about 1.6 ly (0.5 parsec), because from here on the dilution becomes too great [202]. With increasing E-class, also the radius of the expanding nebula is growing. Gurzadyan [206] provides mean values for  $R_n$  [ly] which however may scatter considerably for the individual nebulae.

E-Class	E1	E3	E5	E7	E9	E11	E12+
$R_n$ [ly]	0.5	0.65	0.72	1.0	1.2	1.4	1.6

## 24.6 Emission Lines identified in the Spectra of Nebulae

The appearance and intensity of emission lines in the spectra of the individual Nebulae are different. Therefore here follows a compilation with identified emission lines from *Plasma Recombination Lasers in Stellar Atmospheres* [200] and *Frank Gieseke* [202]. So-called "Forbidden lines" are written within brackets [].

*Ne III* 3869 [*Ne III*] 3967.5 *He I* 4026.2 [*S II*] 4068.6 *Hδ* 4101.7 *C II* 4267.3 *Hγ* 4340.5  
 [*O III*] 4363.2 *He I* 4387.9 *He I* 4471.5 *He II* 4541.6 [*Mg I*] 4571.1 [*N III*] 4641 *He II* 4685.7  
 [*Ar IV*] 4740.3 *Hβ* 4861.3 *He I* 4921.9 [*O III*] 4958.9 [*O III*] 5006.8 *N I* 5198.5 *He II* 5411.5  
 [*Cl III*] 5517.2 [*Cl III*] 5537.7 [*O I*] 5577.4 [*N II*] 5754.8 *He I* 5875.6 [*O I*] 6300.2 [*S III*] 6310.2  
 [*O I*] 6363.9 [*Ar V*] 6434.9 [*N II*] 6548.1 *Hα* 6562.8 [*N II*] 6583.6 *He I* 6678.1 [*S II*] 6717.0  
 [*S II*] 6731.3 [*He II*] 6890.7 [*Ar V*] 7006.3 *He I* 7065.2 [*Ar III*] 7135.8 *He II* 7177.5 [*Ar IV*] 7236.0  
 [*Ar IV*] 7263.3 *He I* 7281.3

## 24.7 Commented Spectra

Because spectra of emission nebulae barely show a continuum, the profiles in the following tables are slightly shifted upwards to improve the visibility of the scaled wavelength axis. The presentation of the following objects is sorted according to ascending excitation classes. For most of the PN, the problem of distance estimation is still not really solved. The information may therefore vary, depending on the sources up to >100%! Correspondingly inaccurate are therefore also the estimated diameters of the nebulae!



By pushing off the envelope and the progressive “exposing” of increasingly hotter, inner stellar layers, central stars of PN may generate spectra, *simulating* substantially more massive and luminous stars. This applies, for example, for all O-, early B- and WR-classifications! However the progenitor stars of planetary nebulae are limited to maximum 8 solar masses, corresponding to the middle B class.

Table 80	Orion Nebula M42, NGC1976	Object type: HII region	Excitation class: <b>E1</b>
----------	---------------------------	-------------------------	-----------------------------

T80 shows the emission spectrum of M42 (approx. 1400 ly) taken in the immediate vicinity of the trapezium  $\theta^1$  *Orionis*. Main radiation source is the C- component, a blue giant of the rare, early spectral type O6 (see Table 3) with a temperature of approx. 40,000K [207]. Together with the other stars of the early B-Class, it is capable to excite the surrounding nebula with the criterion value  $I_{N1+N2}/I_{H\beta} \approx 5$  up to the border area between the classes E1 and E2. The  $H\beta$  line is here just slightly surpassed by the [O III] ( $\lambda$  4959) emission. Due to the enormous apparent brightness the object is spectrographically easy accessible and requires only modest exposure times. (10x30 seconds).

Table 80A	Orion Nebula M42	Intensity profiles within the central part of the nebula
-----------	------------------	--

T80A shows for the [O III] ( $\lambda$ 5007) and  $H\beta$  emission lines the intensity profiles along the entire length of the slit array (some 2.5 ly), within the central region of the nebula (Photo M42: HST). The ratio of these intensities demonstrates indirectly the course of the excitation class. Thanks to the linear arrangement of the three slits, DADOS allows for 2-dimensional appearing objects an improvised "Long-slit" spectroscopy, which enables to gain spectral information, combined with the spatial dimension. These profiles have been generated with Vspec and spectral stripes, rotated by 90° with the IRIS software. On the narrow bridges between the individual slits the intensity curve is supplemented with dashed lines. After recording of the spectra in each case a screenshot of the slit camera was taken to document the exact location of the slit array within the nebula.

The different width of the three slits (50/25/30  $\mu$ m) plays a little role for this purpose, since just the intensity course is recorded and IRIS averages anyway the gray values within the whole slit width. The slit array was positioned on two places within the central part of M42 and approximately aligned in the North-South direction. The western section runs through the C- component of the brightest Trapezium star  $\theta_1$  *Orionis* C (Table 3) and ends at the so called *Orion Bar*. The eastern section runs along the *Schröter-Bridge*, through the *Sinus Magnus* and finally also the impressive *Orion Bar*, southeast of the *Trapezium*. The intensity scales of the profiles are normalised on the spectral peak value of [O III] = 1 within the *Orion Bar* and the peak of  $H\beta$  on the local ratio there of [O III]/ $H\beta \approx 2.5$ .

Striking is the dramatic increase of intensity within the area of the Trapezium and in the huge ionisation front of the *Orion Bar*. The latter marks the end of the ionised H II region or the so called *Strömgren Radius*. At the end of this transition zone the nebula is heated up to just several 100 K, by the remaining UV photons with energies <13.6 eV which, below this Lyman limit, could not be absorbed by the ionisation processes within the H II area. Outside this transition zone follow chemically increasingly complex molecular clouds [404].

Also remarkable is the sharp drop of the intensity within the dark cloud in the *Sinus Magnus* and the slight increase in the range of the *Schröter Bridge*. The C- component of  $\theta_1$  *Orionis* produces here about 80% of all photons [223]! Without it, only a much smaller part of the nebula would be ionised, i.e. the corresponding Strömgren Radius  $R_s$  would be significantly shorter. Calculated for a relatively "dense" gas (relative to H II regions) of  $10^3 \text{ cm}^{-3}$  and an O6 star with 43,600K yields  $R_s \approx 3 \text{ ly}$  (0.9pc). For B0 stars this value drops to  $R_s \approx 1.2 \text{ ly}$  (0.36pc) [404]. The lower the density of the nebula the greater will be the *Strömgren Radius*, because comparatively lesser photons will be absorbed within the same route.



Table 81	Spirograph Nebula IC 418	Object type: PN	Excitation class: E1
----------	--------------------------	-----------------	----------------------

Spectrum of IC 418 (approx. 2500 ly). The central star has here a temperature of only 35,000K [207]. It is still unstable, highly variable within short periods of time and therefore just able to excite this nebula with the criterion value  $I_{N1+N2}/I_{H\beta} \approx 2.8$  to the lowest class E1 (Gurzadyan: E1 [206]). This is still lower than in the H II region M42. Further  $H\beta$  here even outperforms the intensity of [O III] ( $\lambda$  4959). Accordingly, the PN stage must be still very young and also the diameter of the ionized shell is estimated to just 0.2 ly [207]. The complex spirograph pattern in the nebula is still not understood. Exposure time with the C8 is 3x170 seconds. Photo: HST.



Table 82	Turtle Nebula NGC 6210	Object type: PN	Excitation class: E4
----------	------------------------	-----------------	----------------------

Spectrum of NGC 6210 (approx. 6500 ly). The central star has here a temperature of approx. 58,000K [207] and is classified as O7f. It excites this nebula with the criterion value  $I_{N1+N2}/I_{H\beta} \approx 14$  slightly below the threshold of class E4 (~consistent to Gurzadyan: E4 [206]). In the spectrum appears here, only very weak, the He II line ( $\lambda$  4686). In some cases, this line can also be emitted directly from the central star [206]. Exposure time with the C8 is 4x45 seconds. Photo: HST.



Table 83	Saturn Nebula NGC 7009	Object type: PN	Excitation class: E8
----------	------------------------	-----------------	----------------------

Spectrum of NGC 7009 (approx. 2000 ly). The central White Dwarf has a temperature of approx. 90,000K [207]. It excites this nebula with the criterion value  $\log(I_{N1+N2}/I_{He II (4686)}) \approx 1.9$  up to the class E8. (Gurzadyan: slightly different: E7 [206]). The blue profile is strongly zoomed in the intensity to make the weaker lines visible. Striking are here, despite the high excitation class, still intense H emissions and a too low Balmer decrement of  $D < 2.8$ , (possible influences sect. 24.4). This PN is the first whose expansion could be detected photographically. [202]. Exposure time with the C8 is 7x240 seconds. Photo: HST

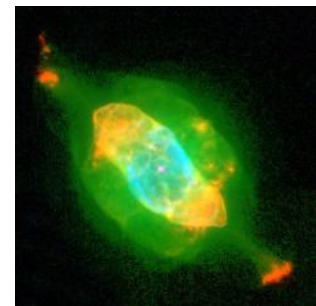


Table 84	Ring Nebula M57, NGC 6720	Object type: PN	Excitation class: E10
----------	---------------------------	-----------------	-----------------------

T84 shows the emission spectrum of M57 (approx. 2300 ly) approximately in the center of the Ring Nebula. The central White Dwarf has a temperature of approx. 150,000K [207]. It excites this nebula with the criterion value  $\log(I_{N1+N2}/I_{He II (4686)}) \approx 1.4$  up to the class E10 (consistent to Gurzadyan: E10 [206]).

Accordingly weak are here the hydrogen lines relative to [O III]. The  $H\alpha$  line here just reaches parity with the weaker [N II] ( $\lambda$  6548) emission. The much stronger [N II] ( $\lambda$  6584) line however is the second-most intense emission behind [O III] ( $\lambda$  5007). Therefore the reddish color within the ring of M57 predominantly originates from [N II] instead of the by far weaker  $H\alpha$  line.

The broadband spectrum (left) was taken with the 90cm CEDES Cassegrain Telescope in Falera, slit width: 25 $\mu$ m, exposure time 5x340 seconds. This was obviously too short to show the weak classification line  $He II$  ( $\lambda$  4686). However, this was later achieved with the

C8, the low-resolution 50 $\mu$ m slit and an exposure time of 3x1270 seconds (excerpt of the spectrum to the right). This reflects the high effort, required for these large appearing PN (in this case 86"x72"). Typical for this high excitation class are the old age of about 20,000 years, and the large extent of the nebula of about 1.4 ly.

Table 84A	M57, Intensity profile along the longitudinal axis of the Ring Nebula
-----------	---

T84A shows for the strongest emission lines [O III] and [N II], the intensity profile along the entire 50 $\mu$ m slit, positioned on the longitudinal axis of the Ring Nebula. This profile has been generated with Vspec and a spectral stripe, rotated by 90° with the IRIS software.

Table 85	M1, NGC 1952	Object type: SNR	Excitation class: E >5
----------	--------------	------------------	------------------------

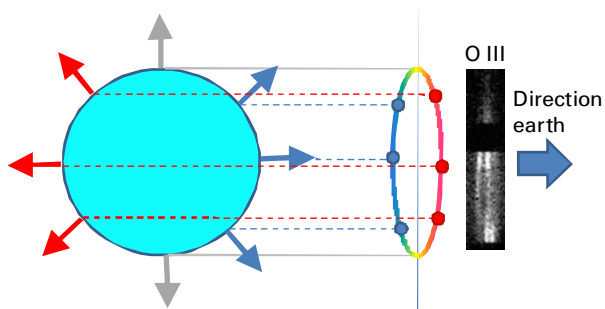
T85 shows the emission spectrum of the Supernova Remnant (SNR) M1 (approx. 6300 ly). The 50 $\mu$ m slit runs in ~N–S direction through the central part of this young SNR. The causal supernova explosion was observed and documented in 1054 by the Chinese. Today, the diameter of the expanding nebula reaches approximately 11 ly.

Vesto Slipher in 1913 recorded the first spectrum of M1. At that time he already noticed a massive split up of the most intense emission lines. Unaware of the nebula expansion, he interpreted this spectral symptom incorrectly as the newly discovered *Stark effect* caused by the interaction with electric fields. 1919 exposed R.F. Sanford, the M1 spectrum with the 2.5m Hooker Telescope, and at that time the "fastest" film emulsions, while no fewer than 48 hours! The result he describes sobering as "dissapointingly weak", a well clear indication that even today this can't be really a beginner object. The expansion of the nebula was found not until 1921 by C.O. Lampland, by comparing different photographic plates!

With the C8, a 200L grating and an Atik 314L+ camera, cooled to –20°C with 2x2 binning mode, after all still 2x30 minutes were needed to record a spectrum of passably acceptable quality. As an annoying side effect of the long exposure time, light pollution and airglow (Table 96) was recorded in a comparable intensity to the signal of M1, despite a quite passable rural sky with a visible magnitude of maximum about 4–5<sup>m</sup>. This disturbing spectrum was therefore recorded separately, just outside the nebula, and afterwards subtracted with Fitswork from the M1 signal.

This apparently almost 1,000 years old expanding shell is meanwhile diluted to such an extent, that it has become optically transparent. This show also the redshifted peaks of the splitted, well shaped emission lines, often appearing of similar intensity like the blue-shifted, but in some cases however significantly weaker.

The chart at right explains the split up of the emission lines due to the Doppler Effect. The parts of the shell which move towards earth cause a blue shift of the lines and the re-treating ones are red shifted. Thereby, they are deformed to a so-called velocity ellipse. This effect is seen here at the noisy [O III] lines of the M1 spectrum – below the 50 $\mu$ m slit, on the top the 25 $\mu$ m slit.



At this low resolution the red-shifted peak of the [O III] ( $\lambda$  4959) emission forms a blend with the blue-shifted peak of the [O III] ( $\lambda$  5007) line. Due to the transparency of the SNR, with the split up of  $\Delta\lambda$ , as already shown in Table 2 and in [30], the total expansion velocity of the matter can be determined, related on the diameter of the shell (here, about

1800 km/s). The *radial velocity* is obtained finally by halving this value. The radial velocity of this young SNR yields just below 1000 km/s – about 50 times higher than in PN.

By contrast, the envelopes of Wolf Rayet stars (Table 5), P Cygni (Table 13/13A) and to an extreme extent also of Novae and Supernovae, are so dense that we see only the *hemisphere* of the expanding shell, heading towards the earth. In these cases we measure *directly* the *radial velocity*, applying the Doppler formula.

Even more spectral symptoms show that SNR are a special case within the family of the emission nebula. In the center of the nebula (Profile **B**), due to synchrotron and bremsstrahlung processes (see [30]) a clear continuum is visible, which is very weak in the peripheral regions of the SNR (**A**). The latter profile was even slightly raised to make here readable the labeling of the wavelength axis. In contrast to the SNR it is difficult to detect a continuum in the spectra of *PN* and H II regions.

The line intensities  $I$  of the profiles **B**<sub>1,2</sub> were adapted relative to the continuum heights ( $I/I_c$ ), to become roughly comparable with those of profile **A**. Apparently in profile **A** and **B** the emissions in the range around  $\lambda$  6500 are of similar intensity. However, in the peripheral area of the nebula (profile **A**), the [O III] lines around  $\lambda$  5000 are several times stronger. Obviously the conditions for forbidden transitions are here much more favourable than in the vicinity of the high-energy pulsar, the stellar remnant of the SN explosion. This statement is relativized by the uncertainty, whether and to what extent the rudimentary subtraction of light pollution has affected the course of the continuum.

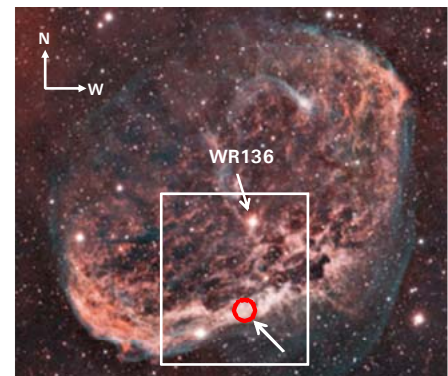
Due to shock wave induced collisional excitation the strikingly intense sulfur doublet ( $\lambda\lambda$  6718/33) becomes clearly visible. This feature is only weak in PN and almost completely absent in H II spectra. This also applies to the [O I] line at  $\lambda$  6300. Anyway at this resolution it can hardly be separated from the [O I] airglow line at the same wavelength (see sect. 27).

Table 86	NGC 6888 Crescent Nebula	Object type: WR-Nebula	Excitation class: <b>E1</b>
----------	--------------------------	------------------------	-----------------------------

T86 shows the emission spectrum of the *Crescent Nebula NGC 6888*, located in the constellation swan (some 4700 Lj). The picture (Wikipedia/Hewholooks) shows the nebula *WR 136*, the location of the recorded spectrum within the shock front, and the position of the image detail on table 86.

Origin and ionising source of *NGC 6888* is the Wolf Rayet star *WR 136*, which is described in sect. 8, table 6. In the previous giant stage, the star has already repelled a part of its gas shell. After the transition to the WR stage, about 30,000 years ago [240], the mass loss intensified dramatically to about  $10^{-5}$  to  $10^{-4} M_{\odot}$  per year [236] and the stellar wind accelerated to more than 1000 km/s. This violent stellar wind collides with interstellar matter and the gas layer, which was repelled earlier during the former giant stage of the star. This process generates an elliptically shaped *shock front*, expanding with some 75 km/s [240] to currently  $\sim 16 \times 25$  ly [237]. Similar to the *SNR*, this shock front is chiefly responsible for the ionisation and also for the fluffy pattern of the Crescent nebula. Within WR Nebulae, these processes apparently run much less violently as within *SNR*. For comparison; the shock wave of M1 expands with  $\sim 1000$  km/s. Anyway, this object is still some 30 times younger than NGC 6888. In WR nebulae also a central pulsar or neutron star is missing, which in SNR generates a permanent, relativistic electron wind, combined with the effects, described in Table 85.

The repelling of the hydrogen shell happens at the very beginning of the Wolf Rayet stage. Accordingly, later on, hydrogen can hardly be detected anymore in the spectra of WR stars



(sect. 8). With a dynamic age of about 30,000 years [240], WR 136 just passed some 10% of the entire, estimated WR sequence of ~200,000 years [237].

The spectrum was recorded with the 25 $\mu$ m slit and the 200L grating, just west of the star HD 192182 and within the outer shock front of the nebula. A continuum cannot be found here. The profile in table 87 was shifted just slightly upwards, to make visible the labelling of the wavelength axis. In contrast to M1 the degree of excitation of the plasma is *E1* and therefore very low. The H $\beta$  emission is even more intense than the [O III] line at  $\lambda$  4959.

Certainly, this can also be attributed to the advanced age of the nebula. In addition to the typical hydrogen- and O III emissions, only neutral helium He I, as well as forbidden lines of ionised nitrogen [N II] can be observed. The forbidden sulfur doublet [S II] at  $\lambda\lambda$  6718/33, a characteristic feature for shock waves, barely rises here above the continuum noise level.

With the C8 and the camera Atik 314L+, cooled to -20° C, after an exposure time of 2x30 minutes in the 2x2-binning mode, a slightly noisy, but for this purpose anyway useful profile resulted. On all shots, the separately recorded light pollution and the airglow (Table 96) had to be subtracted (Fitswork). Under the prevailing conditions, the nebula remained invisible in the flip mirror, even with help of the O III filter. The slit of the spectrograph was positioned on the selected nebula-filament with help of the field stars pattern.

## 24.8 Distinguishing Characteristics in the Spectra of Emission Nebulae

Here, the main distinguishing features are summarised again. Due to the synchrotron and bremsstrahlung *SNR* show, especially in the X-ray part of the spectrum, a clear continuum. X-ray telescopes are therefore highly valuable to distinguish SNR from the other nebula species, particularly by very faint extragalactic objects. For all other types of emission nebulae the detection of a continuum radiation is difficult.

In the optical part of *SNR* and to some extent also in *WR* spectra, the [S II] and [O I] lines are, relative to H $\alpha$ , more intense than at PN and H II regions, due to additionally shock wave induced collision ionisation. The [S II] and [O I] emissions are very weak at PN and almost totally absent in H II regions [204].

In SNR the electron density  $N_e$  is very low, ie somewhat lower than in H II regions. It amounts in the highly expanded, old *Cirrus Nebula* to about 300 cm<sup>-3</sup>. By the still young and compact *Crab Nebula* it is about 1000 cm<sup>-3</sup> [204]. By PN,  $N_e$  gets highest and is usually in the order of 10<sup>4</sup> cm<sup>-3</sup> [204]. In the H II region of M42,  $N_e$  is within the range of 1000–2000 cm<sup>-3</sup> [224]. The determination of  $N_e$  and  $T_e$  from the line intensities is presented in [30].

In H II regions, the excitation by the O- and early B-class stars is relatively low and therefore the excitation class remains in the order of just approx. *E* = 1-2. Planetary nebulae usually pass through all 12 excitation classes, following the evolution of the central star.

In this regard the SNR are also a highly complex special case. By very young SNR, eg the Crab Nebula (M1), dominate higher excitation classes whose levels are not homogeneously distributed within the nebula, according to the complex filament structure [222]. The diagnostic line He II at  $\lambda$  4686 is therefore a striking feature in some spectra of M1, ([222] and Table 85).

TABLE 80

Orion Nebula M42

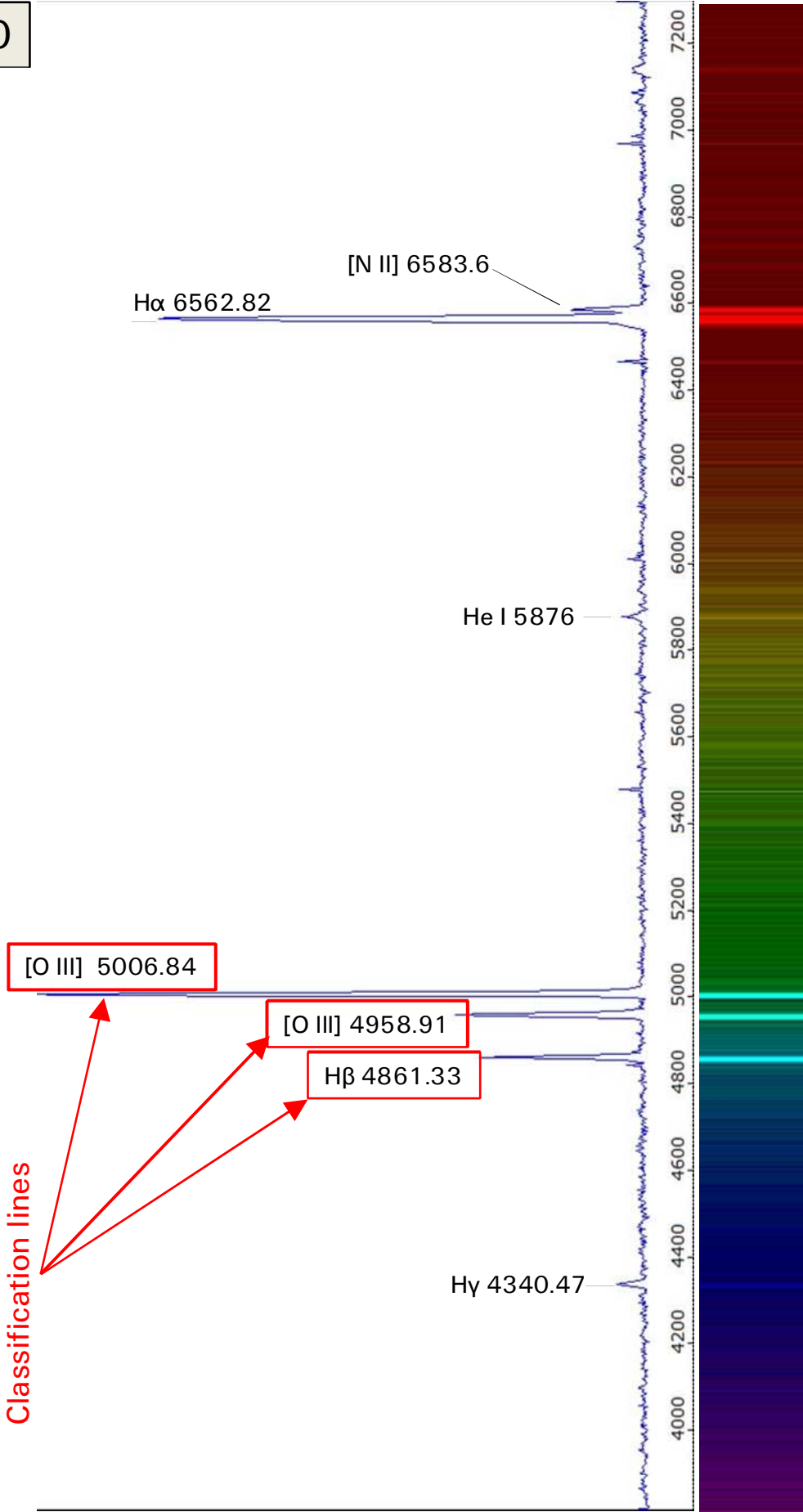


Excitation class E1

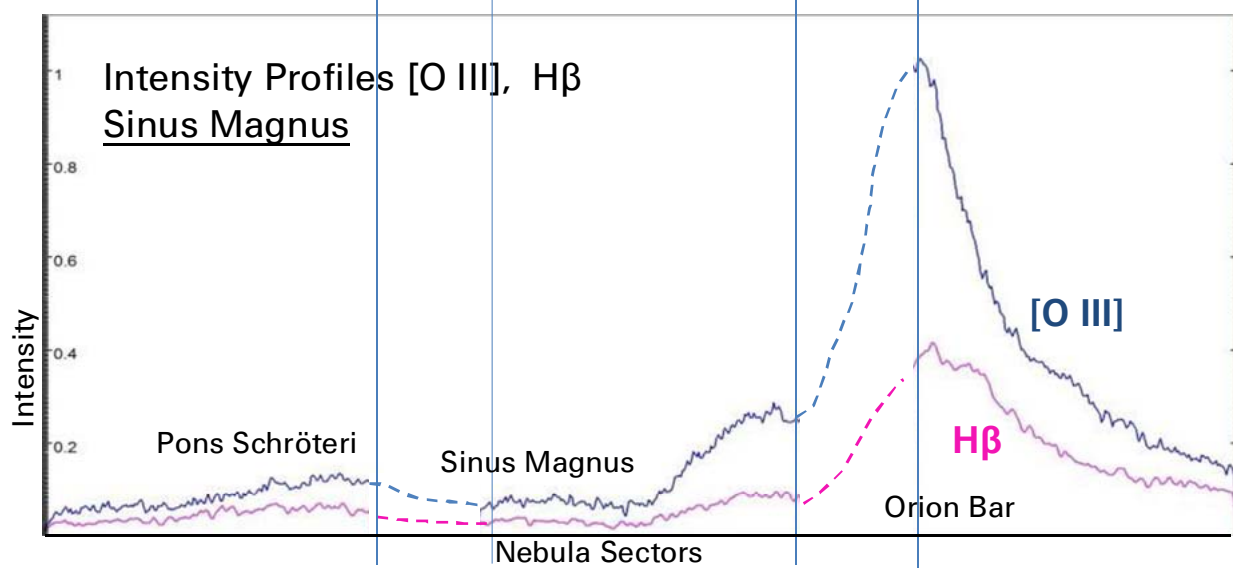
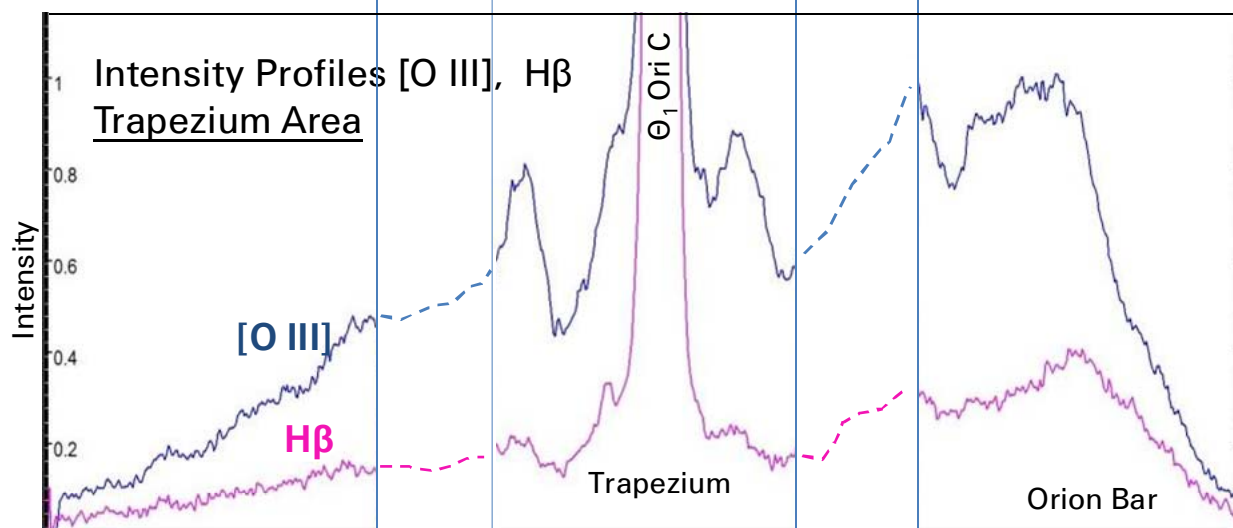
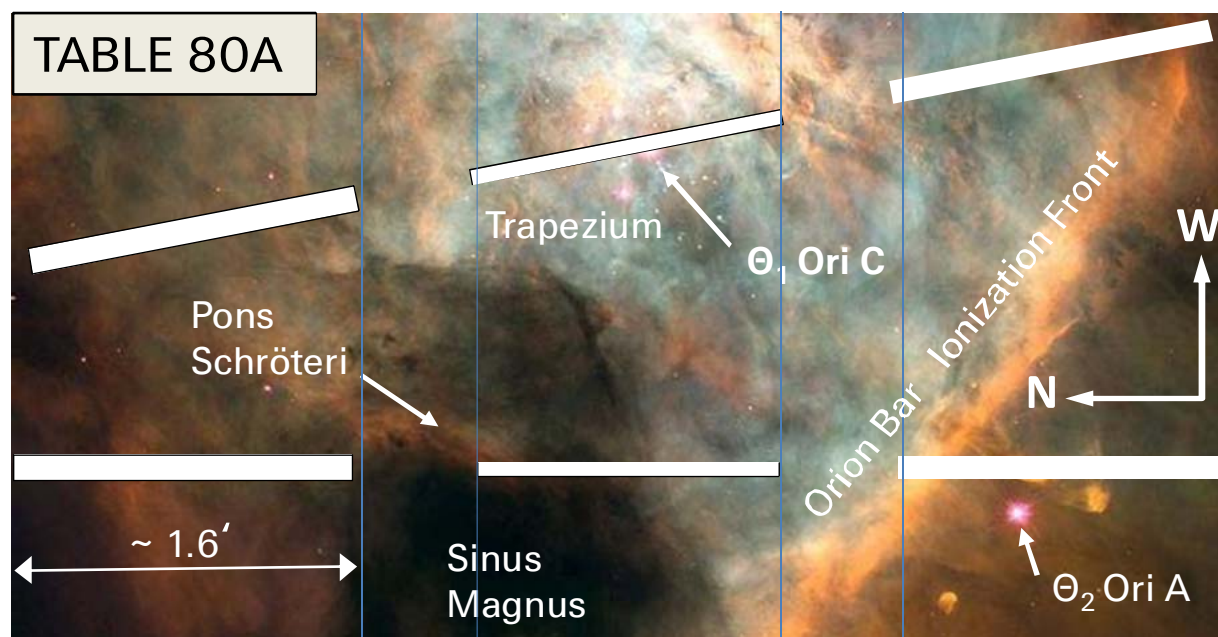
$I_{N1+N2}/H\beta \approx 5$

Criterion  $I_{N1+N2}/H\beta \approx 5$

Classification lines





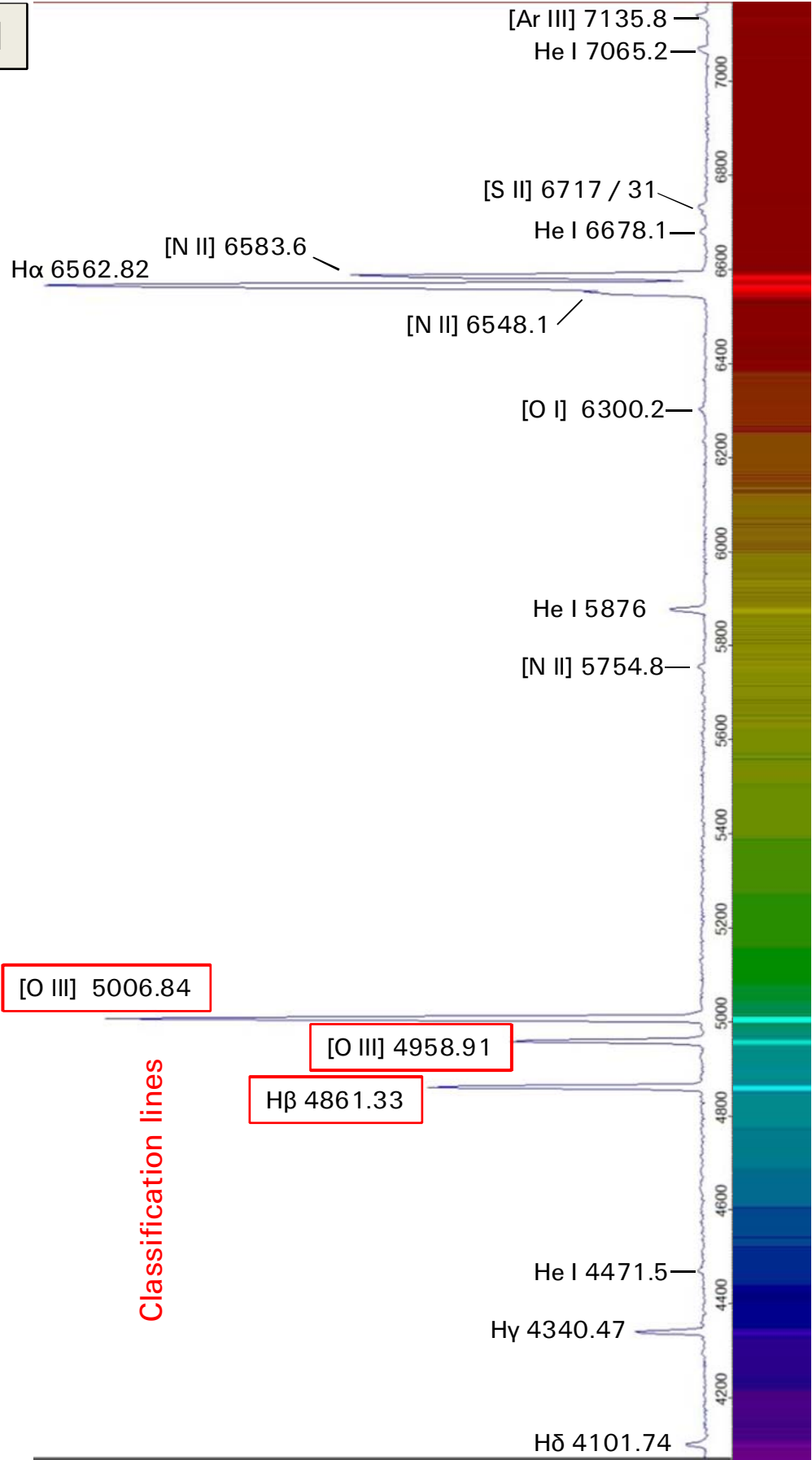




Spirograph Nebula IC 418

Criterion  $I_{N1+N2}/H\beta \approx 2.8$  ➔ Excitation Class E1

TABLE 81



Turtle Nebula NGC 6210

Criterion  $I_{N1+N2}/H\beta \approx 14 \rightarrow$  Excitation Class E3

TABLE 82

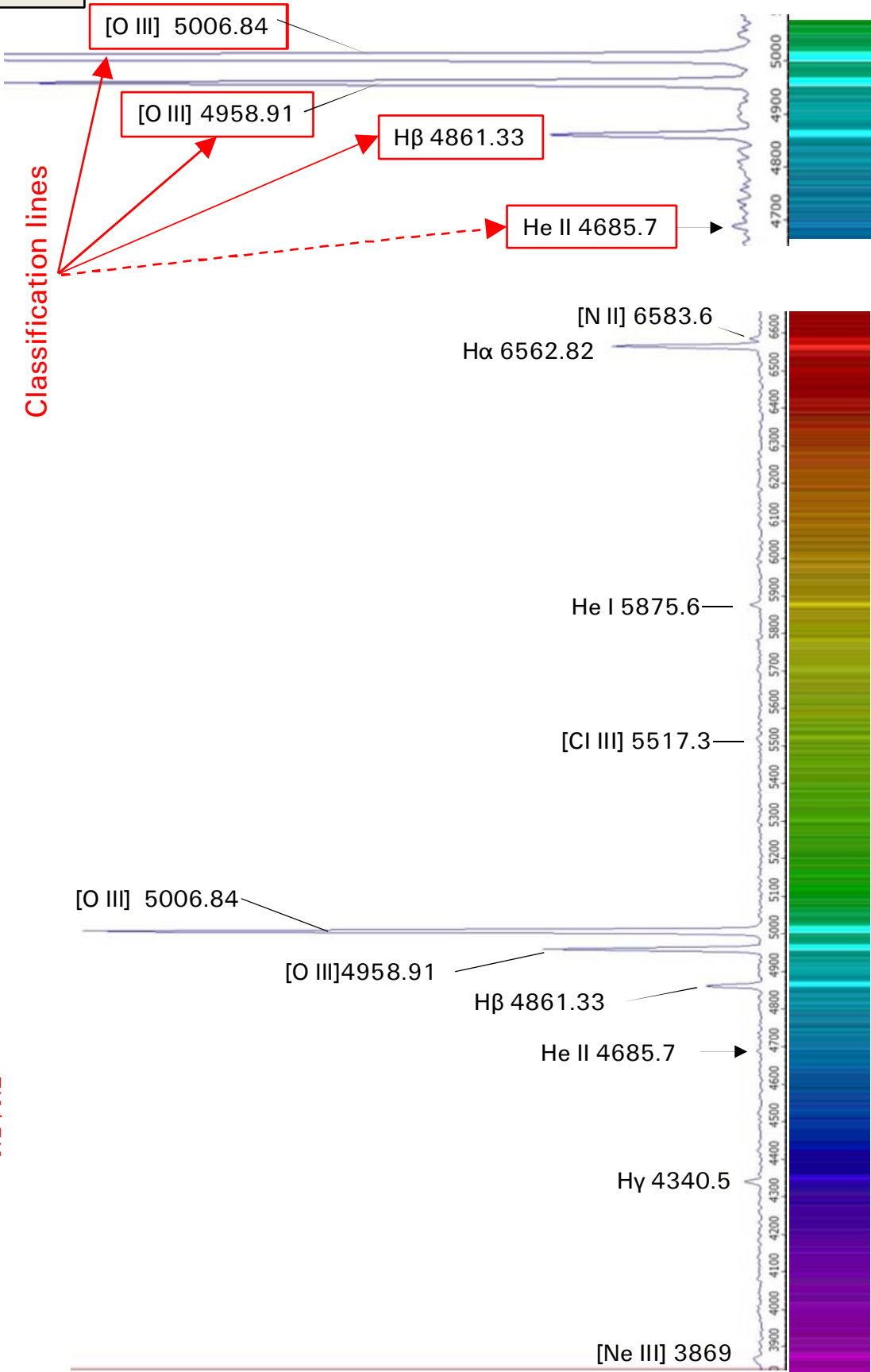


TABLE 83

Saturn Nebula NGC 7009

Criterion  $\log(I_{N1+N2}/I_{He II (4686)}) \approx 1.9 \rightarrow$  Excitation class E8

Classification lines

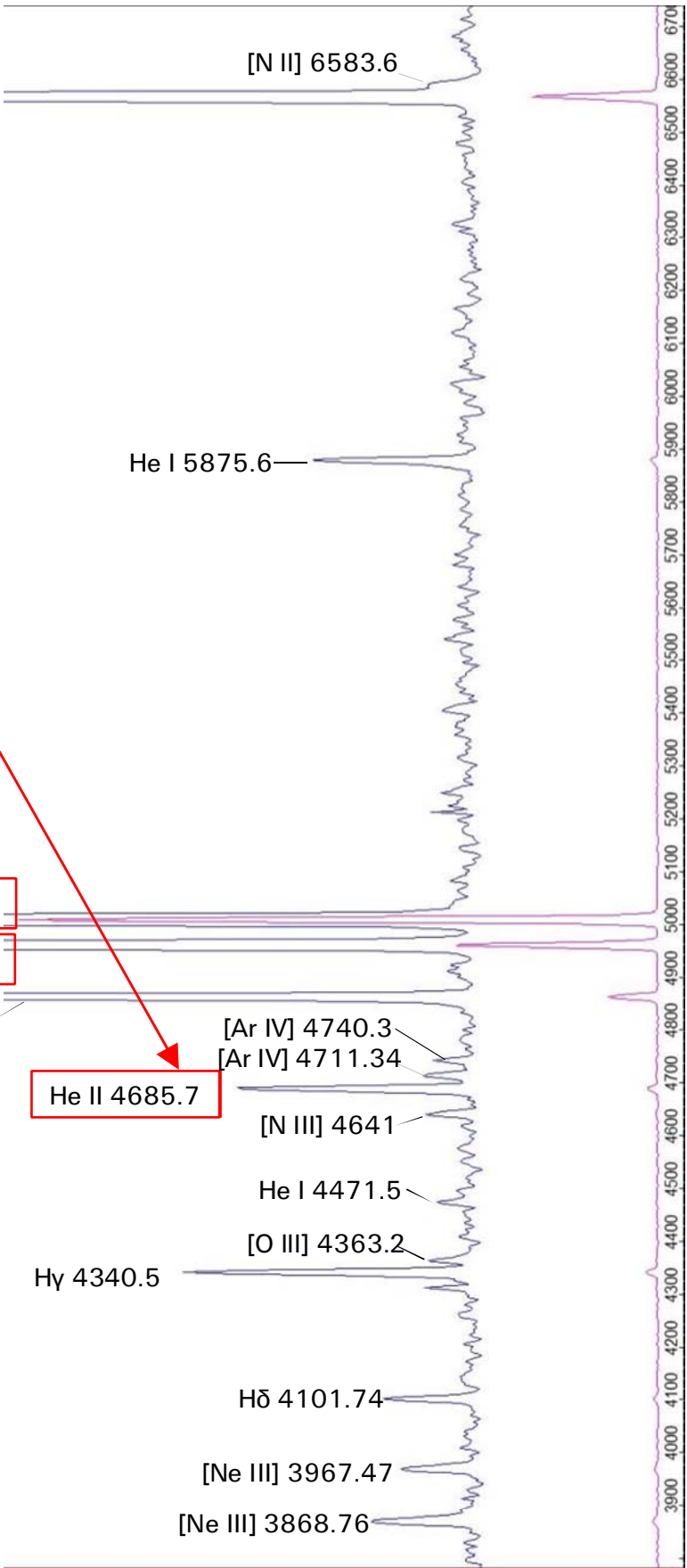


TABLE 84

Ring Nebula M57

Criterion  $\log(I_{N1+N2}/I_{He II (4686)}) \approx 1.4 \rightarrow$  Excitation Class E10

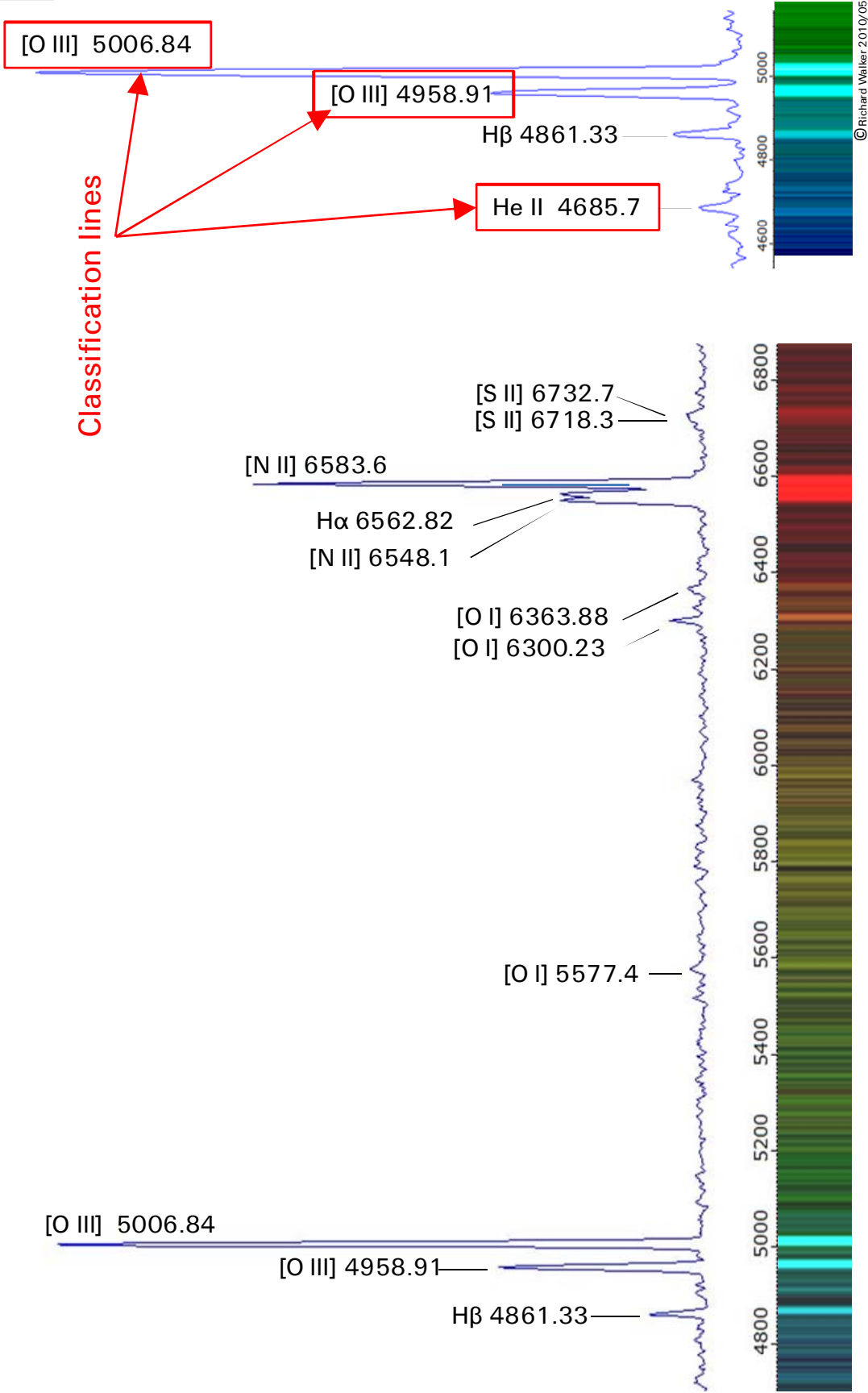


TABLE 84A

## Ring Nebula M57

Longitudinal section through M57. The 50 $\mu$ m slit of DADOS is approximately aligned with the longitudinal axis of the nebula. With Vspec the Intensity profiles of the strongest emissions [O III] and [N II] are generated along the entire length of the slit. The scales of the two profiles are normalized on the peak value of [O III] = 1, proportional to their line intensity in the spectrum. [N II] chiefly generates the reddish yellow edge part of the nebula, [O III] mainly produces the turquoise-blue color in the center of the Nebula (Photo: HST).

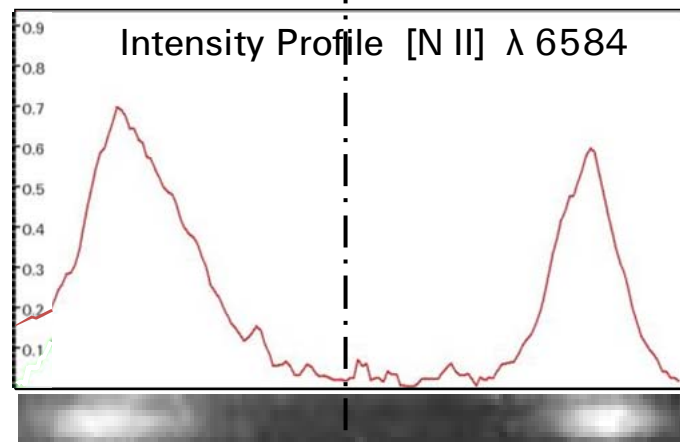
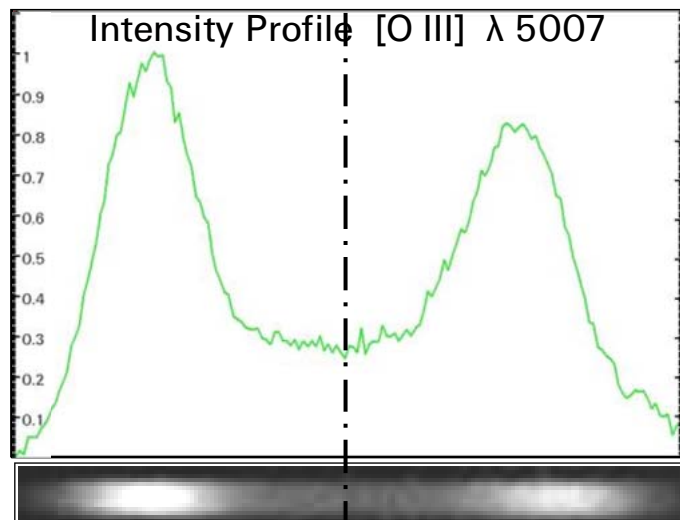
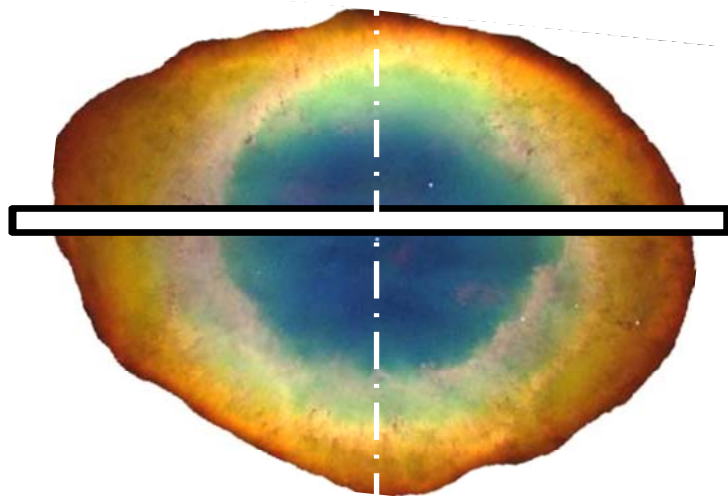


TABLE 85

SNR M1 / NGC 1952

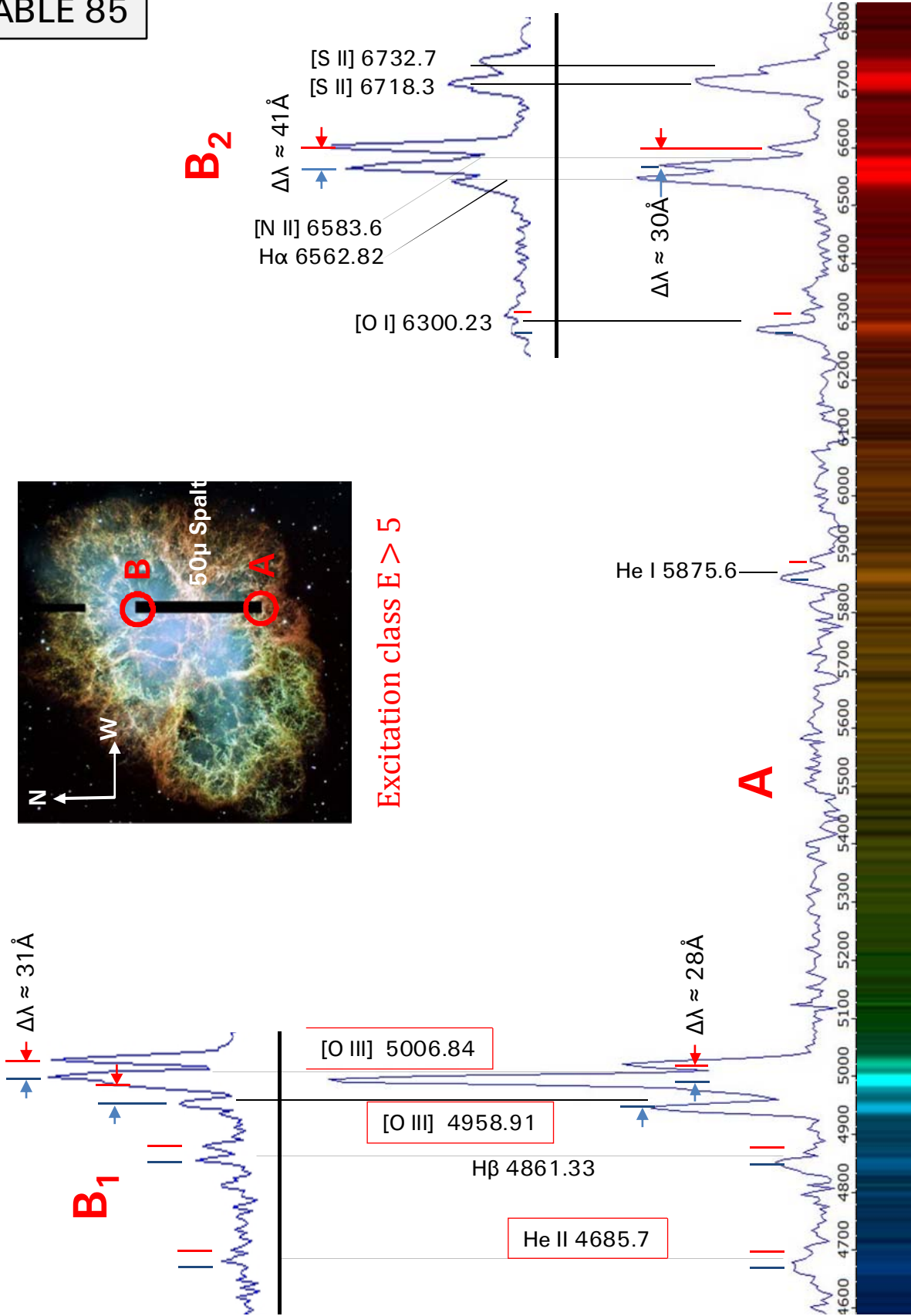
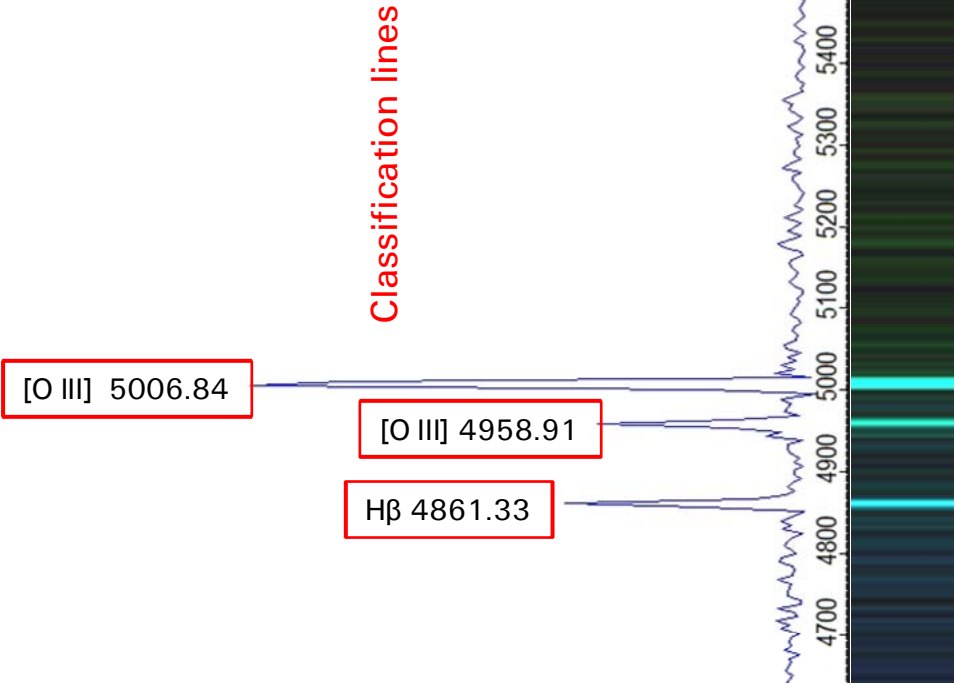




TABLE 86

Crescent Nebula NGC 6888, Type Wolf Rayet (WR136)

Criterion  $I_{N1+N2}/H\beta \approx 3.3 \rightarrow$  Excitation class E1



## 25 Reflexion Spectra of Solar System Bodies

### 25.1 Overview

The objects in our solar system are not self-luminous, and visible only due to reflected sunlight. Therefore, with exception of comets, these spectra always show, not surprisingly, the absorption lines of the Sun. On the other hand the spectral *continua* of the reflected profiles are overprinted, because certain molecules, e.g.  $CH_4$  (methane) in the atmospheres of the large gas planets, are reflecting or absorbing the light differently strong within specific wavelength ranges. According to their characteristics the planetary reflection spectra are separated here into two tables, each compared with the continuum of the sunlight. All profiles (200L grating) have been equally normalised. During the recording of the spectra all objects had an elevation above the horizon of some 30-40°.

### 25.2 Commented Spectra

#### Table 90: Reflection spectra of *Mars* and *Venus*

The extremely dense atmosphere of *Venus* generates on the surface a pressure of about 90 bar, ie approximately 90 times as high as on *Earth*. It consists of about 96% carbon dioxide ( $CO_2$ ). The remaining shares are mainly nitrogen ( $N_2$ ), water vapor ( $H_2O$ ), and sulfur compounds in the form of sulfur dioxide ( $SO_2$ ) and sulfuric acid ( $H_2SO_4$ ).

The extremely thin atmosphere of *Mars* consists similar to *Venus*, to about 96% of  $CO_2$ , but here under a surface pressure of only 0.006 bar, i.e. <1% of the value on the surface of the *Earth*. Here particularly the rocky surface of the planet might determine the reflective properties. In the displayed range the spectra neither of *Venus* nor *Mars* show significant deviations from the shape of the Sun's spectral continuum. In higher resolved spectra, of course experts can recognise and analyse differences.

#### Table 91: Reflection spectra of *Jupiter* and *Saturn*

The outer atmosphere of *Jupiter* consists of about 89% hydrogen and 10% helium, the rest mainly of methane and ammonia.

*Saturn's* outer atmosphere is composed slightly different. It consists of about 93% hydrogen and only close to 7% of helium. Further appear some traces of methane, ammonia and other gases.

Impressive to see here are, concentrated in the near-infrared range, the very broad methane ( $CH_4$ ) and ammonia ( $NH_3$ ) absorption gaps in the spectral continuum. In this wavelength domain, these differences are most pronounced visible in the areas of 6200 and  $\lambda$  7300.

#### Table 94: Comet C/2009 P1 Garradd

Comets, like all other objects in the solar system, reflect the sunlight. However on its course into the inner solar system core material increasingly evaporates, flowing out into the coma, and subsequently into the mostly separated plasma- and dust tails. The increasing solar wind, containing highly ionised particles (mainly protons and helium cores), excites the molecules of the comet. Thus the reflected solar spectrum gets more or less strongly overprinted with molecular emission bands, – chiefly due to vaporised carbon compounds of the cometary material. The most striking features are the  $C_2$  Swan bands, above all, the band heads at  $\lambda\lambda$  5165, 5636 and 4737 (see also sect. 28.2 and the comments on Table 110). Further frequently occurring emissions are CN (cyan) at  $\lambda\lambda$  4380 and 3880,  $NH_2$  (Amidogen Radicals), and  $C_3$  at  $\lambda$  4056. Sometimes also Na I lines can be de-

tected. Only slightly modified is the solar spectrum, recorded from sunlight, which has been exclusively reflected by the *dust tail*. A comprehensive catalog of cometary emission line can be found in [210] and additional data also in [110].

All these facts and the associated effects create complex composite spectra. The influence of the possible components depends primarily on the current intensity of the core eruptions, as well as on our specific perspective, regarding the coma, as well as the plasma- and dust tail.

In Table 94, the coma profile of C/2009 P1 Garradd is presented, taken on November 17 2011, 1730 GMT. Exposure time with the C8: 3x900s. Shown is a montage of the comet profile together with the C<sub>2</sub> Swan bands, generated with a butane gas burner. This comparison clearly shows that in this spectrum of comet Garradd only two of four C<sub>2</sub>-bandheads at  $\lambda\lambda$  5165 and 4715th are visible. The missing two are overprinted by molecular CH, CN and NH<sub>2</sub> emissions. Absorptions of the solar spectrum are hardly recognisable here. This became clear by a test superposition of the comet profile and the solar spectrum.

At the bottom of Table 94 the influence ranges of different molecules on the emissions of the spectrum are presented, according to the tables of [210]. Those are based on spectral profiles, which were obtained with a high-resolution Echelle spectrograph ( $R \sim 40,000$ ). It is noticeable that, apart from some isolated emissions, overlappings of the influence regions can barely be found.

.

# Reflection spectra of Mars and Venus compared to the daylight

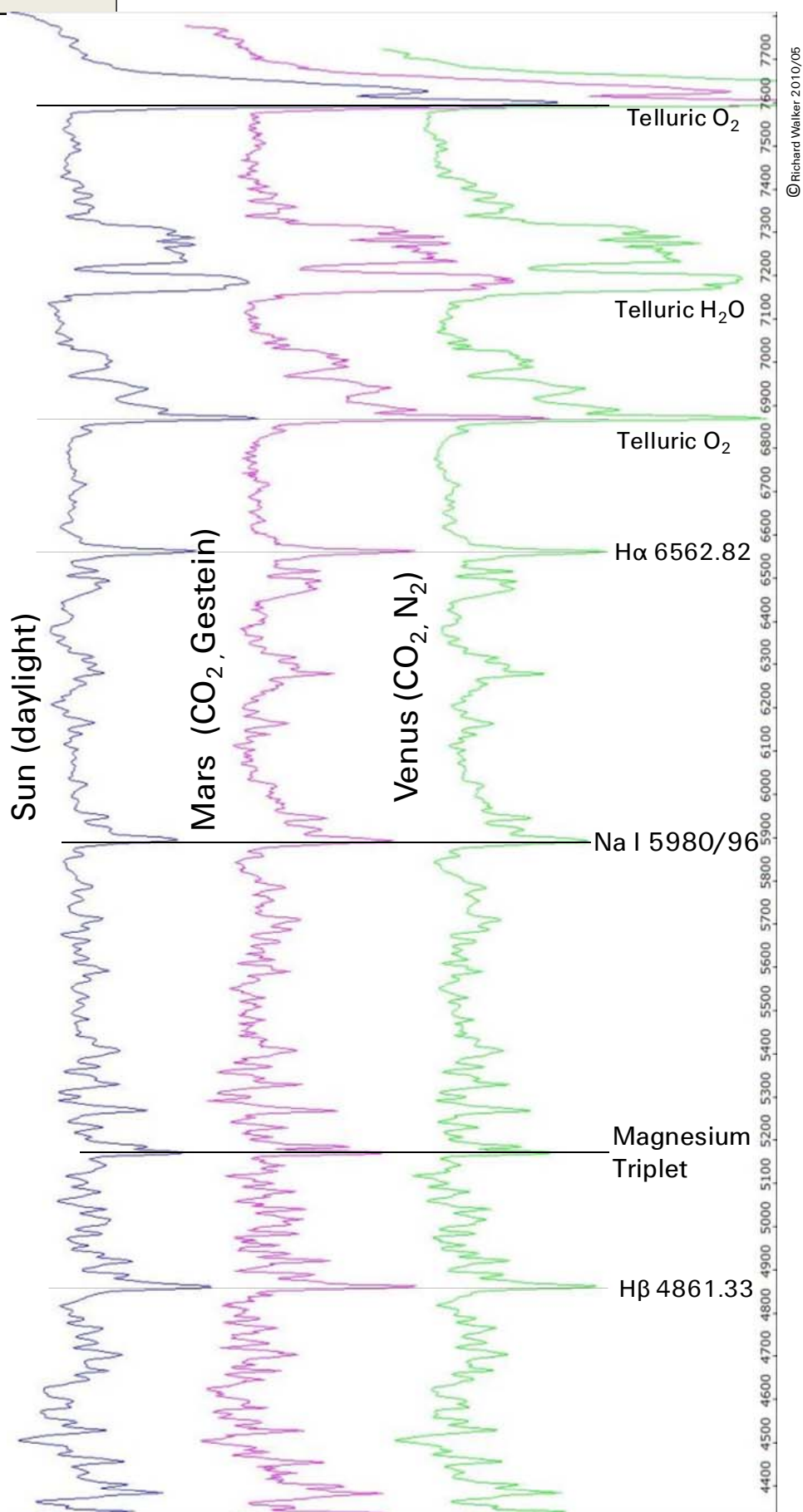
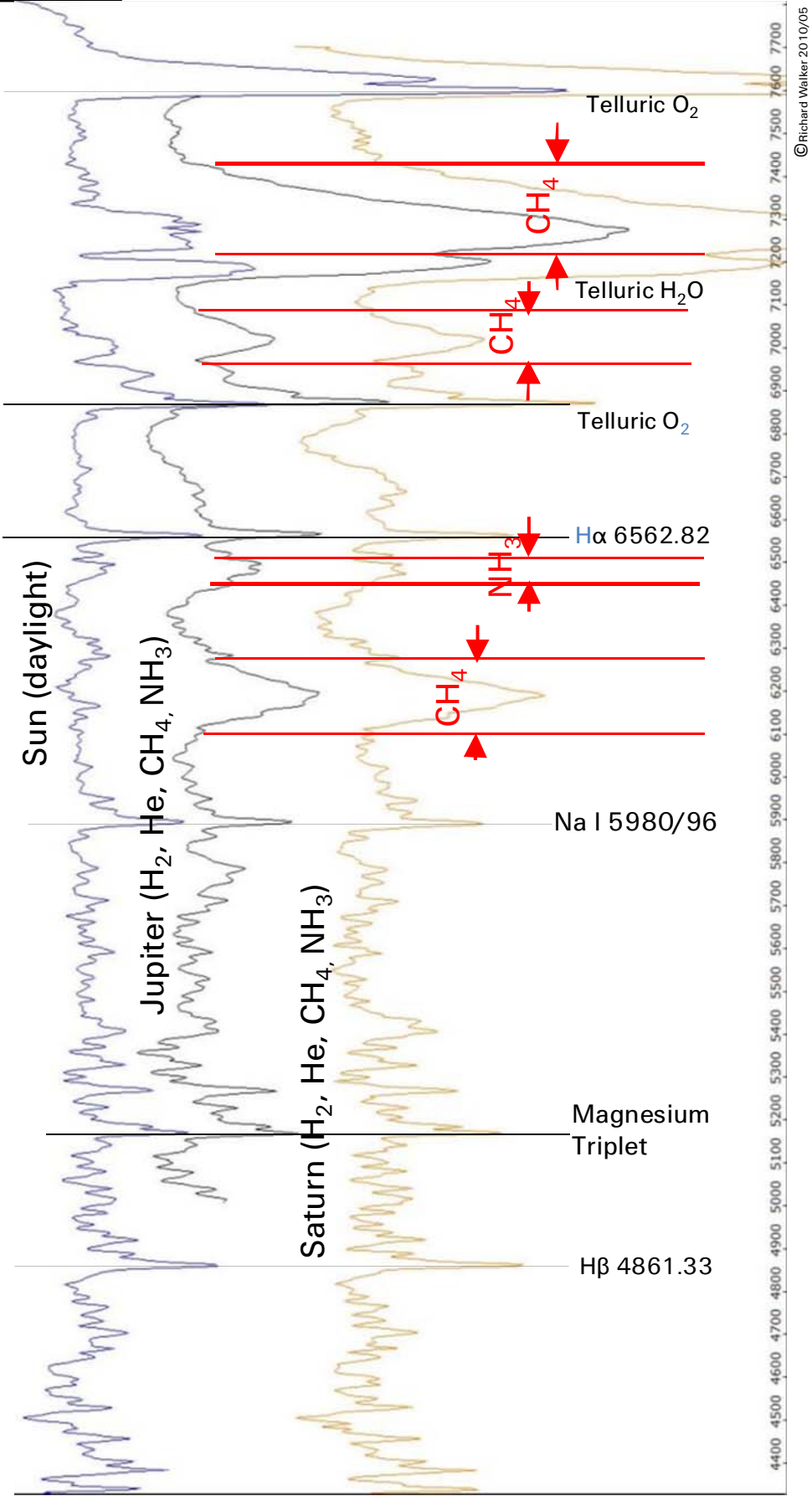
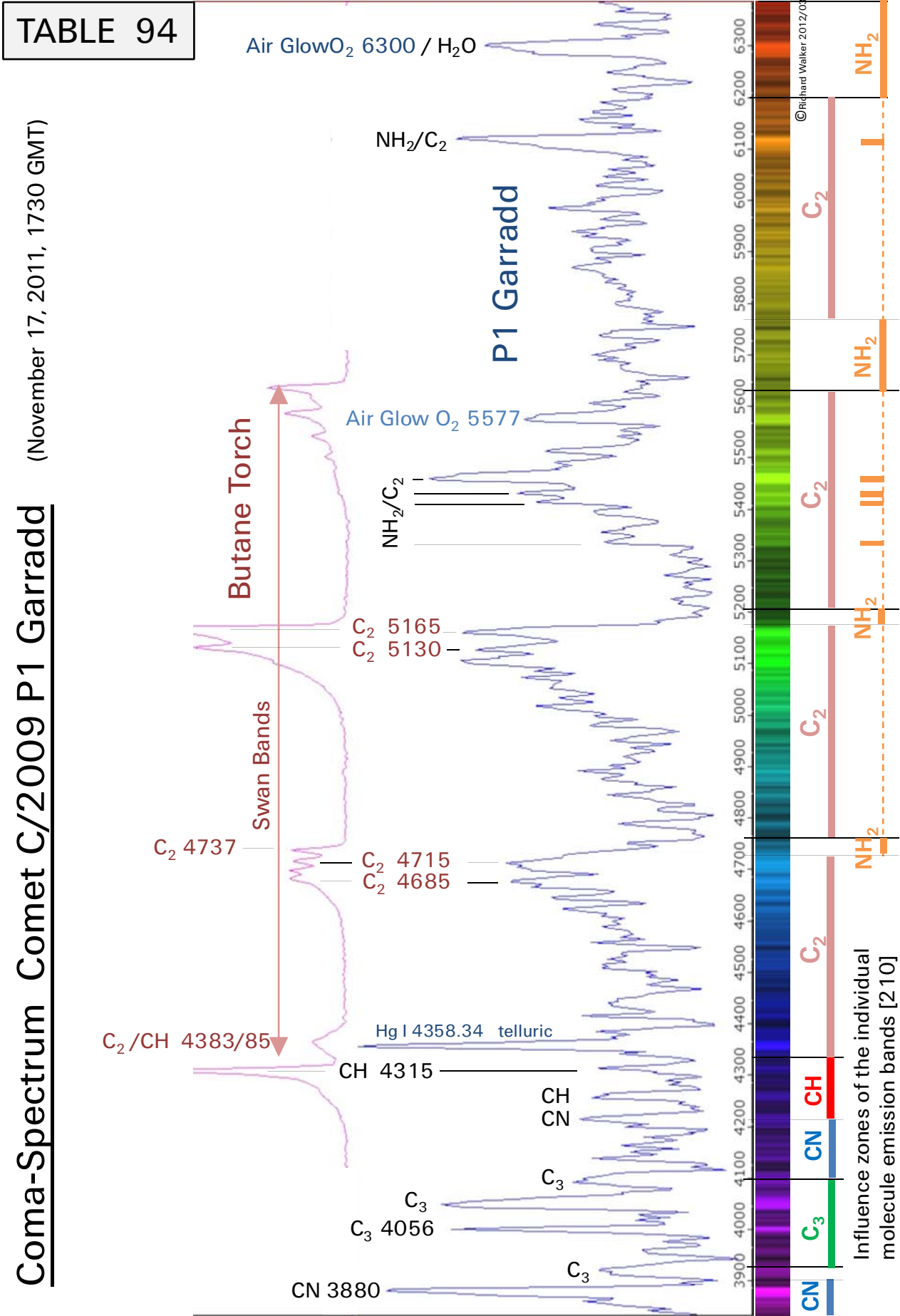


TABLE 91

Reflection spectra of Jupiter and Saturn compared to the daylight



Coma-Spectrum Comet C/2009 P1 Garradd (November 17, 2011, 1730 GMT)





## 26 Telluric Molecular Absorption

Table 95: Overview on the most dominant absorptions caused by the earth's atmosphere.

Between approx.  $\lambda$  6,200 – 7,700 it literally swarms with molecular  $H_2O$ - und  $O_2$  absorption bands, caused by the earth's atmosphere. Few of them appear in the form of discrete lines even beyond  $\lambda$  5,700, unfortunately pretending the presence of stellar absorptions. On *Table 90* the solar spectrum within the domain of  $\lambda$  6,800 – 7,800 is shown (900L grating). These features appear here so impressively that Fraunhofer has labeled them with the letters A and B. At that time he could not know that these lines do not originate from the Sun, but arise due to absorption in the earth's atmosphere.

For astronomers, they are only a hindrance, unless they need fine water vapor lines of known wavelength to calibrate the spectra. These "calibration marks" are generated by complex molecular vibration processes, appearing as a very broad scattered absorption swarm. The atmospheric physicist deduces from the  $H_2O$  absorptions moisture profiles of the troposphere. The  $O_2$  bands (Fraunhofer A and B) allow him conclusions about the layer temperatures of the atmosphere [180].

For the "average amateur" important is just the awareness, that the line identification within this area requests great caution. In most of the cases only the  $H\alpha$  line overtops unambiguously the "jungle" of the telluric absorption lines and bands. This is particularly the case for the early spectral classes, where the maximum of the stellar radiation occurs in the ultraviolet or blue part of the spectrum. Exceptions are here *Wolf-Rayet* and *Be-stars* and those which show mass loss due to strong *P Cygni profiles*. In the latter two cases, at least the helium line  $He I$  at  $\lambda$  6678 can additionally be identified.

Stars of the late *K* and all *M*-classes, as well as the carbon stars, predominantly radiate in the infrared part of the spectrum. Therefore particularly intense *titanium oxide (TiO)* absorption bands are capable to overprint these telluric lines. Further the reflection spectra of the large gas planets show mainly here the impressive gaps in the continua of their spectral profiles.

These telluric bands and lines can be reduced to a certain extent with a relatively large effort – e.g. by subtraction of synthetically produced standard profiles of the telluric lines (see *Vspec* manual) and further by comparison with profiles of standard stars.

Dazu eignet sich auch die Spektralklasse A0, welche in diesem Sektor nur wenige und sehr schwache, stellare Linien zeigt. Very suitable for this purpose is the spectral class A0 which shows just few and very weak stellar lines within this range.

Complicating facts are the influences by weather conditions, elevation angle of the object etc. For further information refer to [180], [181]. Moreover, there is a highly recommended freeware program by *Peter Schlatter*, which allows the almost complete extraction of  $H_2O$  lines [554].

Table 95A: Telluric  $H_2O$  absorptions around the  $H\alpha$  line

These  $H_2O$  lines (*Vspec* database) are usefull for the calibration of high-resolution spectra particularly around the  $H\alpha$  line. As an orientation aid these are shown at two highly resolved spectral profiles ( $R \sim 20,000$ ) with different spectral classes –  $\delta$  *scorpii*, B0.3 IV and the *Sun*, G2V, recorded with the SQUES Echelle spectrograph [600].

Tafel 95B: Telluric  $O_2$  absorptions of the Fraunhofer A- and B-Band

Highly resolved profiles, recorded with the SQUES Echelle spectrograph [600]. The line identification and the according wavelengths are based on [182].

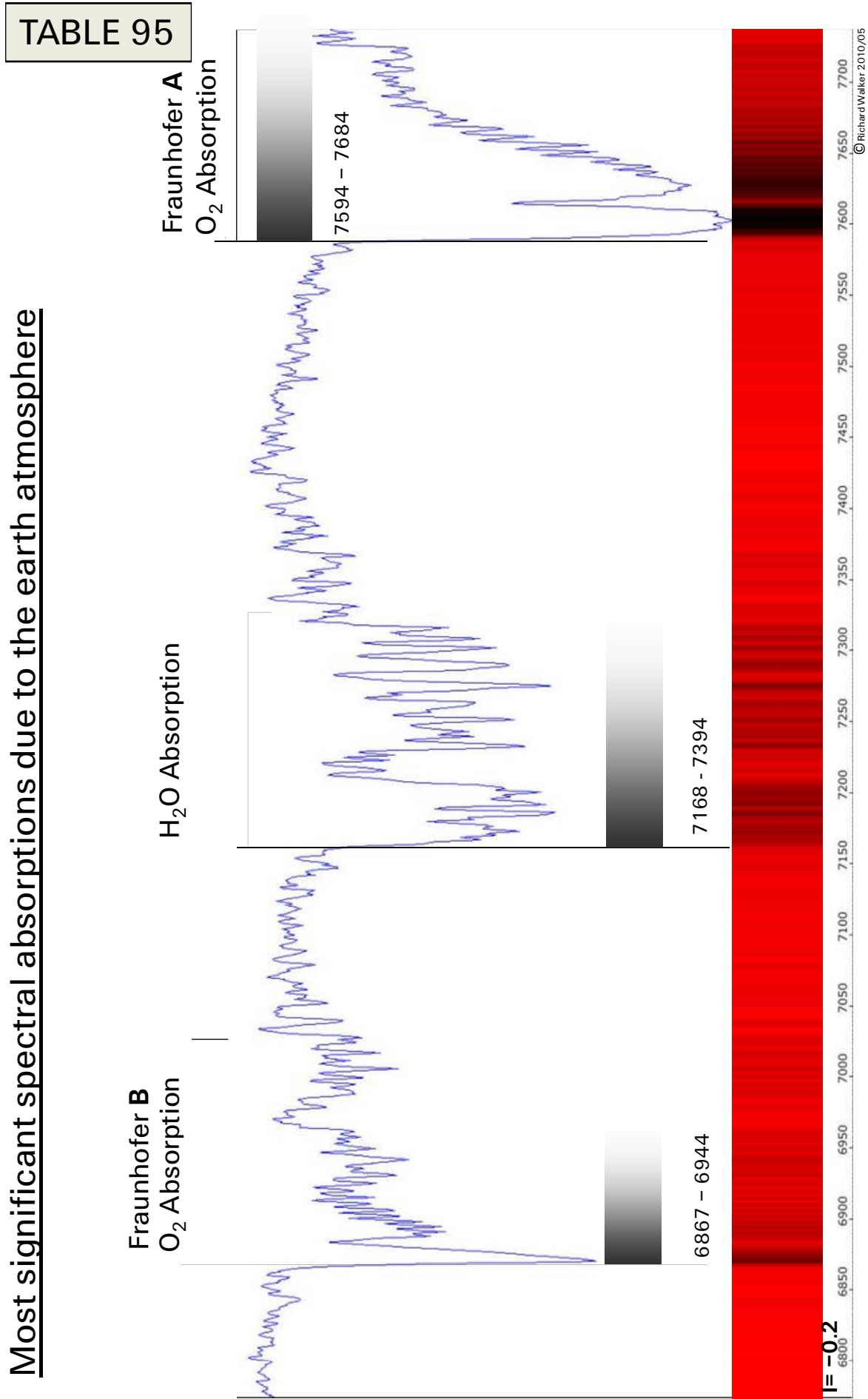


TABLE 95A

Telluric H<sub>2</sub>O Absorptions at H $\alpha$  Line

Recorded with the SQUES Echelle Spectrograph

- Sun
- G2V
- $\delta$  scorp*ii*
- B0.3 IV

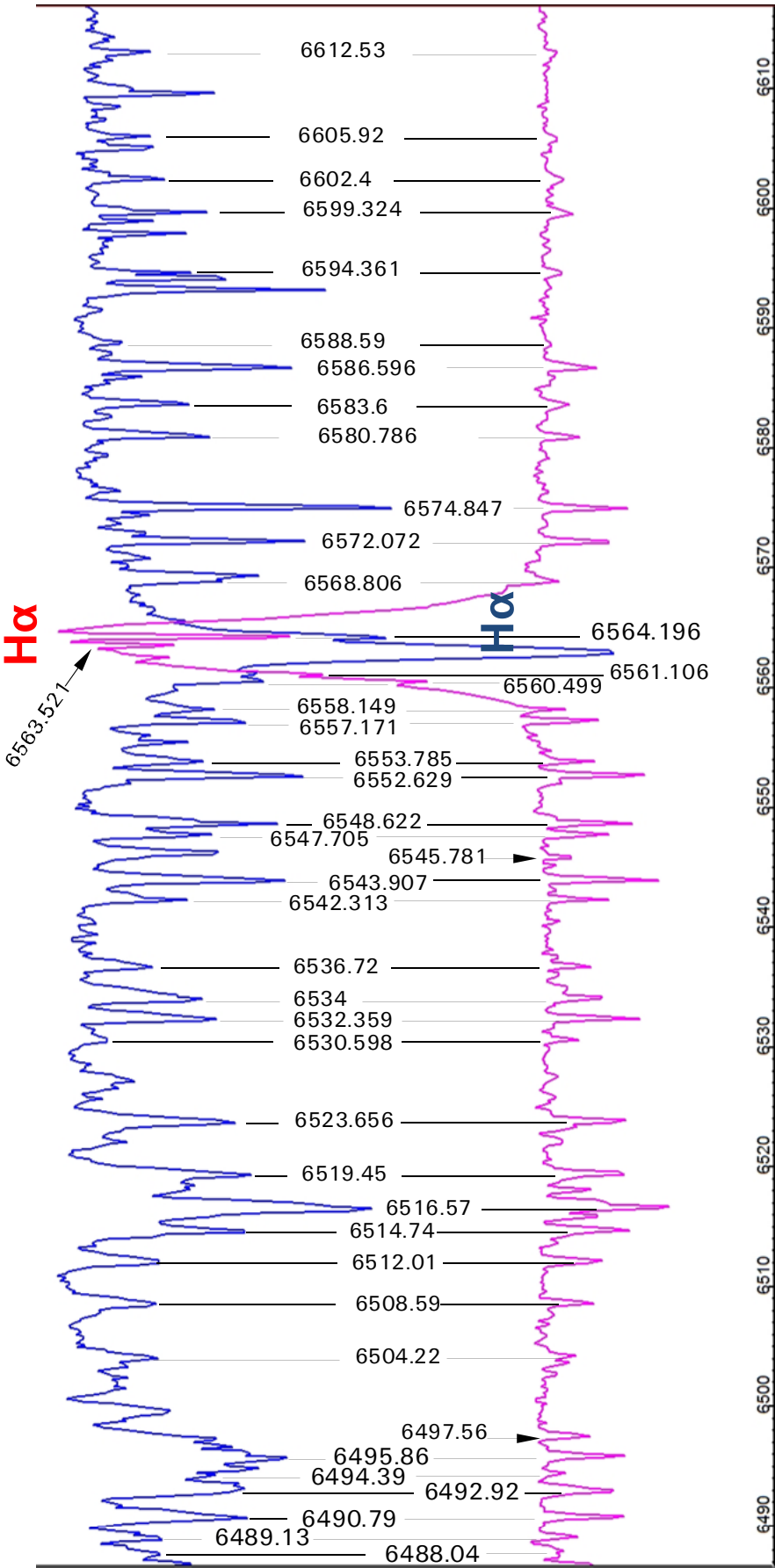
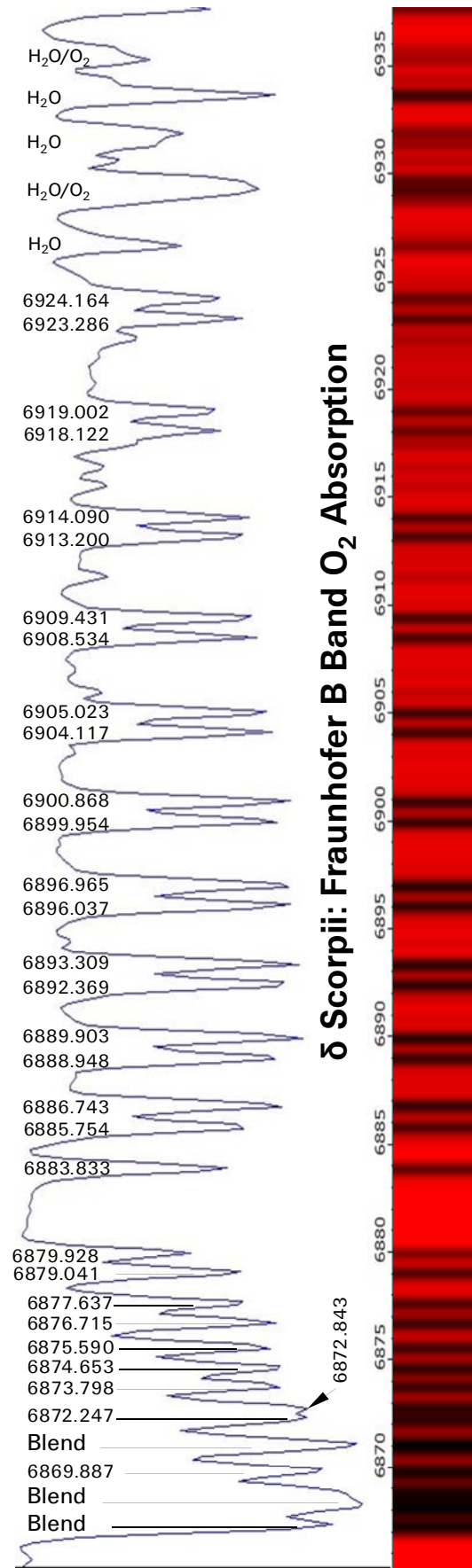
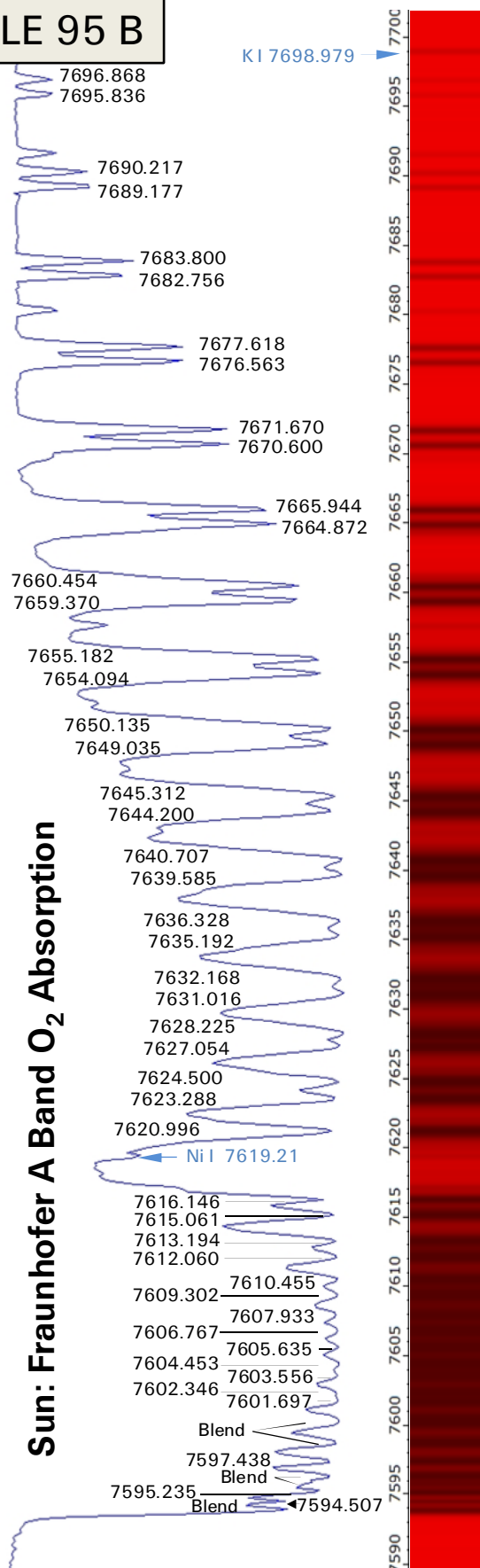


TABLE 95 B

**Telluric O<sub>2</sub> Absorptions: Fraunhofer A and B** SQUES Echelle Spectrograph  
 According to: *Fine Structure of the Red System of Atmospheric Oxygen Bands*, H. D. Babcock and L. Herzberg



## 27 The Night Sky Spectrum

### 27.1 Introduction

Mainly due to light pollution and airglow the night sky is significantly brightened and the astronomical observations thereby seriously hampered.

The light pollution is mainly caused by street lamps and other terrestrial light sources. The light is chiefly scattered by molecules and particles in the mesopause (altitude approx. 80 – 100km).

The airglow is produced during the day in the atmosphere by photoionisation of oxygen as a result of solar UV radiation and chemical reaction chains. At night recombination takes place, causing emission lines at discrete frequencies. Really striking here are only two of the O I lines at  $\lambda$  5577.35 and 6300.23. The latter is visible just under a very good night sky, and therefore lacking in the spectrum of Table 96. Airglow however includes also the rotational and vibrational bands of OH molecules in the near infrared range, detected in 1950 by A. B. Meinel. Further influence, particularly over the continuum of the night sky spectrum, has the diffuse galactic light (DGL), the integrated starlight (ISL) and the reflected zodiacal light (ZL). The latter may also contribute elements of the solar spectrum. (www.caltech.edu)

### 27.2 Effects on the Spectrum

Depending on the quality of the night sky, at long to very long exposure times the emissions of airglow and light pollution can disturbingly superimpose the recorded signal of the examined object, example see M1, Table 85 and 96. The effects of airglow to the spectrum are much less harmful than the light pollution, which can consist of dozens of emission lines, depending on the type of terrestrial light sources in the wider surroundings, as well as meteorological factors. Under a perfect night sky, only the airglow is visible in the spectrum.

### 27.3 Countermeasures

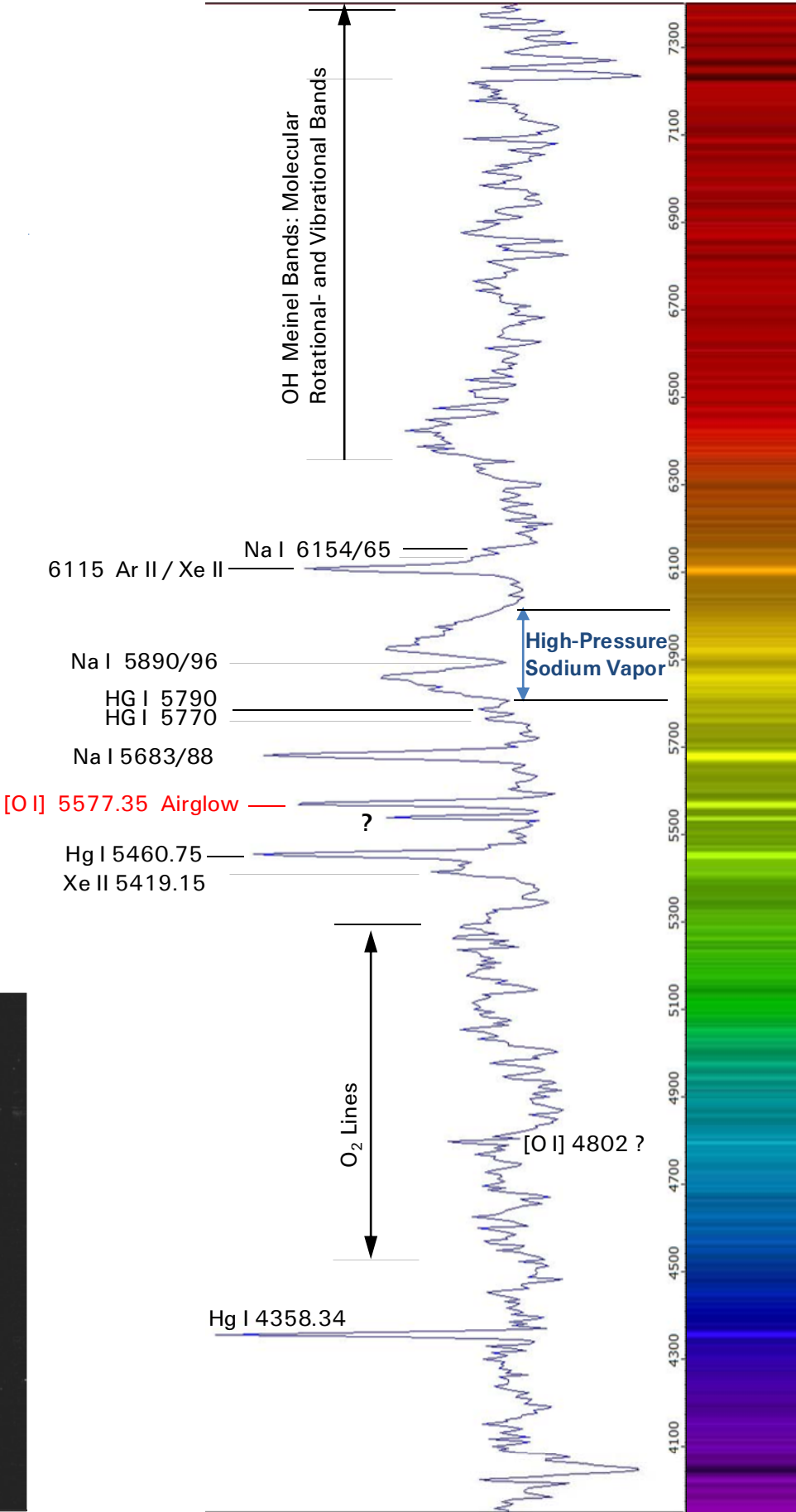
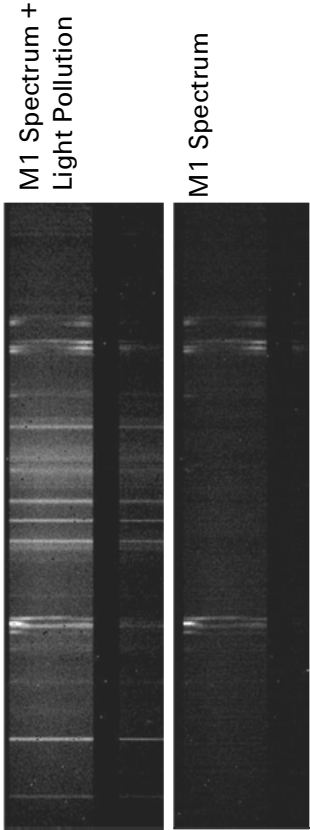
For long term exposures of two-dimensional appearing objects like nebulae, helps the recording of the night sky spectrum in the immediate vicinity of the examined object (with the same exposure time). This must then be subtracted from the object spectrum, eg with Fitswork. For point-like appearing objects, the light pollution can be subtracted together with the sky background (eg IRIS).

### 27.4 Comments to Table 96

This night sky spectrum was recorded to clean the disturbed spectrum of M1 (Table 85). It was taken at my home (Rifferswil Switzerland) about 610m above sea level, under a rather moderately good rural sky with a limiting magnitude of about 4–5<sup>m</sup> and an elevation angle of approximately 50°. For such long exposures (30 Minutes) the C8 was equipped with a long dew cap to reduce the influence of scattered light from the surrounding area. The lighting of the residential area consists of gas discharge lamps, of which some but not all spectral lines appear in the spectrum. Major roads with sodium vapor lamps are some 100m distant without a direct line of sight. As the most harmful source of pollution in literature consistently high-pressure sodium vapor lamps are referred, since they produce a bell-shaped emission around the Fraunhofer D Lines  $\lambda$  5890/96 D (see also Table 104). This feature can hardly be effectively filtered out without impairing of the wanted signal. Not surprisingly the famous sky contamination act („La Ley del Cielo“), affecting the islands of Tenerife and La Palma, severely limits the use of high-pressure sodium vapor lamps [190]!

TABLE 96

Night Sky Spectrum  
Rifferswil Switzerland





## 28 Terrestrial Lightsources

### 28.1 Spectra of Gas Discharge Lamps

Gas discharge lamps play a key role for astronomers. They can be useful, for example to calibrate the spectral profiles - but also represent a disturbing source e.g. by light pollution from the road- and municipal lighting. For beginners they are also usefull exercise objects to study the spectra – particularly during cloudy nights. Further spectra and info to calibration light sources see [32], [34], [35], [508].

Unfortunately, gas discharge lamps are operated with relatively high voltage. This requires, especially for outdoor operation, ie minimal electrical knowledge of relevant safety measures such as isolation transformers, GFCI devices, or DC/AC Power Inverters (ie 12V DC/230V AC).

Table 101: Neon glow lamps

The orange glowing neon glow lamps are used as indicator lights, e.g. for stoves, flat irons, connection plug boards etc. They produce a large number of emission lines, mainly in the red region of the spectrum. Their wavelengths are known with high accuracy. These properties make them very popular as calibration lamps among the amateurs. The disadvantage is that the intense lines are limited to the red region of the spectrum. Further they can only be operated with mains voltage of 230V, therefore posing a safety risk and requiring specific electrotechnical safety measures. With very long exposures, especially in the green area further emissions will appear, but coupled with the disadvantage that the most intense neon lines in the red range of the spectrum become oversaturated at low to moderately high-resolution spectrographs. Such lines can therefore no longer be used for calibration purpose within the same profile. For the calibration of broadband spectra (red to blue) or higher-resolved profiles within the blue range, low cost solutions according to tables 103 and 106, or even better [35] are preferred. In the professional sector or on the senior amateur level, relatively expensive hollow cathode lamps are used, producing a fine raster of eg iron-argon or thorium emission lines.

Table 102: Energy saving lamp ESL Osram Sunlux

Amateurs often use ESL as a complement to the neon lamps, which are limited to the red part of the spectrum. These lamps contain several gases and substances performing different tasks – among other things, fluorescent substances, usually so called *rare earth* metals. The mixture depends largely on the color, the lamp should produce. Anyway for calibration purposes usefull are only the intense lines of the auxiliary gases, e.g. Argon (Ar), Xenon (Xe), and Mercury (Hg). Unfortunately, some of these line positions are located very close together and are therefore difficult to distinguish, such as Ar II (6114.92) and Xe (6115.08).

Table 103: Xenon strobe tube

Better-suited for the broadband calibration of profile graphs, is the spectrum of a xenon strobe light, e.g. kit K2601 from *Velleman*. This kit is designed primarily as position lamp for model aircraft as well as for lighting effects on stages, dancefloors, in shop windows etc. The flicker frequency for the calibration purpose must be adjusted to the maximum and the lamp requires some 15 seconds warmup time to produce accurately the specified lines. This lamp generates some 50 useful lines, distributed over the entire range from the near infrared to violet (about  $\lambda\lambda$  8,000 – 3,900). In the infrared domain further emissions are available, but not documented here. Most emission lines are produced by *xenon*. However the shortwave-end of the spectrum is dominated by lines of *rare earths*. The xenon tube gets very hot during operation. Further it requires also mains voltage of 230V. Therefore an appropriate housing is needed.

Table 104: High pressure sodium vapor lamp for street lighting

This lamp is widely used for street lighting. The sodium generates light in the domain of the Fraunhofer D1, and D2 line. Due to the high gas pressure it's not a real monochromatic light. The continuum, as a result of *pressure and collision broadening*, as well as *self absorption effects*, shows a bell-like shape. Added auxiliary gases, for example Xenon, can produce some discrete lines in the spectrum.

Table 105: High power Xenon lamp

Such high pressure gas discharge lamps are used for lighting of stadiums, position lamps on mountain tops etc.

The line identification in Table 102 – 105 is based on Vspec (*Tools/Elements/elements*), as well as on data sheets from the lamp manufacturers.

Table 106: Glow Starter ST 111 from OSRAM, (4–80W, 220V–240V)

Another alternative for broadband calibration and detailed analysis in the blue range of spectra are modified glow starters for fluorescent lamps. They contain a small gas discharge lamp, which is not used there as light source but as a bimetal switch. For our special purpose it must be wired with a series resistor (details see [34]). OSRAM declares the composition of the gas with hydrogen *H* and argon *Ar*. The light output in the blue range of the spectrum is relatively weak and may require somewhat longer exposure times. For 110V mains, appropriate starters may be used also from other suppliers. The necessary series resistors must be determined by tests. The current must be limited to the extent, that a reasonable light output is achieved without closing the bimetal switch. In the case of ST111 40-80W, ~24 kΩ was evaluated. Rainer Ehlert from Mexico tested the 110V type "Fulgore" and evaluated the same resistor value!

The Glow starter RELCO SC480, in addition to argon and hydrogen, contains also neon and helium. Thus in the optical spectral calibration are about 270 lines available, which is even sufficient for the calibration of high-resolution echelle spectra. An according line atlas, recorded with the DADOS- and SQUES spectrographs, can be found in [35].

Practical note to the calibration in order to avoid transmission errors:

If data from any table of this atlas are used for wavelength calibration, they can be copied with ctrl c from the pdf file and transferred to the Vspec calibration field with shift insert.

TABLE 101

Spectrum Neon Glow lamp

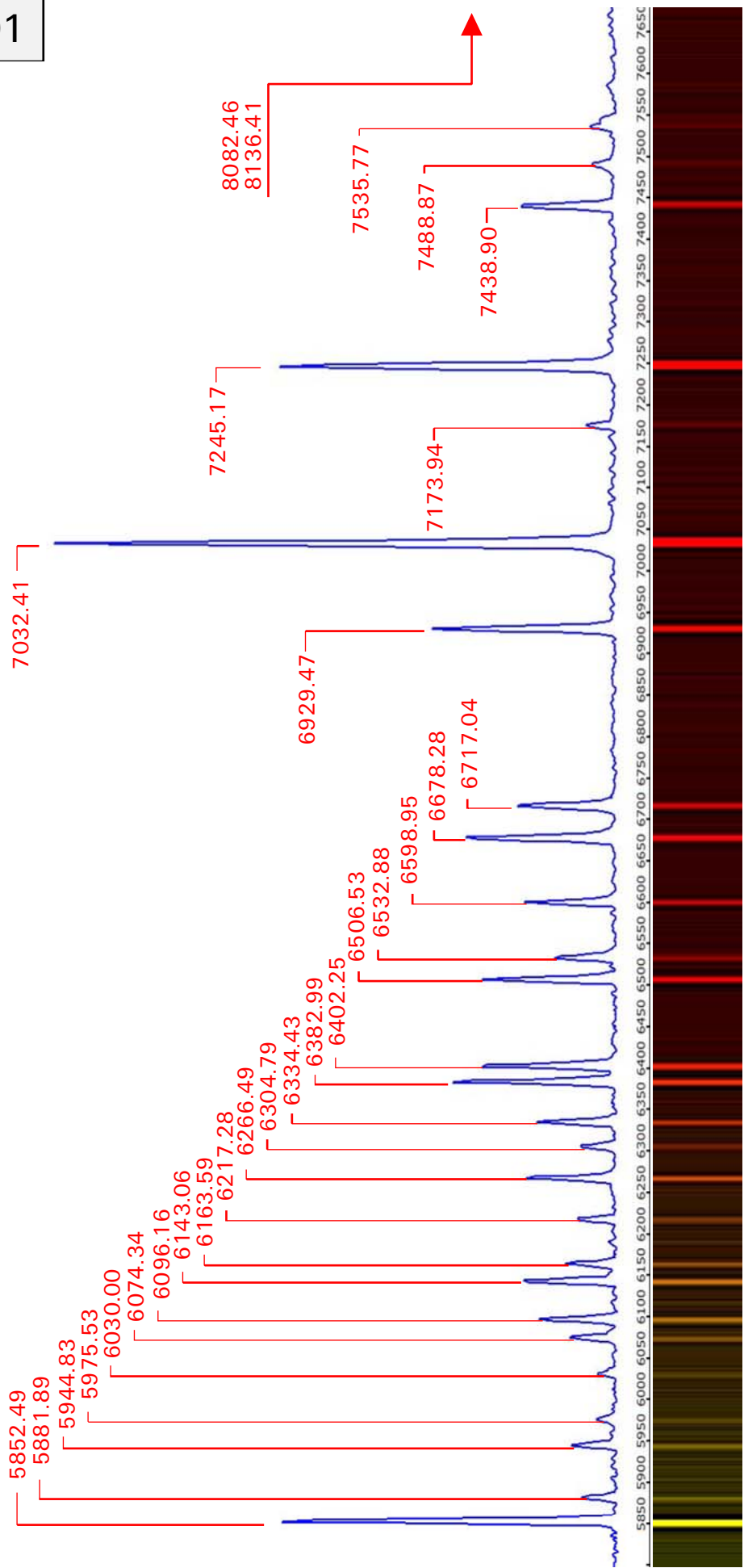


TABLE 102

Spectrum ESL Osram Sunlux

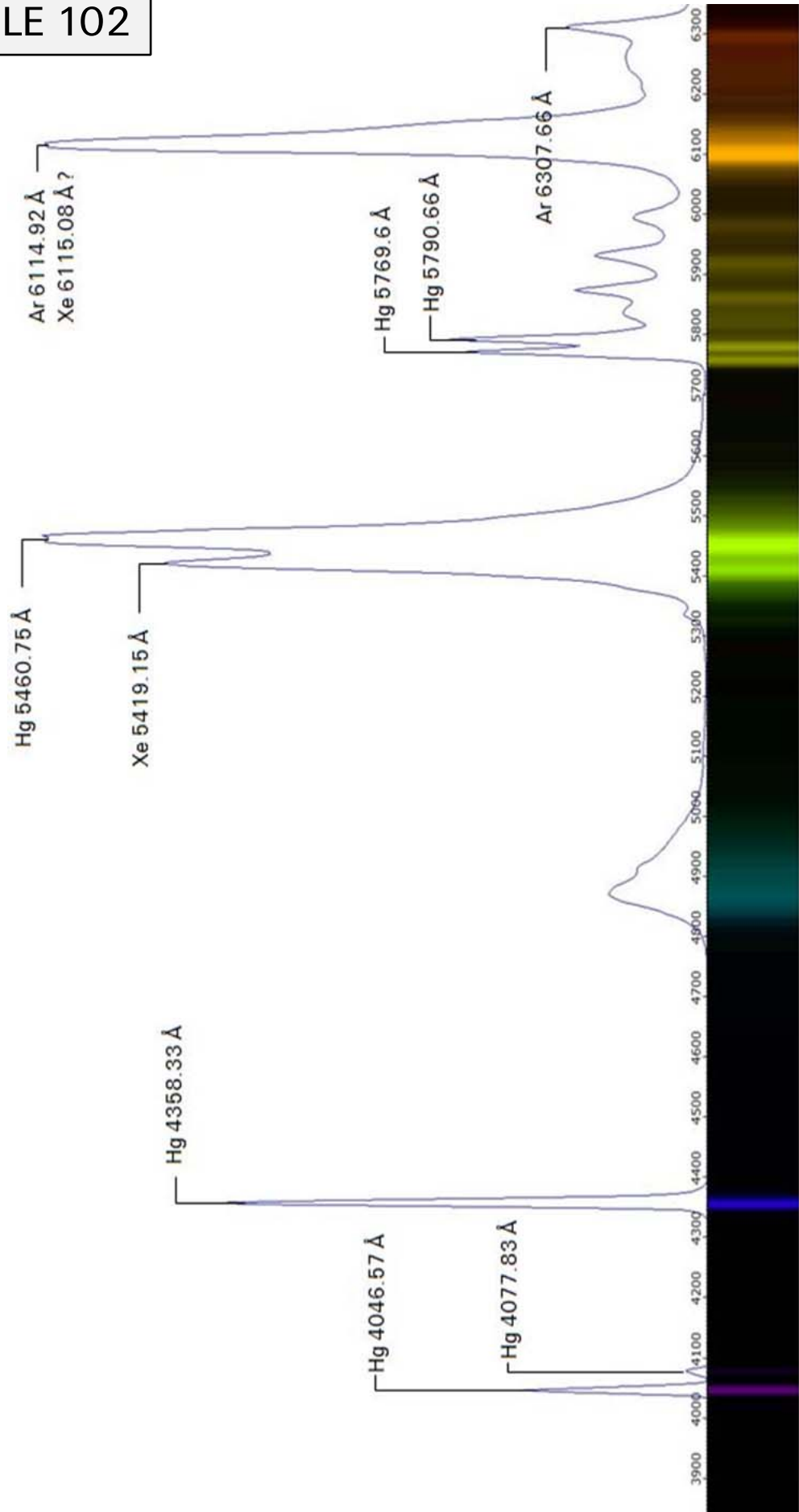


TABLE 103

## Spectrum of the Xenon Strobotube 27 WS Kit: Velleman K2601

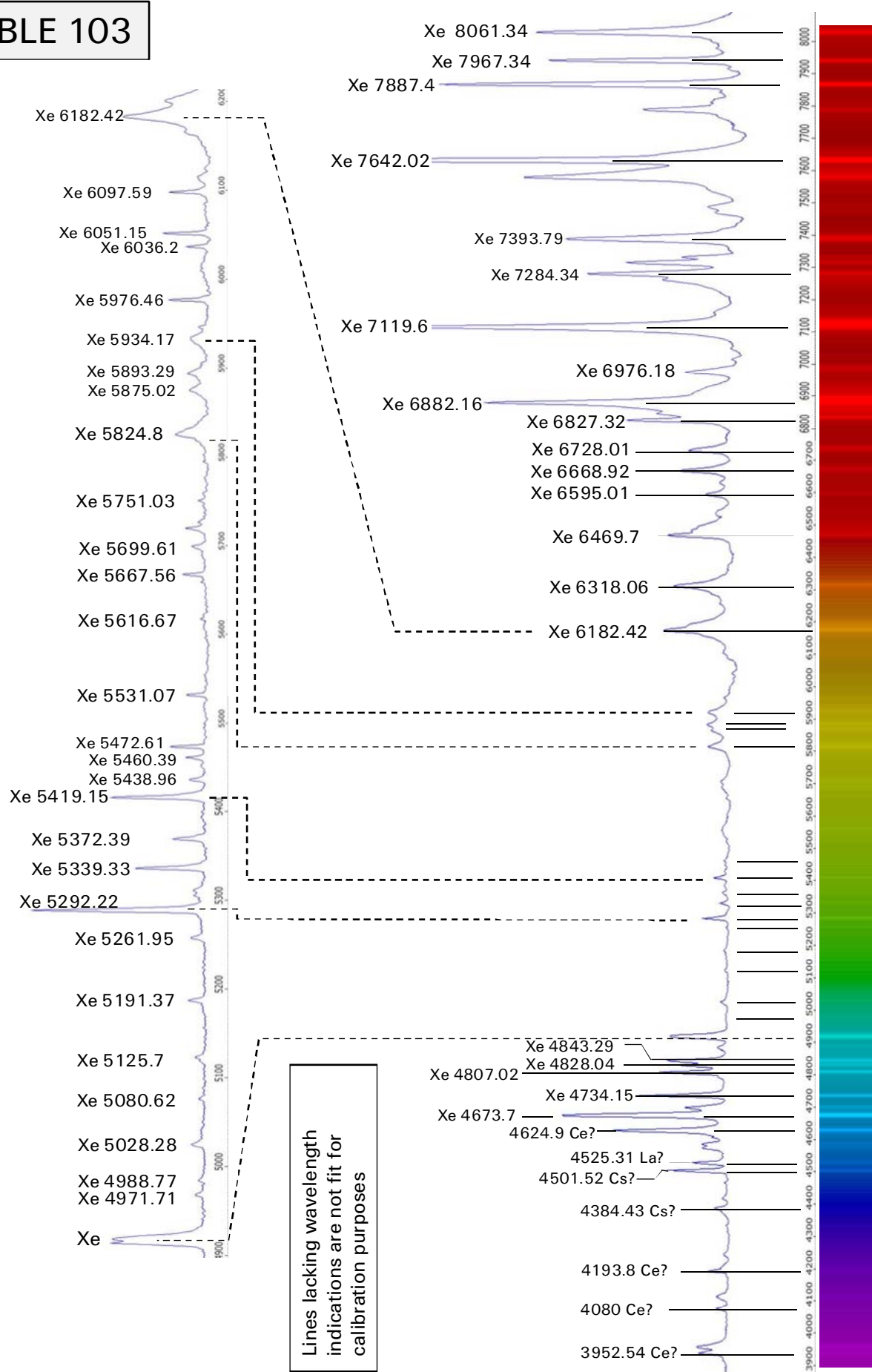


TABLE 104

High pressure sodium vapor lamp

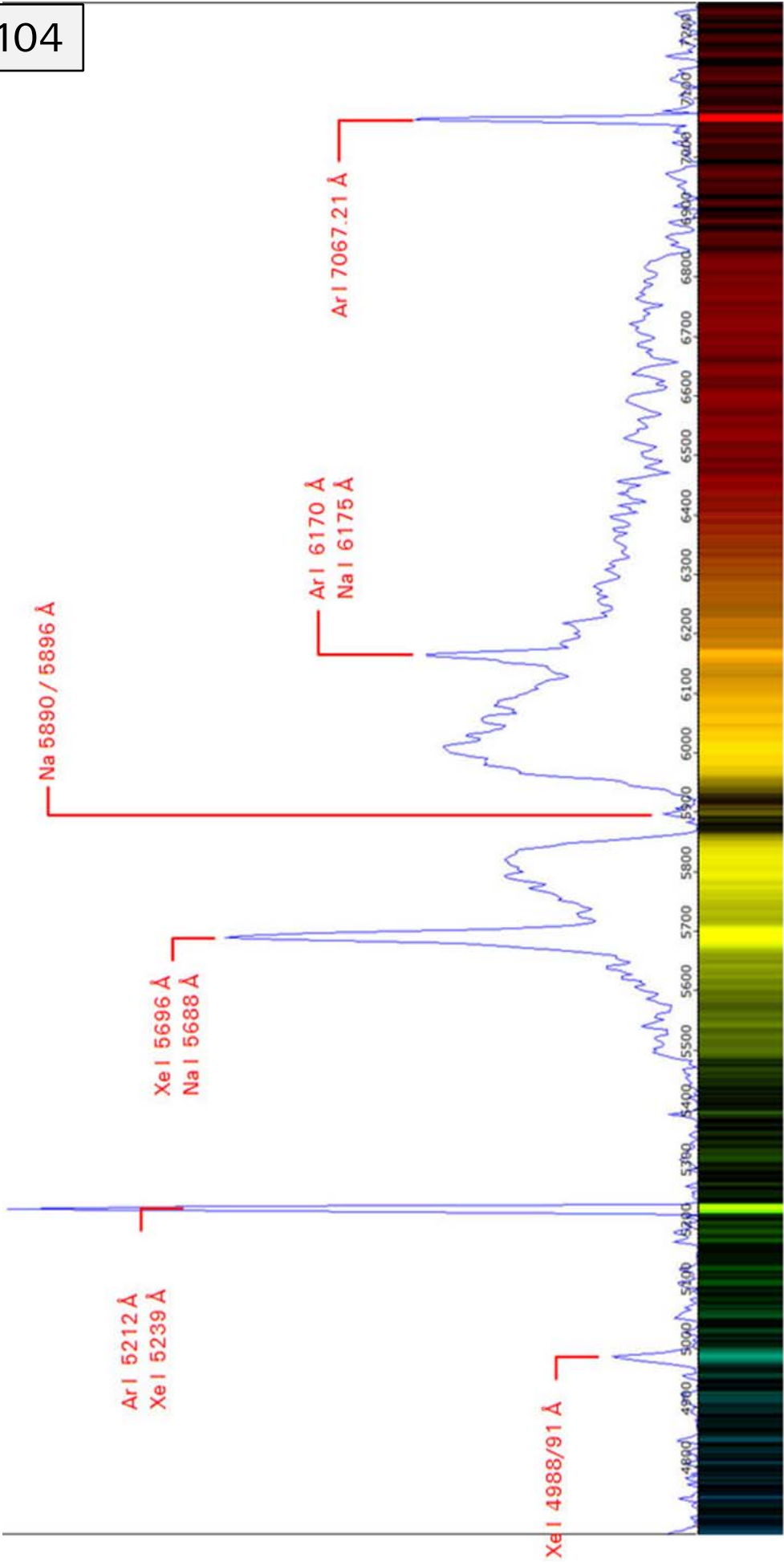




TABLE 105

Xenon high power lamp  
Position lamp on the summit of Mt. Rigi

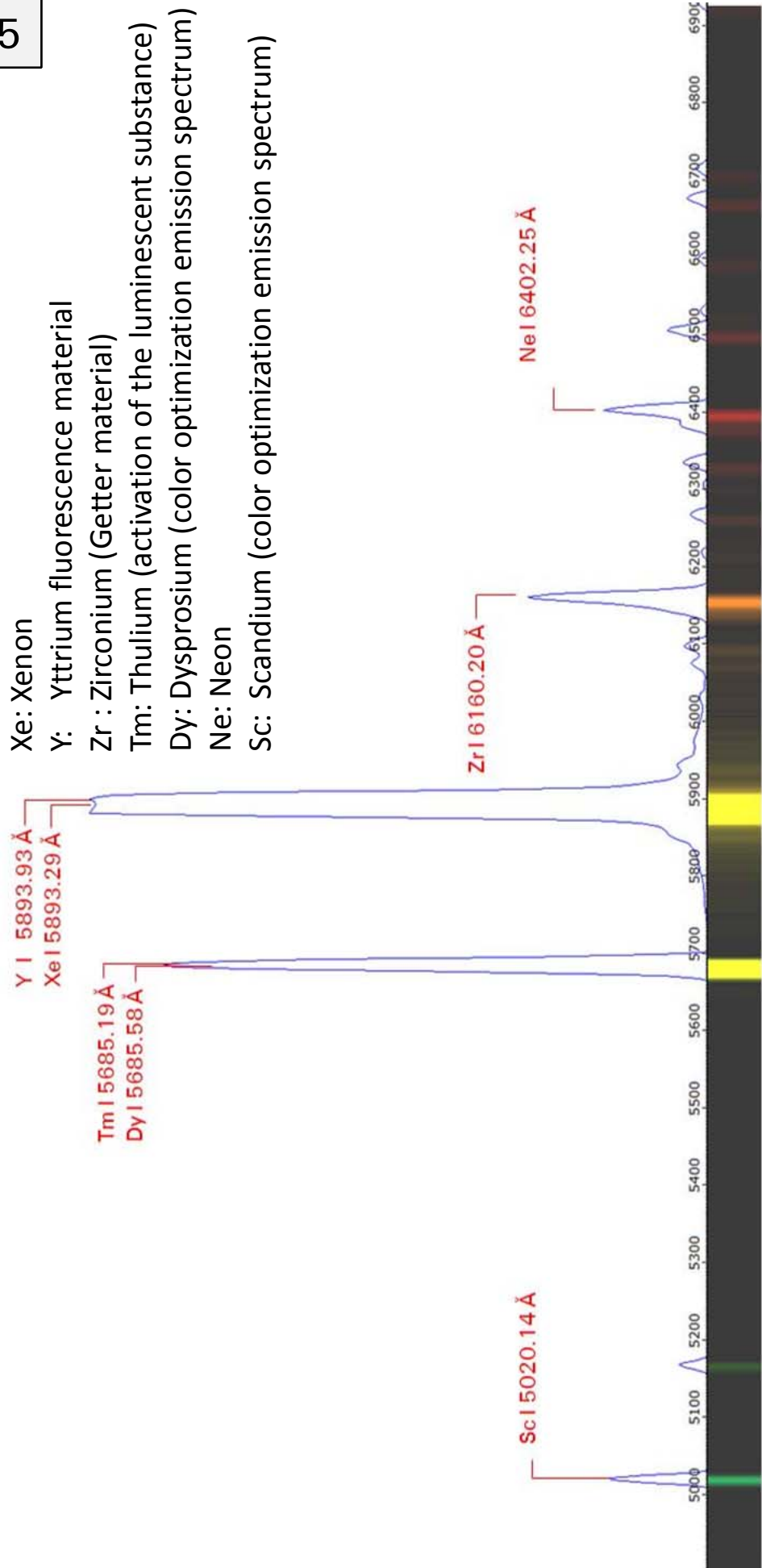
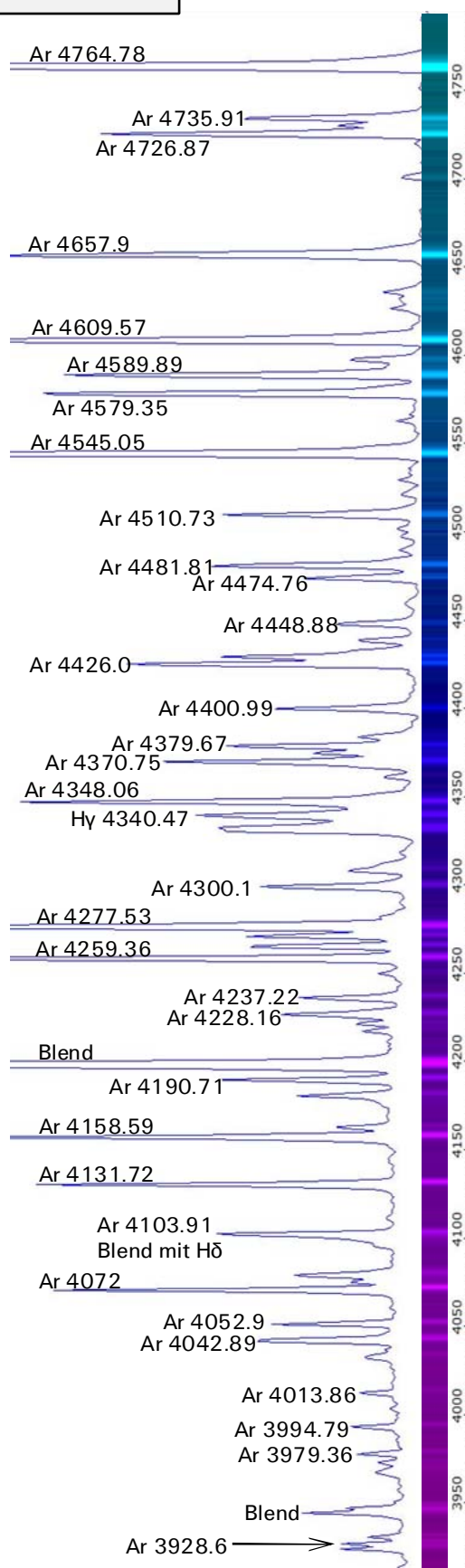
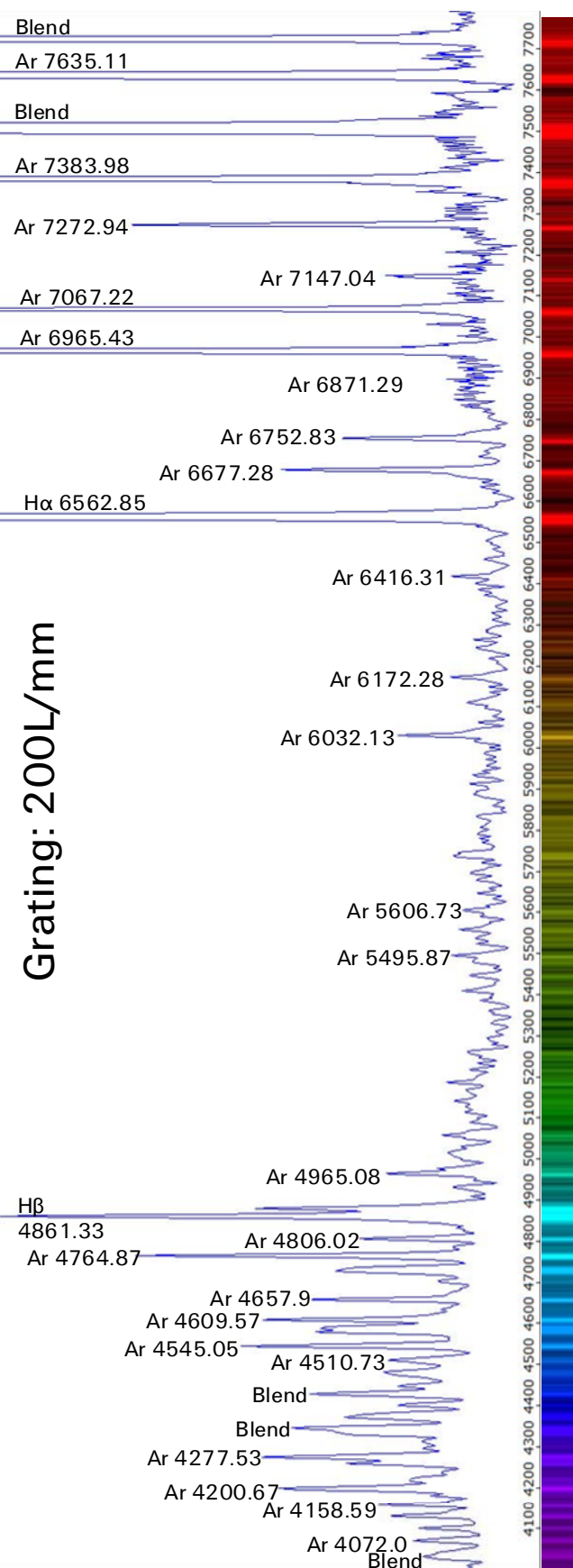


TABLE 106

Spectrum Glow Starter OSRAM ST 111 4-80W Grating: 900L/mm



Grating: 200L/mm



## 28.2 Spectra of Gasflames

Table 110: *Swan Bands* in comparison to the following spectra:  
*butane gas torch, comet Hyakutake* and carbon star *WZ Cassiopeiae*

The Swan Bands, already described in sect. 22, are of great importance for astrophysics. They are generated e.g. in the cool atmospheres of carbon stars as *absorption bands* and in the comets of the solar system as *emission bands*. Molecular band spectra are generated by complex rotational and vibrational processes of heated molecules [3]. The required excitation energy to generate *Swan Bands* is relatively low. Therefore this spectral detail can be easily simulated by the intense combustion of hydrocarbons with do it yourself equipments from the hardware store!

*Table 110* shows the *Swan Bands*, generated with a *butane torch*. The wavelengths of the most intensive *band heads* are  $\lambda\lambda$  6191, 5636, 5165, 4737 and 4383. Further a number of *fainter*  $C_2$  absorptions are still recognisable, with wavelengths according to [110]. Some of these lines are also visible in the profiles of the carbon stars in *Table 65*.

In this *table*, spectra of the butane gas flame ( $C_4H_{10}$ ), comet *Hyakutake* and the carbon star *WZ Cassiopeiae* (excerpt from *Table 67*) are superposed. The shape of the *Hyakutake* profile (March 28, 1998) was transferred to and accordingly scaled up in the drawing from an ESO/Caos project <http://www.eso.org/projects/caos/>.

Striking are the amazingly similar *emission spectra* of the comet *Hyakutake* and the *butane gas flame* within the domain of the  $C_2$  *Swan bands*! That's why for both cases the same physical process is taking effect. *WZ Cassiopeiae* shows the *Swan Bands* in *absorption* instead of *emission*. Therefore the shape of this profile runs inversely to the others.

The line identification is based amongst others on [110], [210].

Tests with acetylen flames ( $C_2H_2$ ), carried out in the workshop of Urs Flükiger, yielded similar results (Photo below).

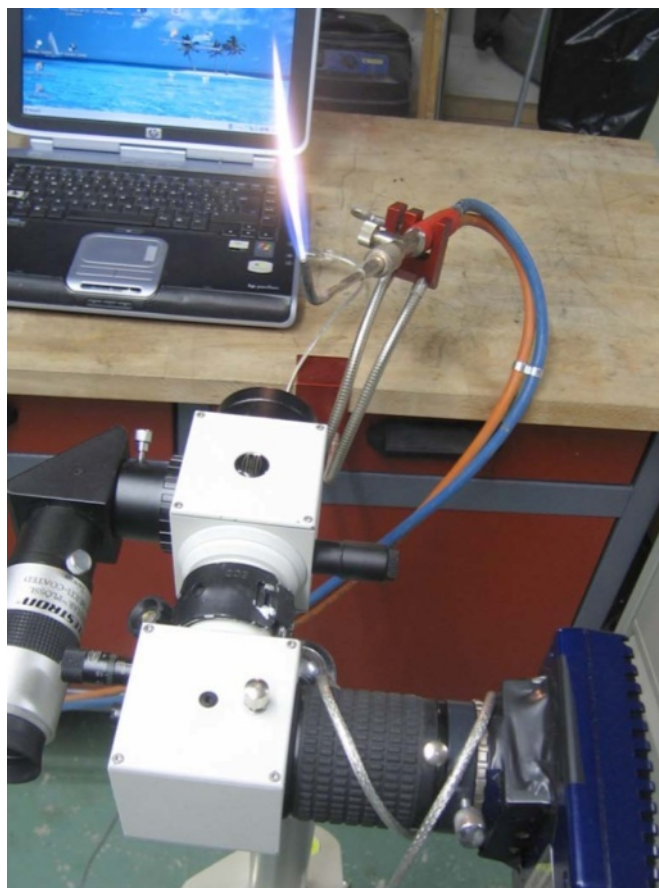
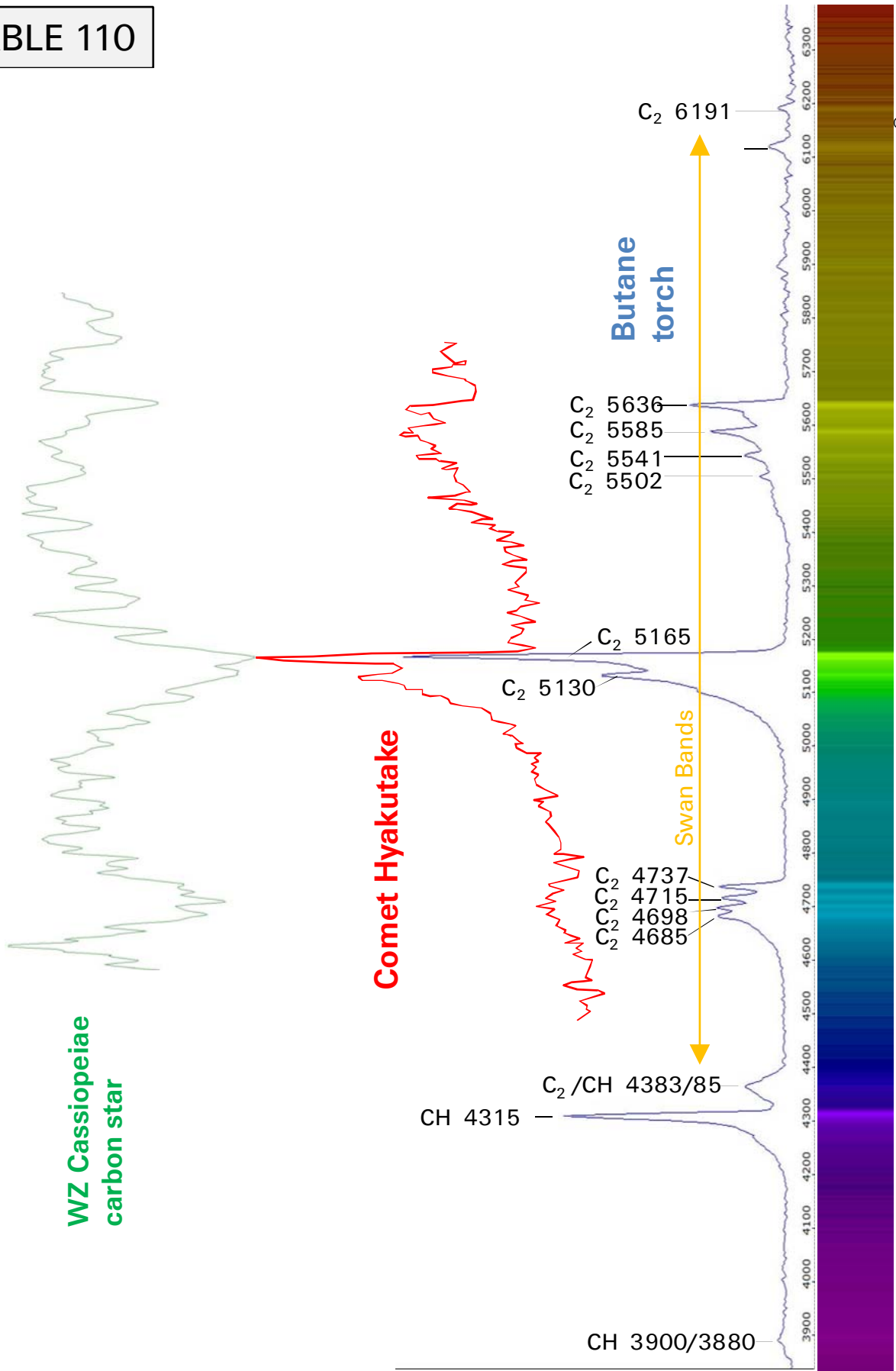


TABLE 110

Swan Bands: Butane torch, Comet Hyakutake and WZ Cas



### 28.3 Spectra of Terrestrial Lightning Discharges

Already since the beginning of the Spectroscopy in 19th century it was attempted to gain spectra of lightning discharges. At the beginning of the 20th Century, also well-known astronomers have been involved, like Pickering and Slipher [708]. Further information and references see also [33].

The following figure shows the spectrum of a lightning that has hit the ground in a distance of approximately 220 m from the observer. Martin Huwiler filmed this event through the closed window pane with a Canon G1X and a 300L mm<sup>-1</sup> transmission grating, mounted in front of the camera lens.



Table 111: Lightning spectrum recorded via cloud reflection

For this, the C8 telescope with the DADOS spectrograph and the Atik 314L+ was built up at night in the living room. It pointed through the closed window on the approaching thunderstorm at the western horizon. Three shots of each 180 seconds in the 2x2 binning mode have been processed. Per image the integrated light of some 5-10 lightnings could be recorded. Since the cloud base was very low, on all shots the light pollution had to be subtracted.

The idea to gain lightning spectra this way, originates from none other than Vesto M. Slipher. With the same intention, he directed on the evening of July 24 1917 his spectrograph at the Lowell Observatory in Flagstaff to a thunderstorm, which raged in a distance of about 10 km above the south slopes of the San Francisco Peaks [708].

Striking here is the very intense CN emission at approximately  $\lambda$  3900. According to [707] this is a characteristic feature for discharges with relatively *long-lasting currents*, generated mainly by the type of "Cloud-to-Ground Lightning and causing a high fire risk. Therefore in the 1980 ies, it was even discussed in the U.S. to detect this spectral feature with satellites, as an early warning criterion for possible forest fires [707]. Anyway on all my shots, with the integrated light of several lightning strikes, this CN emission appeared in comparable intensity.

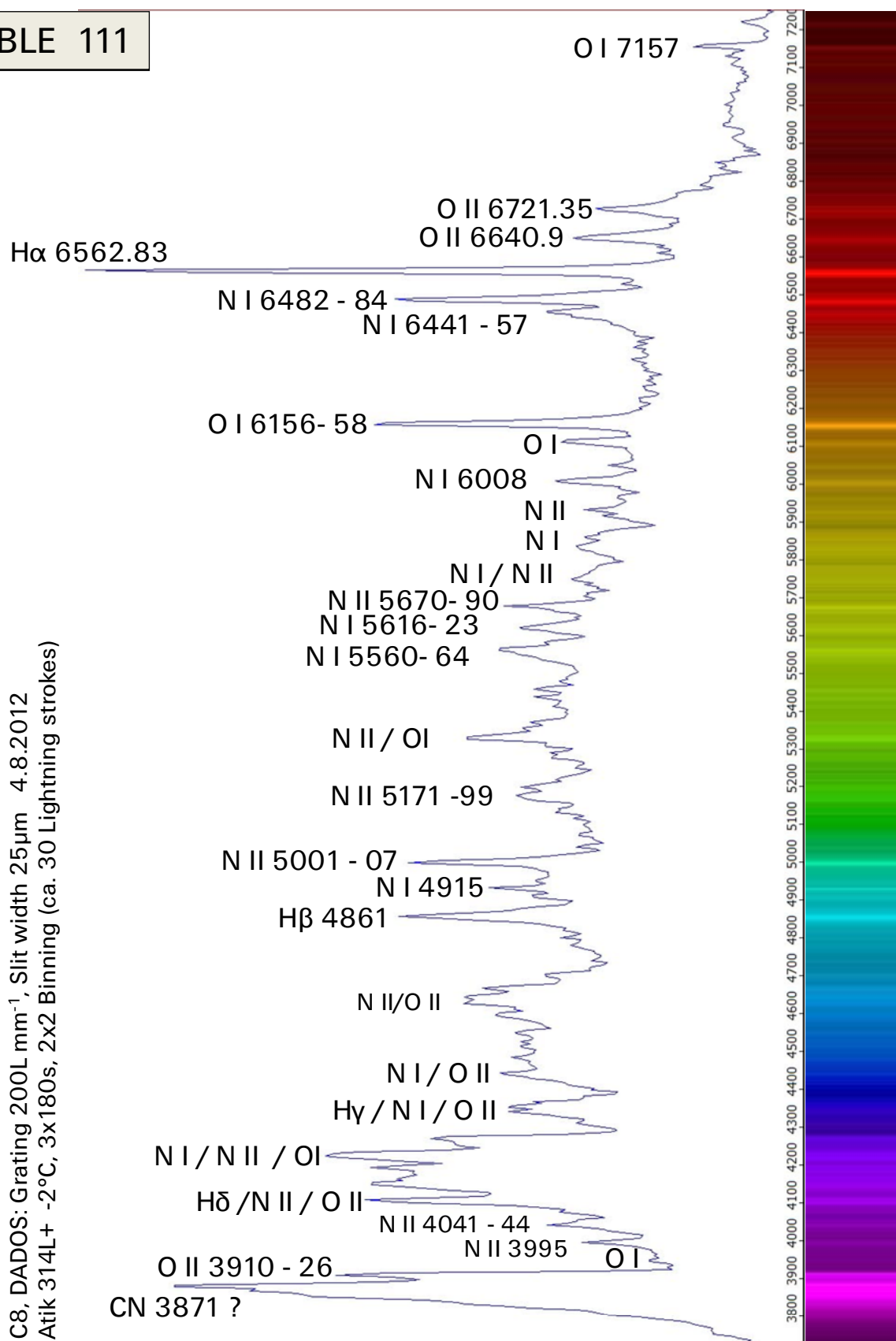
Otherwise, most of the lines of the lightning spectrum are rather complex, broad blends of OII, NII, OI, NI as well as emissions of the H-Balmer series. The raw profile is wavelength calibrated only.



# Lightning Cloud Reflection

C8, DADOS: Grating 200L mm<sup>-1</sup>, Slit width 25μm 4.8.2012  
Atik 314L+ -2°C, 3x180s, 2x2 Binning (ca. 30 Lightning strokes)

TABLE 111





## 29 Spectral Classes and $v \sin i$ – Values of Important Stars

Stars of the spectral classes *O*, *B*, *A*, *F*, *G*, *K*, *M* observable from Central Europe:

Spectral class	Luminosity class	Appar. magn	$v \sin i$ [km/s]	Bayer designation	Proper name
O8	III	3.5		$\lambda$ Ori A	Meissa
O9	III	2.8	130	$\iota$ Ori	Nair al Saif
O9.5	Ib	2.1		$\zeta$ Ori A	Alnitak
	II	2.2		$\delta$ Ori A	Mintaka
	V	3.7	94	$\sigma$ Ori A	
B0	Ia	1.7	87	$\epsilon$ Ori	Alnilam
	IVe	2.5	300	$\gamma$ Cas	
	V	2.8	24	$\tau$ Sco	
B0.5	Ia	2.1	82	$\kappa$ Ori	Saiph
	IV	2.3	181	$\delta$ Sco	Dschubba
	V	2.6		$\beta$ Sco	Acrab
	IV	2.9	153	$\epsilon$ Per	Adid
	V	3.4	46	$\eta$ Ori	Algiebbah
B1	V	1.0	159	$\alpha$ Vir	Spica B
	II-III	2.0	36	$\beta$ CMa	Mirzam
	Ib	2.9	59	$\zeta$ Per	Menkib
	III	3.2	28	$\beta$ Cep	Alfirk
B2	III	1.6	59	$\gamma$ Ori	Bellatrix
	IV	2.8	3	$\gamma$ Peg	Algenib
B3	IV	2.0	201	$\sigma$ Sgr	Nunki
	IV	3.4	19	$\epsilon$ Cas	Segin
B5	Ia	2.5	45	$\eta$ CMa	Aludra
	IIIe	3.0	259	$\delta$ Per	
B6	III	3.2	31	$\zeta$ Dra	Aldhibah
	III	3.7	215	17 Tau	Electra
	IVe	4.2	282	23 Tau	Merope
B7	V	1.4	329	$\alpha$ Leo	Regulus
	III	1.7	71	$\beta$ Tau	Alnath
	IIIe	2.9	215	$\eta$ Tau	Alcyone
B8	IIpe	3.4		$\beta$ Lyr	Sheliak
	Ia	0.1	33	$\beta$ Ori	Rigel
	V	2.1	65	$\beta$ Per	Algol
	IIIp Hg Mn	2.6	41	$\gamma$ Crv	Gienah Corvi
	Ve	2.9	276	$\beta$ Cmi	Gomeisa
	III	3.9	39	20 Tau	Maia
	III	3.6	212	27 Tau	Atlas
	Ve			$\beta$ Cyg	Albireo B
	III	3.2	68	$\phi$ Sgr	
	IVp Mn Hg	2.1	56	$\alpha$ And	Alpheratz
B9	III	3.2	76	$\gamma$ Lyr	Sulafat

Spectral class	Luminosity class	Appar. magn	$v \sin i$ [km/s]	Bayer designation	Proper name
A0	Va	0.0	15	$\alpha$ Lyr	Vega
	p Cr	1.8	38	$\varepsilon$ UMa	Alioth
	IV	1.9	32	$\gamma$ Gem	Alhena
A1	Vm	-1.46	13	$\alpha$ CMa A	Sirius A
	V	1.9		$\alpha$ Gem A	Castor A
	V	2.4	39	$\beta$ UMa	Merak
	V	3.8	96	$\varepsilon$ Aqr	Albali
A2	Ia	1.25	21	$\alpha$ Cyg	Deneb
	Vm	2.9		$\alpha$ Gem B	Castor B
	IV	1.9	37	$\beta$ Aur	Menkalinan
A3	V	2.1	121	$\beta$ Leo	Denebola
	III-IV	2.8		$\alpha$ Lib A	Zubenelgenubi
	V	3.4	173	$\zeta$ Vir	Heze
A4	IV	2.6	181	$\delta$ Leo	Zosma
A5	V	2.6	79	$\beta$ Ari	Sharatan
	III	2.1	219	$\alpha$ Oph	Ras Alhague
	III-IV	2.7	113	$\delta$ Cas	Ruchbah
A7	V	0.8	242	$\alpha$ Aql	Altair
	V	2.4	246	$\alpha$ Cep	Alderamin
	III	3.0	139	$\gamma$ Boo	Seginus
A9	III	3.8	141	$\gamma$ Her	

F0	Iae	3.0	29	$\varepsilon$ Aur A	Alanz
	III	3.4	84	$\zeta$ Leo	Adhafera
	IV	3.5	111	$\delta$ Gem	Wasat
	V	2.8		$\gamma$ Vir	Porrima
F2	III-IV	2.3	70	$\beta$ Cas	Caph
F5	IV-V	0.4	6	$\alpha$ CMi	Procyon
	Ib	1.8	18	$\alpha$ Per	Mirfak
	Ib-II	2.0	17	$\alpha$ Umi	Polaris
F6	IV	3.4	93	$\alpha$ Tri	Mothallah
F8	Ia	1.9	28	$\delta$ CMa	Wezen
	Ib	2.2	20	$\gamma$ Cyg	Sadr
	V	3.6	3	$\beta$ Vir	Zavijah

G0	IV	2.7	13	$\eta$ Boo	Muphrid
	Ib	2.9	18	$\beta$ Aqr	Sadalsuud
	III	0.1		$\alpha$ Aur	Capella B
G1	II	3.0	<17	$\varepsilon$ Leo	Raselased
G2	V	-26.75	1.9	SOL	Sun
	V	-0.27		$\alpha$ Cen A	Rigil Kentaurus
	Ib-IIa	2.8	13	$\beta$ Dra A	Rastaban
	Ib	3.0	<17	$\alpha$ Aqr	Sadalmelik
G5	II	2.7	<17	$\beta$ Crv	Kraz
	III3e	0.1		$\alpha$ Aur A	Capella A
G7	IIIa	2.8	<19	$\beta$ Her	Kornephoros

Spectral class	Luminosity class	Appar. magn	$v \sin i$ [km/s]	Bayer designation	Proper name
G8	Ib	3.0	<17	$\epsilon$ Gem	Mebstuta
	III Fe I	3.5	<19	$\delta$ Boo	
	IIIa Ba0.3 Fe-0.5	3.5	<17	$\beta$ Boo	Nekkar
G8	IIIab	2.8	<17	$\epsilon$ Vir	Vindemiatrix

K0	IIIb	1.1	<17	$\beta$ Gem	Pollux
	IIIa	1.8	<17	$\alpha$ Uma	Dubhe
	IIIa	2.2	21	$\alpha$ Cas	Shedar
	II - III	2.4		$\epsilon$ Boo	Izar
K1.5	III Fe-0.5	-0.0	<17	$\alpha$ Boo	Arcturus
K2	III Ca-1	2.0	<17	$\alpha$ Ari	Hamal
	IIIb CN1	2.7	<17	$\alpha$ Ser	Unukalhai
	III	2.8	<17	$\beta$ Oph	Cebalrai
K3	IIIa	2.7		$\delta$ Sgr	Kaus Media
	II	2.7	<17	$\gamma$ Aql	Tarazed
	II	3.1		$\beta$ Cyg A	Albireo A
K4	III	2.1	<17	$\beta$ Umi	Kochab
	III Ba0.5	3.5	<17	$\beta$ Cnc	Altarf
K5	III	0.9	<17	$\alpha$ Tau	Aldebaran
	III	2.2	<17	$\gamma$ Dra	Eltanin
	V	5.2	<2	61 Cyg A	
K7	IIIab	2.2		$\alpha$ Lyn	Alsciaukat
	V	6.1	<2	61 Cyg B	

M0	IIIa	2.1		$\beta$ And	Mirach
	III	3.1		$\mu$ Uma	Tania Australis
M0.5	III	2.7		$\delta$ Oph	Yed Prior
M1.5	Ia-Ib	1.0	<20	$\alpha$ Sco	Antares
	IIIa	2.4		$\beta$ Peg	Scheat
M1-2	Ia-Iab	0.5		$\alpha$ Ori	Betelgeuse
	III	2.5		$\alpha$ Cet	Menkar
M3	III	3.3		$\eta$ Gem	Propus
	IIIab	2.9		$\mu$ Gem	Tejat Posterior
	III	3.4		$\delta$ Vir	Auva
M5	Ib - II	3.1		$\alpha$ Her	Ras Algethi
M7	IIIe	3-10		$\circ$ Cet	Mira (variable)

### Lower case letters of the Greek alphabet

$\alpha$	Alpha
$\beta$	Beta
$\gamma$	Gamma
$\delta$	Delta
$\epsilon$	Epsilon
$\zeta$	Zeta

$\eta$	Eta
$\theta$	Theta
$\iota$	Iota
$\kappa$	Kappa
$\lambda$	Lambda
$\mu$	My

$\nu$	Ny
$\xi$	Xi
$\omicron$	Omikron
$\pi$	Pi
$\rho$	Rho
$\sigma$	Sigma

$\tau$	Tau
$\upsilon$	Ypsilon
$\phi$	Phi
$\chi$	Chi
$\psi$	Psi
$\omega$	Omega

### 30 Required Ionisation Energies for the Individual Elements

This table shows the required energies [eV], which are needed for the ionisation of a certain element, starting from the ground state  $n = 1$ . Source: [201].

Z	Element	Required excitation energy [eV] to reach the following ionisation stages							
		II	III	IV	V	VI	VII	VIII	IX
1	H	13.6							
2	He	24.6	54.4						
3	Li	5.4	75.6	122.5					
4	Be	9.3	18.2	153.9	217.7				
5	B	8.3	25.2	37.9	259.4	340.2			
6	C	11.3	24.4	47.9	64.5	392.1	490.0		
7	N	14.5	29.6	47.5	77.5	97.9	552.0	667.0	
8	O	13.6	35.1	54.9	77.4	113.9	138.1	739.3	871.4
9	F	17.4	35.0	62.7	87.1	114.2	157.2	185.2	953.9
10	Ne	21.6	41.0	63.5	97.1	126.2	157.9	207.3	239.1
11	Na	5.1	47.3	71.6	98.9	138.4	172.2	208.5	264.2
12	Mg	7.6	15.0	80.1	109.2	141.3	186.5	224.9	265.9
13	Al	6.0	18.8	28.4	120.0	153.7	190.5	241.4	284.6
14	Si	8.2	16.3	33.5	45.1	166.8	205.1	246.5	303.2
15	P	10.5	19.7	30.2	51.4	65.0	230.4	263.2	309.4
16	S	10.4	23.3	34.8	47.3	72.7	88.0	280.9	328.2
17	Cl	13.0	23.8	39.6	53.5	67.8	98.0	114.2	348.3
18	Ar	15.8	27.6	40.7	59.8	75.0	91.0	124.3	143.5
19	K	4.3	31.6	45.7	60.9	82.7	100.0	117.6	154.9
20	Ca	6.1	11.9	50.9	67.1	84.4	108.8	127.7	147.2
21	Sc	6.5	12.8	24.8	73.5	91.7	111.1	138.0	158.7
22	Ti	6.8	13.6	27.5	43.3	99.2	119.4	140.8	168.5
23	V	6.7	14.7	29.3	46.7	65.2	128.1	150.2	173.7
24	Cr	6.8	16.5	31.0	49.1	69.3	90.6	161.1	184.7
25	Mn	7.4	15.6	33.7	51.2	72.4	95.0	119.3	196.5
26	Fe	7.9	16.2	30.7	54.8	75.0	99.0	125.0	151.1
27	Co	7.9	17.1	33.5	51.3	79.5	102	129	157
28	Ni	7.6	18.2	35.2	54.9	75.5	108	133	162
29	Cu	7.7	20.3	36.8	55.2	79.9	103	139	166
30	Zn	9.4	18.0	39.7	59.4	82.6	108	134	174
31	Ga	6.0	20.5	30.7	64				

## 31 Bright Planetary Nebulae sorted by Excitation Classes

This table shows the Planetary Nebulae up to apparent magnitude 11<sup>m</sup>, sorted by excitation class E, according to *Gurzadyan* et al [206]. The temperatures of the central stars are from J. Kaler [207], the spectral classes from CDS / SIMBAD [500], magnitudes from Karkoschka or Wikipedia.

E	Catalogue	Popular Name	Constellation	App. mag.	Central Star	
					Spectral class	Temperature T <sub>eff</sub> [K]
1	IC418	Spirograph Nebula	Hare	9m3	O7fp	35,000
2	IC2149		Charioteer	10m6	O7.5	
2	IC4593		Hercules	10m9		35,000
2	IC4776		Archer	11m5		
2	IC4997		Archer	11m5		49,000
3	IC3568		Giraffe	11m5		57,000
4	NGC6210	Turtle	Hercules	8m8	O7f	58,000
4	NGC6790		Eagle	10m5		76,000
4	NGC6891		Dolphin	10m5		
5	NGC6543	Cat's Eye	Drache	8m1	O7+WR	80,000
5	NGC6803		Eagle	11m4		
7	NGC6884		Swan	10m9		87,000
7	NGC7009	Saturn Nebula	Water Bearer	8m3		90,000
7	NGC6572	Blue Racquetball	Serpent Bearer	9m0	Of+WR	100,000
7	NGC7293	Helix Nebula	Water Bearer	7m5	DA0	110,000
8	NGC1514		Bull	10m9	DB8	
8	NGC1535		River	10m6		
8	NGC3587	Owl Nebula	Great Bear	9m9		
9	NGC3132	South. Ring Nebula	Sails	8m2		
9	NGC6886		Arrow	11m4		168,000
9	NGC6741	Phantom Streak	Eagle	11m0		180,000
9	NGC3242	Ghost of Jupiter	Fem Water Snake	7m7		90,000
9	NGC3918		Centaur	8m5		
10	NGC7662	Blue Snowball	Chained Maiden	8m3		110'000
10	NGC7027		Swan	8m5	invisible	
10	NGC6853	Dumbbell Nebula	Fox	7m5	DO7	160'000
10	NGC2438		Puppis Stern	10m1		
10	NGC650	Small Dumbb. Nebula	Hero	10m1		
10	NGC6818		Archer	9m3		155'000
10	NGC6302	Bug Nebula	Scorpion	9m6		
10	NGC6720	Ring Nebula	Lyre	8m8		150'000
10	NGC2392	Eskimo Nebula	Twins	9m1		65'000
11	NGC6826	Blinking Planetary	Swan	8m8		100'000
11	NGC2818		Compass	8m2		
11	NGC7008		Swan	10m7		
12	NGC1360		Furnace	9m4		
12+	NGC246		Sea Monster	10m9		
12+	NGC4361		Crow	10m9		

## 32 Terminology of the Spectroscopic Wavelength Domains

Terminology for wavelength domains is used inconsistently in astrophysics [2] and depends on the context. Furthermore many fields of astronomy, various satellite projects etc. often use different definitions.

Here follows a summary according to [2], [11] and Wikipedia (*Infrared Astronomy*). Given are either the center wavelength  $\lambda$  of the corresponding photometric band filters, or their approximate passband.

Optical region UBVRI  $\lambda$  3300 – 10,000 (Johnson/Bessel/Cousins)

Center wavelength		Astrophysical wavelength domain	Required instruments
$\lambda$ [ $\mu\text{m}$ ]	$\lambda$ [ $\text{\AA}$ ]		
0.35	3,500	<b>U</b> – Band (UV)	Most optical telescopes
0.44	4,400	<b>B</b> – Band (blue)	
0.55	5,500	<b>V</b> – Band (green)	
0.65	6,500	<b>R</b> – Band (red)	
0.80	8,000	<b>I</b> – Band (infrared)	

Further in use is also the *Z-Band*, some  $\lambda$  8,000 – 9,000 and the *Y-Band*, some  $\lambda$  9,500 – 11,000 (ASAHI Filters).

Infrared region according to Wikipedia (*Infrared Astronomy*)

Center wavelength		Astrophysical wavelength domain	Required instruments
$\lambda$ [ $\mu\text{m}$ ]	$\lambda$ [ $\text{\AA}$ ]		
1.25	10,250	<b>J</b> – Band	Most optical- and dedicated infrared telescopes
1.65	16,500	<b>H</b> – Band	
2.20	22,000	<b>K</b> – Band	
3.45	34,500	<b>L</b> – Band	Some optical- and dedicated infrared telescopes
4.7	47,000	<b>M</b> – Band	
10	100,000	<b>N</b> – Band	
20	200,000	<b>Q</b> – Band	
200	2,000,000	Submillimeter	Submillimeter telescopes

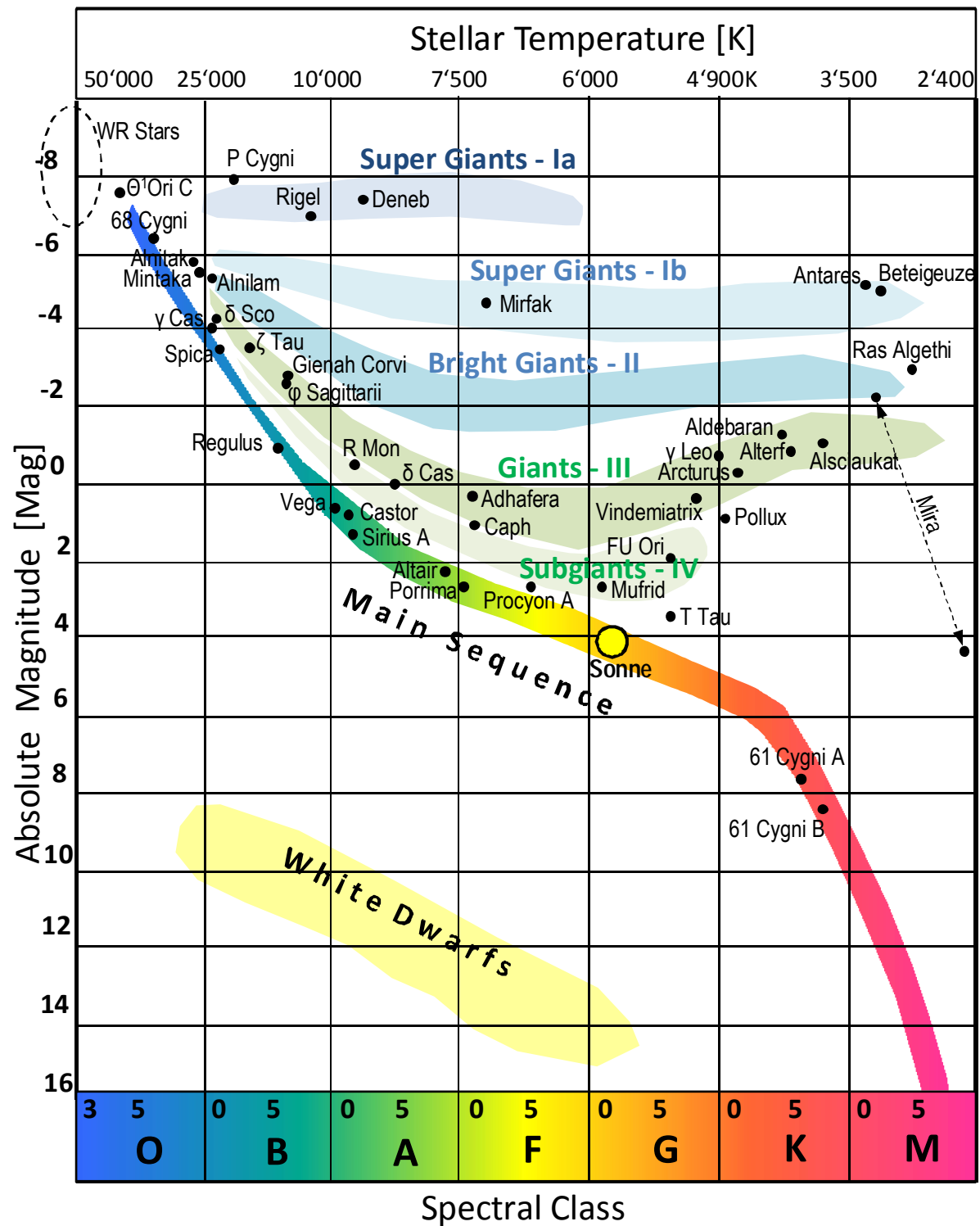
For ground based telescopes mostly the following terminology is in use [ $\text{\AA}$ ]:

- Far Ultraviolet (FUV):  $\lambda < 3000$
- Near Ultra Violet (NUV):  $\lambda$  3000 – 3900
- Optical (VIS):  $\lambda$  3900 – 7000
- Near Infrared (NIR):  $\lambda$  6563 ( $\text{H}\alpha$ ) – 10,000
- Infrared or Mid-Infrared:  $\lambda$  10,000 – 40,000 (J, H, K, L – Band 1 – 4  $\mu\text{m}$ )
- Thermal Infrared:  $\lambda$  40,000 – 200,000 (M, N, Q – Band 4 – 20  $\mu\text{m}$ )
- Submillimeter:  $\lambda > 200,000$  (200  $\mu\text{m}$ )



### 33 Positions of the Atlas-Stars in the HRD

This diagram shows the positions of the stars in the HRD, which are documented in the Atlas. Not included are the spectral classes *S* and *C* on the *Asymptotic Giant Branch*, since their distances and absolute magnitudes are very difficult to determine. These stars are located in an area, somewhat above Mira and with comparable variability. In this area, also the M-giants Antares, Betelgeuse and Ras Algethi can be found. However their masses are much bigger and they will end up as *SN* and not by the emission of a *PV*.



## 34 Appendix

### 34.1 Constellations

Constellation Latin genitiv	Abbr ev.	Proper name
Andromedae	And	Chained Maiden
Antliae	Ant	Air Pump
Apodis	Aps	Bird of Paradise
Aquarii	Aqr	Water Bearer
Aquilae	Aql	Eagle
Arae	Ara	Altar
Arietis	Ari	Ram
Aurigae	Aur	Charioteer
Bootis	Boo	Herdsmen
Caeli	Cae	Engraving Tool
Camelopardalis	Cam	Giraffe
Cancri	Cnc	Crab
Canum Venaticorum	CVn	Hunting Dogs
Canis Majoris	CMA	Great Dog
Canis Minoris	CMi	Lesser Dog
Capricorni	Cap	Sea Goat
Carinae	Car	Keel
Cassiopeiae	Cas	Seated Queen
Centauri	Cen	Centaur
Cephei	Cep	King
Ceti	Cet	Sea Monster
Chamaeleontis	Cha	Chameleon
Circini	Cir	Compass
Columbae	Col	Dove
Comae Berenices	Com	Bernice's Hair
Coronae Australis	CrA	Southern Crown
Coronae Borealis	CrB	Northern Crown
Corvi	Crv	Crow
Crateris	Crt	Cup
Crucis	Cru	Southern Cross
Cygni	Cyg	Swan
Delphini	Del	Dolphin
Doradus	Dor	Dolphinfish
Draconis	Dra	Dragon
Equulei	Equ	Little Horse
Eridani	Eri	River
Fornacis	For	Furnace
Geminorum	Gem	Twins
Gruis	Gru	Crane
Herculis	Her	Hercules
Horologii	Hor	Clock
Hydrae	Hya	Female Water Snake
Hydri	Hyi	Male Water Snake
Indi	Ind	Indian

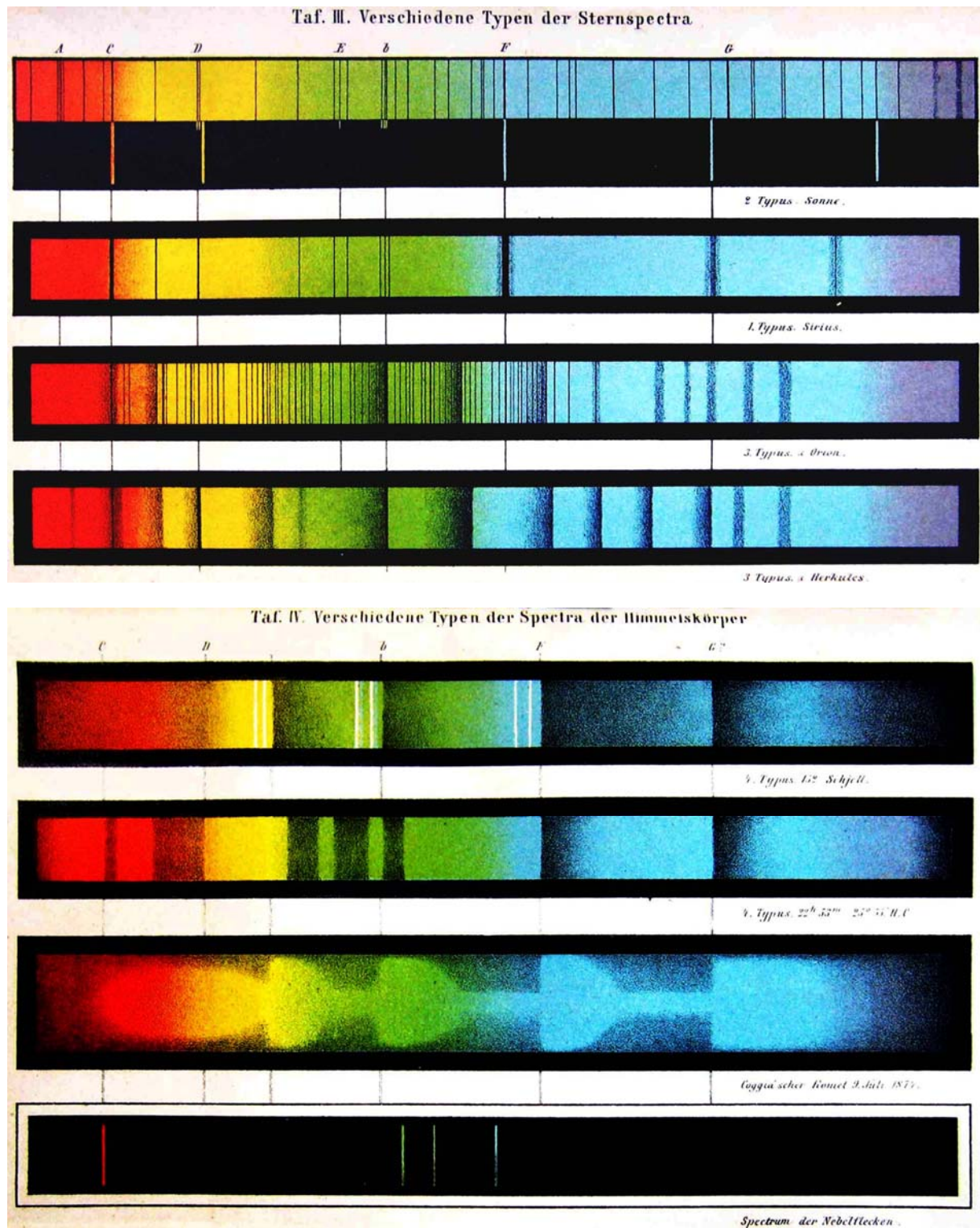
Constellation Latin genitiv	Abbr ev.	Proper name
Lacertae	Lac	Lizard
Leonis	Leo	Lion
Leonis Minoris	LMi	Lesser Lion
Leporis	Lep	Hare
Librae	Lib	Scales
Lupi	Lup	Wolf
Lyncis	Lyn	Lynx
Lyrae	Lyr	Lyre
Mensae	Men	Table Mountain
Microscopii	Mic	Microscope
Monocerotis	Mon	Unicorn
Muscae	Mus	Fly
Normae	Nor	Carpenter's Square
Octantis	Oct	Octant
Ophiuchi	Oph	Serpent Bearer
Orionis	Ori	Hunter
Pavonis	Pav	Peacock
Pegasis	Peg	Winged Horse
Persei	Per	Hero
Phoenicis	Phe	Phoenix
Pictoris	Pic	Painter's Easel
Piscium	Psc	Fishes
Piscis Austrini	PsA	Southern Fish
Puppis	Pup	Stern
Pyxidis	Pyx	Mariners Compass
Reticuli	Ret	Reticule
Sagittae	Sge	Arrow
Sagittarii	Sgr	Archer
Scorpii	Sco	Scorpion
Sculptoris	Scl	Sculptor
Scuti	Sct	Shield
Serpentis	Ser	Serpent
Sextantis	Sex	Sextant
Tauri	Tau	Bull
Telescopii	Tel	Telescope
Trianguli	Tri	Triangle
Trianguli Australis	TrA	Southern Triangle
Tucanae	Tuc	Toucan
Ursae Majoris	UMa	Great Bear
Ursae Minoris	UMi	Lesser Bear
Velorum	Vel	Sails
Virginis	Vir	Maiden
Vulpeculae	Vul	Fox
Volantis	Vol	Flying Fish

## 34.2 Periodic Table of Elements

[illegible]

### 34.3 Some Excerpts of Historical and up to date Spectral Atlases

The very first *Spectral Atlas* was written by Father *Angelo Secchi* at the Vatican Observatory, illustrating his classification system. Many sources call him therefore "Father of the modern astrophysics". The tables with the hand drawn spectra are taken from the german translation of his book *Die Sterne, Grundzüge der Astronomie der Fixsterne* (1878). Courtesy by Martin Brunold [705].





Supergiants 09.5-A0

	Ca II K	He	N II 3995	He I 4009	He I 4026	Sr II 4089	H8	Sr II-He I	He I 4144	4200	Hγ	O II 4349	He I 4387	O II 4415-7	He I 4471	Sr II 4552	C III 4650
9 Cam																	
ε Ori																	
κ Cas																	
ξ Per																	
χ <sup>2</sup> Ori																	
η CMa																	
β Ori																	
HR 1040																	

S II 4128-30      Fe II 4233      Fe II 4351      Mg II 4481

All of the above stars are of luminosity class I. Eastman

[illegible]





### 34.4 Instruments

Telescope: Celestron C8, aperture 8 inch, focal length some 200 cm  
Mount: Equatorial, Vixen Sphinx SXD

Spectrographs: – DADOS, Baader Planetarium [603], reflexion grating 200 and 900L/mm,  
Slit width: 25, 35, 50 $\mu$ m,  $R_{900L} \approx 4000$   $R_{200L} \approx 900$   
Dispersion with Atik 314L+: 2.55 Å/Pixel

– SQUES Echelle, Eagleowloptics Switzerland [600],  $R \approx 20'000$   
adjustable slit width: ~15 - 90 $\mu$ m  
Dispersion with Atik 314L+: 0.18 Å/Pixel

Cameras: Atik 314L+, Meade DSI II and III,  
Location: Rifferswil, Switzerland Elevation: 610m above sea level



Below: Some spectra of Deep Sky Objects have been recorded with the CEDES Cassegrain Telescope of the *Mirasteilas* Observatory in Falera, Switzerland: aperture 90 cm, focal length 900 cm, and Nasmith Fokus. For more details refer to [706].

Martin Huwiler (left), technical head of the observatory.



Finally sincere thanks are given to *Martin Huwiler*, for his valuable collaboration and support, as well as to the successful Asteroid hunter *Jose de Queiroz* for his kind hospitality during our stay!

## 35 Bibliography and Internet

### Literature

- [1] James Kaler, *Stars and their Spectra*
- [2] Richard Gray, Christopher Corbally, *Stellar Spectral Classification*, Princeton Series in Astrophysics
- [3] Keith Robinson, *Spectroscopy, The Key to the stars*
- [4] Stephen Tonkin, *Practical Amateur Spectroscopy*
- [5] Waltraut Carola Seitter, *Atlas for Objective Prism Spectra – Bonner Spektralatlas*, Astronomisches Institut Bonn, Duemmler Verlag 1970/1975. Out of print today, but recently available as Download: <http://www.archive.org/search.php?query=bonner%20atlas>
- [6] H.A. Abt, A.B. Meinel, W.W. Morgan, J.W. Tapscott, 1968. *An Atlas of Low Dispersion Grating Stellar Spectra*, Out of print.
- [7] N. Houk, N. Irvine, D. Rosenbush, Univ. Michigan 1968. *An Atlas of Objective-Prism Spectra*, Out of print.
- [8] Ginestet, N.; et al. 1992. *Atlas de Spectres Stellaires, Standards de Classification MK*, / Observatoire Midi-Pyrenees, Out of print.
- [9] Jack Martin, *A Spectroscopic Atlas of Bright Stars*, Springer Verlag 2010
- [10] Erich Karkoschka, *Atlas für Himmelsbeobachter*, 3. Auflage, Kosmos Verlag
- [11] Brian D. Warner, *Lightcurve Photometry and Analysis*
- [12] Ken M. Harrison, *Astronomical Spectroscopy for Amateurs*, Springer Verlag 2010
- [13] J.-P. Rozelot, C. Neiner et al, *Astronomical Spectrography for Amateurs*, EDP Sciences: EAS Publication Series, Volume 47, 2011.
- [14] G.A. Gurzadyan, 1997, *The Physics and Dynamics of Planetary Nebulae*,
- [15] David F. Gray, 2005, *The Observation and Analysis of Stellar Photospheres*,
- [16] Fritz Kurt Kneubühl, *Repetitorium der Physik*, Teubner Studienbücher Physik, Kap. *Relativistischer Doppler-Effekt der elektromagnetischen Wellen*

### Articles by the Author and Reviews to the Spectroscopic Atlas

- [25] Richard Walker, *Die Fingerabdrücke der Sterne – Ein Spektralatlas für Amateurastronomen*, June/July 2012, Interstellarium No. 82
- [26] Urs Flückiger, *Kostenfreier Spektralatlas*, April 2011, Sterne und Weltraum
- [27] Thomas Eversberg, *Spektralatlas für Astroamateure von Richard Walker*, VDS Journal für Astronomie, III/2011

### Internet Links

#### Author

The following scripts on the subject (some of them in german) are downloadable under this link:  
<http://www.ursusmajor.ch/astrospektroskopie/richard-walkers-page/index.html>

- [30] *Analysis and Interpretation of Astronomical Spectra, Theoretical Background and Practical Applications for Amateur Astronomers*
- [31] *Das Aufbereiten und Auswerten von Spektralprofilen mit den wichtigsten IRIS und Vspec Funktionen*
- [32] *Kalibrierung von Spektren mit der Xenon Stroboskoplampe*

[33] *Atomic Emission Spectroscopy with Spark- or Arc Excitation, Experiments with the DADOS Spectrograph and Simple Makeshift Tools*

[34] *Kalibrierung von Spektren mit dem Glimmstarter ST 111 von OSRAM*

[35] *Glow Starter RELCO SC480 – Atlas of Emission Lines*

[36] *Quasar 3C273, Optical Spectrum and Determination of the Redshift*

### **Spectral atlases and commented spectra**

[50] *An atlas of stellar spectra, with an outline of spectral classification*, Morgan, Keenan, Kellman (1943): [http://nedwww.ipac.caltech.edu/level5/ASS\\_Atlas/frames.html](http://nedwww.ipac.caltech.edu/level5/ASS_Atlas/frames.html)

[51] *Revised MK Spectral Atlas for Stars earlier than the Sun* W.W. Morgan, H.A. Abt, and J.W. Tapscott, (1978), Yerkes Observatory, University of Chicago and Kitt Peak National Observatory <http://nedwww.ipac.caltech.edu/level5/March02/Morgan/frames.html>

[52] *Digital Spectral Classification Atlas* von R.O. Gray, (2000): <http://nedwww.ipac.caltech.edu/level5/Gray/frames.html>

[53] *Moderate-resolution spectral standards from lambda 5600 to lambda 9000* von Allen, L. E. & Strom, K. M: <http://adsabs.harvard.edu/full/1995AJ....109.1379A>

[54] Paolo Valisa, *Osservatorio Astronomico Schiaparelli, Varese*. <http://www.astrogeo.va.it/astronom/spettri/spettrien.htm>

[55] *An atlas of low-resolution near-infrared spectra of normal stars* Torres Dodgen, Ana V., Bruce Weaver: <http://adsabs.harvard.edu/abs/1993PASP..105..693T>

[56] *Contemporary optical spectral classification of the OB stars - A digital atlas* : N. R. Walborn, E.L. Fitzpatrick (1990) <http://adsabs.harvard.edu/full/1990PASP..102..379W>

[57] *An Atlas of yellow-red OB Spectra* N. R. Walborn (1980), <http://articles.adsabs.harvard.edu/full/1980ApJS...44..535W>

[58] *A Standard Stellar Spectral Sequence in the Red/Near Infrared Classes: K5 to M9*, Kirkpatrick et al. <http://articles.adsabs.harvard.edu/full/1991ApJS...77..417K>

[59] *The Interactive Database of Spectral Standard Star Atlases*. <http://alobel.freeshell.org/>  
[http://spectra.freeshell.org/SpectroWeb\\_news.html](http://spectra.freeshell.org/SpectroWeb_news.html)

[60] UCM: *Librerías de espectros estelares* <http://www.ucm.es/info/Astrof/invest/actividad/spectra.html>

[61] *Spectral Synthesis of TiO Lines*, J.A. Valenti et al. <http://adsabs.harvard.edu/abs/1998ApJ...498..851V>

### **Sun**

[80] Highly resolved solar spectrum, Bass2000 [http://bass2000.obspm.fr/download/solar\\_spect.pdf](http://bass2000.obspm.fr/download/solar_spect.pdf)

[81] Lunettes Jean Roesch (Pic du Midi), Highly resolved solar spectrum, recorded on the Jungfraujoch Switzerland, Université de Genève: <http://ljr.bagn.obs-mip.fr/observing/spectrum/index.html>

### **Carbon Stars**

[100] *A Moderate Resolution Spectral Atlas of Carbon Stars*, Cecilia Barnbaum, P. Keenan et al. <http://articles.adsabs.harvard.edu/full/1996ApJS..105..419B>

[101] *A High Resolution Spectral Atlas of Carbon Stars*, Cecilia Barnbaum, <http://articles.adsabs.harvard.edu/full/1994ApJS...90..317B>

- [102] *The Chemical Composition of the Rare J-Type Carbon Stars*, Carlos Abia et al.  
[http://arxiv.org/PS\\_cache/astro-ph/pdf/9912/9912025v1.pdf](http://arxiv.org/PS_cache/astro-ph/pdf/9912/9912025v1.pdf)
- [103] *Near-Infrared Spectra of 29 Carbon Stars, Simple Estimates of Effective Temperature*, Masuo Tanaka et al. <http://pasj.asj.or.jp/v59/n5/590508/590508.pdf>
- [104] *Radial Velocity Distribution and Line strengths of 33 Carbon Stars in the Galactic Bulge*, 1991, D. Tyson et al. <http://articles.adsabs.harvard.edu/full/1991ApJ...367..547T>
- [105] *Carbon Stars, Hydrostatic Models and Optical/Near Infrared Interferometry*, S. Schneiderbauer, 2008, Univ. Vienna, [http://othes.univie.ac.at/1627/1/2008-10-13\\_9940129.pdf](http://othes.univie.ac.at/1627/1/2008-10-13_9940129.pdf)
- [106] *Understanding Carbon Star Nucleosynthesis from Observations*, 2003, C. Albia et al.  
[http://www.publish.csiro.au/?act=view\\_file&file\\_id=AS03021.pdf](http://www.publish.csiro.au/?act=view_file&file_id=AS03021.pdf)
- [107] *Revised MK Classification of the Red Carbon Stars*, 1993, P. Keenan  
<http://adsabs.harvard.edu/full/1993PASP..105..905K>
- [108] *Photometric and Spectroscopic Investigation of a New Carbon Star in the Auriga Region*, 1978, M. Vetesnik, Brno University <http://articles.adsabs.harvard.edu/full/1979BAICz..30....1V>
- [109] *SiC<sub>2</sub> in carbon stars: Merrill Sanford Absorption Bands between 4100 and 5500Å*, P. J. Sarre et al. <http://articles.adsabs.harvard.edu/full/2000MNRAS.319..103S>
- [110] *Band-Head Wavelengths of C<sub>2</sub>, CH, CN, CO, NH, NO, O<sub>2</sub>, OH and Their Ions*, L. Wallace 1962  
<http://adsabs.harvard.edu/full/1962ApJS....7..165W>

### **Spectral Class S**

- [140] *Spectral types of S and SC stars on the revised MK system*, 1979, Keenan, & Boeshaar  
<http://articles.adsabs.harvard.edu/full/1980ApJS...43..379K>
- [141] *Molecular Spectra of pure S-Stars*, 1978, S. Wyckoff, R.E.S. Clegg  
<http://adsabs.harvard.edu/abs/1978MNRAS.184..127W>

### **Evolution AGB Stars**

- [160] *On the evolution and properties of AGB stars*, 1993, Martin Arnold Theodoor Groenewegen, Universität Amsterdam <http://dare.uva.nl/>, 103726 in das Suchfeld eingeben.

### **Telluric Absorptions**

- [180] *High Resolution Spectral Atlas of Telluric Lines*, G. Catanzaro, Università di Messina.  
<http://webusers.ct.astro.it/gca/papers/telluric.pdf>
- [181] *A Method of Correcting Near-Infrared Spectra for Telluric Absorption*. W. D. Vacca et al.  
<http://www.journals.uchicago.edu/doi/pdf/10.1086/346193>
- [182] *Fine Structure of the Red System of Atmospheric Oxygen Bands*, H. D. Babcock and L. Herzberg <http://adsabs.harvard.edu/full/1948ApJ...108..167B>

### **Light Pollution and Airglow**

- [190] *Measuring Light Pollution on La Palma*, Chris R. Benn, Isaac Newton Group, Spain  
[http://www.starlight2007.net/pdf/proceedings/C\\_Benn.pdf](http://www.starlight2007.net/pdf/proceedings/C_Benn.pdf)
- [191] *The High-Resolution Light-polluted Night-Sky Spectrum at Mount Hamilton, California*, T. G. Slinger P. C. Cosby et al. 2003: <http://adsabs.harvard.edu/abs/2003PASP..115..869S>
- [192] *Where the shadows lie – The dark skies of Chile*, Ferdinando Patat – ESO,  
[http://www.eso.org/~fpatat/science/skybright/zenit/zenit\\_paper.htm](http://www.eso.org/~fpatat/science/skybright/zenit/zenit_paper.htm)

### **Planetary Nebulae and Emissionsline Objects**

- [200] *Emission Lines Identified in Planetary Nebulae*, Y.P. Varshni, et al., 2006 Univ. Ottawa  
<http://laserstars.org/>  
<http://laserstars.org/data/nebula/identification.html>

- [201] *Gallery of Planetary Nebula Spectra*, Williams College  
<http://www.williams.edu/astronomy/research/PN/nebulae/>  
<http://www.williams.edu/astronomy/research/PN/nebulae/legend.php>
- [202] *Planetarische Nebel*, Frank Giesekeing, 6 articles, SUW 1983.
- [203] *Balmer Line Ratios in Planetary Nebulae*, Osterbrock et al., Univ. Wisconsin 1963  
[http://articles.adsabs.harvard.edu/cgi-bin/nph-iarticle\\_query?1963ApJ...138...62O&defaultprint=YES&filetype=.pdf](http://articles.adsabs.harvard.edu/cgi-bin/nph-iarticle_query?1963ApJ...138...62O&defaultprint=YES&filetype=.pdf)
- [204] *3D Spektrofotometrie Extragalaktischer Emissionslinienobjekte*, Dissertation J. Schmoll, AIP  
<http://www.aip.de/groups/publications/schmoll.pdf>
- [205] *An Evaluation of the Excitation Parameter for the Central Stars of Planetary Nebulae*, W. A. Reid et al, Univ. Sydney 2010 [http://arxiv.org/PS\\_cache/arxiv/pdf/0911/0911.3689v2.pdf](http://arxiv.org/PS_cache/arxiv/pdf/0911/0911.3689v2.pdf)
- [206] *Excitation Class of Nebulae – an Evolution Criterion?* G. A. Gurzadyan, A.G. Egikyan, Byurakan Astrophysical Observatory 1990 <http://articles.adsabs.harvard.edu/full/1991Ap%26SS.181...73G>
- [207] *The Planetary Nebulae*, J. Kaler, <http://stars.astro.illinois.edu/sow/pn.html>
- [210] *A HighResolution Catalogue of Cometary Emission Lines*, M.E Brown et al. 1996 Caltech  
<http://www.gps.caltech.edu/~mbrown/comet/echelle.html>
- [220] *Optical Spectra of Supernova Remnants*, Danziger, Dennefeld, Santiago de Chile 1975,  
<http://articles.adsabs.harvard.edu/full/1976PASP...88...44D>
- [221] *Optical and Radio Studies of SNR in the Local Group Galaxy M33*, Danziger et al. 1980, ESO  
<http://www.eso.org/sci/publications/messenger/archive/no.21-sep80/messenger-no21-7-11.pdf>
- [222] *Emission-line spectra of condensations in the Crab Nebula*, Davidson 1979  
<http://adsabs.harvard.edu/abs/1979ApJ...228..179D>
- [223] *ISM and Star Formation, The Orion Bar*, Harvard Astronomy 201b/2011  
<http://ay201b.wordpress.com/2011/05/01/the-orion-bar/>
- [224] *Complex ionized structure in the theta-2 Orionis region*, J. R. Walsh, Univ. Manchester, 1981  
<http://articles.adsabs.harvard.edu/full/1982MNRAS.201..561W>

### **Wolf Rayet Stars**

- [230] *C IV  $\lambda$ 5806 in Wolf Rayet Stars*, Anne B. Underhill  
<http://articles.adsabs.harvard.edu/full/1988PASP..100.1269U/0001269.000.html>
- [231] *Atlas for Wolf-Rayet Stars*, Harvard Center for Astrophysics  
<https://www.cfa.harvard.edu/~pberlind/atlas/htmls/wrstars.html>
- [232] *The VII<sub>th</sub> catalogue of galactic Wolf-Rayet stars*, Karel A. van der Hucht  
[www.astrosurf.com/luxorion/Documents/wrcat.pdf](http://www.astrosurf.com/luxorion/Documents/wrcat.pdf)
- [233] *Spectral Classification of Wolf-Rayet Stars*, W.A. Hiltner, R.E. Schild, 1965 Chicago  
<http://articles.adsabs.harvard.edu/full/1966ApJ...143..770H>
- [234] *Physical Properties of Wolf-Rayet Stars*, Paul A. Crowther,  
<http://www.stsci.de/wr140/pdf/crowther2006.pdf>
- [235] *WR stars with the O VI 3811, 3834 A emission doublet*. A.M. Cherepashchuk, D.N Rustamov,  
<http://articles.adsabs.harvard.edu/full/1990Ap%26SS.167..281C>
- [236] *Chapter 11, Pre-supernova evolution of massive stars*, lecture University of Bonn  
[www.astro.uni-bonn.de](http://www.astro.uni-bonn.de)
- [237] *The Interaction of NGC 6888 and HD 192163 With the Surrounding Interstellar Medium*  
 Cappa, C. E et al. <http://articles.adsabs.harvard.edu/full/1996AJ....112.1104C>
- [238] *HST Observations of the Wolf-Rayet Nebula NGC 6888*, Brian D. Moore et al  
<http://arxiv.org/abs/astro-ph/0003053>

[239] *Non-LTE spectral analyses of Wolf-Rayet stars: The nitrogen spectrum of the WN6 prototype HD 192163 (WR136)*, W.-R. Hamann, et al. <http://adsabs.harvard.edu/abs/1994A&A...281..184H>

[240] *Suzaku Observations of the Prototype Wind-Blown Bubble NGC 6888*, Svetozar A. Zhekov <http://arxiv.org/pdf/1012.3917>

[241] *Chandra Detects the rare Oxygen Type Wolf-Rayet Star WR 142 and OB Stars in Berkeley 87* Kimberly R. Sokal et al. <http://arxiv.org/abs/1004.0462>

[242] *The WO stars IV. Sand 5: a variable WO star?*, V.F. Polcaro et al. <http://adsabs.harvard.edu/full/1997A%26A...325..178P>

[243] *Discovery of a WO Star in the Scutum-Crux Arm of the inner Galaxy*, Janet E. Drew et al. <http://arxiv.org/pdf/astro-ph/0403482.pdf>

### **Be Stars**

[250] *High and intermediate-resolution spectroscopy of Be stars*, J. Chauville et al. A&A 2002 [http://www.aanda.org/index.php?option=com\\_article&access=standard&Itemid=129&url=/articles/aa/abs/2001/42/aa1599/aa1599.html](http://www.aanda.org/index.php?option=com_article&access=standard&Itemid=129&url=/articles/aa/abs/2001/42/aa1599/aa1599.html)

[251]: *Spectra of the Brightest Be stars and Objects Description*, A. Miroshnichenko, University of North Carolina, [www.astrospectroscopy.de/Heidelbergtagung/Miroshnichenko2.ppt](http://www.astrospectroscopy.de/Heidelbergtagung/Miroshnichenko2.ppt)

[252] *Summary of Experiences from Observations of the Be-binary  $\delta$  Sco*, A. Miroshnichenko, University of North Carolina, [www.astrospectroscopy.de/Heidelbergtagung/Miroshnichenko1.ppt](http://www.astrospectroscopy.de/Heidelbergtagung/Miroshnichenko1.ppt)

[253] *Properties of the  $\delta$  Scorpii Circumstellar Disk from Continuum Modeling*, A. Miroshnichenko et al.: University of North Carolina, [http://libres.uncg.edu/ir/uncg/f/A\\_Miroshnichenko\\_Properties\\_2006.pdf](http://libres.uncg.edu/ir/uncg/f/A_Miroshnichenko_Properties_2006.pdf)

[254] *High resolution emissionline spectroscopy of Be Stars*, Reinhard W. Hanuschik, Astronomisches Institut Universität Bochum. <http://articles.adsabs.harvard.edu/full/1986A%26A...166..185H>

[255] *V/R Variations of Binary Be Stars*, S. Stefl et al. ESO 2007 <http://www.arc.hokkai-s-u.ac.jp/~okazaki/Meetings/sapporo/361-0274.pdf>

[256] *The Optical Counterpart of the X-ray Transient RX J0117.6-7330R*. Soria, Siding Spring Observatory Coonabarabran, Australia <http://articles.adsabs.harvard.edu/full/1999PASA...16..147S>

[257] *Spektroskopische Beobachtungen der H $\alpha$ - und der He I 6678-Emission am Doppelsternsystem  $\delta$  Scorpii*, E. Pollmann: <http://www.bav-astro.de/rb/rb2009-3/151.pdf>

### **Herbig Ae/Be Stars**

[270] *Spectrophotometry of R Monocerotis*, K.H. Böhm et al. 1976, University of Washington <http://adsabs.harvard.edu/full/1976A%26A....50..361B>

[271] *Spectroscopy of R Monocerotis and NGC 2261*, Alan Stockton et al. Univ. of Hawaii 1974, <http://adsabs.harvard.edu/full/1975ApJ...199..406S>

[272] *Toward Understanding the Environment of R Monocerotis from high Resolution Near-Infrared Polarimetric Observations*, M.A. Jolin et al. Université de Montréal, 2010 [http://iopscience.iop.org/0004-637X/721/2/1748/fulltext/apj\\_721\\_2\\_1748.text.html](http://iopscience.iop.org/0004-637X/721/2/1748/fulltext/apj_721_2_1748.text.html)

[273] *Iron Emission Lines in the Spectra of Herbig Ae/Be stars Viewed through Their Proto-Planetary Disks*. C.A. Grady et al. 183<sup>rd</sup> AAS Meeting, Washington DC <http://articles.adsabs.harvard.edu/full/1993AAS...183.4109G>

[274] *Spektroskopische Variationen des Herbig Ae/Be Sterns HD 163296*. Diploma Thesis Stefan Noll, University Heidelberg 1999, [http://www.lsw.uni-heidelberg.de/projects/hot-stars/Diplom\\_Noll.pdf](http://www.lsw.uni-heidelberg.de/projects/hot-stars/Diplom_Noll.pdf)

[275] *Carbon Monoxide Observations of R Monocerotis, NGC 2261 and Herbig Haro 39: The Interstellar Nozzle*. J Canto et al. Univ. Mexico 1980. <http://articles.adsabs.harvard.edu/full/1981ApJ...244..102C>



**T Tauri Stars**

[280] *Spectra of T Tauri Stars*, A. McKay  
<http://astronomy.nmsu.edu/>

[281] *Understanding Stellar Birth Through the Photometric and Spectroscopic Variability of T Tauri Stars*, MW Eastwood, N. Mahmud, C.M. Johns, Rice University Houston Texas 2011,  
[http://www.as.utexas.edu/ugrad\\_symposium/?a=3](http://www.as.utexas.edu/ugrad_symposium/?a=3)

**FU Orionis Stars**

[286] *The FU Orionis Phenomenon*, Lee Hartmann, Scott J. Kenyon, Harvard-Smithsonian Center for Astrophysics 1996, [www.ifa.hawaii.edu/~reipurth/reviews/hartmann.ps](http://www.ifa.hawaii.edu/~reipurth/reviews/hartmann.ps)

[287] *The Periodic Spectroscopic Variability of FU Orionis*, Stacie L. Powell et al. 2012  
<http://arxiv.org/abs/1209.0981>

[288] *Veränderungen im Spektrum von FU Orionis*, P. Wellmann 1951  
<http://adsabs.harvard.edu/full/1951ZA.....29..154W>

[289] *Models of the Spectral Energy Distributions of FU Orionis Stars*, N. J. J. Turner et al. 1996  
<http://iopscience.iop.org/0004-637X/480/2/754/>

[290] *Line Structure in the Spectrum of FU Orionis*, P.P. Petrov, G.H. Herbig  
<http://arxiv.org/abs/0806.4053>

**Extragalactic Objects**

[300] Caltech: Spektralatlases for extragalactic Objekts  
<http://nedwww.ipac.caltech.edu/level5/catalogs.html>

[301] *A Spectrophotometric Atlas of Galaxies*, Robert C. Kennicutt, Steward Observatory  
<http://articles.adsabs.harvard.edu/full/1992ApJS...79..255K>

[302] *Aktive Galaxien, Quasare, Schwarze Löcher*, Vorlesung Universität Potsdam 2005  
[www.mpia-hd.mpg.de/home/jahnke/lectures/gqs\\_05/introduction1.pdf](http://www.mpia-hd.mpg.de/home/jahnke/lectures/gqs_05/introduction1.pdf)

[303] *Active Nuclei and their Host Galaxies: Observations of Seyfert Galaxies*, 2008, S. Harrold, J. Kajubi [www.pas.rochester.edu/~advlab/reports/harrold\\_kajubi\\_astro2.pdf](http://www.pas.rochester.edu/~advlab/reports/harrold_kajubi_astro2.pdf)

[304] *Spectroscopic Atlas of the Central 24"x 20" of the Seyfert 2 Galaxy NGC 1068*, B. Garcia-Lorenzo et al. <http://iopscience.iop.org/0004-637X/518/1/190/>

[305] Spectral classification of emission-line galaxies from the Sloan Digital Sky Survey, 2009, F. Lamareille et al.:

Part I <http://adsabs.harvard.edu/abs/2009arXiv0910.4814L>,

Part II: <http://arxiv.org/abs/1105.0488>

[306] Testing the Seyfert Unification Theory: Chandra HETGS observations of NGC 1068, P. M. Ogle et al. <http://arxiv.org/abs/astro-ph/0211406>

[307] Spectral Classification of Emission Line Galaxies, 1986 S. Veilleux, D. Osterbrock  
<http://adsabs.harvard.edu/abs/1987ApJS...63..295V>

[308] M. J. Avara, *Precision X-Ray Spectroscopy of 3C273 Jet Knots*, MIT 2008  
<http://dspace.mit.edu/bitstream/handle/1721.1/44464/297176629.pdf?sequence=1>

[309] B.M. Peterson et al. *Are Forbidden Lines Present in the Optical Spectrum of the QSO 3C 273?* Ohio State University 1984 <http://articles.adsabs.harvard.edu/full/1984ApJ...283..529P>

[310] B.M. Peterson et al. *Central Masses and Broad-Line Region Sizes of Active Galactic Nuclei. II. A Homogeneous Analysis of a Large Reverberation-Mapping Database*. The Astrophysical Journal 2004 <http://arxiv.org/abs/astro-ph/0407299>

[311] S. Paltani, M. Türlér: *The mass of the black hole in 3C273*, 2005 Marseille, Geneva  
<http://arxiv.org/abs/astro-ph/0502296>

[312] A. Boksenberg et al. *New Spectrometric Results on the Quasar 3C273*, 1974, University London <http://adsabs.harvard.edu/full/1975MNRAS.172..289B>

[313] J.B. Oke: *The Optical Spectrum of 3C273*, CALTECH 1964  
<http://adsabs.harvard.edu/abs/1965ApJ...141....60>

### **Monographs**

[340] *Time-series Analysis of Line Profile Variability in Optical Spectra of  $\epsilon$  Orionis*, Gregory B. Thompson <http://etd.ohiolink.edu/send-pdf.cgi/Thompson%20Gregory%20Brandon.pdf?toledo1249511358>

[341] *Spektralatlas P Cygni*, O. Stahl, Landessternwarte Heidelberg  
[http://seds.org/Maps/Stars\\_en/Spectra/pcyg.html](http://seds.org/Maps/Stars_en/Spectra/pcyg.html)

[341a] *The Spectrum of P Cygni 1964*, L.S. Luud, Academy of Science Estonian SSR 1964  
<http://adsabs.harvard.edu/full/1967SvA....11..211L>

[341b] *Of the Spectrum and Nature of P Cygni*, Maart de Groot, Astr. Inst. Nederlands, 1968  
<http://adsabs.harvard.edu/full/1969BAN....20..225D>

[342] Christian Buil: *Vega Spectrum Atlas, a full commented spectrum*  
<http://astrosurf.com/buil/us/vatlas/vatlas.htm>

[343] O.C. Wilson: *The Wolf-Rayet Spectroscopic Binary HD 190918*, Mount Wilson 1948  
<http://articles.adsabs.harvard.edu/full/1949ApJ...109...76W>

[344] *A Study of the moderately wide Wolf Rayet Spectroscopic Binary HD190918*, A. Underhill et al. <http://adsabs.harvard.edu/full/1994ApJ...432..770U>

[345] Lesley A. Morgan 1971: *The Emission Line Spectrum of the Orion Nebula...*  
[http://articles.adsabs.harvard.edu/cgi-bin/nph-iarticle\\_query?1971MNRAS.153..393M&defaultprint=YES&filetype=.pdf](http://articles.adsabs.harvard.edu/cgi-bin/nph-iarticle_query?1971MNRAS.153..393M&defaultprint=YES&filetype=.pdf)

[346] S. V. Marchenko et al.: *The unusual 2001 Periastron Passage in the „Clockwork“ Colliding Wind Binary WR 140*, <http://www.stsci.de/wr140/pdf/marchenko2003.pdf>

[347] *Multi Frequency Variations of Wolf Rayet System HD193793*, P.M. Williams et al. 1989  
<http://esoads.eso.org/abs/1990MNRAS.243..662W>

[348] *Spectral Analysis of a Peculiar Star WZ Cassiopeiae*, Masanori Hirai, University of Tokyo,  
<http://adsabs.harvard.edu/full/1969PASJ...21...91H>

[349] *The 6708 resonance line of Li I in the spectrum of the N-type variable star WZ Cassiopeiae*, McKellar 1941, <http://articles.adsabs.harvard.edu/full/1941Obs....64....4M/0000004.000.html>

[350] *Cyclic variability of the circumstellar disk of the Be star  $\zeta$  Tau*, S. Stefl et al., ESO,  
[http://arxiv.org/PS\\_cache/arxiv/pdf/0907/0907.2250v1.pdf](http://arxiv.org/PS_cache/arxiv/pdf/0907/0907.2250v1.pdf)

[351] *Visual/infrared interferometry of Orion Trapezium stars: preliminary dynamical orbit and aperture synthesis imaging of the  $\theta$ 1 OrionisC system*, S. Kraus, Y. Y. Balega et al. 2006,  
[www.skraus.eu/papers/kraus.T1OriC.pdf](http://www.skraus.eu/papers/kraus.T1OriC.pdf)

[352] *Spectrum variability of 68 Cygni, an O(f) star at the center of a ring nebula*, V. I. Alduseva, A. A. Aslanov et al. 1982, <http://adsabs.harvard.edu/full/1982SvA....8..386A>

### **Lectures and practica**

[400] *Versuchsanleitung zum Astrophysikalischen Praktikum, Grobe Klassifikation von Sternspektren*, Kiepenheuer Institut: [http://www.kis.uni-freiburg.de/fileadmin/user\\_upload/kis/lehre/praktika/sternspektren.pdf](http://www.kis.uni-freiburg.de/fileadmin/user_upload/kis/lehre/praktika/sternspektren.pdf)

[401] F. Royer: *Rotation des étoiles de type A*, Vorlesung Ecole d'Astronomie de CNRS  
<http://adsabs.harvard.edu/abs/1996udh..conf..159R>

[402] *Vorlesung Astrophysik*, Max Planck Institut München:  
[www.mpa-garching.mpg.de/lectures/TASTRO](http://www.mpa-garching.mpg.de/lectures/TASTRO)

[403] *Vorlesung Astrophysik*, Astrophysikalisches Institut Potsdam  
<http://www.aip.de/People/MSteinmetz/classes/WiSe05/PPT/>

[404] Astrophysics graduate course 25530-01 Lecture 6 and 7, Univ. Basel  
[http://phys-merger.physik.unibas.ch/~cherchneff/Site\\_2/Teaching\\_at\\_UniBasel.html](http://phys-merger.physik.unibas.ch/~cherchneff/Site_2/Teaching_at_UniBasel.html)

**Databases**

[500] CDS Strassbourg: *SIMBAD Astonomical Database*  
<http://simbad.u-strasbg.fr/simbad/>

[501] NASA *Extragalactic Database (NED)*  
<http://nedwww.ipac.caltech.edu/>

[502] *The SAO/NASA Astrophysics Data System*,  
<http://adsabs.harvard.edu/index.html>

[503] *NIST Atomic Spectra Database*:  
[http://physics.nist.gov/PhysRefData/ASD/lines\\_form.html](http://physics.nist.gov/PhysRefData/ASD/lines_form.html)

[504] Simulated emission spectra for all elements  
<http://bmauclaire.free.fr/astronomie/spectro/simulation/noblet/index2.htm>

[505] *The Bright Star Catalogue, 5th Revised Ed. (Preliminary Version) (Hoffleit+, 1991)*  
Datenzugang über [http://www.alcyone.de/search\\_in\\_bsc.html](http://www.alcyone.de/search_in_bsc.html)

[506] James Kaler <http://stars.astro.illinois.edu/sow/sowlist.html>

[507] AAVSO, American Association of Variable Star Observers <http://www.aavso.org/>

[508] *Spectral Atlas Central*, Atlas of Calibration lines, *National Optical Astronomy Observatories*  
NOAO <http://www.noao.edu/kpno/specatlas/>

**Spectrographic software**

[550] IRIS: Webpage of *Christian Buil*  
<http://www.astrosurf.com/buil/>

[551] Vspec: Webpage of *Valerie Désnoux*  
<http://astrosurf.com/vdesnoux/>

[552] RSPEC: Webpage of *Tom Field*  
<http://www.rspec-astro.com/>

[553] MIDAS, ESO  
<http://www.eso.org/sci/software/esomidas//>

[554] Spectro Tools: Freeware program by Peter Schlatter for the extraction of the H<sub>2</sub>O lines  
<http://www.peterschlatter.ch/SpectroTools/>

**Spectrographs and Cameras**

[600] SQUES Echelle Spectrograph, Eagleowloptics Switzerland,  
<http://www.eagleowloptics.com/>

[603] DADOS Spectrograph, Baader Planetarium, Germany:  
[http://www.baader-planetarium.com/pdf\\_download.htm](http://www.baader-planetarium.com/pdf_download.htm)

[605] Shelyak Instruments: <http://www.shelyak.com/>

[606] Datasheet Sony Chip ICX285AL:  
<http://www.datasheetcatalog.org/datasheet/sony/a6803068.pdf>

[607] SBIG Spectrograph DSS-7, <http://ftp.sbig.com/dss7/dss7.htm>

**General links**

[700] Isabelle A. Grenier: *The Gould Belt, star formation and the interstellar medium*  
[http://arxiv.org/PS\\_cache/astro-ph/pdf/0409/0409096v1.pdf](http://arxiv.org/PS_cache/astro-ph/pdf/0409/0409096v1.pdf)

[700a] *3D Evolution of the Gould Belt*, Christophe Perrot , Isabelle Grenier  
<http://arxiv.org/pdf/astro-ph/0303516>

[701] Gene Smith, University of California, San Diego, *Astronomy Tutorial, Stellar Spectra*  
<http://cass.ucsd.edu/public/tutorial/Stars.html>

- [702] H.A. Abt: *New Data on A-Type Disk stars*, The Astrophysical Journal 2007,  
[http://iopscience.iop.org/0067-0049/174/2/499/pdf/0067-0049\\_174\\_2\\_499.pdf](http://iopscience.iop.org/0067-0049/174/2/499/pdf/0067-0049_174_2_499.pdf)
- [703] H. M. Qiu et al.: *The Abundance Patterns of Sirius and Vega*, The Astrophysical Journal 2001  
[http://iopscience.iop.org/0004-637X/548/2/953/pdf/0004-637X\\_548\\_2\\_953.pdf](http://iopscience.iop.org/0004-637X/548/2/953/pdf/0004-637X_548_2_953.pdf)
- [704] U.K. Gehlich: *Differential Fine Analysis Sirius versus Vega*, Astronomy & Astrophysics, 1969  
<http://articles.adsabs.harvard.edu/full/1969A%26A.....3..169G>
- [705] Martin Brunold, CH-Abtwil <http://www.astrolabe.ch/index.aspx>
- [706] *Mirasteilas*, Observatory, Falera <http://www.sternwarte-mirasteilas.ch/>
- [707] Richard E. Orville and Ronald W. Henderson:  
*Absolute Spectral Irradiance Measurements of Lightning from 375 to 880 nm*  
<http://journals.ametsoc.org/doi/pdf/10.1175/1520-0469%281984%29041%3C3180%3AASIMOL%3E2.0.CO%3B2>
- [708] Vesto M. Slipher, *The Spectrum of Lightning*, Bulletin No. 79, Lowell Observatory Sept 1917, Flagstaff Arizona <http://adsabs.harvard.edu/full/1917LowOB...3...55S>